Numerical modelling of convection-reaction-diffusion problems using electrical analogues

Sabawoon Shafaq

PhD 2014

Numerical modelling of convection-reaction-diffusion problems using electrical analogues

By Sabawoon Shafaq BEng

Submitted to Dublin City University for the award of PhD.

July 2014

Dr Joseph Stokes

Head of School

Dr Alan Kennedy

Supervisor

Dr Yan Delauré

Co-supervisor

School of Mechanical and Manufacturing Engineering

I hereby certify that this material, which I now submit for assessment on the programme of study leading to the award of PhD is entirely my own work, and that I have exercised reasonable care to ensure that the work is original, and does not to the best of my knowledge breach any law of copyright, and has not been taken from the work of others save and to the extent that such work has been cited and acknowledged within the text of my work.

Signed: _____ ID No.: 54800834 Date: _____

Contents

Acknowledgement

I would like to thank my family and friends for their support over the years, which I spent completing this project, and I remain indebted to their kindness. I sincerely like to thank Dr Alan Kennedy for his support, time, enthusiasm and hard work required to complete this project; his efforts will always be remembered. I would also like to show my gratitude to Dr Yan Delauré and Dr Joseph Stokes who provided the right support and honest opinions at times when they were needed the most. I finally like to thank the Irish Research Council for Science, Engineering & Technology (IRCSET), for providing the funds required for the first three years of this research.

Nomenclature

a	Constant or as per description in the chapters
α	Constant or as per description in the chapters
$A_{i,j}$	A cell value of matrix **A** located at row *i* and column *j*
$\mathbf{A}$	A 2×2 matrix
$\mathbf{b}$	A 2×1 matrix
b	Constant or as per description in the chapters
$b_{i,j}$	A cell value of matrix **b** located at row *i* and column *j*
C	Thermal capacitance of materials or per description in the chapters
C_d	Distributed capacitance
C_l	Left side lumped capacitance in an electrical circuit
C_r	Right side lumped capacitance in an electrical circuit
D	Diffusion coefficient
Δx	Length of a segment or spatial discretization
D_n	Diffusion coefficient value at the location of node *n*
$D^{AA}_{n+\frac{1}{2}}$	Interpolated value of the diffusion coefficient between node *n* and *n*+1 calculated from the average values of the diffusion coefficient over volume corresponding to node n
$D^{An}_{n+\frac{1}{2}}$	Average value of the diffusion coefficient over over space between node *n* and *n*+1
$D^{BA}_{n+\frac{1}{2}}$	Average value of the diffusion coefficient between node *n* and *n*+1
$D^{Bn}_{n+\frac{1}{2}}$	Value of the diffusion coefficient between node *n* and *n*+1
D^{HA}_{n}	Harmonic mean value of the diffusion coefficient over space between node *n* and *n*+1 calculated from the average values of the diffusion coefficient over volume corresponding to node n

$\overline{D_n}, \overline{K_n}, \overline{S_n}$	Average values of coefficients over the volume corresponding to node n
$\mathrm{dA}^{\mathrm{Rel}}$	Relative difference between the coefficients of the equations for the Lumped-circuit and transmission line
E	Error
${}^{*}E_{h-h_0}$	Difference between two solutions; one solved using a grid size of h and the other using h_0, where $h_0 << h$
E_{Abs}	Absolute error
$E_{\mathrm{Abs}}^{\mathrm{LCM}}$	Absolute error in LCM solution
${}^{*}E_{m}^{\mathrm{Abs}}$	Approximate absolute error calculated at midpoint of the domain
E_{m}^{Rel}	Relative error in the solutions calculated at midpoint of the domain
${}^{*}E_{m}^{\mathrm{Rel}}$	Approximate relative error calculated at midpoint of the domain
$\mathbf{F}$	Flux vector
f	Reference to CV face or as per description in the chapters
$\mathrm{FVM}^{\mathrm{An}}$	Reference to errors and solutions of FVM method solved with $D^{An}_{n+\frac{1}{2}}$
$\mathrm{FVM}^{\mathrm{BA}}$	Reference to error and solution of FVM method solved with $D^{BA}_{n+\frac{1}{2}}$
$\mathrm{FVM}^{\mathrm{Bn}}$	Reference to errors and solutions of FVM method solved with $D^{Bn}_{n+\frac{1}{2}}$
$\mathrm{FVM}^{\mathrm{HA}}$	Reference to error and solution from FVM method solved with D_n^{HA}
$\mathrm{FVM}^{\mathrm{BHA}}$	Reference to error and solution from FVM method solved with D_n^{BHA}
G_d	Distributed shunt conductance
G_l	Left side lumped inductance in an electrical circuit
G_r	Right side lumped inductance in an electrical circuit
h	Distance between two adjacent nodes (spatial discretization) or length of a control volume
I	Current

I_d	Distributed current source
$I_{i,n}$	Input current at the location of node *n*
I_l	Left side lumped current source in an electrical circuit
$I_{o,n}$	Output current at the location of node *n*
I_r	Right side lumped current source in an electrical circuit
j	Reference to material layer or lmaginary number
K	Reaction coefficient
k	Thermal conductivity or as per description in the chapters
λ	Length of the domain
L_d	Inductance of a transmission line
$L_{j,i}$	Part of layer *j* overlapping section *i*
L_{N_s}	Length of a segment, similar to L*j*,*i*
m	Node located at the midpoint of the domain or as per description in the chapters
n	Node number
$\mathbf{n}$	The unit outward vector normal
N_L	Number of layers in a domain
N	Number of nodes in a domain
N_s	Number of segments in a section
ω	Angular velocity of sinusoidal current
P	Impedance ratio or as per description in the chapters
$\mathbf{p}$	Vector representing the position of a points in space or as per description in the chapters
ϕ	Unknown scalar in the CRDE (i.e. concentration of diffusant)

$\mathbf{q}$	Vector representing the position of a points in space
R_d	Distributed resistance
R	Lumped resistance of an electrical circuit
ρ	Reflection coefficient, density or as per description in the chapters
ρ_{LR}	Reflection coefficient for a voltage incident from left to right
ρ_{RL}	Reflection coefficient for a voltage incident from right to left
S	Source term
τ	Transmission coefficient
τ_{LR}	Transmission coefficient for a voltage incident from left to right
τ_{RL}	Transmission coefficient for a voltage incident from right to left
T	Temperature
u	Propagation speed or Phase velocity of a signal
v	Convection velocity (scalar)
$\mathbf{v}$	Convection velocity (vector)
Vil	Voltage incident from the left
$V_{i,n}$	Input voltage of a TL at the location of node n
Vir	Voltage incident from the right
V	Voltage
V_L	Constant voltage at the left−hand side boundary located at $x = 0$ where $x \in [0, \lambda]$
V_n	Voltage at the location of node n
$V_{n,m}$	Voltage at the location of node n,m in a 2D domain
V_{exact}	Exact solution

$V_{o,n}$	Output voltage of a TL at the location of node *n*
V_R	Constant voltage at the right−hand side boundary located at $x = \lambda$ where $x \in [0, \lambda]$
Vsl	Voltage scattered to the left
Vsr	Voltage scattered to the right
$V_{x_2,x_1}(x)$	Voltage at all points between x_1 and x_2 in the domain where $x \in (0, \lambda)$
x	Spatial location of nodes in the domain
x_L	Spatial location of a layer boundaries
Z	Impedance of the transmission line

Abstract

Convection-reaction-diffusion equations can describe a diverse range of physical phenomena. The development of efficient, reliable, and accurate numerical methods for the solution of such equations is ongoing, especially for certain types of problems (e.g. ones in which convection dominates). In this thesis, a new method, called the Lumped-component Circuit Method (LCM), developed previously for one-dimensional steady-state reaction-diffusion, is tested and extended for modelling both steady-state and transient reaction-diffusion and convection-reaction-diffusion in one and two dimensions. It is developed for solving equations with piecewise-constant coefficients, but its application is not restricted to such problems.

Like the Transmission Line Method (TLM), it is an indirect method in which the problem to be solved is first represented by an analogous transmission line (TL). Unlike with TLM, however, the TL is then modelled using a lumped-component circuit, and the voltages at nodes within that circuit are calculated. For transient modelling, a time-stepping scheme is required. Traditional schemes can be used when calculating the node voltages over time, but TLM (a simple, explicit, and unconditionally stable time-stepping technique) can also be used for this purpose.

The LCM method is compared with FVM (Finite Volume Method) schemes. It is validated, where possible, using analytical solutions and existing solutions to real physical problems. When solving equations with piecewise-constant coefficients, with nodes that are not positioned to correspond with the discontinuities, the FVM solutions do not converge consistently as the node spacing is decreased. That is not the case with LCM. In general, the LCM scheme is more accurate than the FVM schemes tested, and, while the computational cost of LCM is higher, results suggest that it is generally more accurate, especially when one or more of the coefficients are piecewise constant.

Chapter 1

1 Introduction

The main objective of the research presented here has been to develop a new numerical method and assess its ability to produce accurate, robust, consistently convergent and bounded solutions for convection-reaction-diffusion equations (CRDEs).

Convection-reaction-diffusion equations have attracted a great deal of interest due to their use in modelling a broad range of natural and industrial processes. They can describe phenomena in chemistry [1], biology [2], semiconductors physics [3-4], ecology [5], finance [6-7], physics and other fields of science. Applications can range from simple predator-prey models in ecology [8] to complex chemical reactions in chemistry [9].

The CRDE, which accounts for the three processes of convection, reaction and diffusion, can be derived from conservation laws [9-10]. The conservation of the transported quantity ϕ is governed by

$$\frac{\partial \phi}{\partial t} = \nabla \cdot \left(D \nabla \phi \right) - \nabla \cdot \left(\mathbf{v} \phi \right) - K\phi + S \tag{1.1}$$

where the coefficients of diffusivity, D, convection, $\mathbf{v}$, reaction, K, and the source term, S, may all be dependent on space, time or ϕ. The modelling of problems with time-varying and/or non-linear coefficients is not considered here.

A broad range of numerical methods already exist that can be used to estimate solutions of Eq. (1.1) [11-12]; however, their accuracy, consistency and computational cost vary

significantly [10]; Research is still ongoing in this field and new methods and schemes continue to be developed for solving these equations [13]. The efficient solution of some types of problems (in particular, those in which the convection term dominates) remains a problem.

A novel numerical scheme, called LCM (Lumped-component Circuit Method), is developed in this thesis. While the method is designed for solving physical problems modelled by equations with piecewise-constant coefficients (e.g. problems concerning heat transfer through layers of different materials), it can also be used to solve more general problems. The basic method solves CRDEs with convection terms expressed in non-conservative form,

$$\frac{\partial \phi}{\partial t} = \nabla \cdot \left(D \nabla \phi \right) - \mathbf{v} \cdot \nabla \phi - K\phi + S \tag{1.2}$$

but could be used to solve equations of the form given in Eq. (1.1) by simply adjusting the reaction coefficient to

$$K^* = K + \nabla \cdot \mathbf{v} \tag{1.3}$$

The method depends on the fact that, under steady-state conditions, the equation for the voltage along a length of transmission line (TL), i.e. a pair of parallel conductors, can have the same form as the one-dimensional CRDE with constant coefficients. Similarly, a series of connected TL segments, each with different properties, can be an exact analogue for a one-dimensional steady-state convection-reaction-diffusion problem with piecewise-constant coefficients.

In one-dimensional LCM for steady-state problems, once the domain is divided into a series of nodes, simple lumped-component circuit elements (composed of resistors, conductances and current sources) are found that exactly model the sections of TL between each pair of adjacent nodes. The entire problem can then be modelled by these circuit elements connected in series. Once the boundary conditions are implemented, it is a straightforward matter to calculate the voltages at the nodes (i.e. the solution of the problem being solved). In this study, the method is assessed by comparing its solutions with those obtained from equivalent Finite Volume Method (FVM) models. The

implementations are validated using existing numerical and analytical solutions where available.

Chapter 2 provides an overview of some physical applications of CRDE models, the Finite Volume Method, the Transmission Line Method (TLM) which is similar in many respects to LCM, properties of numerical methods such as consistency of convergence, and the validation and comparison of such schemes.

Chapter 3 introduces the method for one-dimensional steady-state reaction-diffusion problems. It is applied to problems with piecewise-constant coefficients and to problems that are more general (i.e. ones with coefficients that vary continuously over space). Results are compared with those obtained using FVM schemes. In particular, the behaviour of both schemes is examined when modelling problems with discontinuities when the nodes are not positioned to align with those discontinuities.

In Chapter 4, LCM is extended to solve transient one-dimensional reaction-diffusion problems. Time stepping is implemented for both the LCM and FVM schemes using both a traditional first-order technique and using TLM. The sources and nature of errors in LCM solutions are partially investigated.

Chapter 5 extends the LCM method to allow modelling of convection-reaction-diffusion problems and the solution errors are investigated further.

In Chapter 6, it is shown how two-dimensional convection-reaction-diffusion problems can be solved using LCM by first representing them with a network of interconnected transmission lines (as in TLM).

.

Chapter 2

2 Literature Review

2.1 Convection-reaction-diffusion equation (CRDE) and its applications

The transport equation (Eq. (1.1)), derived from the conservation law [9, 14-15], expresses conservation of a property ϕ taking account of diffusive, convective [16-19] and reactive [20] processes and allowing for the existence of a source term. The solution may represent, for example, concentrations of charge carriers in semiconductors [4, 21], bacteria and molecules [22], pollutants in a river [23], numbers of animals [2] or plants in models of ecological systems, or the spread of disease during epidemics [24].

The diffusion equation with a convection and/or reaction term has been used to provide approximate models of a broad range of processes. The equation has been applied to a range of problems in chemistry [25], biology [26], ecology [5], electronics [27] and physics [28].

An example of the application of the diffusion equation in electronics is the modelling of heat conduction in high power semiconductor devices such as insulated gate bipolar transistors (IGBTs). These devices, consisting of distinct layers with different properties [27], handle high voltages and currents and require carefully designed systems to dissipate the heat generated within them. The modelling process allows designers to reduce the size of components and improve their performance.

An example of the application of CRDEs in electronics is in modelling the movement of charge carriers in semiconductors, sometimes through distinct layers within the devices

(giving piecewise-constant coefficients). In these devices, charge carriers (i.e. electrons and/or holes) diffuse over time, and can recombine (modelled using reaction terms) and drift under the influence of external electric fields (modelled using convection terms) [4].

Some bio-separation processes used in biochemistry can also be represented using convection-reaction-diffusion equations. One such process involves organic compounds diffusing and migrating through different gel layers under the influence of an electric field [29].

An example in ecology is the predator-prey interaction model. Population dynamics deal with changes in population size through the birth and death of species and predator-prey interactions. Commonly, these models represent a system in which two species compete for resources while one consumes the other. The number of prey, *U*, and predators, *V*, satisfy a system of two coupled equations

$$\frac{\partial U}{\partial t} = D_u \frac{\partial^2 U}{\partial x^2} + A\left(U\right) - B\left(U, V\right)$$

$$\frac{\partial V}{\partial t} = D_V \frac{\partial^2 V}{\partial x^2} - C\left(V\right) + B\left(U, V\right) \tag{2.1}$$

where the term $B(U,V)$ models the interaction between the prey and the predator, $A(U)$ controls the rate at which the prey numbers grow, and $C(V)$controls the rate at which the predators die. Both equations have the form of standard reaction-diffusion equations and, given correct initial and boundary conditions , can be solved to find the population numbers over time [8].

A convection-reaction-diffusion equation that is widely used in financial modelling for option pricing is the Black-Scholes equation [7].

$$\frac{\partial V}{\partial t} + \frac{1}{2}\sigma^2 x^2 \frac{\partial^2 V}{\partial x^2} + rx\frac{\partial V}{\partial x} - rV = 0 \tag{2.2}$$

It has the same form as Eq. (1.1) but with non-conservative convection and diffusion terms. It can be used to model variations in option prices over time and to find the optimum price at which an option should be sold [30].

Air pollution models are solved using Navier-Stokes equations, which require numerical coupling of a number of equations [31-32]. Such models often have time-dependent coefficients, non-linear reaction terms, and unknown velocity and diffusion coefficients, but can be simplified to the form of Eq. (1.1) by using estimated **v** and D and by assuming that reactions are first order [23].

Convection-reaction-diffusion equations are also used in modelling heat conduction (diffusion) [10, 19], heat conduction in extrusion processes (convection-diffusion) [33], pattern formation (reaction-diffusion) [34], drug delivery in the brain (convection-reaction-diffusion) [35], flood routing (convection-diffusion) [36], diffusion of packaging constituents into food products (diffusion) [37], oil reservoir engineering (convection-diffusion) [38], semiconductors (convection-reaction-diffusion) [3], the expansion of invasive organisms (convection-reaction-diffusion) [39] and a range of Computational Fluid Dynamics (convection-reaction-diffusion) problems [9].

In the vast majority of practical applications, exact analytical solutions are not available [40] and numerical methods are required to deal with non-linearities in material properties and complex problem geometries [41]. This thesis describes novel numerical techniques but makes use of analytical solutions, when available, for validation purposes.

2.2 Numerical solutions

A number of existing numerical schemes, such as the Finite Element Method (FEM) [42], the Method of Lines [43], Cellular Automata [44], the Finite Volume Method (FVM) [45] and the Transmission Line Modeling Method (TLM) [46], have been and are used to solve convection-reaction-diffusion equations. In this section, attention is focused on two specific methods which are (i) FVM, as it is widely used for the solution of the CRDE and is similar in some ways to LCM, and (ii) TLM, which, in common with the LCM method described in this thesis, is based on the use of a transmission line analogue for the problem being solved.

Three potential properties of numerical methods, conservativeness, boundedness and consistency, are desirable in practice. For a convection-diffusion problem with no source term and with boundaries such that no diffusant can enter or leave the domain,

the total quantity of diffusant within the domain should remain constant over time. If a numerical scheme is conservative, then, for such a problem, the total quantity of diffusant represented by the numerical solution should also remain constant from one time step to the next. It should be noted that this property may have no relevance if the equation being solved has a non-conservative convection term (since, then, if the convection velocity varies over space, conservation is not guaranteed).

In the solution of a convection-diffusion equation with no source term, for example, the values of the diffusing quantity, ϕ, at all points will be bounded by the values of ϕ at the boundaries. A numerical scheme is said to produce bounded solutions if the solution values also all lie between those values[9]. In other words, boundedness is a method's ability to produce physically meaningful solutions that do not cross the limits set at the boundaries on the solution. In practice, this is not the case for many numerical schemes when used to solve convection-diffusion problems in which the Peclet number, $P_e = hv/D$, where h is the node spacing, is greater than a prescribed value. For example, when using standard finite volume and finite difference methods with central difference approximations, solutions will not be bounded when $P_e > 2$ [9, 47]. Solutions produced by such schemes under those circumstances may exhibit non-physical "wiggles" – i.e. the values of the solution can oscillate from one node to the next and some can fall below or above the boundary values.

Consistency refers to the ability of a numerical scheme to produce solutions that will converge on the exact solution as the spatial and temporal discretizations are reduced to zero [9].

FVM has been used extensively to solve conservative convection-reaction-diffusion equations, largely because of its ability to enforce mass conservation [10, 45]. Numerous discretization schemes have been proposed to improve its boundedness, in particular for modelling convection-dominated problems and processes involving sharp gradients or discontinuities in the flow or material properties. Commonly used methods for approximating convection terms include the exponential [48-49], upwind-differencing, QUICK, power-law, hybrid differencing [9-10] and total variation diminishing (TVD) [50] schemes.

The similarity between the equation governing the voltage along a generalised transmission line and the convection-reaction-diffusion equation is the basis of an existing TLM scheme for solving convection-diffusion problems [51-52]. In that, it is similar to the LCM scheme presented below. The standard TLM method for diffusion, originally developed by Johns [46] and the basis of all TLM methods for diffusion and convection-diffusion, has specific advantages over many comparable schemes when solving transient problems as it is explicit and unconditionally stable (i.e. the solution will not be unstable, with values growing unbounded over time, no matter how long a time-step is used) [53-57].

Some details of both the FVM and TLM schemes are outlined below.

2.2.1 The Finite Volume Method (FVM)

FVM has been widely used for the solution of convection, reaction and diffusion equations, and it is particularly well-suited to solving the conservative form of the CRDE [9, 58]. This section provides a brief description of the method.

FVM starts by using the integral form of the CRDE (or "transport equation") to enforce conservation over each control volume (CV) comprising the model domain. See Figure 1 for an example of one possible domain discretization. The domain, in this case, is discretized using an orthogonal mesh and each CV is assigned a computational node (for example *P*) located at its centre. The integral form of the CRDE equation for a CV can be expressed in coordinate free form as

$$\underbrace{\int_{CV} \frac{\partial \phi}{\partial t} dx}_{Transient\_Term} = \underbrace{\int_{CV} \nabla \cdot \left(D \nabla \phi \right) dV}_{Diffusion\_Integral} - \underbrace{\int_{CV} \nabla \cdot \left(\mathbf{v} \phi \right) dV}_{Convection\_Integral} - \underbrace{\int_{CV} K \phi dV}_{Reaction\_Integral} + \underbrace{\int_{CV} S dV}_{Source\_Integral} \tag{2.3}$$

The Gauss divergence theorem provides an equivalent equation written in terms of surface fluxes

$$\int_{CV} \left(\nabla \cdot \mathbf{F} \right) d\mathbf{v} = \oint_{S} \left(\mathbf{F} \cdot \mathbf{n} \right) ds \tag{2.4}$$

where **F** is a flux vector which can be either the diffusive flux vector ($D\nabla\phi$) or the convective flux vector ($\mathbf{v}\phi$) and **n** is the unit outward vector normal to the surface *S* which bounds the CV.

The CV is bounded by *m* discrete faces so that the surface integral in Eq. (2.4) can be discretized using

$$\oint_S (\mathbf{F}\cdot\mathbf{n})\,ds = \sum_{f=1}^{m}\left(\int_f (\mathbf{F}\cdot\mathbf{n})\,ds\right) = \sum_{f=1}^{m} F_f S_f \tag{2.5}$$

where the index *f* identifies the CV faces, F_f is the value of *F* interpolated at the face centre from its value at neighbouring cell centres, and S_f is the distance between the two adjacent nodes. This involves two approximations: (i) **F** is assumed to be constant over the entire face, and, (ii), the interpolation generally relies on a first or second order approximation. The CV highlighted in Figure 1 has four faces. The value of **F** at the centre of the face labeled *e* can be, for example, calculated by interpolation from the values at two or more cell centres (e.g. those labeled P and E).

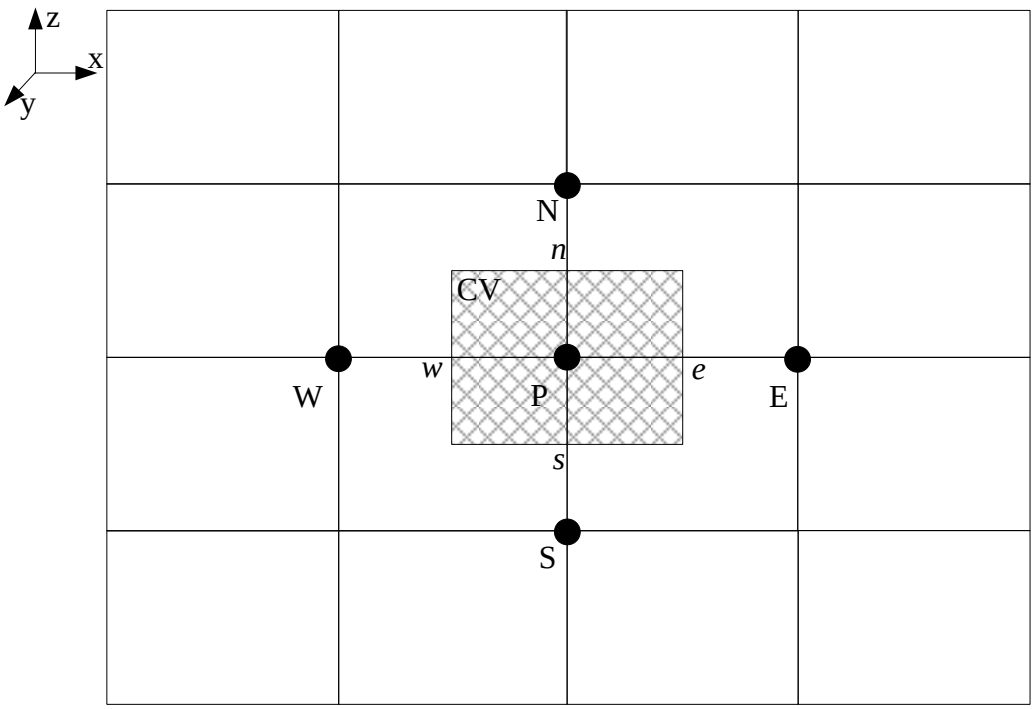

Figure 1: A control volume (CV) with a node denoted by capital letter P located at the centroid and flat faces denoted by lower case letters *e, w, n, s* to refer to the east, west north and south faces respectively.

Consider the application of this to the convection term in the integral form of the CRDE (Eq.(2.3)). The volume integral of the convection term can be represented as a discrete sum of convective fluxes

$$\int_{CV} (\nabla \cdot \mathbf{v}\phi) dv = \sum_{f=1}^{m} v_f \phi_f S_f \tag{2.6}$$

where ϕ_f is the value of the unknown scalar at the control volume face, and v_f (or $\mathbf{v}\cdot\mathbf{n}$) is the component of the velocity field perpendicular to the control volume face, both of which need to be approximated using interpolation. Several differencing schemes exist for this purpose and a number of them are examined here.

One that is commonly used is the central difference scheme (CD), which evaluates the value of ϕ at the CV faces using a linear interpolation of the form [10]:

$$\phi(\mathbf{q}) = \phi(\mathbf{p}) + \nabla\phi \cdot (\mathbf{q} - \mathbf{p}) \tag{2.7}$$

where $\mathbf{q}$ and $\mathbf{p}$ are vectors representing the positions of two points in space. For the domain shown in Figure 1, for face *e*, the value of ϕ can be approximated as

$$\phi_e = \alpha\phi_P + (1-\alpha)\phi_E \tag{2.8}$$

where $\alpha = \overline{eE}/\overline{PE}$, where $\overline{eE}$ and $\overline{PE}$ are the distances from face *e* to the node *E*, and from *P* to *E*, respectively. The CD scheme can be shown to be second-order accurate on uniform grids but its formal accuracy drops to first order on non-uniform grids. Like other second and higher-order schemes, CD produces unbounded solutions under certain conditions (for example, when the convection term dominates in the solution of the CRDE).

The Quadratic Upstream Interpolation for Convective Kinetics (QUICK) scheme approximates the value of ϕ_e using a quadratic interpolation which results in

$$\phi_e = \frac{3}{8}\phi_E + \frac{6}{8}\phi_P - \frac{1}{8}\phi_W \tag{2.9}$$

for a grid as shown in Figure 1 when the convection velocity at *e* is positive. This scheme is third-order accurate when used on orthogonal uniform grids but it produces

second-order solutions on non-uniform grids. QUICK cannot guarantee boundedness, but, when it does produce non-physical spurious “wiggles” in solutions, they tend to be significantly smaller than those produced by other discretization schemes with an order higher than first [9, 59].

The upwind differencing [10, 60], the hybrid differencing [15], the power-law [9], exponential [48] and total variation diminishing schemes (TVD) [50] are among others that are used. The upwind and hybrid schemes are formally first-order accurate. The properties of the power-law schemes are very similar to those of hybrid schemes, but they can provide more accurate solutions when used in one dimension [9]. Exponentially-fitted methods can be used to produce bounded solutions for convection-dominated and singularly-perturbed (i.e. where the diffusion coefficient is very small when compared with the other coefficients) problems [61-63]. In general, such methods are used for solving the non-conservative form of the CRDE equation (or problems in which the convection-velocity is constant over space).

Similarly, the volume integral of the diffusion integral, evaluated over the volume, is

$$\int_{CV} \nabla \cdot \left(D \nabla \phi \right) dV = \sum_{f=1}^{n} D_f S_f \left(\nabla \phi \right)_f \tag{2.10}$$

The solution, ϕ, can be estimated using linear interpolation (as in Eq.(2.7)) when calculating $\left(\nabla \phi\right)_f$. For the grid shown in Figure 1, the term $(\nabla \phi)_e$ can be approximated using a second order scheme:

$$\left(\nabla \phi\right)_e = \frac{\phi_E - \phi_P}{\overline{PE}} \tag{2.11}$$

It can be shown that assuming a quadratic variation (as in the QUICK scheme) produces the same approximation formula [9].

Reaction and source terms are treated in the same way by neglecting variations in the integrands over the CV giving

$$\int_{CV} \left(K \phi \right) dV = \overline{K} \phi_P \tag{2.12}$$

This approximation is again second order [15].

The time discretization involves integrating Eq.(2.3) over the time discretization step, giving

$$\int_t^{t+\Delta t}\left[\int_{CV}\frac{\partial\phi}{\partial t}dV\right]dt=\int_t^{t+\Delta t}\left[\int_{CV}\nabla\cdot\left(D\nabla\phi\right)dV-\int_{CV}\nabla\cdot\left(v\phi\right)dV-\int_{CV}K\phi dV+\int_{CV}SdV\right]dt \quad (2.13)$$

Various explicit and implicit time-stepping schemes exist that allow Eq.(2.13) to be converted into an algebraic equation once evaluation of the spatial integrals is completed. These schemes differ in terms of their accuracy and order of accuracy, stability and efficiency.

In this study, it is assumed that the CRDE coefficients are either known throughout space or only at the nodes and that they remain constant over time.

When using FVM to model problems with piecewise-constant coefficients, nodes are normally positioned at the discontinuities when possible [64]. If two discontinuities are close together (e.g. in a model of a physical system that includes a very thin layer of material) then at least one very small control volume may be required. When using conditionally-stable explicit time-stepping schemes, the maximum time step allowed is determined by the node spacing. The existence of one very small control volume may mean that a very short time step is required.

Alternatively, material properties can be averaged over control volumes. One way of doing this that is recommended specifically for problems with abrupt spatial variations in material properties and for models involving shock waves is the harmonic mean approximation [10]. The harmonic mean of the diffusion coefficient evaluated at face *e* for the mesh shown in Figure 1 is, for example,

$$D_e=\frac{2\overline{D}_E\overline{D}_P}{\overline{D}_E+\overline{D}_P} \quad (2.14)$$

here $\overline{D}$ for a given CV is the value of *D* averaged over that control volume.

In fluid dynamics experience has shown that using the conservative form of the transport equation produces more accurate and stable solutions when discontinuities

(caused, for example, by shocks) in the flow properties exist, than when the non-conservative form of the equation is used. Use of the non-conservative form can lead to instability and inaccuracy in solutions [65].

2.2.2 The Transmission Line Method (TLM)

It can be shown that the Telegrapher's Equation, which governs the voltage along a transmission line (e.g. a pair of parallel conductors) with distributed resistance, inductance and capacitance, is analogous to diffusion equations that describe a range of physical phenomena [53, 57, 66]. Because of this analogy, solving for the voltages along a transmission lines can provide a solution of a diffusion equation. TLM is a straightforward method for doing that.

To demonstrate this analogy, consider the 1D Telegrapher's Equation

$$\frac{1}{C_d}\frac{\partial V}{\partial t} = \frac{\partial}{\partial x}\left(\frac{1}{R_d}\frac{\partial V}{\partial x}\right) - \frac{L_d}{R_d}\frac{\partial^2 V}{\partial t^2} \tag{2.15}$$

It is analogous to the diffusion equation of the form

$$\frac{\partial \phi}{\partial t} = \frac{\partial}{\partial x}\left(D\frac{\partial \phi}{\partial x}\right) \tag{2.16}$$

when

$$D = \frac{1}{R_d},\ L_d = 0 \text{ and } C_d = 1 \tag{2.17}$$

In order to model a transmission line using TLM, the TL must have a non-zero distributed inductance (L_d). As a result of this inductance, the equation being solved has a wave term (the last term on the right in Eq. (2.15)) that, when modelling diffusion, causes errors in transient solutions. The distributed inductance required in the TL being modelled depends on Δt, the time step length, and Δx, the node spacing. It can be shown that the wave term is then proportional to $\Delta t^2/\Delta x^2$ and so using a small enough time step can ensure that these errors are negligible [67-68].

2.2.2.1 Propagation of a signal along a transmission line

A transmission line, in its simplest form, can be characterized by its distributed inductance L_d, resistance, R_d, and capacitance, C_d. The line impedance, Z, at any point on the line is

$$Z = \sqrt{\frac{L_d}{C_d}} \tag{2.18}$$

This property is important in TLM as will be shown below.

If the voltage at a point along a transmission line is changed (e.g. by being connected to a voltage source), then the voltage along the entire line will not change instantaneously. Instead, voltage waves (and accompanying current waves) will travel along the TL at a finite speed. This speed, the propagation velocity, is important in TLM and is given by

$$u = \sqrt{\frac{1}{L_d C_d}} \tag{2.19}$$

When modelling diffusion problems, the distributed capacitance of the TL, C_d, can be set equal to one as mentioned above. When solving a heat conduction equation of the form

$$\rho c \frac{\partial \phi}{\partial t} = \frac{\partial}{\partial x}\left(D \frac{\partial \phi}{\partial x} \right) \tag{2.20}$$

however, the distributed capacitance must be set to

$$C_d = \rho c \tag{2.21}$$

as is clear from comparing Equations (2.15) and. (2.20)

In TLM, the propagation velocity along any TL section linking adjacent nodes must equal $\Delta x/\Delta t$. This ensures that a voltage wave leaving a node at one time step will arrive at an adjacent node at the next time step. Therefore, in TLM

$$u = \frac{\Delta x}{\Delta t} \tag{2.22}$$

Combining Equations (2.22) and (2.19) gives

$$L_d = \frac{1}{C_d}\frac{\Delta t^2}{\Delta x^2}$$

for a given section of transmission line. In the case where C_d is one, the actual equation solved is therefore

$$\frac{\partial \phi}{\partial t} = \frac{\partial}{\partial x}\left(D\frac{\partial \phi}{\partial x}\right) - D\frac{\Delta t^2}{\Delta x^2}\frac{\partial^2 \phi}{\partial t^2} \tag{2.23}$$

due to wave term in Eq. (2.15). If C_d is constant over the length of a section of TL between two nodes Δx apart, then combining Equations (2.18), (2.19) and (2.22) gives the impedance as,

$$Z = \frac{\Delta t}{C_d \Delta x} \tag{2.24}$$

2.2.2.2 Implementing TLM

TLM models can be separated into two main types [46]; the first type uses lossy transmission lines (i.e. TLs with non-zero distributed resistance) to solve diffusion equations, while the second type uses lossless TLs (i.e. TLs with zero resistance) to solve wave equations. The Lossless TLM method is well established and has been used for a wide variety of wave modelling applications [21, 53, 69]. Since the subject of this investigation is related to diffusion modelling, attention is focussed here on lossy TLM.

In TLM, the transmission line to be modelled is divided into sections, each section linking a pair of adjacent nodes. These lossy TL sections are modelled as segments of uniform (i.e. with L_d and C_d both constant along their lengths) lossless TL segments linked by lumped resistors. There are two possible configurations referred to as the "link-line" configuration and the "link-resistor" configuration. In this section, only the link-resistor configuration is explained. It is illustrated in Figure 2. Each TL section is modelled using two TL segments linked by two lumped resistors. The alternative link-line configuration, and the differences between the two, is discussed briefly below.

The lumped resistors in any section represent the distributed resistance of the section of TL being modelled. If R_d is constant between adjacent nodes, then each resistor is simply

$$R = R_d \Delta x / 2 \tag{2.25}$$

The impedance of each lossless TL segment, Z, is given by (2.24).

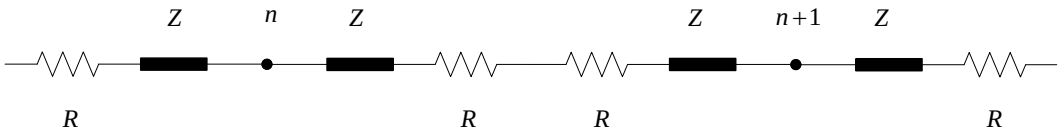

Figure 2: This shows how the TL section between two nodes is modelled by two lossless TL segments, one connected to each node (when using a link-resistor configuration), linked by two lumped resistors.

Implementing the lossy TLM method involves keeping track of Dirac voltage pulses (i.e. voltage waveforms that, at any point in time, are nonzero at one point in space and zero elsewhere) that leave nodes at each time step. Part of any pulse returns back to the node from which it originated, while the rest of the pulse travels on to the adjacent node. All pulses arrive at nodes at the next time step. This synchronization ensures that the method is straightforward to implement.

2.2.2.3 Implementation of lossy link-resistor TLM

The iterative TLM process can be understood by first considering the incident voltages (Dirac voltage pulses) arriving at a node n at a time step k, one arriving from the left, Vil_n^k, and one arriving from the right, Vir_n^k, as shown in Figure 3(a). The two incident pulses raise the voltage on the TL at the node to V_n^k, the node voltage, which represents the solution of the problem being modelled at that node. The difference between the incident voltages and the node voltage causes two voltage pulses to be scattered from the node at the same instant, one to the left, Vsl_n^k, and one to the right, Vsr_n^k. The scattered voltage in a given direction is simply the difference between the node voltage and the incident voltage from that direction. The scattered voltages travel along the TL segments towards the neighbouring nodes.

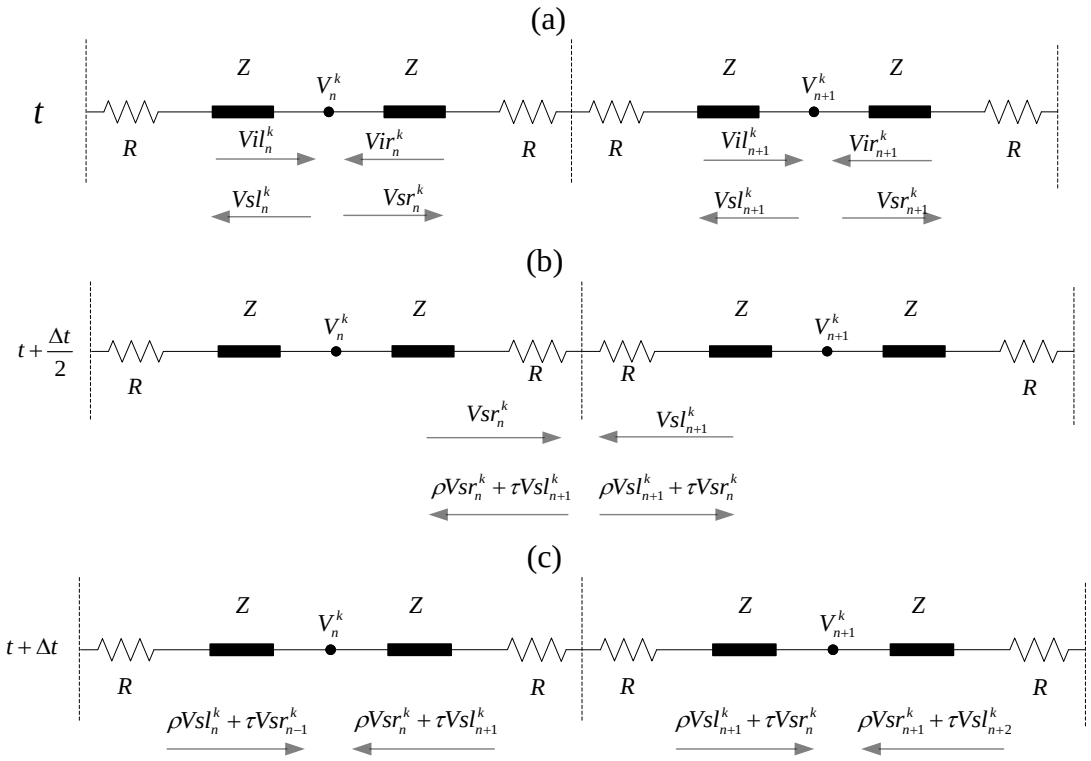

Figure 3: Two nodes in a TLM model (with link-resistor configuration) with incident pulses, *Vil* and *Vir*, and scattered pulses *Vsl* and *Vsr* at time *t* (corresponding to time step *k*) indicated, (a), *Vsl* and *Vsr* pulses arriving at an impedance discontinuity at $t + \Delta t/2$, (b), and the resulting V*il* and *Vir* at time $t + \Delta t$ (i.e. time step k+1), (c).

In a link-resistor configuration (as in Figure 3), one half time step (i.e. $\Delta t/2$) after leaving nodes, the scattered voltage pulses arrive at impedance discontinuities (i.e. differences between the TL impedances and the resistance of the lumped resistors). As a result, a fraction, ρ, of each pulse is reflected back towards the node from which it originated, while the remaining fraction, τ, is transmitted onwards towards the adjacent node (as shown in Figure 3(b)).

A further half time step later, these pulses form the new incident pulses arriving at the nodes (as shown in Figure 3(c)) and the process repeats itself in this manner. At any time step, the node voltages represent the solution of the problem being solved.

The voltage at node *n* at time step *k* can be calculated from the incident pulses. For the simple diffusion model illustrated in Figure 3,

$$V_n^k = Vil_n^k + Vir_n^k \tag{2.26}$$

The scattered voltages are simply

$$Vsl_n^k = V_n^k - Vil_n^k \tag{2.27}$$

$$Vsr_n^k = V_n^k - Vir_n^k \tag{2.28}$$

Following the scattering process at node *n* shown in Figure 3(a), the scattered voltages Vsl_n^k (voltage scattered to the left) and Vsr_n^k (voltage scattered to the right) arrive at the discontinuity caused by the resistor after $\Delta t/2$. Part of the scattered pulse is transmitted and part of it is reflected. The resulting transmitted and reflected pulses from adjacent nodes form a new pulse that travels towards the node. After travelling for a further $\Delta t/2$, the new incident pulses arrive at the node *n* at the next time step $k+1$. Their voltages are

$$Vil_n^{k+1} = \rho Vsl_n^k + \tau Vsr_{n-1}^k \tag{2.29}$$

and

$$Vir_n^{k+1} = \rho Vsr_n^k + \tau Vsl_{n+1}^k \tag{2.30}$$

where, again, for the diffusion model shown in Figure 3,

$$\tau = \frac{Z}{Z+R} \tag{2.31}$$

is the transmission coefficient and

$$\rho = \frac{R}{(R+Z)} \tag{2.32}$$

is the reflection coefficient. The derivation of equivalent formulae for a more general model is presented in Appendix A. Equations (A.15) and (A.16), for constant *Z*, simplify to Equations (2.31) and (2.32)). In Eq. (2.29), the pulse incident at node *n* from the left at time step $k+1$ is the sum of that part of the pulse scattered from node $n-1$ at time step *k* that has transmitted towards node *n*, and that part of the pulse scattered from node *n* that was reflected.

To summarise, the lossy link-resistor TLM method can be used to solve the second order Telegrapher's equation, which is analogous to the diffusion equation. The method starts with pulses incident at the nodes at any time step, selected to produce the correct

initial node voltages. Voltage pulses scatter from the nodes in all directions, and $\Delta t/2$ later, arrive at impedance discontinuities caused by the resistors. Parts of the scattered voltage pulses are reflected and parts are transmitted. From these, the new incident voltage pulses can be calculated and the process repeated.

At the first time step, the incident pulses at each node are set equal to half the required node voltage (i.e. to half the value of the initial solution at each node). Unlike with other numerical methods, there is an error associated with this initialisation process, referred to as the "inconsistent first time step error" that arises from the fact that the initial conditions prescribed are not consistent with the TLM scheme [70]. The inconsistency in the first time step becomes evident when the TLM solution for the diffusion equation for a single instantaneous injection is compared with the exact solution (pure diffusion of a single injection of diffusant at a single point in space and time results in a Gaussian-shaped distribution of diffusant concentration that spreads over time) [71]. The TLM solution is approximately Gaussian in shape, however, the diffusant does not spread initially at the correct rate. This error only persists in the earlier part of the transient, however, it becomes insignificant as the modelling period extends. An approach proposed by Enders, Pulko and Stubbs [70] can improve the transient solution in the earlier part of the model if the error that arises due to this inconsistency is significant. Also, Kennedy and O'Connor [71] have shown that the accuracy of the solution can be improved under certain circumstances by adjusting the transmission coefficient at a single time step.

Since TLM uses a TL with non-zero L_d to model diffusion, Eq.(2.15), which governs the voltage along the TL, includes a wave term, and there are resulting errors in TLM solutions. This error can be minimized by making the inductance very small (it is proportional to $\Delta t^2/\Delta x^2$), [67-68], but cannot be eliminated completely.

Only the link-resistor configuration is detailed above. The alternative link-line configuration can also be used when solving diffusion problems in lossy TLM. The two are similar but, in the link-line configuration, the nodes are positioned between the pairs of resistors [54, 57]. Two-dimensional link-line models can be marginally more efficient than equivalent link-resistor models, but not when the parameters vary over space. Only link-resistor models are implemented in the work presented here.

2.2.2.4 2D link-resistor TLM

The lossy TLM method can be easily extended to model diffusion in two dimensions. The problem being solved is approximated using a network of interlinked lossy transmission lines. These are then modelled, as in one dimension, using lengths of lossless TL in series with lumped resistors. In a link-resistor formulation, the transmission lines intersect at the nodes in both *x* and *y* directions, as shown in Figure 4. At a node *n,m*, an incident impulse sees three transmission lines in parallel.

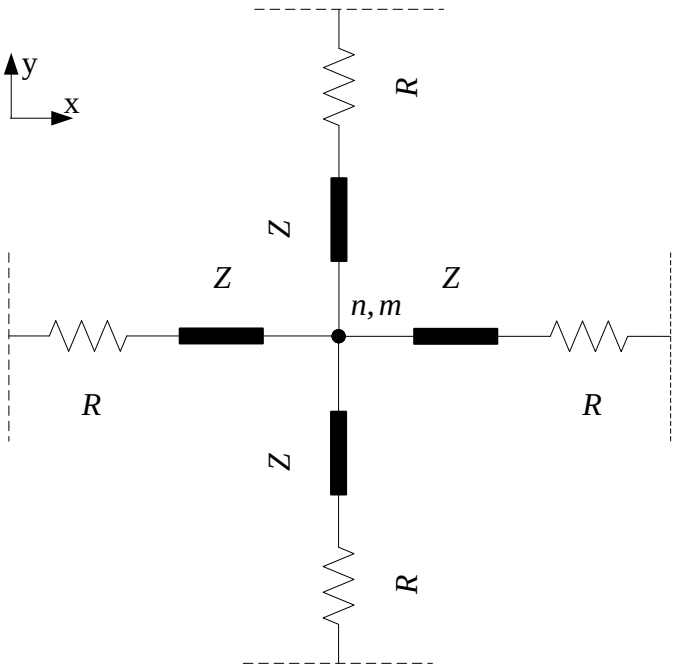

Figure 4: 2D link-resistor configuration.

In 2D, there are four pulses arriving simultaneously at any node *n,m* at each time step, from both *x* and *y* directions. The pulse scattered in any direction is the difference between the node voltage and the incident voltage from that direction, as in one dimension. The reflection and transmission of pulses at each impedance discontinuity, after a time interval of $\Delta t/2$, and the calculation of the reflection coefficient, ρ, and transmission coefficient, τ, are also all similar to what they are in 1D.

2.2.3 TLM methods for convection-reaction-diffusion

TLM has been widely used to model diffusion, however, its application to convection-diffusion (or "drift-" or "advection-diffusion") and reaction-diffusion (or "diffusion with recombination") problems has been limited [4, 51, 53, 72-73]. For recombination,

Gui and de Cogan [72] proposed a method in which recombination is modelled using a TL with both distributed series resistance, R_d, and distributed shunt conductance (i.e. conductance between the two parallel conductors in the transmission line), G_d. The voltage along such a TL is governed by

$$\left(R_d C_d + L_d G_d\right)\frac{\partial V}{\partial t} = \frac{\partial^2 V}{\partial x^2} - R_d G_d V + L_d C_d \frac{\partial^2 V}{\partial t^2} \tag{2.33}$$

where the $R_d G_d V$ term is equivalent to the reaction term in the one-dimensional form of Eq. (1.1). The diffusion effect was modelled using two different approaches; the first approach modelled the diffusion using series resistance and shunt capacitance, C_d, while the second used series inductance and shunt resistance. Both approaches produced identical solutions under circumstances examined [72].

One of the earliest techniques proposed for solving convection-reaction-diffusion problems was that of de Cogan and Henini [21]. In their method, the convection and diffusion processes are treated independently. The entire node voltage distribution is moved by one node (i.e. a distance of Δx) in the direction of the velocity at regular intervals, the interval being chosen such that, on average, the distribution is transported at the convection velocity, **v**. Meanwhile, at each iteration, the diffusion process is allowed to proceed as normal. This approach is limited in terms of its accuracy and its applicability.

Al-Zeben and Saleh [4] proposed an alternative method in which a voltage-controlled current generator is added at each node to a standard TLM diffusion model with shunt conductance. The additional current added at each node is $I_n = g_n \Delta V_x$ (where g_n is a constant and ΔV_x is given as $V_x = (V_{n+1} + V_{n-1})/2$). They show that, for $L_d << R_d$, the resulting circuit models a TL with the governing equation

$$R_d C_d \frac{\partial V}{\partial t} = \frac{\partial^2 V}{\partial x^2} + g_n R_d \frac{\partial V}{\partial x} + G_d R_d V$$

which is analogous to the CRDE. The results presented show accurate solutions for the limited cases examined.

Kennedy and O'Connor [51-52] proposed the alternative "varied impedance" method, in which convection-diffusion problems are solved using TLs whose properties vary exponentially. The circuits modelled require no active components and are therefore unconditionally stable. The method produces highly accurate solutions for steady-state convection-diffusion equations, and can produce exact solutions when $\mathbf{v}(x)$ and $D(x)$ are known over the domain. The method can be extended to solve the conservative form of the convection-diffusion equation, but it then requires active current sources

Although, in their second paper on the method [52] they showed that steady-state solutions can be calculated directly, in their first paper, the steady-state solutions were found by running the transient solution to steady-state. As with standard TLM for diffusion [51], they found that there is an optimum time-step length that minimizes the number of time steps required to reach a steady-state solution. In general, the number of steps can be minimized by increasing the size of the time step, however, in TLM this leads to increased wave-like behaviour that takes time to settle down. Further unpublished work has shown that the varied impedance method can be modified to produce solutions with 4^{th}-order accuracy for problems with coefficients that vary over space, and that steady-state solutions can be calculated by more efficient means than those published.

Kennedy and O'Connor developed a second TLM method, called the convection-line (CL) method [74], in which a lossless transmission line is coupled with a lossy one to model the convection process. The lossless transmission line has a notional "diode" at each node that allows voltage pulses (either positive or negative) to pass only in one direction. The results published suggest that the CL method can be more accurate than the varied impedance TLM method, but the nature of the scheme means that it is difficult to adapt it to solve more general one-dimensional problems and problems in two and three dimensions.

The scheme introduced in the next chapter is related to the varied impedance scheme but includes the modelling of reaction terms and has been specifically developed for solving problems with piecewise-constant coefficients.

2.3 Errors and method validation

There are two main types of errors in solutions obtained using numerical methods, truncation and round-off errors.

Round-off errors arise in digital computers due to the use of finite arithmetic (i.e. because numbers such as π, 1/3 or e cannot be stored in a finite number of bits in a computer). Even numbers such as 0.1 must be rounded-off when stored in floating-point binary form. The difference between the value to be stored and the value that is actually stored is the round-off error. These errors are essentially random in nature [10] and small, but can accumulate, for example, in calculations that require many steps, leading to significant errors in solutions.

Truncation errors arise from the use of approximations. The size of a truncation error depends on the size of the discretization used in the approximation. The order of the error for a particular approximation specifies how the truncation errors are related to the discretization. The orders of the errors in the approximations used in solving differential equations (e.g. using FVM), and the resulting errors in the solutions obtained using those approximations, can be found using the Taylor series. The orders of the truncation errors may be different for different terms in an approximation of a CRDE. The order of errors in the solution of the overall scheme will equal that of the lowest order approximation used.

The term discretization error is used here to describe the global error that is dependent on the spatial and temporal discretization, while the term truncation error is used to refer to the error that is defined by the truncated Taylor series for the differencing scheme used. On a uniform grid, the discretization and truncation errors exhibit similar order of accuracy, but for non-uniform grids, they often do not correspond, and their order is dependent on the uniformity of the grid [75-76]. For example, a non-uniform grid with a single step change in the grid size will generally exhibit a discretization error with an order higher than the truncation error.

The order of accuracy of a method is important as it indicates how quickly the method will converge on the exact solution as the discretization (i.e. the node spacing or time step length) is decreased. Higher order methods are generally more accurate for a given

level of discretization, but, in some cases, the higher computational cost of implementing such schemes makes them less efficient than lower order methods.

Implementations of numerical schemes must be validated and that can be done by comparing results with analytical or existing (and previously validated) numerical solutions. Validation may also involve checking that the implemented method acts as expected, e.g. that the order of the discretization errors is as expected.

To calculate exactly the error in a numerical solution, it is necessary to have the corresponding exact solution. Exact solutions are, however, often not available except in very limited cases. In some of the testing presented here, the method of manufactured solutions is used to ensure that exact solutions are available, and, in other testing, errors are estimated by comparing numerical solutions with more accurate benchmark numerical solutions. Details are given below.

2.3.1 The method of manufactured solutions (MMS)

The method of manufactured solutions (MMS) [77] can be used to efficiently formulate problems with known solutions. The approach involves choosing a desired solution and then working backwards to find the parameters for the differential equation that has that solution. To illustrate this, consider a steady-state, non-linear, non-conservative convection-reaction-diffusion problem in one dimension of the form

$$\frac{\partial}{\partial x}\left(D(\phi)\frac{\partial \phi}{\partial x}\right) - v(\phi)\frac{\partial \phi}{\partial x} - K\phi + S = 0 \tag{2.34}$$

(i.e. with a non-conservative convection term) where

$$D(\phi) = \phi^3,\ v(\phi) = \phi \text{ and } K = 4 \tag{2.35}$$

If the desired solution is

$$\phi(x) = x^2 + 1 \tag{2.36}$$

then Eq.(2.34) can be rewritten as

$$\frac{\partial}{\partial x}\left(\left(x^2+1\right)^3\frac{\partial\left(x^2+1\right)}{\partial x}\right)-\left(x^2+1\right)\frac{\partial\left(x^2+1\right)}{\partial x}-4\left(x^2+1\right)+S=0 \qquad (2.37)$$

This allows $S(x)$ to be found. The boundary conditions must simply be consistent with the desired solution. This approach can provide exact solutions that can be used for validating numerical methods, and is applicable even when exact solutions are difficult to find for specified problems. The approach cannot be used when the coefficients are discontinuous. It is also limited in that one coefficient cannot be varied without changing another.

2.3.2 Order of convergence

With a consistent scheme, the numerical solution for any given problem will converge towards the exact solution for that problem as any solution discretizations, e.g. the node spacing and/or time step length, approach zero. For a steady-state CRDE problem, the systematic error in any given solution value (i.e. the error due to the scheme and not including round-off errors), calculated using a consistent scheme, is dependent on the node spacing, h [78-79]. A solution value estimated with node spacing h can be written as

$$V_h = V_{exact} + c_1 h^p + c_2 h^{p+1} + c_3 h^{p+2} + \ldots \qquad (2.38)$$

where V_{exact} is the corresponding exact solution value. As h approaches zero, this becomes

$$\lim_{h\to 0} V_h = V_{exact} + c_1 h^p$$

The value of p will depend on the nature of the approximations inherent in the numerical scheme and determines the order of accuracy of the scheme. For example, if $p = 2$ for a given scheme, then it is said to be second-order accurate. The order of the accuracy determines the rate at which a numerical solution will converge on the exact solution as the node spacing is decreased, and so, for example, a second-order scheme is generally preferable to a first-order scheme.

The values of c in Eq. (2.38) will depend on the problem coefficients and solution. They will also depend on h. In general, they will change monotonically as h is decreased, approaching constant values as h approaches zero. As a result, the error in any solution value will, as h approaches zero, always reduce when h is reduced in a manner that is consistent with the order of the scheme. For example, with a second-order accurate scheme, the error in any solution value will reduce by a factor of approximately four when the node spacing is halved.

For some types of problems, numerical schemes may not be "consistently convergent", i.e. the error at a point in the solution may not always decrease as h is decreased, even as h approaches zero, or may decrease as h is decreased, but not in a way that is consistent with the order of the method.

The value of p for a given scheme can be estimated empirically in a number of ways, giving an estimated order of convergence (EOC). If an exact solution is known then it can be estimated as [80]

$$EOC = \frac{\ln\left(e_h / e_{h/2}\right)}{\ln 2} \tag{2.39}$$

where e_h is the error in the solution obtained using a step size h [81]. When an exact solution is not available, the EOC can be estimated using

$$EOC = \frac{\ln\left(\left(V_h - V_{h/2}\right)/\left(V_{h/2} - V_{h/4}\right)\right)}{\ln 2} \tag{2.40}$$

where V_h , $V_{h/2}$ and $V_{h/4}$ are corresponding solution values estimated using step sizes of h, $h/2$ and $h/4$, respectively [80].

If the results used to estimate the order of convergence are obtained using a scheme that is consistently convergent for the problem tested, then, as h approaches zero, and assuming that round-off errors in the results are insignificant, the estimated order of convergence should approach the order of accuracy of the scheme (e.g. for a second-order scheme, the value of EOC should approach two as h is decreased).

2.3.3 Benchmark numerical solutions

A benchmark numerical solution is simply a highly accurate numerical approximation that can be used to estimate errors in less accurate estimates, and to compare the accuracy of different methods. They can be used in situations where exact solutions are not available and where the method of manufactured solutions is not applicable.

In general, when numerically solving differential equations that are dependent on both space and time, as the size of the spatial and temporal discretizations approach zero, the solution approaches the exact solution. The computational cost of producing very accurate benchmark solutions can be prohibitively high, especially when solving over both space and time. In addition, small discretizations can lead to significant accumulated round-off errors in the solutions obtained. The use of Richardson extrapolation can allow accurate solutions, which are not significantly affected by round-off errors, to be found in an efficient manner.

2.3.3.1 Richardson extrapolation

Richardson extrapolation can be used to find improved estimations of the solutions of CRDEs [78] for both steady-state [82] and transient problems [83-84]. It can be used to calculate highly accurate solutions from less accurate ones [85].

For Richardson extrapolation to produce accurate results, the solution errors must be dependent in a known and predictable way on the discretization used, i.e. the order of the errors must be known and the errors must reduce in a consistent manner as the discretization is reduced (i.e. the errors must "converge consistently") [79]. An extrapolation can be made from two solutions (each calculated with a different discretization), but higher accuracy can be achieved if three or more solutions are used.

The extrapolations performed below are for second-order methods from which an estimate obtained with a step size of h, V_h, is assumed to have an error $c_1h^2 + c_2h^3 + c_3h^4 + \cdots$ so that

$$V_h = V_{exact} + c_1h^2 + c_2h^3 + c_3h^4 + \cdots \tag{2.41}$$

Similarly, a corresponding estimate obtained with a step size of $h/2$ and $h/4$ will be

$$V_{h/2} = V_{exact} + c_1 \frac{h^2}{4} + c_2 \frac{h^3}{8} + c_3 \frac{h^4}{16} + \cdots \tag{2.42}$$

$$V_{h/4} = V_{exact} + c_1 \frac{h^2}{16} + c_2 \frac{h^3}{64} + c_3 \frac{h^4}{256} + \cdots \tag{2.43}$$

Ignoring the fourth term and onward on the right hand side of these equations, Eq. (2.41) can be approximated as

$$c_1 h^2 \approx V_h - V_{exact} - c_2 h^3 \tag{2.44}$$

Using this to replace the $c_1 h^2$ term in Equations (2.42) and (2.43) gives

$$8V_{h/2} \approx 6V_{exact} + 2V_h - c_2 h^3 \tag{2.45}$$

$$64V_{h/4} \approx 60V_{exact} + 4V_h - 3c_2 h \tag{2.46}$$

Combining these gives

$$V_{exact} \approx \frac{32V_{h/4} - 12V_{h/2} + V_h}{21}$$

This formula is used below for calculating benchmark numerical solutions.

2.3.4 Error calculation and estimation

Errors in numerical solutions can be presented as either relative or absolute. For relative errors, the difference between the numerical and exact solution is divided by the exact solution. This may be desirable in situations where the solution values change significantly in size over the domain or between tests. The relative error in the numerical solution value at node *n* at time step *k*, i.e. in ϕ_n^k is

$${}_k E_n^{\mathrm{Rel}} = \left| \frac{\phi_n^k - \phi_{exact,n}^k}{\phi_{exact,n}^k} \right| \tag{2.47}$$

where $\phi_{exact,n}^k$ is the exact solution at the corresponding point in space and time.

The absolute error on the other hand is simply the difference between the numerical and exact solutions. The maximum absolute error is defined here, at time step *k*, as

$$\left\| \phi^k - \phi^k_{exact} \right\|_\infty = \max \left| \phi^k_n - \phi^k_{exact,n} \right|, \quad n = 1 \text{ to } N \tag{2.48}$$

where the exact solution is not available, a benchmark solution may be used instead of ϕ^k_{exact} when calculating errors.

2.3.5 Implicit and explicit time-stepping schemes

Many of the transient solutions presented below have been produced using the standard first order explicit FTCS time-stepping scheme. The time-stepping errors, for a given temporal discretization, are very similar for the different schemes tested here, no matter what time-stepping method is used. There is therefore little to be learned from testing the different schemes with different time-stepping methods.

Time-stepping schemes may be unstable, causing the solution values to grow in an unbounded manner over time. Stability may be dependent on the problem coefficients and the time-step length, Δt. An unconditionally stable method is one that is stable for any value of Δt, while a conditionally stable method is one that is only stable if Δt is below a certain value, normally dependent on the problem coefficients.

The main advantage of the FTCS scheme is its simplicity. Its low accuracy when compared with that of, for example, the second order implicit Crank-Nicolson scheme is not a significant disadvantage in most of the tests presented here because a short time step can be used without causing excessively long model run-times. It is conditionally stable, becoming unstable if

$$\Delta t > \frac{h^2}{2D} \tag{2.49}$$

but, again, that is not a problem in most of the tests presented here in which the time step is chosen to ensure that time-stepping errors are negligible.

2.3.6 Boundedness and conservativeness of numerical schemes for convection-diffusion

Under steady-state conditions, the values of the exact solution of a convection-diffusion problem, with no source term, will be, at any point in space, within the upper and lower limits of the solution values at the boundary. For example, in a one-dimensional problem, if the solution value is 10 at one boundary and 100 at the other, then the exact solution at all points between will be bounded by the values 10 and 100. A “bounded” numerical scheme for convection-diffusion is one that always produces solutions that are bounded in this way (i.e. that lie between the boundary-value limits).

The exact solution of a one-dimensional steady-state convection- diffusion equation will also either monotonically increase or monotonically decrease over space, depending on the boundary conditions. The solutions from bounded numerical schemes also have this quality. In contrast, solutions from unbounded schemes may exhibit unphysical “wiggles” [9] i.e. solution values may go up and down over space, as well as falling outside the boundary-value limits.

If the quantity of diffusant represented by an exact solution does not change over time (i.e. the diffusant may diffuse and be convected over space, but none is added or removed from the domain) then the problem is conservative. A “conservative” numerical scheme is one that, for a conservative problem, produces a solution that represents a quantity of diffusant that does not change over time[9].

Chapter 3

3 Steady-state one-dimensional reaction diffusion

3.1 Introduction

This chapter examines and extends a novel numerical method originally developed by Dr. Kennedy at Dublin City University for solving steady-state one-dimensional reaction-diffusion equations (RDEs) with piecewise-constant coefficients. This work has not been published to date. The method is described here and extended for modelling more general reaction-diffusion problems. Tests are presented and results are compared with equivalent ones obtained from finite volume schemes.

As with the TLM methods presented in previous sections, this scheme, called here the lumped-component circuit method (LCM), is based on the similarity of the equation for the steady-state voltage along a general transmission line

$$\frac{\partial}{\partial x}\left(\frac{1}{R_d}\frac{\partial V}{\partial x}\right)-\frac{\partial}{\partial x}\left(\frac{1}{R_d}\right)\frac{\partial V}{\partial x}-G_d V+I_d=0 \tag{3.1}$$

(where C_d, R_d, G_d and I_d are the distributed capacitance, resistance, inductance and source current, respectively) and convection- reaction-diffusion equations of the form

$$\frac{\partial}{\partial x}\left(D\frac{\partial \phi}{\partial x}\right)-v\frac{\partial \phi}{\partial x}-K\phi+S=0 \tag{3.2}$$

As will be shown below, the scheme involves solving a set of equations for the voltages at a series of nodes in a circuit. These equations are similar in form to those for the finite volume method. It is partly for that reason that comparison is made between the two techniques. FVM is also suited to the solution of problems with discontinuous coefficients as examined here [64, 86].

It should be noted that the purpose of the comparison made here between LCM and some FVM schemes is simply to establish if the novel method has advantages over such schemes. Comparison could be made with other methods, such as finite element schemes, and other finite volume implementations, but that is beyond the scope of this work.

Unlike FVM, LCM can solve the steady-state RDEs with piecewise-constant coefficients exactly. In more general situations, where the coefficients K, D, and S are only known at the nodes, its performance is dependent on the nature of problem being solved. In situations where one or more of the coefficients varies in a piecewise-constant fashion, but the others are only known at the nodes (e.g. a problem in which one or more of the coefficients is a function of the solution, but others are piecewise-constant), it is shown below that LCM can produce significantly more accurate results than the standard FVM schemes tested here.

In Chapter 4, this scheme is further extended for modelling transient reaction-diffusion problems. The method is adapted for modelling convection-reaction-diffusion in Chapter 5 and for solving 2D problems in Chapter 6.

3.2 The Lumped-component Circuit Method

As mentioned above, a non-uniform transmission line can act as an analogue for a one-dimensional reaction-diffusion problem. The lumped-component circuit method requires such a non-uniform TL to be modelled using a series of uniform TL segments (i.e. segments with G_d, R_d and I_d, all constant along their lengths). The distributed capacitance, C_d, and inductance, L_d, of the TL segments can be set to zero, because, under steady conditions, the current entering a capacitor and the voltage across an inductor are both zero.

As with other numerical methods, LCM calculates the solution values (i.e. values of the voltage along the TL being modelled) at discrete nodes in space. In LCM, each pair of adjacent nodes is linked by one or more uniform TL segments. In this context, a uniform TL segment can be treated as a "black box" in that only the relationship between the input and output (I/O) voltages and currents (indicated in Figure 5) is of interest (since the voltage between nodes is not being calculated). As will be shown in the next section, this relationship can be found through a straightforward analysis of a uniform segment.

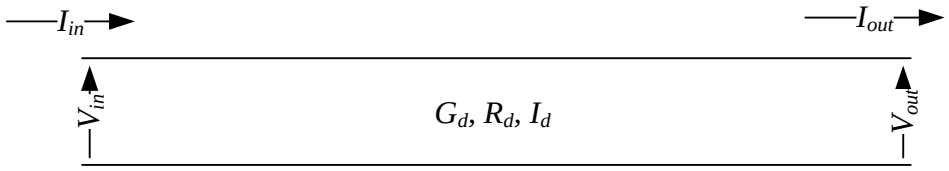

Figure 5: A segment of uniform transmission line with distributed properties and input and output voltages and currents indicated. Note that the "input" and "output" ends of the section have been assigned arbitrarily.

It will also be shown in the next section that a lumped-component circuit of the form given in Figure 6, can, in terms of inputs and outputs, and under steady-state conditions, act in the same way as a section of TL (whether uniform or non-uniform). A relationship can be easily established between the outputs and the inputs for this equivalent circuit element. By comparing this relationship with the equivalent one for the TL section being modelled, it is possible to determine what lumped-component parameters (i.e. what values of the resistance R, conductances G_l and G_r, and currents I_l and I_r) will produce a lumped-component circuit element that models a TL section exactly. Calculation of the node voltages along a series of such elements is more straightforward than calculating the node voltages when the nodes are linked by TL segments. This also opens up other possibilities that will be discussed elsewhere in this thesis.

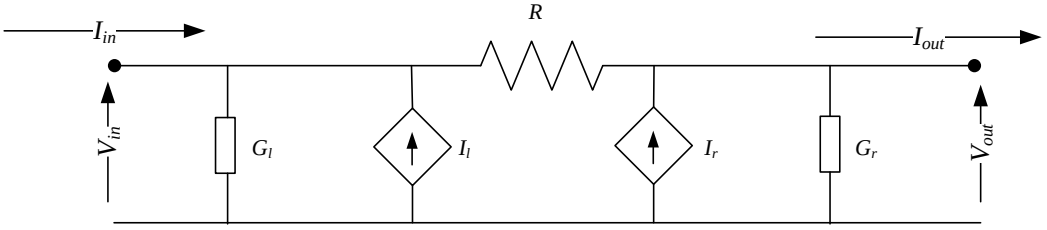

Figure 6: A lumped-component circuit element for modelling a section of TL linking two nodes.

To illustrate the method further, and to introduce the notation used here, consider an example of a heat transfer problem with piecewise-constant parameters. The problem has layers of different uniform materials, each having different physical properties, as shown in Figure 7.

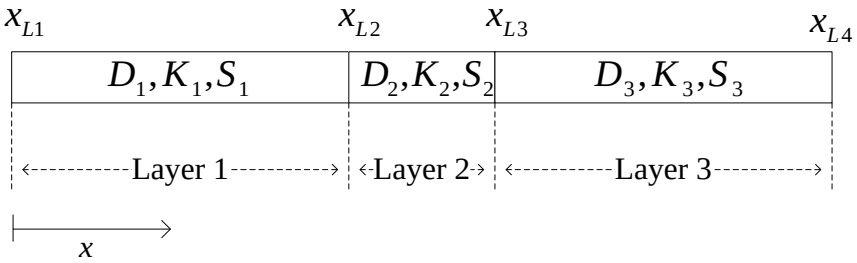

Figure 7: Physical layers for sample problem with layer coefficients and layer boundary positions indicated.

The heat equation for this problem is of the form,

$$\frac{\partial}{\partial x}\left(D\frac{\partial \phi}{\partial x}\right) - K\phi + S = 0 \tag{3.3}$$

where

$$\left.\begin{aligned} D &= D_j \\ K &= K_j \\ S &= S_j \end{aligned}\right\} x_{Lj} \le x < x_{L(j+1)}$$

and $j = 1,2,\ldots,N_L$, where the x_{Lj} values give the locations of the boundaries of the N_L layers (as shown in Figure 7).

By comparing Equations (3.1) and (3.3) for the situation where the diffusion coefficient is piecewise constant, it is clear that the relationship between the TL parameters and the RDE coefficients must be

$$R_{dj} = \frac{1}{D_j},\ G_{dj} = K_j, I_{dj} = S_j \tag{3.4}$$

and that Eq. (3.1) simplifies to

$$\frac{\partial}{\partial x}\left(\frac{1}{R_d}\frac{\partial V}{\partial x}\right) - G_d V + I_d = 0 \tag{3.5}$$

To solve the problem, nodes must be positioned along the domain. The notation used for their positions is illustrated in Figure 8 where x_i is the location of node i and h_i is the length of the section between nodes i and i+1. The length of that part of layer j that overlaps section i is denoted as $L_{j,i}$.

The section of TL between nodes 1 and 2 is uniform and can therefore be represented by a lumped-component circuit element of the form shown in Figure 6. The same can be done for the section between nodes 3 and 4, but the section between nodes 2 and 3 is composed of three segments of uniform TL (as shown in Figure 8) and, therefore, it is a more complex problem to determine the parameters for the equivalent lumped-component circuit element for that section.

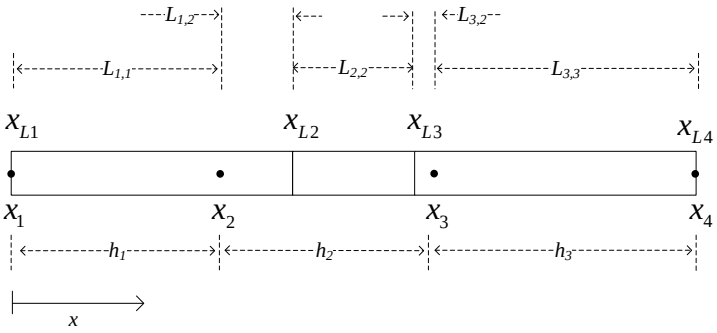

Figure 8: Physical layers, node positions, node spacings and TL segment lengths for sample problem.

The I/O relationship can be found for each of the three uniform TL segments between nodes 2 and 3. The full section can be represented by 3 black boxes in series as shown in Figure 9. The I/O relationship for the whole section can be easily determined given the I/O relationship for each segment. Once that is done, comparison with the I/O relationship for the standard lumped-component circuit element gives the parameters for a circuit that will model the section (i.e. the three TL segments in series) exactly (in terms of the inputs and outputs of the section).

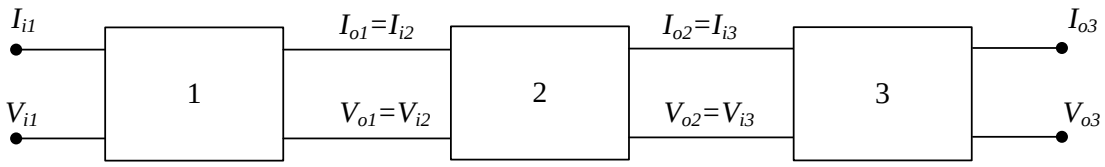

Figure 9: Black box representation of the TL section between nodes x_2 and x_3 in the sample problem. Each box represents a segment of uniform TL.

Once the parameters for the three lumped-component circuit elements (i.e. for the circuit elements connecting each pair of adjacent nodes in the model) are found, and the boundary conditions are set, it is a straightforward process to calculate the voltages at the nodes.

To summarize, the I/O relationship for a uniform TL segment under steady-state conditions is known. To model a transmission line with piecewise-constant coefficients, it must first be broken into sections linking adjacent nodes. Each section can be composed of one or more segments of uniform TL. A lumped-component circuit element can then be found to model each section. Once the parameters for these elements are calculated and the boundary conditions are set, the voltages at the nodes can be found.

3.2.1 Derivation of LCM equations

The first step in deriving the equations for the method is to find the relationship between the inputs and the outputs for a length of uniform transmission line with distributed R_d, G_d, I_d, C_d and L_d. The governing equations for voltage and current along a transmission line are derived in Appendix B for a TL segment suitable for modelling a general transient CRDE. Under steady-state conditions with zero convection, Equations (B.2) and (B.4) in Appendix B simplify to

$$\frac{\partial I}{\partial x} = I_d - G_d V \tag{3.6}$$

and

$$\frac{\partial V}{\partial x} = -IR_d \tag{3.7}$$

These first-order coupled ordinary differential equations govern the current and voltage along a segment of uniform TL. Consider a segment of length Δx between $x = x_0$ and $x = x_0 + \Delta x$. If the voltage and current at the "input" end are

$$V(x_0) = V_i,\ I(x_0) = I_i \tag{3.8}$$

then Equations (3.6) and (3.7) can be solved to give the voltage and current at the output end (i.e. at $x = x_0 + \Delta x$), V_0 and I_0. The result is

$$\begin{bmatrix} V_o \\ I_o \end{bmatrix} = \begin{bmatrix} \alpha & -\beta/\zeta \\ -\beta\zeta & \alpha \end{bmatrix} \begin{bmatrix} V_i \\ I_i \end{bmatrix} + \begin{bmatrix} (1-\alpha)/(\gamma\zeta) \\ \beta/\gamma \end{bmatrix} I_d \tag{3.9}$$

or

$$\begin{bmatrix} V_o \\ I_o \end{bmatrix} = \mathbf{A}_{\mathbf{TL}} \begin{bmatrix} V_i \\ I_i \end{bmatrix} + \mathbf{b}_{\mathbf{TL}} \tag{3.10}$$

where

$$\alpha = \cosh(\gamma\Delta x),\ \beta = \sinh(\gamma\Delta x),\ \gamma = \sqrt{G_d R_d},\ \zeta = \sqrt{G_d/R_d} \tag{3.11}$$

In a situation where reaction is zero, Eq. (3.9) simplifies to

$$\begin{bmatrix} V_o \\ I_o \end{bmatrix} = \begin{bmatrix} 1 & -R_d\Delta x \\ 0 & 1 \end{bmatrix} \begin{bmatrix} V_i \\ I_i \end{bmatrix} + \begin{bmatrix} -R_d\Delta x^2/2 \\ \Delta x \end{bmatrix} I_d \tag{3.12}$$

The second step in deriving the equations for the method is to establish the equivalent I/O relationship for the lumped-component circuit element shown in Figure 10.

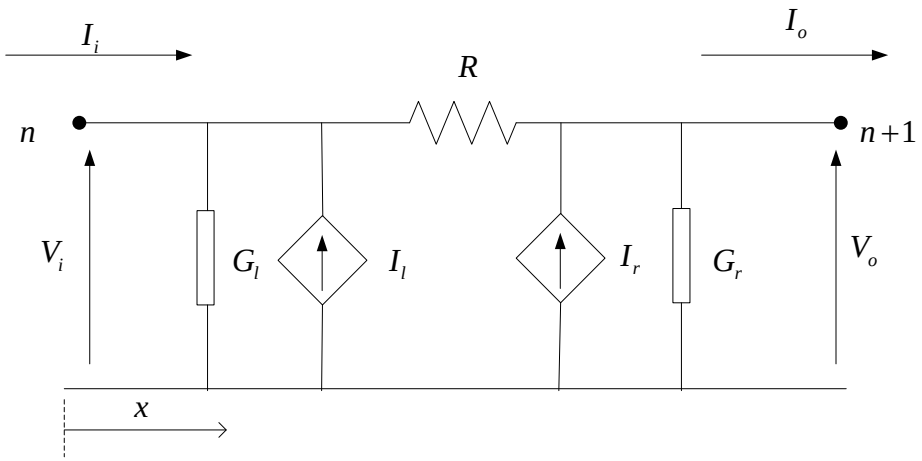

Figure 10: Lumped-component circuit element.

It is important to note that this circuit is just one of many possible circuits that could represent a segment of uniform TL. From Kirchhoff's current law, the sums of the currents at nodes *n* and *n*+1 must both be zero giving

$$I_i - G_l V_i + I_l + \frac{V_o - V_i}{R} = 0 \tag{3.13}$$

and

$$\frac{V_i - V_o}{R} + I_r - G_r V_o - I_o = 0 \tag{3.14}$$

Solving these for V_0 and I_0 gives,

$$\begin{bmatrix} V_o \\ I_o \end{bmatrix} = \begin{bmatrix} G_l R + 1 & -R \\ -G_l\left(G_r R + 1\right) - G_r & G_r R + 1 \end{bmatrix} \begin{bmatrix} V_i \\ I_i \end{bmatrix} + \begin{bmatrix} -R I_l \\ I_r + \left(G_r R + 1\right) I_l \end{bmatrix} \tag{3.15}$$

or

$$\begin{bmatrix} V_o \\ I_o \end{bmatrix} = \mathbf{A_{LC}} \begin{bmatrix} V_i \\ I_i \end{bmatrix} + \mathbf{b_{LC}} \tag{3.16}$$

Equations (3.10) and (3.16) both have the same form. In order for the lumped-component circuit element to be equivalent to the TL segments, the component values must be chosen so that

$$\mathbf{A_{LC}} = \mathbf{A_{TL}}\,,\ \mathbf{b_{LC}} = \mathbf{b_{TL}} \tag{3.17}$$

That gives

$$R = -\mathrm{A}_{\mathrm{TL},1,2} \tag{3.18}$$

$$G_l = -\frac{\mathrm{A}_{\mathrm{TL}\ 1,1} - 1}{\mathrm{A}_{\mathrm{TL}\ 1,2}} \tag{3.19}$$

$$G_r = -\frac{\mathrm{A}_{\mathrm{TL}\ 2,2} - 1}{\mathrm{A}_{\mathrm{TL}\ 1,2}} \tag{3.20}$$

$$I_l = \frac{\mathrm{b}_{\mathrm{TL}\ 1,1} - 1}{\mathrm{A}_{\mathrm{TL}\ 1,2}} I_d \tag{3.21}$$

$$I_r = \frac{\mathrm{b}_{\mathrm{TL}\ 2,1} - \dfrac{\mathrm{b}_{\mathrm{TL}\ 1,1}}{\mathrm{A}_{\mathrm{TL}\ 1,2}}}{\mathrm{A}_{\mathrm{TL}\ 2,2}} I_d \tag{3.22}$$

Note that, for situations where there is only one uniform segment in a section, G_l and G_r are equal.

Equations (3.18) to (3.22) can be used to calculate the component values for an equivalent circuit that can exactly represent a TL segment with known distributed coefficients. They can also be used to calculate the parameters for a circuit that models a section composed of multiple uniform TL segments once the I/O relationship can be established (i.e. $\mathbf{A}_{\mathrm{TL}}$ and $\mathbf{b}_{\mathrm{TL}}$ can be found) for such a section.

First, consider a TL section (i.e. the section linking nodes n and $n + 1$) composed of two uniform segments as shown in Figure 11. Eq. (3.10) for the segment between $x_{L,1}$ and $x_{L,2}$ in Figure 11 is given by

$$\begin{bmatrix} V_{o,1} \\ I_{o,1} \end{bmatrix} = \mathbf{A}_{\mathbf{TL}}^{1,n} \begin{bmatrix} V_{i,1} \\ I_{i,1} \end{bmatrix} + \mathbf{b}_{\mathbf{TL}}^{1,n} \tag{3.23}$$

Similarly, for the segment between $x_{L,2}$ and $x_{L,3}$

$$\begin{bmatrix} V_{o,2} \\ I_{o,2} \end{bmatrix} = \mathbf{A}_{\mathbf{TL}}^{2,n} \begin{bmatrix} V_{i,2} \\ I_{i,2} \end{bmatrix} + \mathbf{b}_{\mathbf{TL}}^{2,n} \tag{3.24}$$

where $\mathbf{A}_{\mathbf{TL}}^{1,n}$ represents the matrix $\mathbf{A}_{\mathbf{TL}}$ for segment 1 in the section n. Since $V_{o,1}=V_{i,2}$ and $I_{o,1}=I_{i,2}$, combining Equations (3.23) and (3.24) gives

$$\begin{bmatrix} V_{o,2} \\ I_{o,2} \end{bmatrix} = \mathbf{A}_{\mathbf{TL}}^{2,n} \mathbf{A}_{\mathbf{TL}}^{1,n} \begin{bmatrix} V_{i,1} \\ I_{i,1} \end{bmatrix} + \mathbf{A}_{\mathbf{TL}}^{2,n}\ \mathbf{b}_{\mathbf{TL}}^{1,n} + \mathbf{b}_{\mathbf{TL}}^{2,n} \tag{3.25}$$

The general I/O relationship for a section with N_n layers between nodes n and $n + 1$ is

$$\begin{bmatrix} V_{o,(n+1)} \\ I_{o,(n+1)} \end{bmatrix} = \mathbf{A}_{\mathbf{TL}}^{n} \begin{bmatrix} V_{i,n} \\ I_{i,n} \end{bmatrix} + \mathbf{b}_{\mathbf{TL}}^{n} \tag{3.26}$$

where

$$\mathbf{A}_{\mathbf{TL}}^{n} = \prod_{i=N_n}^{1} \mathbf{A}_{\mathbf{TL}}^{i,n} \tag{3.27}$$

$$\mathbf{b}_{\mathbf{TL}}^{n} = \left(\sum_{i=2}^{N_n} \mathbf{A}_{\mathbf{TL}}^{i,n} \mathbf{b}_{\mathbf{TL}}^{i-1,n} \right) + \mathbf{b}_{\mathbf{TL}}^{N_n,n} \tag{3.28}$$

As before, once these are calculated for a section, the equivalent circuit parameters can be determined using Equations (3.18) to (3.22).

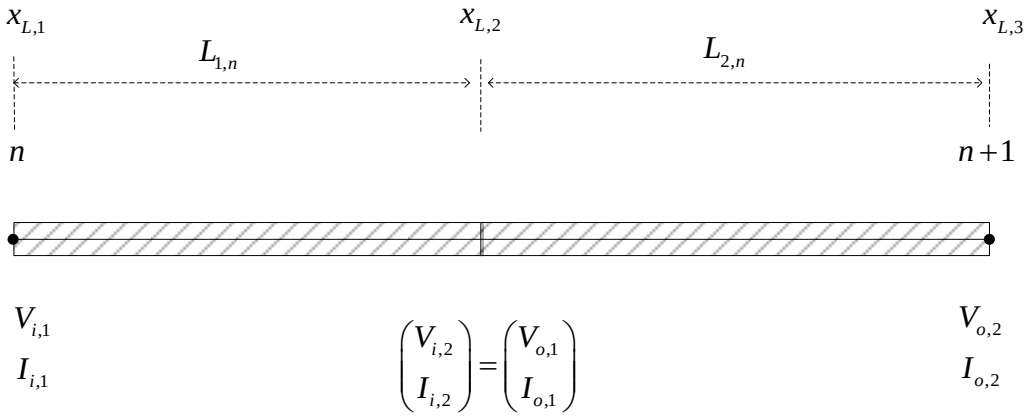

Figure 11: A section linking nodes n and $n + 1$ composed of two uniform segments.

The nodes in a model are linked by lumped-component circuit elements. The next step is to determine the node voltage at any node *n* in terms of the voltages at the surrounding nodes. Consider the two elements shown in Figure 12.

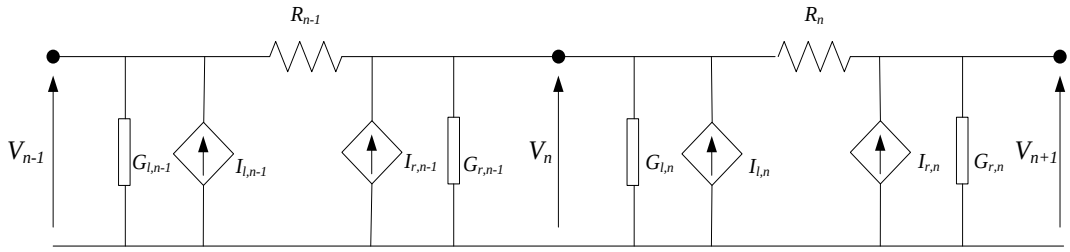

Figure 12: Three nodes in a lumped-component circuit model.

From Kirchhoff's current law, the sum of the currents at node *n* is zero, and so

$$\left(\frac{V_{n+1}-V_n}{R_n}\right)-\left(\frac{V_n-V_{n-1}}{R_{n-1}}\right)-V_n\left(G_{r,n-1}+G_{l,n}\right)+I_{r,n-1}+I_{l,n}=0 \tag{3.29}$$

This equation is similar in form to an equivalent standard FVM equation. Unlike with the finite volume method (or finite difference methods), the derivation of this equation does not involve any approximation of derivatives. For a reaction-diffusion problem with piecewise-constant coefficients, an exact TL analogue can be found. In terms of voltages and currents at the nodes, this can be represented exactly by a lumped-component circuit. If the boundary conditions are implemented with no errors, then the node voltages will match the solution of the RDE, i.e. the method will produce an exact solution (see Appendix C).

For more general problems where the coefficients (i.e. *D*, *K* and *S*) of the equations are varying continuously over space, LCM requires the approximation of the coefficients using piecewise-constant functions. The remaining steps for modelling such problems are similar to those for problems with piecewise-constant coefficients described above. If the continuously varying coefficients are only known at the nodes then one possible approximation is illustrated in Figure 13. Discontinuities are located midway between adjacent nodes giving two TL segments per section. The values of the coefficients at the nodes are used as the values for the corresponding segments, as illustrated by the diffusion coefficients indicated in Figure 13.

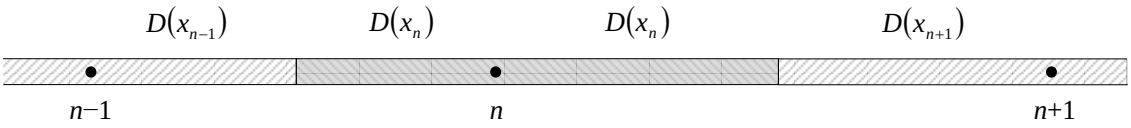

Figure 13: Part of a model with coefficients known only at the nodes. The coefficients over x are approximated by piecewise-constant functions with the discontinuities midway between adjacent nodes as indicated. Only the diffusion coefficients for each segments are shown here.

All tests presented in this chapter are for problems with Dirichlet boundary conditions. The voltages at the boundary nodes in each model are simply fixed at the desired values.

3.3 Testing and results

Testing has shown that LCM can produce exact solutions of the one-dimensional steady-state RDE (to within the limits of computer-storage and calculation accuracy) for problems with piecewise-constant coefficients. In situations where one or more of the coefficients vary continuously over space, however, the physical problem cannot be modelled exactly. As is shown below, the errors in the solutions then depend on how the coefficients vary. A continuous spatial variation of any coefficient means that it must be approximated using a piecewise-constant function, because LCM requires all coefficients to be piecewise constant. The result is that the LCM parameters will differ from what they should be, giving rise to errors in the solutions. These solution errors are compared here with errors produced by equivalent FVM models.

The reasons for choosing FVM for comparison with LCM are; firstly, there is a similarity between the FVM and LCM equations; secondly, FVM is a well-established method for solving reaction-diffusion equations; and thirdly, FVM is widely used for problems with discontinuous coefficients [64, 86]. In FVM, for a problem with discrete physical layers (giving piecewise-constant coefficients) nodes are generally placed so that either volume faces or nodes correspond to the points of discontinuity [10, 64, 87-89]. In order to compare FVM with LCM fully, however, FVM models are implemented here with node and volume positions that do not necessarily correspond to physical layers. As a result, situations can arise like that illustrated in Figure 14, for example, in which a thin layer (layer 2 in the example) lies within a volume. The source and reaction terms in the finite volume equations take account of the source and reaction coefficients of layer 2; however, the diffusion coefficient of layer 2 is not accounted for in a standard FVM implementation because only the diffusion coefficients at the

volume faces (such as those labelled $n - ½$ and $n + ½$ in Figure 14) are used, and those are calculated using only the values of D at the nodes.

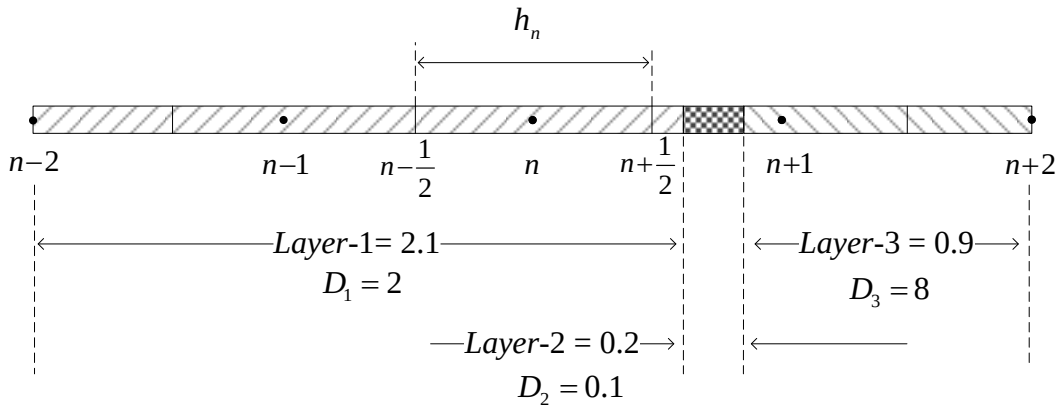

Figure 14: A model with a narrow physical layer located within the FVM volume corresponding to node $n+1$.

In an attempt to overcome this problem, a number of different methods (both standard and non-standard) are used here for calculating the values of D required in the FVM equations. These are outlined briefly in Table 1 with further details given in Appendix D. The purpose of the tests presented here is not to investigate the FVM method and to find the best implementation for a particular problem or type of problem, or to determine how the method could be improved under such circumstances, but only to compare LCM to a variety of FVM schemes, Table 1 gives the formulas used for calculating $D_{n+½}$ for each implementation tested, and includes sample calculations of the diffusion coefficient at the face between elements n and $n+1$ for the example in Figure 14. This gives some indication of the possible variation in the value used.

Table 1: The different formulas used for the calculation of the value of D at the face between elements n and $n + 1$ in FVM models, and the calculation of that value at $n + ½$ for the problem shown in Figure 14.

Scheme	Formula	Calculation
Average of node value: FVM^{An}	$D^{An}_{n+\frac{1}{2}} = \frac{D_n + D_{n+1}}{2}$	$D^{An}_{n+\frac{1}{2}} = \frac{4+8}{2} = 6$
Average of average values: FVM^{AA}	$D^{AA}_{n+\frac{1}{2}} = \frac{\overline{D}_n + \overline{D}_{n+1}}{2}$	$D^{AA}_{n+\frac{1}{2}} = \frac{4+5\frac{21}{40}}{2} = 4\frac{61}{80}$
Average between the nodes: FVM^{BA}	$D^{BA}_{n+\frac{1}{2}} = \frac{\int_{x_n}^{x_{n+1}} D dx}{x_{n+1} - x_n}$	$D^{BA}_{n+\frac{1}{2}} = \frac{0.5\times 2 + 0.2\times 0.1 + 0.1\times 8}{0.5+0.2+0.1} = 3\frac{21}{40}$
Harmonic mean of average values: FVM^{HA}	$D^{HA}_{n+\frac{1}{2}} = \frac{2\overline{D}_n \overline{D}_{n+1}}{\overline{D}_n + \overline{D}_{n+1}}$	$D^{HA}_{n+\frac{1}{2}} = \frac{2\times 4\times 5\frac{21}{40}}{4+5\frac{21}{40}} = 4\frac{57}{89}$
Alternative harmonic average: FVM^{BHA}	$D^{BHA}_{n+\frac{1}{2}} = \frac{1}{\sum_{j=1}^{N_s} \frac{L_j / h}{D_j}}$	$D^{BHA}_{n+\frac{1}{2}} = \frac{1}{\frac{0.5/0.8}{2} + \frac{0.2/0.8}{0.1} + \frac{0.1/0.8}{8}} = \frac{3}{8}$
Boundary node value: FVM^{Bn}	$D^{Bn}_{n+\frac{1}{2}} = D_{n+\frac{1}{2}}$	$D^{Bn}_{n+\frac{1}{2}} = 4$

The schemes labelled FVM^{An}, FVM^{HA} and FVM^{BA} are standard schemes [10], while the others are less standard.

The first non-standard approach, FVM^{AA}, is only used where D is piecewise-constant. Unlike the standard scheme, FVM^{An}, it takes account of the diffusion coefficient at all points, including by first calculating average values of D over each volume. For the example in Figure 14, the value of D at $n + ½$ calculated using FVM^{AA}, is, therefore, lower than the value calculated using FVM^{An}, because it is affected by the diffusion coefficient of layer 2.

The diffusion coefficient in layer 2 in Figure 14 is significantly lower than the diffusion coefficients in layers 1 and 3. If it were reduced towards zero, diffusion between nodes n and $n + 1$ would stop. That would happen even if the width of that layer were reduced. The averaging used in the second non-standard scheme, FVM^{BHA}, gives greater weight

to a low D value in a narrow layer than that used in the other schemes. This is clear from values of D at $n + ½$ for the example in Figure 14 given in Table 1.

Most standard schemes assume that values of the diffusion coefficient are only known at the nodes, but that is not the case for piecewise-constant problems examined here. The third non-standard method, FVM ^{Bn}, simply uses the values of D at the volume faces.

The values of D at one volume face, calculated in Table 1 for the sample problem, vary significantly over the range of schemes tested. This estimation is, however, only one source of errors in an FVM solution, and errors from different sources can tend to accumulate or to cancel each other out. Therefore, even if one scheme gives, in general, better estimates of D at the volume faces it will not necessarily produce more accurate solution values.

The reaction integral in Eq. (2.3), given in section 2.2.1 above, can either be approximated using Eq. (2.12) or assuming a linear variation of the unknown ϕ over the volume. In this chapter, the latter method is used and details of it are given in Appendix E.

The main purpose of this section is to establish whether the LCM method has the potential to be an accurate method for solving particular types of steady-state problems. Tests examine the accuracy and properties of the method for different types of scenarios in which the coefficients vary continuously over space. Where possible, numerical solutions are compared with analytical solutions and errors are calculated. In most cases, in order to simplify the presentation of results, errors are only calculated at the node corresponding to the mid-point of the domain. For some tests, analytical solutions are not available or are too complex to obtain. In such situations, numerical results are compared with benchmark solutions (i.e. with highly accurate numerical solutions of the problem in question, calculated here using Richardson extrapolation as described in Chapter 2).

All results presented here are for models with $x \in [0,1]$ and with Dirichlet boundary conditions, $V(0)=V_L$ and $V(1)=V_R$, where the values of V_L and V_R are specified below for each test.

The tests are detailed in Table 2. Test 1 involves the solution of a general problem with all coefficients varying continuously over space using models with unevenly spaced nodes. It is used to investigate the order of the discretization errors. Tests 2 and 3 involve models of a semiconductor gas sensor (a reaction-diffusion problem with constant coefficients) and heat transfer through building walls (a diffusion problem with piecewise-constant coefficients) respectively. These two tests show that LCM can produce exact solutions for such problems. In each of tests 4 to 6, two of the coefficients (*D*, *K* and *S*) vary in a piecewise-constant manner over space while the third coefficient varies continuously over space. Each model tested has three "physical layers" giving two discontinuities (at at $x = 0.3$ and $x = 0.6$). Where a coefficient is piecewise constant, the three values of the coefficient corresponding to the three layers are given in the table (e.g. the notation {2, 3, 5}, when used for values of *D*, denotes that $D = 2$ between $x = 0$ and $x = 0.3$, $D = 3$ between $x = 0.3$ and $x = 0.6$, and $D = 5$ between $x = 0.6$ and $x = 1$).

Table 2: Table of tests conducted using steady-state LCM.

Test No.	***D*(*x*)**	***K*(*x*)**	***S*(*x*)**	***h***	**Purpose**	**References**
1	All varying continuously			Uneven	Investigation of order of errors of methods when node spacing is uneven	
2	Constant			Even	Testing with problems with constant coefficients	Sakai 2001 [90], Matsunaga 2003 [91]
3	Piecewise-Constant			Even	Testing with problems with piecewise-constant coefficients	Sami A. Al-Sanea [64], B. A. Price [89]
4	{2, 3, 5}	{25, 15, 45}	$1+\alpha x^2$	Even	Testing of problems with a continuously varying source term coefficient	
5	{2, 3, 5}	$1+\alpha x^2$	{2, 30, 5}	Even	Testing of problems with a continuously varying reaction coefficient	
6	$1+\alpha x^2$	{25, 15, 45}	{2, 3, 5}	Even	Testing of problems with a continuously varying diffusion coefficient	

3.3.1 Test 1: Order of convergence on uneven grids

This test involves a reaction-diffusion model with coefficients varying continuously over space on a grid with uneven node spacings. The objective of this test is to show LCM's general applicability, to compare its results with those from FVM schemes, and to determine the order of its solution errors when implemented on an uneven grid.

The truncation errors in FVM are second order when the node spacings are even and first order when uneven. The literature suggests, however, that there is no

straightforward way to determine these orders from test results because the errors in such results can appear second order even when the node spacings are uneven [92-93]. There is no attempt made here to determine the order of the LCM errors analytically. Instead, they are estimated from numerical results.

In the problem tested here, all the coefficients are varying continuously over space. The coefficients are

$$S = \sin(x)\left(x^2 + e^x + 1\right) - 2x\cos(x),\ D = x^2 + 1,\ K = e^x \tag{3.30}$$

The Dirichlet boundary conditions at $x = 0$ and $x = 1$ are consistent with the exact solution

$$V(x) = \sin(x) \tag{3.31}$$

The coefficients $D(x)$ and $K(x)$ have been selected so they are far from piecewise-contant, and, so, significant errors may occur in the LCM solutions. The solution has been chosen and the source term, $S(x)$, has been found using the method of manufactured solutions (see Section 2.3.1).

The grids used have a change in volume length at $x = 0.5$, h being constant on either side of that point. Results are presented for two different node/element configurations as shown in Figure 15. In each test, similar configurations have been used for both LCM and FVM. When the configuration shown in Figure 15(a) is used, and the number of nodes is varied, the positions of the nodes change. As a result, instead of the solution error at a particular node being presented below, the maximum error at any node is given. That is not the case with the configuration illustrated in Figure 15(b).

In this test, only FVM^{An} and FVM^{Hn} are included as the coefficients are varying continuously over space, and it is assumed that they are known only at the nodes. Under such circumstances, the other schemes listed in Table 1 above cannot be implemented

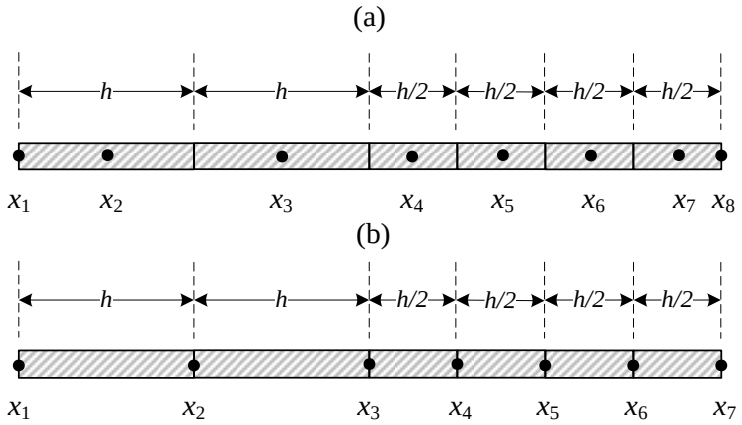

Figure 15: Node positions for models in Test 1, with nodes located at the centre of the volumes, (a), and nodes located at the boundary of the volume, (b).

Table 3 includes the maximum absolute solution error and the corresponding estimated orders of errors for the LCM and FVM schemes tested on grids as shown in Figure 15(a). The order of the error is calculated as shown in Section 2.3.3. Table 4 contains similar results tested on grids as shown in Figure 15(b). In all cases, when the node spacing, h, is small, the errors are approximately proportional to h^2, i.e. all three schmes appear to be second-order accurate on the uneven grids used. The differences between the FVM^{An} and FVM^{Hn} errors are small, but the errors in the LCM results are significantly smaller than for either FVM scheme.

Table 3: Maximum absolute error for LCM and FVM schemes calculated on grids as illustrated in Figure 15(a) with different numbers of nodes. The estimated orders of the errors are included in bold.

N	LCM	FVM^{An}	FVM^{Hn}
8	5.2226E−04	1.3398E−03	0.001587264
14	8.8192E−05	4.5360E−04	0.000494113
26	1.2373E−05	1.2733E−04	0.000136652
	2.5	**1.4**	**1.6**
50	2.8492E−06	3.3298E−05	3.58746E−05
	3.0	**1.8**	**1.8**
98	8.1884E−07	8.4908E−06	9.18659E−06
	2.2	**1.9**	**1.9**
194	2.1883E−07	2.1425E−06	2.3249E−06
	1.8	**2.0**	**2.0**
386	5.6524E−08	5.3802E−07	5.84753E−07
	1.9	**2.0**	**2.0**
770	1.4360E−08	1.3480E−07	1.4663E−07
	1.9	**2.0**	**2.0**
1538	3.6117E−09	3.3737E−08	3.67124E−08
	2.0	**2.0**	**2.0**
3074	8.2440E−10	8.4393E−09	9.18535E−09
	1.9	**2.0**	**2.0**

Table 4: Maximum absolute error for LCM and FVM schemes calculated on grids as illustrated in Figure 15(b) with different numbers of nodes. The estimated orders of the errors are included in bold.

N	LCM	FVM^{An}	FVM^{Hn}
7	2.1211E−04	2.5047E−03	2.5951E−03
13	4.3016E−05	6.2617E−04	6.3942E−04
25	1.0133E−05	1.5654E−04	1.5927E−04
	2.4	**2.0**	**2.0**
49	2.4945E−06	3.9136E−05	3.97805E−05
	2.1	**2.0**	**2.0**
97	6.2119E−07	9.7840E−06	9.94285E−06
	2.0	**2.0**	**2.0**
193	1.5515E−07	2.4460E−06	2.48557E−06
	2.0	**2.0**	**2.0**
385	3.8777E−08	6.1150E−07	6.21384E−07
	2.0	**2.0**	**2.0**
769	9.6928E−09	1.5287E−07	1.55345E−07
	2.0	**2.0**	**2.0**
1537	2.3918E−09	3.8217E−08	3.88352E−08
	2.0	**2.0**	**2.0**
3073	3.6570E−10	9.5532E−09	9.71285E−09
	1.8	**2.0**	**2.0**

The results in the two tables demonstrate that LCM can be solved on both grids, shown in Figure 15, but LCM is more accurate in the second case. LCM is also significantly more accurate for this problem than the FVM schemes tested. The results also suggest

an order of convergence that is equivalent to FVM and it shows that LCM can be applied to a general problem with continuously varying coefficients on an uneven grid.

The order of convergence (see Section 2.3.2) estimated from numerical results does not necessarily match the order of convergence of the scheme determined through analysis of the source or sources of errors within it. For example, it is known that FVM is first order when the grid is uneven due to derivative approximations used in its derivation. Here, however, FVM exhibits second order accuracy on this specific grid configuration. Schemes that exhibit this behaviour are called supra-convergent [75-76]. There are suggestions that it is related to the regularity and structure of the grid. For example, grids with periodic structures, or grids with the distances between nodes varying only slightly, can lead to methods exhibiting a higher order of accuracy than expected. What is clear is that the tests presented here do not prove that LCM is a second-order scheme on an uneven grid, but simply show that it may be.

Note that the node/element configurations used in all subsequent tests here are similar to those illustrated in Figure 15(b) but with nodes evenly spaced over the domains.

3.3.2 Test 2: Reaction-diffusion in a thin-film semiconductor gas sensor

Thin-film semiconductor gas sensors, sometimes called metal-oxide sensors, are used to detect gases through a reaction process that takes place at an active sensing layer within them (see Figure 16(a)). The active layer has an electric conductivity that changes when it is in contact with gases, thus allowing gas detection. The reaction that takes place between the sensing layer and the gases is completely reversible [90-91, 94].

(a)

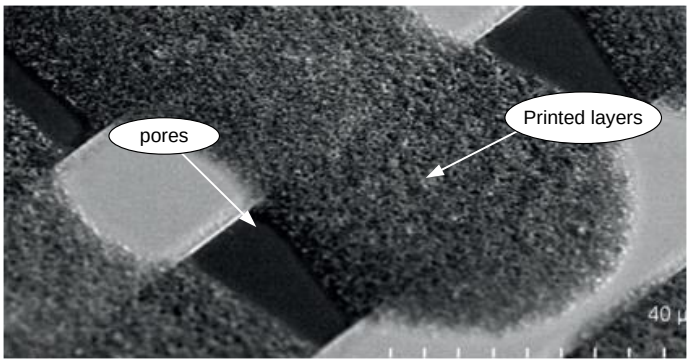

(b)

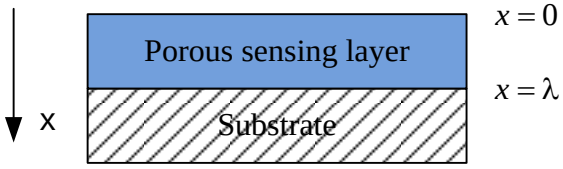

Figure 16: Porous inkjet-printed chromium/titanium-oxide layer (sensing layer) [94], (a). Simplified model of sensor layers, (b).

The physical processes within a thin-film semiconductor gas sensor involve both reaction and diffusion. The gas to be detected diffuses through pores in the sensing layer; if the gas is flammable, then diffusion is followed by a reaction process in which the gas reacts with oxygen in the metal oxide grains. The governing equation, simplified to one dimension as illustrated in Figure 16(b), is [90]

$$\frac{\partial C_A}{\partial t} = D_K \frac{\partial^2 C_A}{\partial x^2} - kC_A$$

where C_A is the target gas concentration.

In these porous materials, gas diffusion depends on the pore size, and, for materials with pore sizes between 1 to 100*nm*, a type of diffusion known as Knudsen diffusion prevails. The diffusion coefficient depends on the radius of the pores, *r*, gas constant, *R*, molecular weight of the gas, *M*, and temperature, *T*, at which the process takes place, and is given by

$$D_K = \frac{4r}{3}\sqrt{\frac{2RT}{\pi M}} \tag{3.32}$$

while the reaction coefficient, sometimes called the rate constant, is

$$k = k_0 \exp\left(-\frac{E_k}{RT}\right) \tag{3.33}$$

where k_0 is called the pre-exponential constant and E_k is the activation energy. The model considered by Sakai et al. [90], shown in Figure 16(b), has boundary conditions

$$C_A(0) = C_{A,s}, \ \frac{\partial C_A(\lambda)}{\partial x} = 0 \tag{3.34}$$

The problem modelled (as in Sakai et al) is an SnO_2 thin film semiconductor gas sensor with a constant pore radius of r = 2nm designed to detect a carbon monoxide (CO) gas with a gas constant R = 297J/KgK and molecular weight M = 28.08g/mol. The temperature at which the detection on the sensing layer takes place is T = 350K. Using Eq. (3.32), the Knudsen diffusion coefficient is calculated as $D_K = 4.1\times10^{12} nm/sec$. Results are presented for five different values of k, k= 4.1×10^{6}, 3.69×10^{7}, , 4.1×10^{8}, 3.69×10^{9} and $4.1\times10^{10} s^{-1}$ (the higher the reaction rate, the lower the solution values, except at the boundaries). The LCM and FVM solutions, and the associated absolute errors in the LCM solutions, are shown in Figure 17. These results, and other testing not reported here, show that LCM produces exact solutions and that the errors plotted are due to round-off.

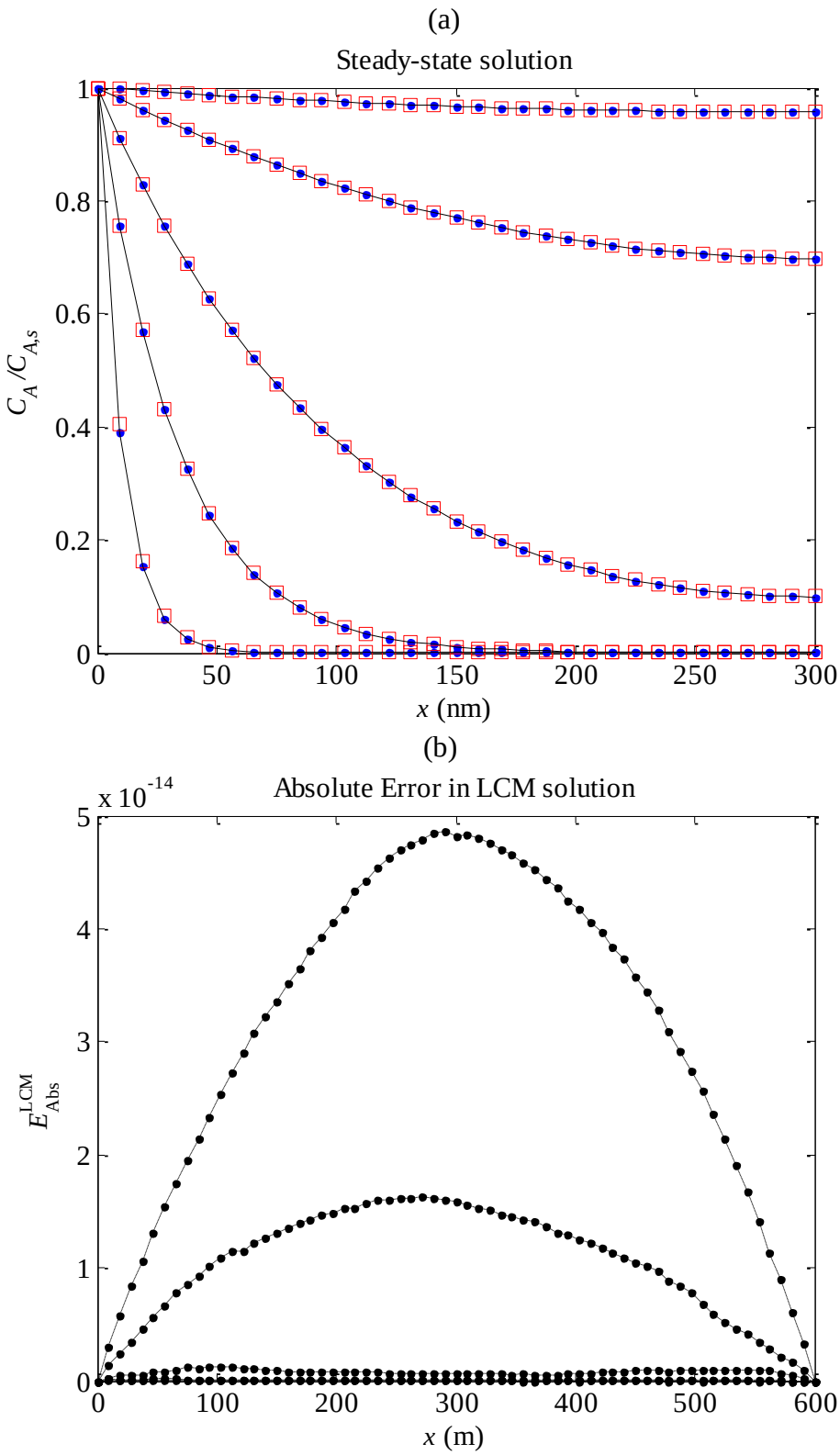

Figure 17: Concentration of SnO_2 over the sensing layer for five different reaction rates, where the blue dots represent the LCM solutions, the red squares represent the FVM solutions, and the black lines represent the exact solution given by Sakai et al. [90], (a). The higher the reaction rate, the lower the solution values. The corresponding absolute errors in the LCM solutions, (b).

3.3.3 Test 3: Heat transfer through insulated walls

Over the years, better building insulation materials and improvements in design have helped to reduce energy losses through walls and roofs; however, it continues to remain an highly active area of research. In this section, the heat transfer through two insulated walls is modelled using the LCM method in order to demonstrate that it can produce exact solutions for diffusion problems with piecewise-constant coefficients.

The one-dimensional steady-state heat equation

$$\frac{\partial}{\partial x}\left(k\frac{\partial T}{\partial x}\right)=0 \tag{3.35}$$

can be solved to find the temperature distribution across a solid wall section within which there is no heat generation. If the wall is composed of several layers of different materials, then the thermal conductivity, k, is a piecewise-constant function of x. The walls in the problem tested are composed of four layers assembled in two different configurations (as shown in Figure 18). In the first, the insulation is placed near the outside, while, in the second, the insulation is located near the inside. The material properties and the thicknesses of each layer are given in Table 5.

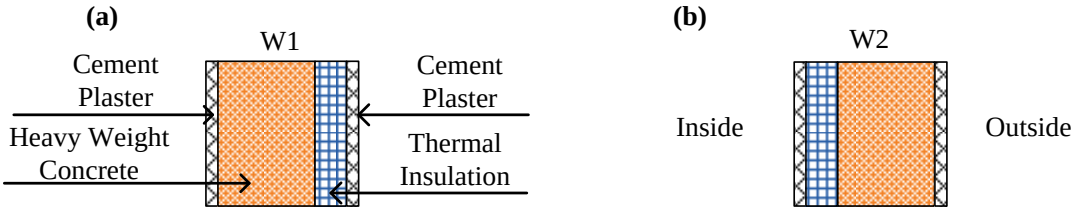

Figure 18: Sections of walls modelled using LCM.

Table 5: Thermal conductivities of the materials used in the walls, and the thicknesses of the wall layers [64].

Material	***k* (W/m K)**	***Thickness* (m)**
Cement Plaster	0.72	0.015
Moulded Polystyrene	0.034	0.088
Heavy-weight concrete	1.73	0.1

The nodes in the models tested are evenly spaced and their locations do not correspond with the physical layers. For simplicity, the boundary conditions used are T_{in} = 25°C and T_{out} = 49°C. Solutions are shown for both walls in Figure 19. The LCM results are compared with the exact solution and results from the FVM^{Hn} scheme.

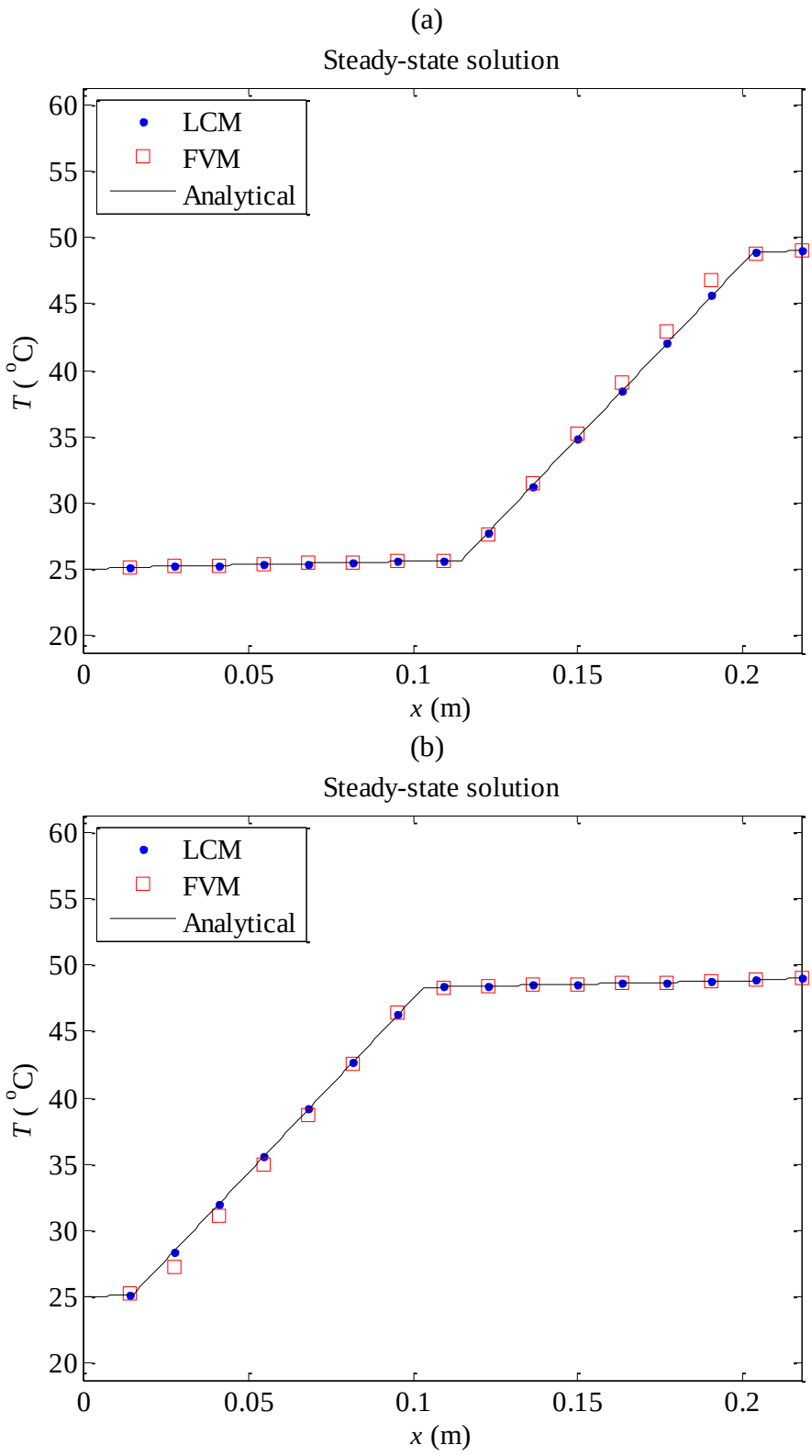

Figure 19: Steady-state temperature distribution across wall 1, (a) and wall 2, (b).

The absolute errors in the LCM and FVM solutions obtained using $N = 11$ are plotted in Figure 20. The size of the LCM solution errors is consistent with them being the result of round-off errors only, i.e. LCM produces exact solutions for this problem. This, and

other testing not presented here, confirms that LCM produces exact solutions for a diffusion problem with piecewise-constant coefficients.

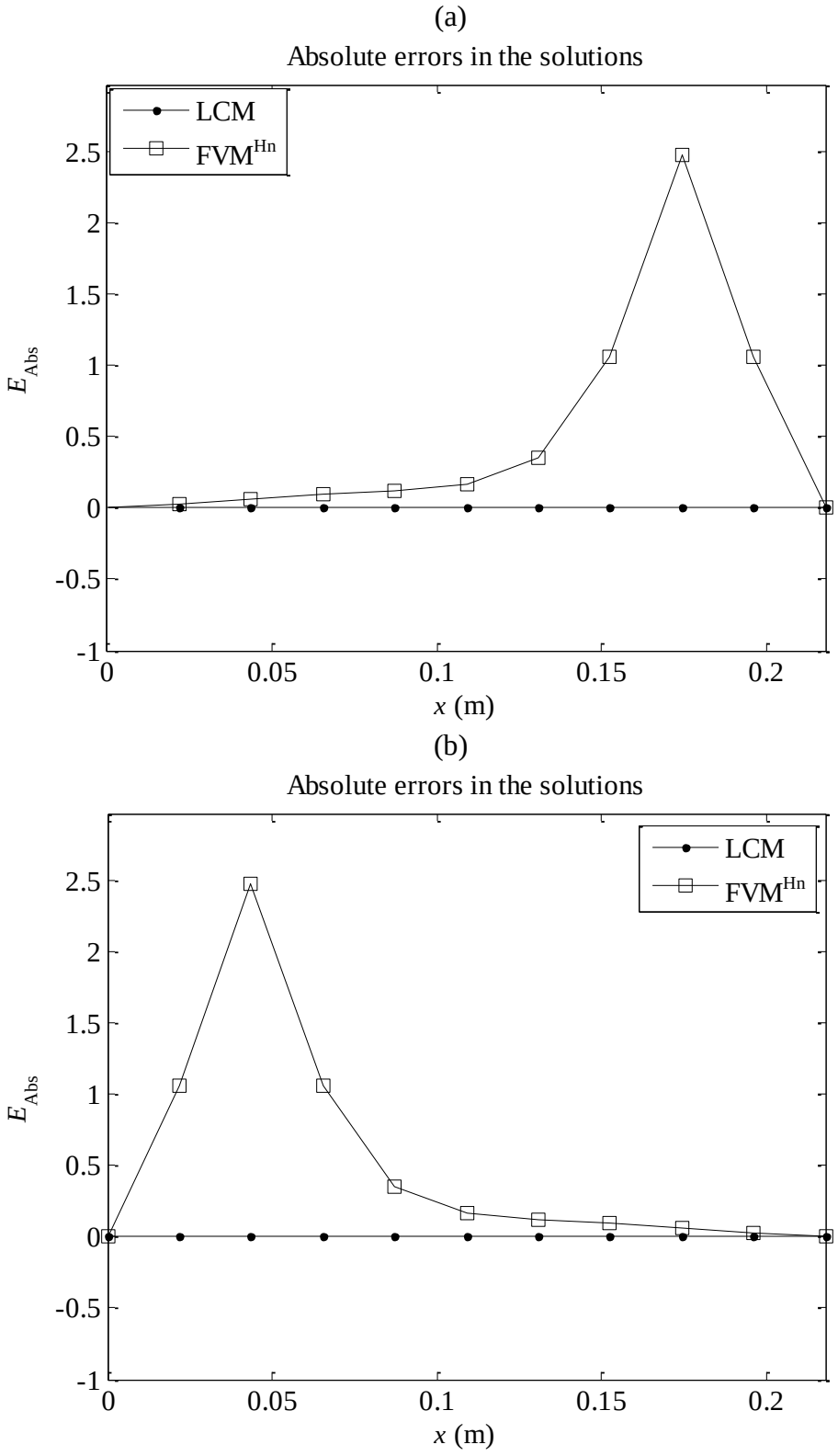

Figure 20: Errors in the solutions shown in Figure 19(a), (a), and in Figure 19(b), (b).

In the next three tests, one of the coefficients varies continuously over space so all methods tested exhibit systematic errors (because the continuously varying coefficient is approximated by a piecewise-constant function). The consistency of convergence of the solutions is examined for situations where, as in Test 3, the node positions do not correspond with coefficient discontinuities, and the accuracy of LCM and FVM is compared.

3.3.4 Test 4: Consistency of convergence with *K* and *D* piecewise-constant

This test models problems with $S(x)$ varying continuously with x and with $D(x)$ and $K(x)$ both piecewise-constant. The coefficients are specified in Table 2 above. The boundary voltages are $V_L = 0$ and $V_R = 1$. It is assumed that the value of $S(x)$ is only known at the nodes, and is therefore approximated using a piecewise-constant function as in Test 1 above. The source term is

$$S(x) = 1 + \alpha x^2 \tag{3.36}$$

where α is a constant for any given test.

Figure 21(a) shows the solution with $\alpha = 1$ obtained using a small node spacing. The approximate errors at $x = 0.5$ for LCM and the different FVM schemes are plotted against h in Figure 21(b). These suggest that the LCM method is significantly more accurate than the FVM schemes tested for this problem.

The approximate errors have been calculated relative to a highly accurate solution obtained using Richardson Extrapolation as described above. The values used in the extrapolation were obtained using the LCM method with 2049, 4096 and 8192 nodes. The reason why the LCM solutions have been used is clear from the results presented in Table 6, where the estimated order of convergence along with the solution values used to calculate them are shown. These results show that the LCM solutions converge in a consistent manner as the node spacing is decreased, unlike the FVM solutions. Richardson extrapolation therefore cannot be used with the FVM results, and it is not possible to estimate the accuracy of the FVM solutions by measuring how much they change as the node spacing is changed.

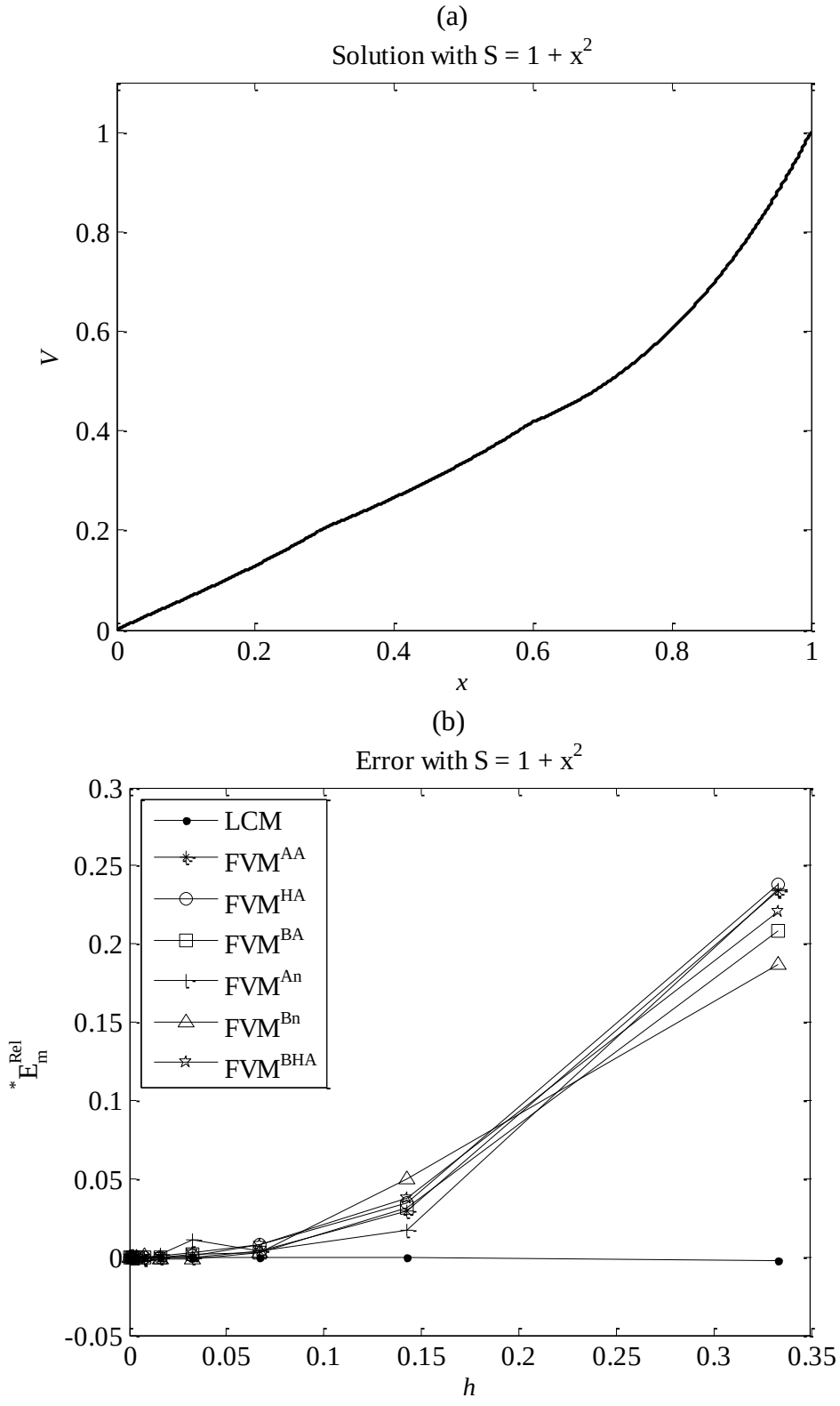

Figure 21: A solution for Test 4 in Table 2. The problem has three layers with discontinuities at $x = 0.3$ and $x = 0.6$, (a). The estimated errors in the solutions at $x = 0.5$ are plotted against h, (b).

Table 6: Values of the solution at the midpoint of the domain obtained using LCM and FVM schemes for different numbers of nodes. The estimated orders of the errors are given in bold font.

N	LCM	FVM^{AA}	FVM^{HA}	FVM^{BA}	FVM^{An}	FVM^{Bn}	FVM^{BHA}
5	0.335323	0.256814	0.255351	0.265277	0.256435	0.272510	0.261024
9	0.335124	0.325179	0.323409	0.324591	0.329395	0.318310	0.322407
17	0.335094	0.333817	0.332410	0.334229	0.336368	0.326172	0.332582
	2.7	**3.0**	**2.9**	**2.6**	**3.4**	**2.5**	**2.6**
33	0.335088	0.335197	0.334927	0.334417	0.331553	0.335464	0.334330
	2.2	**2.6**	**1.8**	**5.7**	**0.5**	**−0.2**	**2.5**
65	0.335086	0.335319	0.335164	0.335115	0.334676	0.335408	0.334917
	2.1	**3.5**	**3.4**	**−1.9**	**0.6**	**7.4**	**1.6**
129	0.335086	0.335235	0.335136	0.335173	0.335443	0.334809	0.335047
	2.1	**0.5**	**3.1**	**3.6**	**2.0**	**−3.4**	**2.2**
257	0.335086	0.335132	0.335049	0.335175	0.335293	0.334685	0.335077
	2.1	**−0.3**	**−1.6**	**4.3**	**2.4**	**2.3**	**2.1**
513	0.335086	0.335137	0.335121	0.335087	0.334916	0.335152	0.335083
	2.0	**4.6**	**0.3**	**−4.9**	**−1.3**	**−1.9**	**2.4**
1025	0.335086	0.335110	0.335100	0.335097	0.335070	0.335115	0.335085
	2.0	**−2.6**	**1.8**	**3.1**	**1.3**	**3.7**	**1.5**
2049	0.335086	0.335097	0.335091	0.335093	0.335110	0.335071	0.335086
	2.0	**1.1**	**1.2**	**1.4**	**2.0**	**−0.3**	**2.1**

It is not surprising that the FVM schemes do not converge in a consistent manner given the ways in which the FVM equation coefficients (in particular, the values of D) are calculated from the problem coefficients, and the fact that the nodes/volumes do not necessarily correspond to the discontinuities in those coefficients.

A clearer comparison of the accuracy of the schemes can be made by looking at the corresponding approximate relative errors listed in Table 7. It is clear that, for this problem, the LCM scheme is significantly more accurate than all of the FVM configurations tested. The difference in accuracy between LCM and FVM is greater than in Test 1. That is expected since two of the coefficients are piecewise constant in this test.

The next question examined here is whether this advantage is maintained if the magnitude of $S(x)$ is increased, leading to larger errors in the LCM parameters and causing the source function to dominate the solution. The estimated absolute errors at $x = 0.5$ obtained from models with $N = 65$ and $S(x) = 1 + \alpha x^2$ are given in Table 8 for a range of values of α. The reason why absolute errors are shown here (rather than

relative errors as given in Table 7) is because the solution values vary significantly with α.

Table 7: Estimated relative errors at the midpoint of the domain in the FVM and LCM solutions for Test 4 for different numbers of nodes (as plotted in Figure 21b).

N	LCM	FVM^{AA}	FVM^{HA}	FVM^{BA}	FVM^{An}	FVM^{Bn}	FVM^{BHA}
5	−7.0647E−04	2.3359E−01	2.3795E−01	2.0833E−01	2.3472E−01	1.8675E−01	2.2102E−01
9	−1.1535E−04	2.9564E−02	3.4848E−02	3.1320E−02	1.6984E−02	5.0065E−02	3.7836E−02
17	−2.5096E−05	3.7868E−03	7.9843E−03	2.5569E−03	−3.8279E−03	2.6601E−02	7.4720E−03
33	−5.7961E−06	−3.3156E−04	4.7402E−04	1.9948E−03	1.0543E−02	−1.1291E−03	2.2565E−03
65	−1.3782E−06	−6.9449E−04	−2.3483E−04	−8.5913E−05	1.2240E−03	−9.6228E−04	5.0415E−04
129	−3.3647E−07	−4.4489E−04	−1.5115E−04	−2.5906E−04	−1.0666E−03	8.2650E−04	1.1529E−04
257	−8.5765E−08	−1.3884E−04	1.0967E−04	−2.6761E−04	−6.1900E−04	1.1974E−03	2.5781E−05
513	−2.3769E−08	−1.5186E−04	−1.0540E−04	−4.1455E−06	5.0559E−04	−1.9628E−04	8.2845E−06
1025	−8.3510E−09	−7.1715E−05	−4.3825E−05	−3.3876E−05	4.5839E−05	−8.6602E−05	1.9092E−06
2049	−4.5564E−09	−3.4693E−05	−1.6500E−05	−2.2791E−05	−7.2842E−05	4.4611E−05	4.4063E−07

Table 8: Absolute errors in the solutions at the midpoint of the domain for Test 4 with N=65 for a range of values of α. Note that the error for LCM with $\alpha = 0$ is due to round-off errors.

α	LCM	FVM^{AA}	FVM^{HA}	FVM^{BA}	FVM^{An}	FVM^{Bn}	FVM^{BHA}
0	−9.4004E−10	−2.3445E−04	−7.8021E−05	−2.9876E−05	4.1281E−04	−3.3225E−04	1.7081E−04
1	−4.6184E−07	−2.3271E−04	−7.8688E−05	−2.8788E−05	4.1016E−04	−3.2245E−04	1.6893E−04
10	−4.6084E−06	−2.1705E−04	−8.4690E−05	−1.8997E−05	3.8628E−04	−2.3422E−04	1.5204E−04
20	−9.2157E−06	−1.9965E−04	−9.1358E−05	−8.1167E−06	3.5974E−04	−1.3620E−04	1.3328E−04
30	−1.3823E−05	−1.8225E−04	−9.8026E−05	2.7633E−06	3.3320E−04	−3.8169E−05	1.1451E−04
40	−1.8430E−05	−1.6485E−04	−1.0470E−04	1.3643E−05	3.0667E−04	5.9857E−05	9.5741E−05
50	−2.3037E−05	−1.4745E−04	−1.1136E−04	2.4523E−05	2.8013E−04	1.5788E−04	7.6974E−05
60	−2.7645E−05	−1.3005E−04	−1.1803E−04	3.5403E−05	2.5359E−04	2.5591E−04	5.8207E−05
70	−3.2252E−05	−1.1264E−04	−1.2470E−04	4.6283E−05	2.2706E−04	3.5394E−04	3.9440E−05
80	−3.6859E−05	−9.5243E−05	−1.3137E−04	5.7163E−05	2.0052E−04	4.5196E−04	2.0672E−05
90	−4.1466E−05	−7.7841E−05	−1.3804E−04	6.8042E−05	1.7398E−04	5.4999E−04	1.9053E−06

The error in the LCM solution increases as α increases. While the relative errors in the values of I_l and I_r may not vary significantly as α is increased, the effect of those errors on the solution would be expected to be greater as the source term increasingly dictates the solution shape. The opposite is true for some of the FVM schemes. In all cases the errors increase in an apparently linear fashion over the range presented (as is clear from Figure 22). There are a number of possible errors leading to discretization errors in the FVM solutions:

1. Errors due to the approximation of the average of $S(x)$ over the length of each volume/element.
2. Errors due to the approximation of $d\phi/dx$ at the volume boundaries in the finite volume scheme. For evenly spaced nodes, this error is dependent on the third spatial derivative of $\phi(x)$
3. Errors due to the values of D used at the volume faces. These will only occur in the vicinity of the discontinuities in this test and will depend on the node positions and the approximation method used. The results in Table 8 are for models with the same node spacing so the errors are only dependent on the method of approximation
4. Errors in the approximation of the integral of $K\phi$ used in implementing the FVM methods (as outlined in Appendix E). In these tests, that will depend on how closely the piecewise-linear approximation of $\phi(x)$ used matches the actual solution

while there is only one source of errors in the LCM solution, the approximation of $S(x)$ with a piecewise-constant function.

Testing has shown that the first, second and third spatial derivatives of the solution vary linearly with α in this example. It would be expected then that the various sources of error in the FVM results would also vary linearly with α. The different FVM implementations only differ in how the diffusion term is approximated, but those differences can be significant as is clear from Figure 22.

As expected, the errors in the LCM solutions approach 0 as α approaches 0. They also vary with α in a linear manner in this case. For larger α values, some of the FVM schemes produce more accurate results than the LCM method. That is not surprising since errors from different sources in the FVM schemes may be positive or negative, and for certain problems they will tend to cancel each other out.

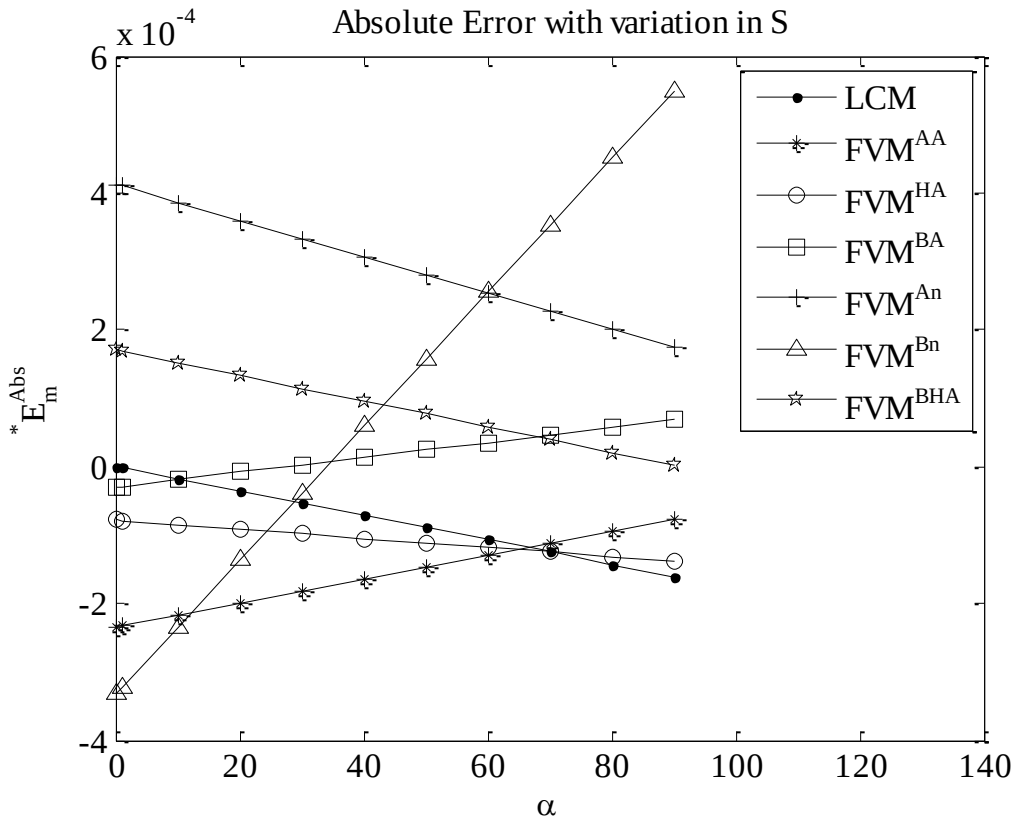

Figure 22: Data in Table 8 in chart form.

3.3.5 Test 5: Consistency of convergence with *D* and *S* piecewise-constant

This test is similar to Test 4 but, in this case, only $K(x)$ varies continuously over space. Figure 23(a) shows the solution with $K(x) = 1 + x^2$. Figure 23(b) shows how the estimated relative errors at the midpoint of the domain vary with the node spacing. Again, it can be seen that the LCM method is significantly more accurate than the FVM schemes tested. Table 9 lists the equivalent solution values along with estimates of the order of convergence. It is clear that none of the FVM solutions converge in a consistent manner. The LCM method, however, converges in a consistently second order manner as h is decreased.

As in Test 4, the highly accurate solution used to estimate the errors was found using Richardson Extrapolation. Table 10 lists the error values plotted in Figure 23(b). It is clear that the LCM scheme is significantly more accurate in this test than the FVM schemes for all node spacings used.

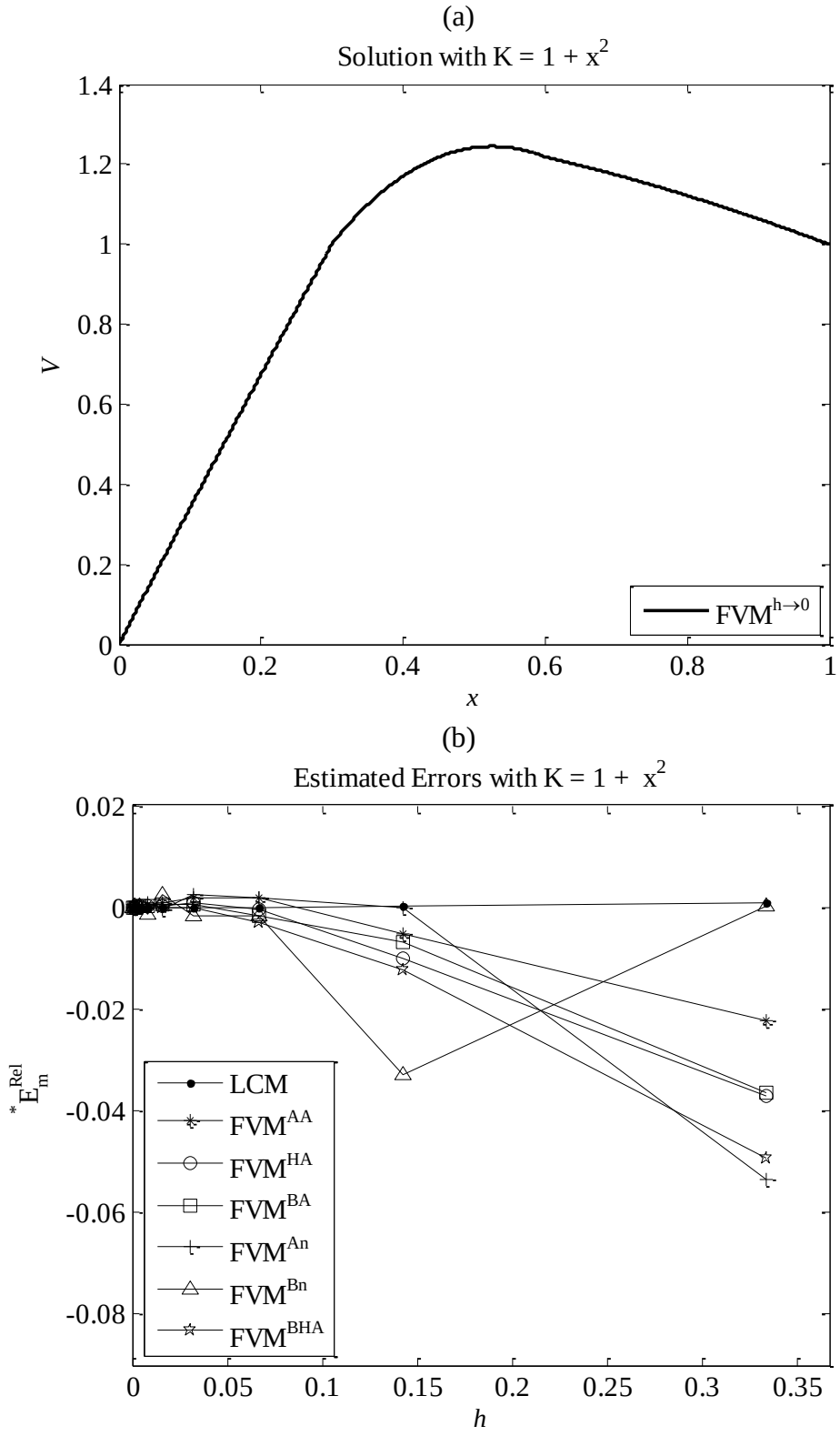

Figure 23: Solution for Test 5 (details of which are given in Table 2) with $\alpha = 1$, (a). The problem has three layers with discontinuities at $x = 0.3$ and $x = 0.6$. The variation in the relative error at $x = 0.5$ with node spacing is also shown, (b).

Table 9: Numerical solution at the midpoint of the domain for both LCM and FVM schemes for different numbers of nodes. The estimated orders of the errors are given in bold font.

N	LCM	FVM^{AA}	FVM^{HA}	FVM^{BA}	FVM^{An}	FVM^{Bn}	FVM^{BHA}
5	1.240758	1.268820	1.287378	1.286618	1.307724	1.241082	1.302625
9	1.241171	1.247864	1.253790	1.249562	1.241211	1.282062	1.256565
17	1.241228	1.239057	1.241709	1.243340	1.251443	1.250688	1.244830
	2.8	**1.3**	**1.5**	**2.6**	**2.7**	**0.4**	**2.0**
33	1.241240	1.239050	1.240108	1.240389	1.238341	1.243185	1.241458
	2.3	**10.3**	**2.9**	**1.1**	**−0.4**	**2.1**	**1.8**
65	1.241243	1.240288	1.240943	1.240587	1.241600	1.238248	1.241385
	2.1	**−7.5**	**0.9**	**3.9**	**2.0**	**0.6**	**5.5**
129	1.241243	1.240731	1.241106	1.240845	1.240272	1.242844	1.241290
	2.1	**1.5**	**2.4**	**−0.4**	**1.3**	**0.1**	**−0.4**
257	1.241244	1.240951	1.241112	1.241168	1.241730	1.241607	1.241256
	2.1	**1.0**	**4.7**	**−0.3**	**−0.1**	**1.9**	**1.5**
513	1.241244	1.241079	1.241146	1.241180	1.241058	1.241351	1.241244
	2.0	**0.8**	**−2.5**	**4.8**	**1.1**	**2.3**	**1.6**
1025	1.241244	1.241172	1.241213	1.241195	1.241257	1.241050	1.241244
	2.0	**0.5**	**−1.0**	**−0.4**	**1.8**	**−0.2**	**5.5**
2049	1.241244	1.241209	1.241232	1.241216	1.241180	1.241341	1.241244
	2.0	**1.3**	**1.8**	**−0.5**	**1.4**	**0.0**	**−0.5**

As in Test 4, the absolute errors at the midpoint have been calculated for a range of values of α (where $K = \alpha(1 + x^2)$) and the results are given in Table 10 and plotted in Figure 24. As before, the LCM errors vary in a similar fashion to those for the FVM schemes but are generally significantly smaller than the FVM errors and are 0 when $\alpha = 0$.

Table 10: Estimated relative errors at the midpoint of the domain in the FVM and LCM solutions for Test 5 calculated using different numbers of nodes.

N	LCM	FVM^{AA}	FVM^{HA}	FVM^{BA}	FVM^{An}	FVM^{Bn}	FVM^{BHA}
5	3.9164E−04	−2.2217E−02	−3.7168E−02	−3.6555E−02	−5.3559E−02	1.3045E−04	−4.9452E−02
9	5.8659E−05	−5.3335E−03	−1.0108E−02	−6.7015E−03	2.6590E−05	−3.2885E−02	−1.2344E−02
17	1.2251E−05	1.7619E−03	−3.7516E−04	−1.6889E−03	−8.2168E−03	−7.6088E−03	−2.8896E−03
33	2.8073E−06	1.7675E−03	9.1503E−04	6.8889E−04	2.3386E−03	−1.5642E−03	−1.7270E−04
65	6.6308E−07	7.6961E−04	2.4225E−04	5.2941E−04	−2.8691E−04	2.4132E−03	−1.1423E−04
129	1.6081E−07	4.1341E−04	1.1108E−04	3.2150E−04	7.8252E−04	−1.2891E−03	−3.7672E−05
257	3.9830E−08	2.3557E−04	1.0614E−04	6.0790E−05	−3.9168E−04	−2.9297E−04	−1.0021E−05
513	9.9613E−09	1.3262E−04	7.8544E−05	5.1425E−05	1.4976E−04	−8.6295E−05	−6.4031E−07
1025	2.5414E−09	5.7636E−05	2.4839E−05	3.9317E−05	−1.1025E−05	1.5577E−04	−4.3356E−07
2049	6.8948E−10	2.8064E−05	9.1732E−06	2.2305E−05	5.1212E−05	−7.8200E−05	−1.4497E−07

Table 11: Absolute errors in the solution at the midpoint of the domain for models for Test 5 with $N = 65$ for a range of values of α. Note that the error for LCM with $\alpha = 0$ is due to round−off errors.

α	LCM	FVM^{AA}	FVM^{HA}	FVM^{BA}	FVM^{An}	FVM^{Bn}	FVM^{BHA}
0	3.3705E−09	9.6382E−04	3.0026E−04	6.6233E−04	−3.6458E−04	3.0331E−03	−1.4757E−04
1	8.2302E−07	9.5528E−04	3.0069E−04	6.5712E−04	−3.5613E−04	2.9953E−03	−1.4178E−04
10	7.1605E−06	8.8972E−04	3.0739E−04	6.1826E−04	−2.8513E−04	2.6943E−03	−9.2176E−05
20	1.2397E−05	8.3564E−04	3.1863E−04	5.8813E−04	−2.1614E−04	2.4268E−03	−4.2343E−05
30	1.6250E−05	7.9551E−04	3.3177E−04	5.6736E−04	−1.5628E−04	2.2123E−03	2.0929E−06
40	1.9093E−05	7.6524E−04	3.4548E−04	5.5294E−04	−1.0435E−04	2.0375E−03	4.1490E−05
50	2.1185E−05	7.4202E−04	3.5896E−04	5.4282E−04	−5.9272E−05	1.8934E−03	7.6284E−05
60	2.2713E−05	7.2388E−04	3.7176E−04	5.3562E−04	−2.0139E−05	1.7730E−03	1.0692E−04
70	2.3812E−05	7.0943E−04	3.8361E−04	5.3038E−04	1.3840E−05	1.6713E−03	1.3384E−04
80	2.4583E−05	6.9766E−04	3.9437E−04	5.2642E−04	4.3345E−05	1.5845E−03	1.5743E−04
90	2.5103E−05	6.8783E−04	4.0399E−04	5.2329E−04	6.8955E−05	1.5097E−03	1.78E−04

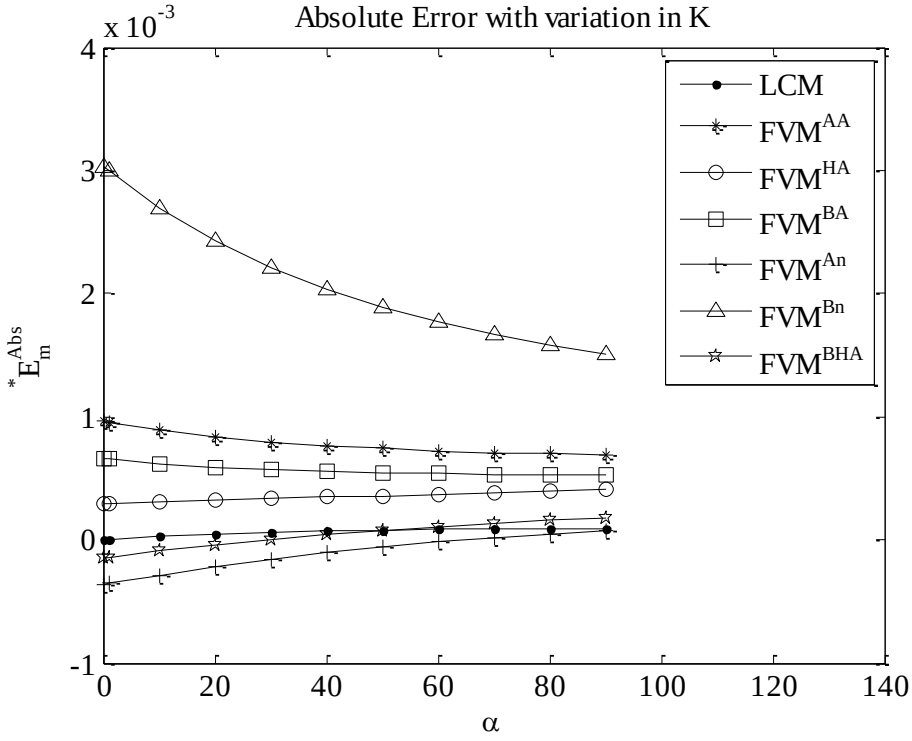

Figure 24: Data in Table 11 shown in chart form.

3.3.6 Test 6: Consistency of convergence with *K* and *S* piecewise-constant

This test is similar to Tests 4 and 5 but, in this case, only $D(x)$ varies continuously over space. Since it is assumed that the values of $D(x)$ are only known at the nodes, only two of the FVM schemes can be implemented, FVM^{An} and FVM^{Hn}.

The results in Figure 25, the data for which is given in Table 12 (and the estimated relative errors in Table 13), are consistent with those from Tests 4 and 5 in that the

LCM scheme is significantly more accurate than the FVM schemes tested, and in that it converges in a consistent manner as *h* is reduced.

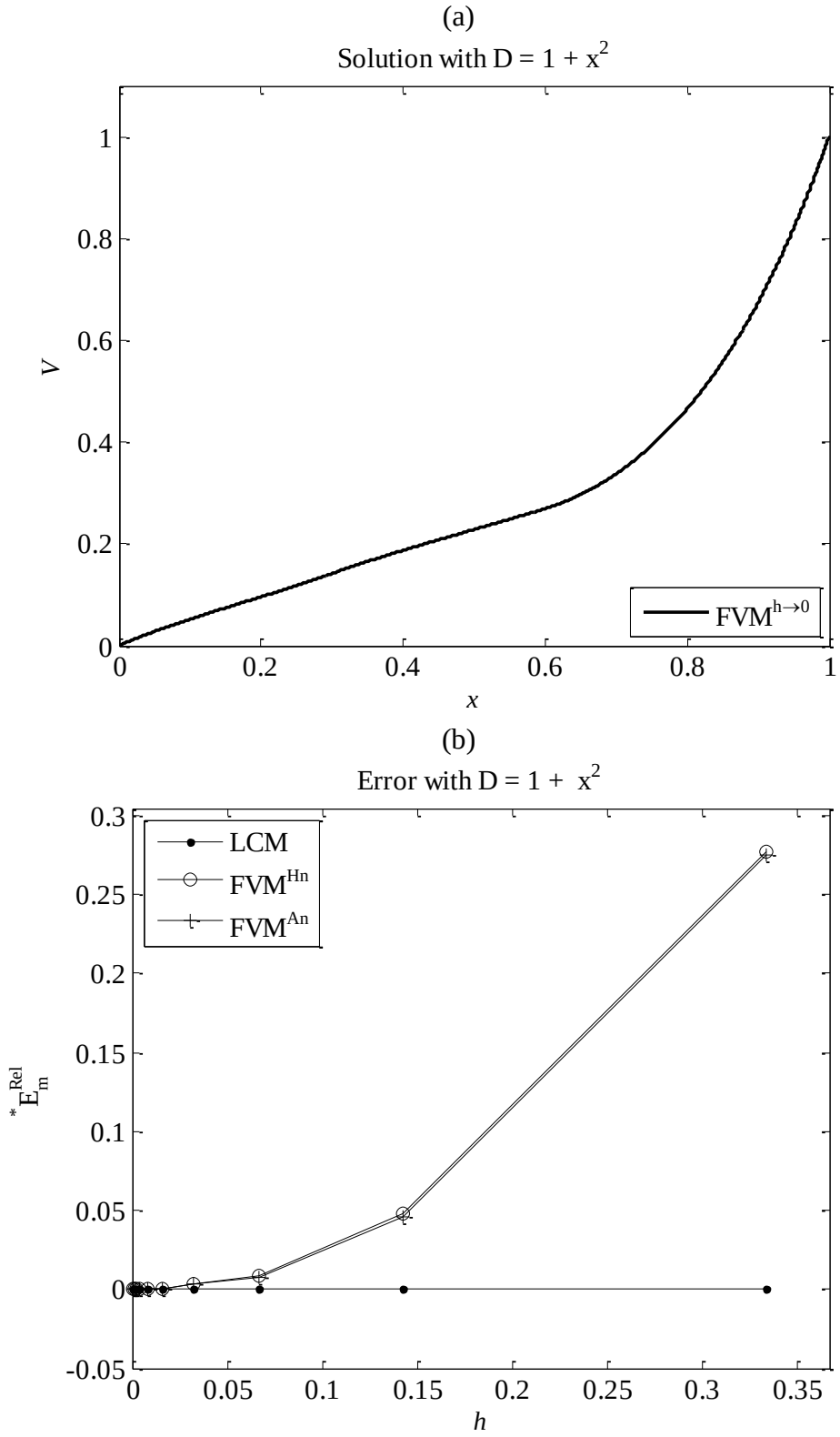

Figure 25: Solution for Test 6 (details of which are given in Table 2) with $\alpha = 1$, (a). The problem has three layers with discontinuities at $x = 0.3$ and $x = 0.6$. The variation in the relative error at $x = 0.5$ with node spacing is also shown, (b).

Table 12: Numerical solution at the midpoint of the domain for LCM and FVM schemes calculated with different numbers of nodes. The estimated orders of the errors are given in bold.

N	LCM	FVM^{An}	FVM^{Hn}
5	0.227817	0.164841	0.165323
9	0.227981	0.217039	0.217427
17	0.227958	0.226050	0.226159
	2.8	**2.5**	**2.6**
33	0.227967	0.227274	0.227301
	1.3	**2.9**	**2.9**
65	0.227971	0.227832	0.227839
	1.5	**1.1**	**1.1**
129	0.227972	0.227937	0.227939
	1.8	**2.4**	**2.4**
257	0.227972	0.227965	0.227966
	2.0	**1.9**	**1.9**
513	0.227972	0.227969	0.227969
	1.9	**2.8**	**2.8**
1025	0.227972	0.227971	0.227971
	2.0	**1.0**	**0.9**
2049	0.227972	0.227972	0.227972
	2.0	**2.3**	**2.4**

Table 13: Estimated relative errors in the FVM and LCM solution for Test 6 at the midpoint of the domain for different numbers of nodes (as plotted in Figure 25).

N	LCM	FVM^{An}	FVM^{Hn}
5	6.3718E−04	2.7692E−01	2.7481E−01
9	2.6580E−04	4.7957E−02	4.6254E−02
17	8.9762E−06	8.4286E−03	7.9508E−03
33	1.8510E−07	3.0632E−03	2.9410E−03
65	4.0184E−07	6.1553E−04	5.8480E−04
129	6.0534E−08	1.5086E−04	1.4316E−04
257	2.7265E−08	2.9131E−05	2.7207E−05
513	8.5126E−09	1.1245E−05	1.0764E−05
1025	3.2929E−09	2.3300E−06	2.2097E−06
2049	1.8758E−09	5.8070E−07	5.5062E−07

Table 14: Absolute errors in the solution at the midpoint of the domain for models for Test 6 with $N = 65$ for a range of values of α. Note that the error for LCM with $\alpha = 0$ is due to round-off errors.

α	LCM	FVM^{An}	FVM^{Hn}
0	6.7833E−12	1.4108E−04	1.4108E−04
1	-9.1288E−08	1.4032E−04	1.3332E−04
10	2.6794E−05	9.8899E−05	5.4206E−05
20	2.9679E−05	6.5202E−05	4.1267E−05
30	2.7432E−05	4.4614E−05	4.5698E−05
40	2.4476E−05	3.0820E−05	5.4615E−05
50	2.1603E−05	2.0811E−05	6.4764E−05
60	1.8956E−05	1.3092E−05	7.5082E−05
70	1.6535E−05	6.8481E−06	8.5180E−05
80	1.4312E−05	1.6065E−06	9.4915E−05
90	1.2253E−05	-2.9277E−06	1.0424E−04

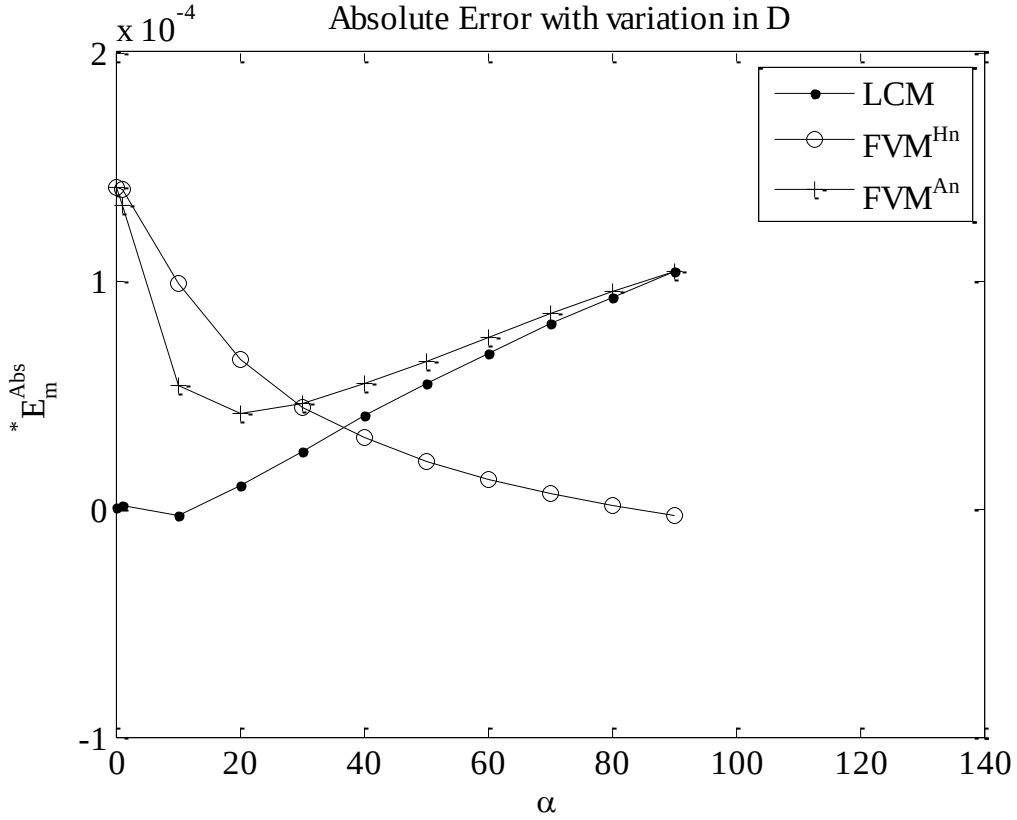

Figure 26: Data in Table 14 presented in chart form.

To summarize:

- LCM produces exact solutions for steady-state reaction-diffusion problems with piecewise-constant coefficients

- It can be applied to general problems with coefficients continuously varying over space on both even and uneven grid with an order of error similar to FVM and higher accuracy than the FVM schemes tested. It may be second order on uneven grids but that has not been established
- When one coefficient varies continuously over space while the others are piecewise constant, the method is, in general, significantly more accurate than FVM
- Results strongly suggest that LCM converges on the exact solution consistently when the node locations do not correspond to the layer boundaries. They also suggest that this is not the case for the FVM schemes tested here

Chapter 4

4 Transient one-dimensional reaction diffusion

4.1 Introduction

There are three steps in implementing steady-state LCM as outlined in the previous chapter:

1. Modelling of the problem in question using a series of uniform TL segments with zero capacitance and inductance
2. Modelling of those segments using a series of lumped-component circuit elements
3. Calculation of the voltages at the nodes given the specified boundary conditions

When extended to modelling reaction-diffusion in the time domain, each of these steps is affected.

Firstly, the basis for the method is the similarity between the reaction-diffusion equation

$$\frac{\partial \phi}{\partial t} = \frac{\partial}{\partial x}\left(D\frac{\partial \phi}{\partial x} \right) - K\phi + S \tag{4.1}$$

and the Telegrapher's equation for the voltage along a TL

$$C_d \frac{\partial V}{\partial t} = \frac{\partial}{\partial x}\left(\frac{1}{R_d}\frac{\partial V}{\partial x} \right) - G_d V + I_d \tag{4.2}$$

It is clear that in transient LCM, the TL being modelled must have non-zero distributed capacitance, C_d.

Secondly, it is not possible to have a lumped-component circuit element that behaves under transient conditions (in terms of the input and output currents and voltages) in exactly the same manner as a uniform TL segment (or a series of uniform TL segments) with distributed capacitance. Therefore, unlike in steady state, this step, in time-domain modelling, introduces errors.

Thirdly, the voltages at the nodes must now be calculated over time and so a time-stepping technique is required. Further errors will be introduced in the solution because of temporal discretization.

In the previous chapter, it was shown that LCM has a number of features that potentially make it superior to FVM when solving steady-state one-dimensional reaction-diffusion problems with piecewise-constant coefficients. In this chapter, tests are carried out to investigate whether or not those advantages are maintained under transient conditions. LCM solutions are compared with those from equivalent FVM schemes in terms of accuracy and convergence, and TLM time-stepping schemes are tested for both LCM and FVM.

In the testing presented in Chapter 3, a variety of methods have been used for calculating D at the control volume faces in FVM implementations. The accuracy and consistency of each approximation depends on the situation being modelled and no clear pattern can be seen in the results. In order to reduce the quantity of transient results presented in this chapter, and, since, in literature, for piecewise-constant coefficients, the harmonic mean approximation is recommended [10], in most cases only results obtained using it are presented here (i.e., unless otherwise stated, the FVM results given below have been obtained using the FVM^{HA} scheme).

Since analytical solutions are not readily available for transient problems, benchmark numerical solutions, as detailed in section 2.3, are used here when estimating errors. The spatial errors for the benchmark solutions have been kept small by using a node spacing that is at least one quarter of the smallest node spacing used in each test. The time-stepping errors have been minimized by using the 4th order Runge-Kutta methods,

implemented using the MATLAB ode45 function [95], with a relative tolerance of 1×10^{-7} (i.e. any time-stepping error is less than 1×10^{-7} times the solution value [96]).

4.2 Equations for TL segments and lumped-component circuit elements

The equation governing the voltage along a uniform TL can be derived from the equivalent equation for a more general TL derived in Appendix B. For a uniform TL segment with constant C_d, this simplifies to Eq. (4.2).

In steady state, the LCM equations are derived by solving the first order telegrapher's equations analytically for a uniform TL segment to find the I/O relationship. For transient modelling, that method is not possible because closed-form solutions of the relevant equations

$$\frac{\partial I(x,t)}{\partial x} = I_d - G_d V(x,t) - C_d \frac{\partial V(x,t)}{\partial t} \tag{4.3}$$

and

$$\frac{\partial V(x,t)}{\partial x} = -L_d \frac{\partial I(x,t)}{\partial t} - I(x,t) R_d \tag{4.4}$$

are difficult to solve analytically. A solution can, however, be found for the quasi-steady-state situation, where the current and voltages are varying sinusoidally over time, using a phasor analysis.

If the voltage and current at the "input" of a uniform segment with distributed capacitance are given by

$$V_i = V(0,t) = V_{\max} \cos(\omega t + \varphi) \tag{4.5}$$

$$I_i = \tilde{I}(0,t) = I_{\max} \cos(\omega t + \theta) \tag{4.6}$$

they allow Equations (4.3) and (4.4) to be solved. Coverting these to complex sinusoidal form, substituting into Equations (4.3) and (4.4), and solving gives

$$\begin{bmatrix} V_o \\ I_o \end{bmatrix} = \begin{bmatrix} \alpha & -\beta\eta/\mu \\ -\beta\eta/R_d & \alpha \end{bmatrix} \begin{bmatrix} V_i \\ I_i \end{bmatrix} + \begin{bmatrix} (1-\alpha)/\mu \\ \beta/\eta \end{bmatrix} I_d \tag{4.7}$$

where

$$\alpha = \cosh(\eta \Delta x) \tag{4.8}$$

$$\beta = \sinh(\eta \Delta x)$$

$$\eta = \sqrt{\mu R_d} \tag{4.9}$$

$$\mu = G_d + jC_d\omega \tag{4.10}$$

This relationship is similar to the one derived in section 3.2.1, for steady-state LCM. The equivalent I/O relationship for the lumped-component circuit element shown in Figure 27 is

$$\begin{bmatrix} V_o \\ I_o \end{bmatrix} = \begin{bmatrix} (G_l + j\omega C_l)R + 1 & -R \\ \Pi & (G_r + j\omega C_r)R + 1 \end{bmatrix} \begin{bmatrix} V_i \\ I_i \end{bmatrix} + \begin{bmatrix} -RI_l \\ I_r + (G_r R + j\omega C_r R + 1) I_l \end{bmatrix} \tag{4.11}$$

where

$$\Pi = -G_l - G_r - R\left(G_l G_r - C_l C_r \omega^2 + j\,\omega(C_l G_r + C_r G_l)\right) - j\,\omega(C_l + C_r) \tag{4.12}$$

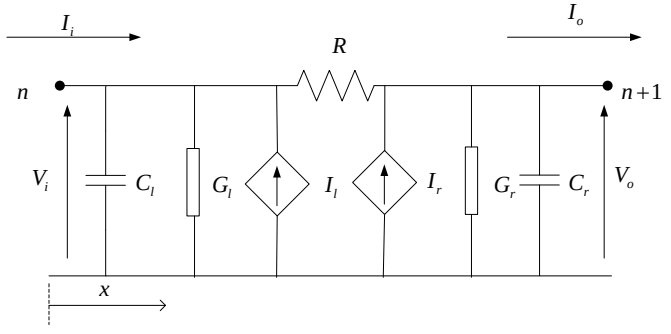

Figure 27: Lumped-component circuit element with capacitors.

In order to implement the method as before, the coefficients in Equations (4.7) and (4.11) must be equated, giving equations for the lumped-component circuit parameters

in terms of the distributed properties of the TL segment being modelled. Unfortunately, this cannot be done for all values of ω. As a result, an alternative approach is required.

4.3 Derivation of transient LCM equations

The alternative approach taken here involves calculating R, G_l, G_r, I_l and I_r as in section 3.2.1 (i.e. using values that will make the lumped-component circuit element equivalent to the TL segment being modelled under steady-state conditions). That leaves the question of how to calculate the values of C_l and C_r. Values for C_l and C_r cannot be found that will make the two equivalent and so an alternative method is employed.

For any very short section of a uniform TL segment of length Δx, the current flowing into the distributed capacitance is $C_d \Delta x dV/dt$. This current affects the currents at the ends of the TL, which consequently affects the voltages at those points. How it affects the currents at the ends depends on the variation in R_d and G_d along the TL segment. The two capacitors in the equivalent lumped-component element should affect the currents at both its ends in the same way, and so the calculation of their values must take into account that variation.

Similarly, for a short TL segment, the current flowing out of the distributed current source is $I_d \Delta x$. Again, the additional current at either end of the segment that results from this, depends on how R_d and G_d vary along the segment. It is already known how to calculate the values of the two current sources in the lumped-component element to account for that, i.e. the relationships between I_l and I_r and the distributed properties, I_d, R_d and G_d, are known. Assuming that dV/dt is constant over the length of the segment, the relationship between C_l, C_r and the distributed properties C_d, R_d and G_d must be similar. Given this assumption, the two lumped capacitors can be calculated as

$$C_l = \frac{\mathrm{b}_{\mathrm{TL}\,1,1} - 1}{\mathrm{A}_{\mathrm{TL}\,1,2}} C_d \tag{4.13}$$

and

$$C_r = \frac{\mathrm{b}_{\mathrm{TL}\,2,1} - \dfrac{\mathrm{b}_{\mathrm{TL}\,1,1}}{\mathrm{A}_{\mathrm{TL}\,1,2}}}{\mathrm{A}_{\mathrm{TL}\,2,2}} C_d \tag{4.14}$$

Testing has shown that the use of these equations produces highly accurate results.

If a section between two nodes is composed of more than one uniform TL segment, then the capacitances for the lumped-component circuit element that represents the entire TL section are calculated in the same way as is used for the current sources (as presented above for steady-state modelling).

As with R_d, G_d and I_d the distributed capacitance, C_d, of a TL represents a certain property in a reaction-diffusion equation. For example, in a heat equation given as

$$\rho c \frac{\partial \phi}{\partial t} = \frac{\partial}{\partial x}\left(D \frac{\partial \phi}{\partial x} \right) - K\phi + S \tag{4.15}$$

the distributed capacitance in the TL is analogous to the thermal capacitance ρc of the material through which the heat flows. If this property varies over space and/or time, then C_d in the TL analogue must vary in a similar manner. Note that such variations are not implemented here, but could be implemented in LCM for reaction diffusion by setting C_d equal to ρc.

The last step in implementing LCM for transient reaction-diffusion is to determine the voltage at a node n, in the equivalent lumped-component circuit, in terms of the voltages at adjacent nodes. Consider two elements in a model that connects three nodes as shown in Figure 28. It is straightforward to show that

$$\left(C_{l,n+1} + C_{r,n}\right)\frac{dV_n}{dt} = \left(\frac{V_{n+1} - V_n}{R_{n+1}}\right) - \left(\frac{V_n - V_{n-1}}{R_n}\right) - V_n\left(G_{r,n} + G_{l,n+1}\right) + I_{r,n} + I_{l,n+1} \tag{4.16}$$

The time derivative term at the left hand side of Eq. (4.16) can be discretized using standard methods commonly used for FVM and finite difference modelling.

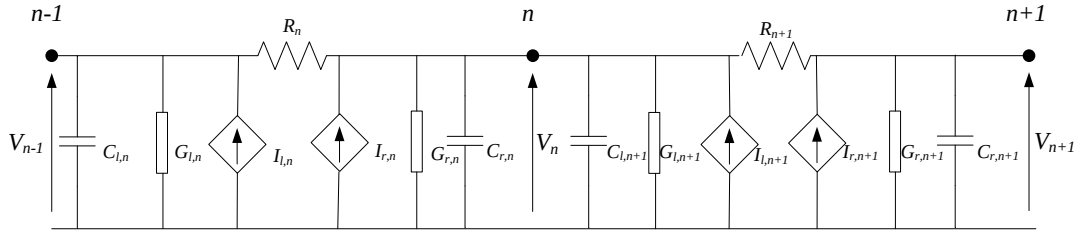

Figure 28: Three nodes in a lumped-component circuit model for the solution of transient reaction-diffusion problems.

4.4 Time-stepping and associated errors

Under transient conditions, LCM does not produce exact solutions when the coefficients are piecewise constant. For the tests that follow, a first-order explicit time–stepping scheme is used. A TLM time-stepping method is also presented and tested for both LCM and FVM schemes. Spatial discretization errors are examined under transient conditions 4.5.

In all the tests, the time step Δt is constant, but there is no reason why Δt could not be varied over time if required [67, 97-98].

4.4.1 TLM as time-stepping method for LCM

Unlike in standard TLM, in which the method is used to directly model a transmission line that approximates the problem being solved, this section uses TLM as a time-stepping method for LCM by modelling the capacitors in the lumped-component circuit. The capacitors in the circuit are first replaced by uniform lossless TL segments as shown in Figure 29. These have the required capacitance, but in order to allow the TLM method to be used, they must also have non-zero inductance. This will lead to wave-like errors as in standard TLM [67, 72, 97, 99]; nevertheless, these errors will tend towards zero as the time step length is reduced. These errors are examined in Chapter 5.

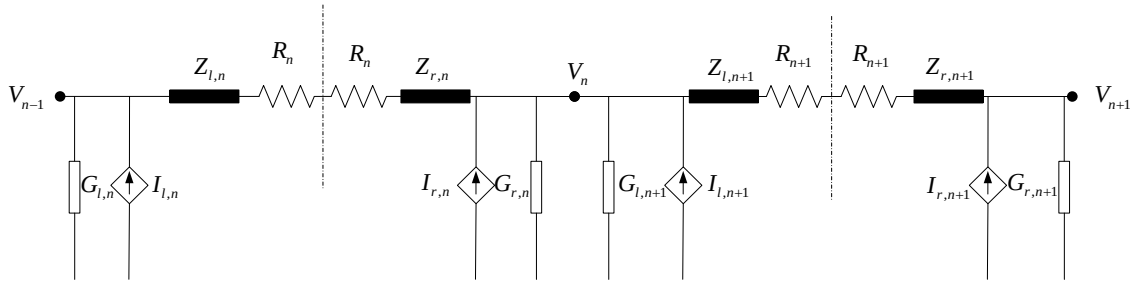

Figure 29: Two lumped-component circuit elements with capacitors modelled by TL segments.

In order to have the correct capacitance, and to ensure that pulses arriving at one end of any TL segment will arrive at the other end $\Delta t/2$ later, the two TL segments between nodes $n-1$ and n must have impedances

$$Z_{r,n} = \frac{\Delta t}{2C_r^n} \text{ and } Z_{l,n+1} = \frac{\Delta t}{2C_l^{n+1}} \tag{4.17}$$

For a pulse scattered to the left from a node at a given time step, the fraction that will arrive at the adjacent node to the left at the next time step is shown in Appendix A to be

$$\tau_{LR} = \frac{2Z_r}{Z_r + Z_l + 2R} \tag{4.18}$$

The fraction of such a pulse that will be reflected back to the node from which it originated is

$$\rho_{LR} = 1 - \frac{Z_l \tau_{LR}}{Z_r}$$

For pulses scattered to the right from the node, the equivalent transmission and reflection coefficients are

$$\tau_{RL} = \frac{2Z_l}{Z_r + Z_l + 2R} \text{ and } \rho_{RL} = 1 - \frac{Z_r \tau_{RL}}{Z_l} \tag{4.19}$$

According to Kirchhoff's current law, the sum of the currents at node n at any instant must be zero, giving

$$\frac{Vil_n^k}{Z_{r,n}} + \frac{Vir_n^k}{Z_{l,n+1}} + I_{r,n} + I_{l,n+1} = \frac{Vsl_n^k}{Z_{r,n}} + \frac{Vsr_n^k}{Z_{l,n+1}} + G_{r,n}V_n^k + G_{l,n+1}V_n^k \tag{4.20}$$

As in standard lossy TLM, the voltage scattered from a node at time step k is equal to the node voltage minus the voltage incident at the node at that instant, and so

$$Vsl_n^k = V_n^k - Vil_n^k \tag{4.21}$$

and

$$Vsr_n^k = V_n^k - Vir_n^k \tag{4.22}$$

Using Equations (4.21) and (4.22) to replace the scattered voltages in Eq. (4.20), and rearranging gives the node voltage in terms of the incident voltages

$$V_n^k = \frac{2Vil_n^k / Z_{r,n} + 2Vir_n^k / Z_{l,n+1} + I_{r,n} + I_{l,n+1}}{1/Z_{r,n} + 1/Z_{l,n+1} + G_{r,n} + G_{l,n+1}} \tag{4.23}$$

The incident voltages at the next time step are then

$$Vil_n^{k+1} = \tau_{LR,n} Vsr_{n-1}^k + \rho_{RL,n} Vsl_n^k \tag{4.24}$$

and

$$Vir_n^{k+1} = \tau_{RL,n+1} Vsl_{n+1}^k + \rho_{LR,n+1} Vsr_n^k \tag{4.25}$$

At time $t = 0$, either the incident or the scattered voltages can be used to initialize the model. If the initial incident voltages from right and left at each node are equal (which is standard in TLM diffusion models) then the initial scattered pulses must be

$$Vsl_n^0 = Vsr_n^0 = V_n^0 - \frac{\left(V_n^0\left(1/Z_{r,n} + 1/Z_{l,n+1} + G_{r,n} + G_{l,n+1}\right) - I_{r,n} - I_{l,n+1}\right) Z_{r,n} Z_{l,n+1}}{2\left(Z_{r,n} + Z_{l,n+1}\right)} \tag{4.25}$$

In all models tested below, there are nodes positioned at the domain boundaries and only Dirichlet boundary conditions are implemented. The node voltages at the boundaries are simply fixed at the desired values.

4.4.2 TLM as a time-stepping method for FVM

Consider the FVM approximation of a reaction-diffusion equation

$$\frac{\partial \phi_n}{\partial t} h = D_{n+\frac{1}{2}} \frac{\left(\phi_{n+1} - \phi_n\right)}{h} - D_{n-\frac{1}{2}} \frac{\left(\phi_n - \phi_{n-1}\right)}{h} - K_n \phi_n + S_n h \tag{4.26}$$

When compared with the equivalent equation for LCM

$$\left(C_{l,n+1} + C_{r,n}\right)\frac{dV}{dt} = \left(\frac{V_{n+1} - V_n}{R_{n+1}}\right) - \left(\frac{V_n - V_{n-1}}{R_n}\right) - V_n\left(G_{r,n} + G_{l,n+1}\right) + I_{r,n} + I_{l,n+1} \tag{4.27}$$

it is clear that a lumped-component circuit with parameters

$$R_{n+1} = \frac{h}{D_{n+\frac{1}{2}}},\ R_n = \frac{h}{D_{n-\frac{1}{2}}} \tag{4.28}$$

$$I_{r,n} + I_{l,n+1} = S_n h \tag{4.29}$$

$$G_{r,n} + G_{l,n+1} = K_n h \tag{4.30}$$

$$C_{r,n} + C_{l,n+1} = h \tag{4.31}$$

is analogous to the FVM approximation. Solving the equations for the voltage at nodes in such a circuit is the same as solving the FVM equations. As with LCM, the capacitors can be replaced with TL segments and the time stepping can be performed using TLM as described above.

4.4.3 Testing of the TLM time-stepping scheme for LCM and FVM

To test the two schemes, a problem involving heat conduction in a plate with piecewise-constant coefficients is considered here. The domain consists of three physical layers with piecewise-constant coefficients $D = \{0.02,0.08,0.05\}\text{cm}^2/\text{s}$, $S = \{0.04,0.6,0.14\}$ °C/s and $K = \{0.2,0.4,0.6\}\text{s}^{-1}$, as shown in . The node spacing is $h = 0.1$ cm with discontinuities at $x = 0.3$ cm and $x = 0.6$ cm. The boundary conditions (i.e. the temperatures at the two faces of the plate) are $V(0,t) = 0$ and $V(1,t) = 1$, and the initial conditions are $V(x,0) = 0$.

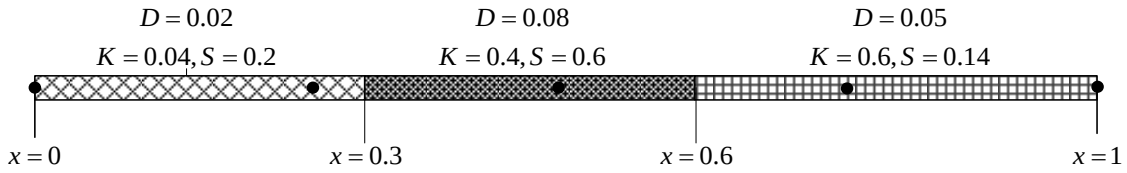

Figure 30: Problem geometry, coefficients and the positions of $N = 5$ evenly spaced nodes.

Values of the solution at $x = 0.5$cm and $t = 1$s are shown in Figure 31 for a range of time-step lengths. The values labeled LCM_{TLM} and FVM_{TLM} have been obtained using TLM time-stepping while those labelled LCM and FVM have been obtained using first-order explicit (i.e. FTCS) time-stepping. These values are also presented in Table 15 along with values of the estimated order of the time-stepping errors. It is clear that, as expected, the TLM time-stepping scheme is second order. It is also simple to implement, explicit, and unconditionally stable.

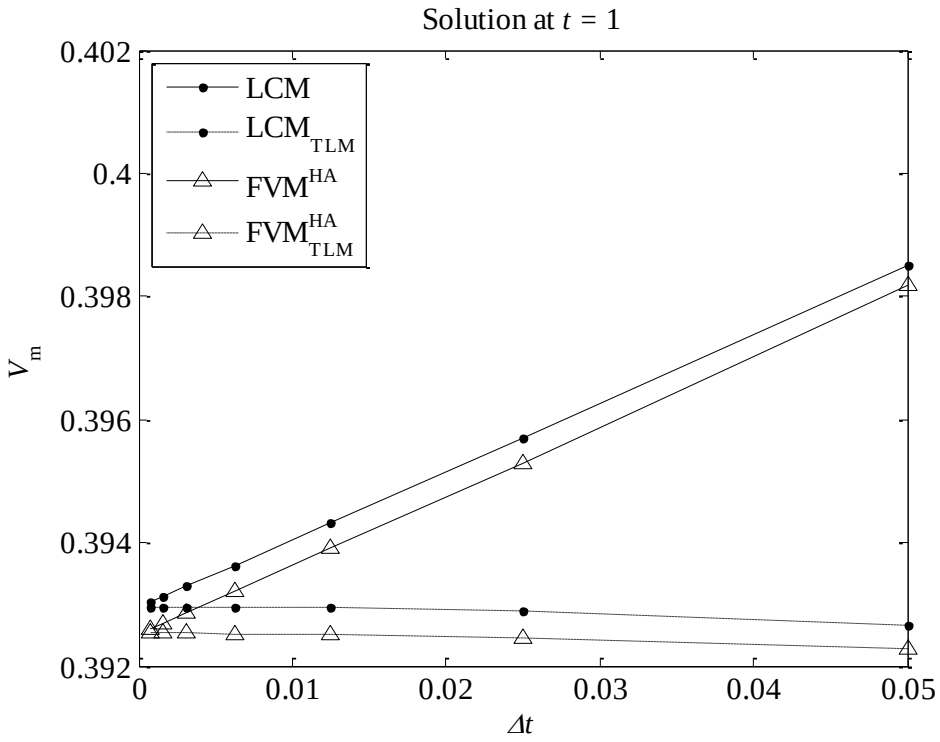

Figure 31: Transient solution values at $x = 0.5$ obtained using a range of time-step lengths. The results labelled LCM and FVM^{HA} are from models using first-order explicit time stepping while the other results are from similar models using TLM time stepping.

Table 15: Values plotted in Figure 31 and corresponding estimates of the orders of the errors.

$1/\Delta t$	LCM_{TLM}	LCM	FVM^{HA}_{TLM}	FVM^{HA}
20	0.392659	0.398511	0.392282	0.398174
40	0.392884	0.395689	0.392467	0.395303
80	0.392939	0.394312	0.392512	0.393904
	2.0	**1.0**	**2.0**	**1.0**
160	0.392952	0.393632	0.392524	0.393213
	2.0	**1.0**	**2.0**	**1.0**
320	0.392956	0.393294	0.392526	0.392869
	2.0	**1.0**	**2.0**	**1.0**
640	0.392957	0.393125	0.392527	0.392698
	2.0	**1.0**	**2.0**	**1.0**
1280	0.392957	0.393041	0.392527	0.392613
	2.0	**1.0**	**2.0**	**1.0**

4.5 Testing and spatial errors under transient conditions

This section examines the spatial errors in transient solutions of reaction-diffusion problems with piecewise-constant coefficients. Such problems are solved exactly by LCM when in steady state. The objective of this section is to determine whether or not the advantages exhibited by LCM in steady state are also exhibited when solutions are changing over time.

4.5.1 Breast model with embedded tumour

Breast thermography is used as a complementary examination method for breast cancer identification. It is a painless procedure involving the use of infrared imaging to measure skin temperature. Since, for a breast with a developing tumour, this temperature can be higher than normal by 1 to 3 degrees, it can be used to detect such tumours [26, 100-101]. Numerical modelling has been used to understand and help predict how tumours of different sizes and at different locations affect the skin temperature.

The model considered here is similar to that examined by Amri et al.[26]. The governing equation used to model the heat transfer in a breast is, when simplified to one dimension,

$$k\frac{\partial^2 T}{\partial x^2} = \rho c\frac{\partial T}{\partial t} + \omega_b \rho_b c_b \left(T - T_a\right) - Q_m \tag{4.32}$$

where ρ, c and k are the tissue density, heat capacity and thermal conductivity, ω_b is the blood perfusion rate, c_b is the blood heat capacity, Q_m is metabolic heat generation rate and T_a is the arterial blood temperature.

In the one-dimensional transient study conducted by Amri et al, the surface of the breast is located at $x = 0$ and the tumour is located at a distance of $x = \lambda$. The surface of the breast is assumed to be at a constant temperature, T_∞, which could be produced through contact with a hot or cold plate. The temperature of the tumour is also assumed to be constant, T_c. The model is illustrated in Figure 32.

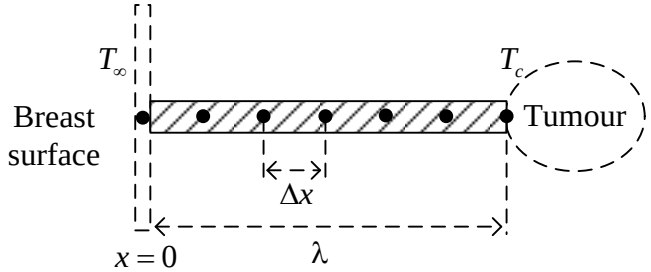

Figure 32: One-dimensional model of the healthy tissue between tumour and breast surface.

The initial temperature is given by [26]

$$T(x,0) = T_a + \frac{Q_m}{\omega_b \rho_b c_b} + \frac{\left(T_c - T_a - Q_m/\omega_b\rho_b c_b\right)\left[\sqrt{A}\cosh\left(\sqrt{A}x\right) + \left(h_0/k\right)\sinh\left(\sqrt{A}x\right)\right]}{\sqrt{A}\cosh\left(\sqrt{A}\lambda\right) + \left(h_0/k\right)\sinh\left(\sqrt{A}\lambda\right)} + \frac{\left(h_0/k\right)\left(T_c - T_a - Q_m/\omega_b\rho_b c_b\right)\sinh\left[\sqrt{A}\left(\lambda - x\right)\right]}{\sqrt{A}\cosh\left(\sqrt{A}\lambda\right) + \left(h_0/k\right)\sinh\left(\sqrt{A}\lambda\right)} \tag{4.33}$$

where $A = \omega_b\rho_b c_b/k$.

The results presented here are for a problem with model length $\lambda = 50$mm, tissue properties of $\rho = \rho_b = 1050\text{kg/m}^3$, $c = c_c = 3800\text{J/kg°C}$, $h_0 = 20\text{W/m}^2$, $\omega_b =$, $1\times10^{-3}\text{s}^{-1}$, $Q_m = 400\text{W/m}^3$, and $k = 0.5\text{W/m°C}$, and with temperatures of $T_c = T_a = 37$°C, $T_f = 28$°C and $T_\infty = 49$°C. The temperature profile between the skin and the tumour has been calculated using transient LCM and the central difference FVM scheme. In both cases, the first order explicit time-stepping scheme has been used. Results are presented in Figure 33 for three points in time, $t = 100$s, $t = 500$s and $t = 1000$s, calculated using $\Delta t = 0.1$s.

The results shown in Figure 33 are in agreement with those by Amri et al and the LCM solutions show good agreement with FVM solutions. This shows that the LCM scheme can be used in a real, though relatively straightforward, transient-modelling situation.

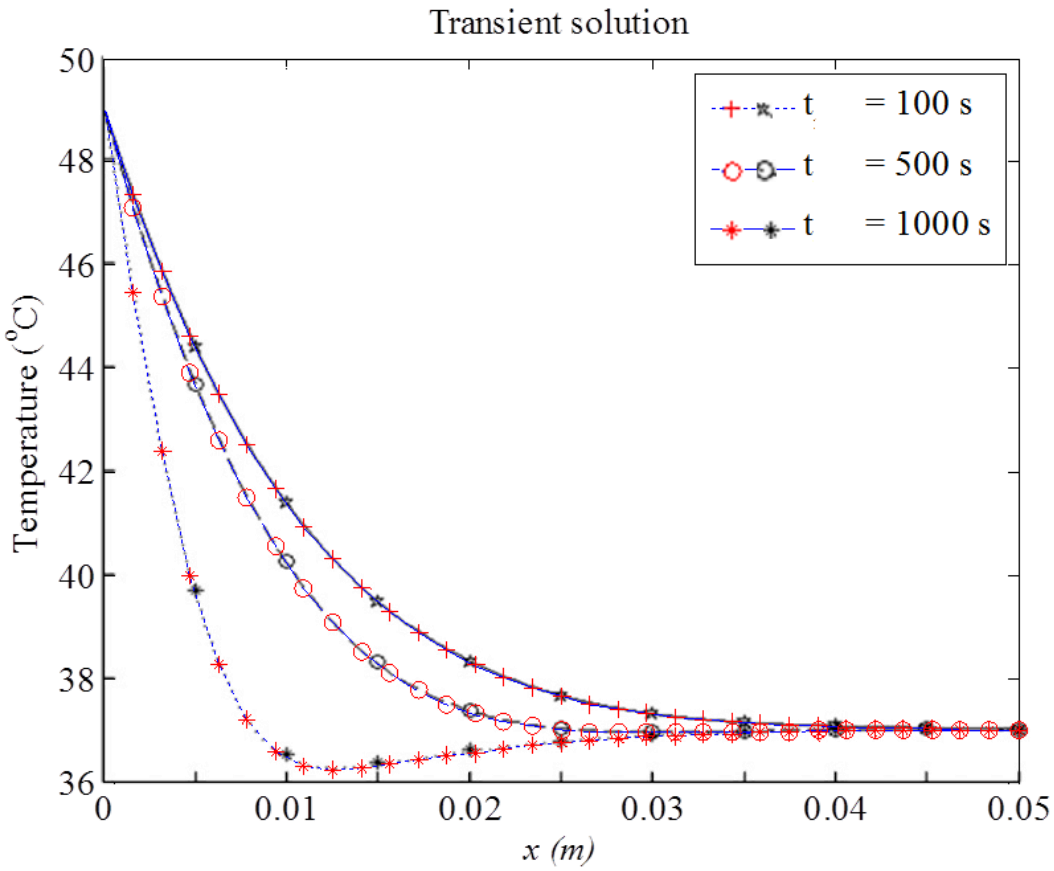

Figure 33: Transient temperature distribution for a one-dimensional breast model at three points in time. The blue lines indicate the LCM results, the red symbols indicate the FVM results, and the gray symbols indicate the equivalent results from Amri et al.[26].

4.5.2 Spatial discretization error for piecewise-constant problems

The purpose of this test is to examine transient models with piecewise-constant coefficients. In Chapter 3, it is shown that LCM is more accurate than FVM in steady state and the question of whether LCM has similar advantages when modelling transient problems is examined here.

Consider a model of a problem with three layers with $D = \{2,3,5\}$, $K = \{25,15,45\}$ and $S = \{2,3,5\}$ over a domain $x \in [0,1]$ with discontinuities at $x = 0.3$, $x = 0.6$, run until $t = 0.008$ with $\Delta t = 1.0\times10^{-7}$. The model end-time has been chosen because voltages are changing rapidly at that point, and the time-step Δt used ensures time-stepping errors in the solution are small compared with the spatial errors. The first-order explicit time-

stepping scheme is used in both LCM and FVM models. The boundary conditions are $V(0,t) = 0$ and $V(1,t) = 1$, and the initial conditions are $V(x,0) = 0$, $x \neq 1$. The solution is shown in Figure 34(a) while estimated errors at $x = 0.5$ are plotted in Figure 34(b) for different node spacings.

The corresponding solution-values are given in Table 16 along with values of the estimated order of the error.

The results suggest that, in terms of accuracy, the advantage of LCM in this case is small when h is large (and further tests with other values of the piecewise-constant parameters suggest that there is not always an advantage). However, LCM converges consistently as the node spacing is reduced while FVM does not (as is the case in steady state) and LCM can be significantly more accurate than FVM when h is small.

The behavior of the error in the LCM and FVM solution over time is different because, for a problem with piecewise-constant coefficients, an LCM model starts with zero spatial error at $t = 0$ and ends with zero spatial error when $t = \infty$, however, an FVM model only has zero spatial error when $t = 0$. As a result, the spatial errors must vary over time in different ways for the two methods.

In general, it would be impossible to develop a numerical method that has zero spatial errors under transient conditions because the initial conditions are only defined at the nodes. In practice this lack of information (the fact that the initial condition between the nodes is not known) manifests itself as a spatial error since it is node-spacing dependent. It would be expected that this error would be similar for all schemes.

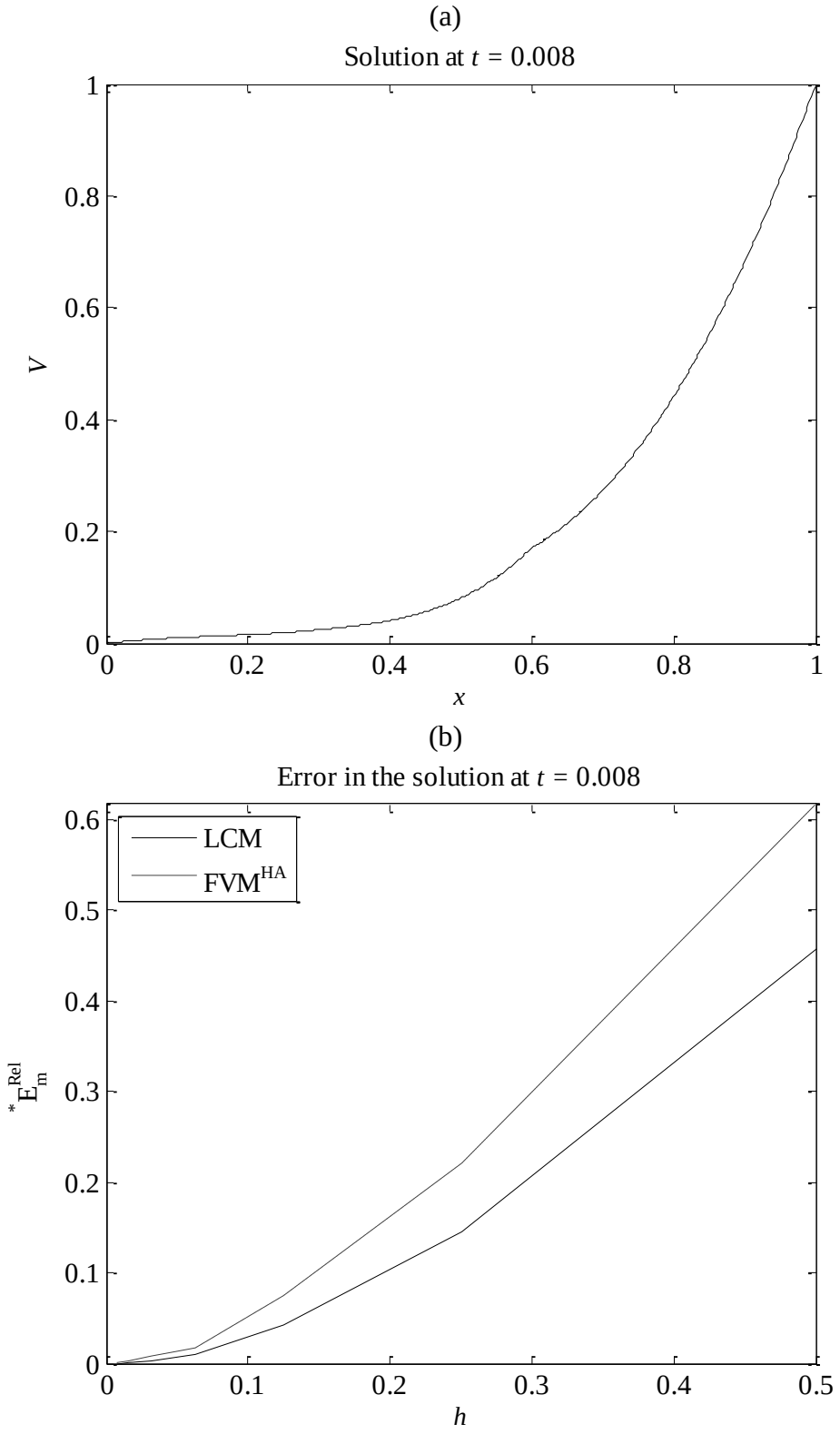

Figure 34: Solution of a problem with piecewise constant coefficient and three layers with discontinuities at x = 0.3 and x = 0.6 (a), and the relative absolute errors in the LCM and FVM solutions for a range of node spacings, (b).

Table 16: Numerical solution values at $x = 0.5$ for LCM and FVM for different numbers of nodes. The estimated orders of the errors are given in bold.

N	LCM	FVM^{HA}
3	0.117953	0.130869
5	0.092720	0.098856
9	0.084372	0.087040
	1.6	**1.4**
17	0.081776	0.082339
	1.7	**1.3**
33	0.081134	0.081675
	2.0	**2.8**
65	0.080971	0.081100
	2.0	**0.2**
129	0.080930	0.081034
	2.0	**3.1**
257	0.080920	0.080940
	2.0	**−0.5**
513	0.080917	0.080948
	2.0	**3.5**

Also, the LCM model has errors due to the modelling of TL segments using lumped-component circuit elements that do not act in the same way except when $\omega = 0$. It would be expected that these errors would be small when ω is small (i.e. when the solution is dominated by low temporal frequency components).

The estimated maximum absolute errors plotted in Figure 34(b) show that LCM under transient conditions cannot produce exact solutions; however, transient LCM solutions can converge consistently even when the nodes do not correspond with discontinuities in the problem coefficients.

4.5.3 Equivalence of FVM and LCM for diffusion problems

This section shows that, for problems with $K = 0$, and with piecewise-constant coefficients that only change at evenly spaced nodes, the LCM scheme is the same as FVM.

Consider the FVM solution of the diffusion equation with a source term of the form

$$\frac{\partial \phi}{\partial t} = \frac{\partial}{\partial x}\left(D \frac{\partial \phi}{\partial x} \right) + S \tag{4.34}$$

on a domain with volumes of equal length h, and material properties that change in a piecewise-constant manner at nodes (i.e. D and S are constant) as illustrated in Figure 35.

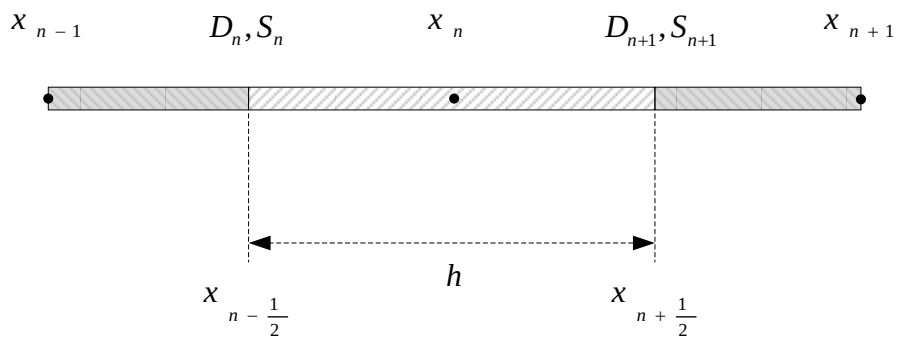

Figure 35: discretized part of the domain showing a single control volume and the problem coefficients.

Integration of Eq. (4.34) over volume n

$$\int_{x_{n-\frac{1}{2}}}^{x_{n+\frac{1}{2}}} \frac{\partial \phi}{\partial t}\Delta x = \int_{x_{n-\frac{1}{2}}}^{x_{n+\frac{1}{2}}} \left(\frac{\partial}{\partial x}\left(D\frac{\partial \phi}{\partial x}\right)\right)\Delta x + \int_{x_{n-\frac{1}{2}}}^{x_{n+\frac{1}{2}}} S\Delta x$$

gives

$$\frac{\partial \phi_n}{\partial t}h = \frac{D_{n+1}}{h}\left(\phi_{n+1}-\phi_n\right) - \frac{D_n}{h}\left(\phi_n - \phi_{n-1}\right) + \left(\frac{S_n + S_{n+1}}{2}\right)h \qquad (4.35)$$

The lumped-component circuit parameters can be found easily in terms of G_d, R_d, I_d and C_d using Equations (3.12) and (3.15), with $G_d = 0$, $R_d = 1/D$, $I_d = S$ and $C_d = 1$, the equivalent LCM equation is then

$$h\frac{dV}{dt} = \frac{D_{n+1}}{h}\left(V_{n+1}-V_n\right) - \frac{D_n}{h}\left(V_n - V_{n-1}\right) + \left(\frac{S_n + S_{n+1}}{2}\right)h \qquad (4.36)$$

This is clearly the same as Eq. (4.35).

If the discontinuities in the materials do not correspond to the nodes, or if $K \neq 0$, then the two schemes are not the same.

4.5.4 Analysis of one source of transient spatial errors in LCM

For transient piecewise-constant problems, a series of TL segments can be an exact analogue for the problem being solved. The only sources of errors in LCM are, therefore, time-stepping errors, which can be made insignificant by using a sufficiently short time-step length, and the fact that the lumped-component circuit elements do not exactly model the TL segments except under steady-state conditions. This section explores this latter source of errors.

The I/O relationships, derived from phasor analysis, for a TL segment and the equivalent lumped-component circuit (i.e. Equations (4.7) and (4.11)) can be written as

$$\begin{bmatrix} V_o \\ I_o \end{bmatrix} = \mathbf{A_{TL}} \begin{bmatrix} V_i \\ I_i \end{bmatrix} + \mathbf{b_{TL}} \quad \text{and} \quad \begin{bmatrix} V_o \\ I_o \end{bmatrix} = \mathbf{A_{LC}} \begin{bmatrix} V_i \\ I_i \end{bmatrix} + \mathbf{b_{LC}}$$

where

$$\mathbf{A_{TL}} = \begin{pmatrix} A_{11}^{TL} & A_{12}^{TL} \\ A_{21}^{TL} & A_{22}^{TL} \end{pmatrix} \text{ and } \mathbf{A_{LC}} = \begin{pmatrix} A_{11}^{LC} & A_{12}^{LC} \\ A_{21}^{LC} & A_{22}^{LC} \end{pmatrix}$$

As stated above, these can only be equal when the angular frequency of the input and output voltage and current phasors, ω, is zero. In this section, the difference between these equations is analyzed.

Only the relative differences in two of the coefficients are examined here. They are

$$dA_{11}^{Rel} = \frac{A_{11}^{LC} - A_{11}^{TL}}{A_{11}^{TL}} \text{ and } dA_{12}^{Rel} = \frac{A_{12}^{LC} - A_{12}^{TL}}{A_{12}^{TL}} \tag{4.37}$$

The equations for the coefficients in the $\mathbf{A_{TL}}$ matrix are given in Eq. (4.7) in terms of the distributed properties of the TL segment. Those for the $\mathbf{A_{LC}}$ matrix are given in Eq. (4.11) in terms of the lumped-component circuit parameters. Using Equations (3.18) to (3.22) to replace the lumped-component circuit parameters in Eq. (4.11) allows the relative differences in the two coefficients to be simplified to

$$dA_{11}^{Rel} = \frac{\cosh\left(h\sqrt{R_d G_d}\right) - \cosh\left(h\sqrt{R_d\left(G_d + j\omega C_d\right)}\right) + \dfrac{C_d\omega\left(\cosh\left(h\sqrt{R_d G_d}\right) - 1\right)j}{G_d}}{\cosh\left(h\sqrt{R_d\left(G_d + j\omega C_d\right)}\right)} \quad (4.38)$$

and

$$dA_{12}^{Rel} = \frac{\sinh\left(h\sqrt{R_d G_d}\right)\left(G_d + j\omega C_d\right)}{\sinh\left(h\sqrt{R_d\left(G_d + j\omega C_d\right)}\right)\sqrt{\dfrac{G_d}{R_d}}\sqrt{R_d\left(G_d + j\omega C_d\right)}} - 1 \quad (4.39)$$

The following tests explore, to a limited extent, how these differences depend on R_d, G_d and h, and how they are related to errors in LCM solutions.

Consider a TL segment with $R_d = 1$, $G_d = 0$, $C_d = 1$, $h = 1/32$. The magnitudes of the relative differences calculated using Equations (4.38) and (4.39) with these settings are shown in Figure 36(a) for a range of ω values. The error at $x = 0.5$ for a problem with the same coefficients with an initial condition of $V(x,0) = 100$ and boundary condition of $V(0,t) = 0$ and $V(1,t) = 100$ is plotted over time in Figure 36(b).

The effect on the results of changing R_d from 1 to 10 is shown in Figure 37. The magnitudes of the relative differences, for a given value of ω, have increased by a factor of 100, however, the rate of change of the solution has decreased by a factor of 10 while the manner of the change has remained the same (since R_d is proportional to one over the diffusion coefficient, and since there is no reaction term in this case). The frequency content of the solution, at any point in time, is therefore lower in the second test (i.e. equivalent values of ω are lower). From the values plotted in Figure 37a, the relative differences between the coefficients for the TL segments and the lumped-component circuits are, therefore, affected by the change in R_d. However, the size of the solution errors is unaffected (as is clear from Figure 36(b) and Figure 37(b)).

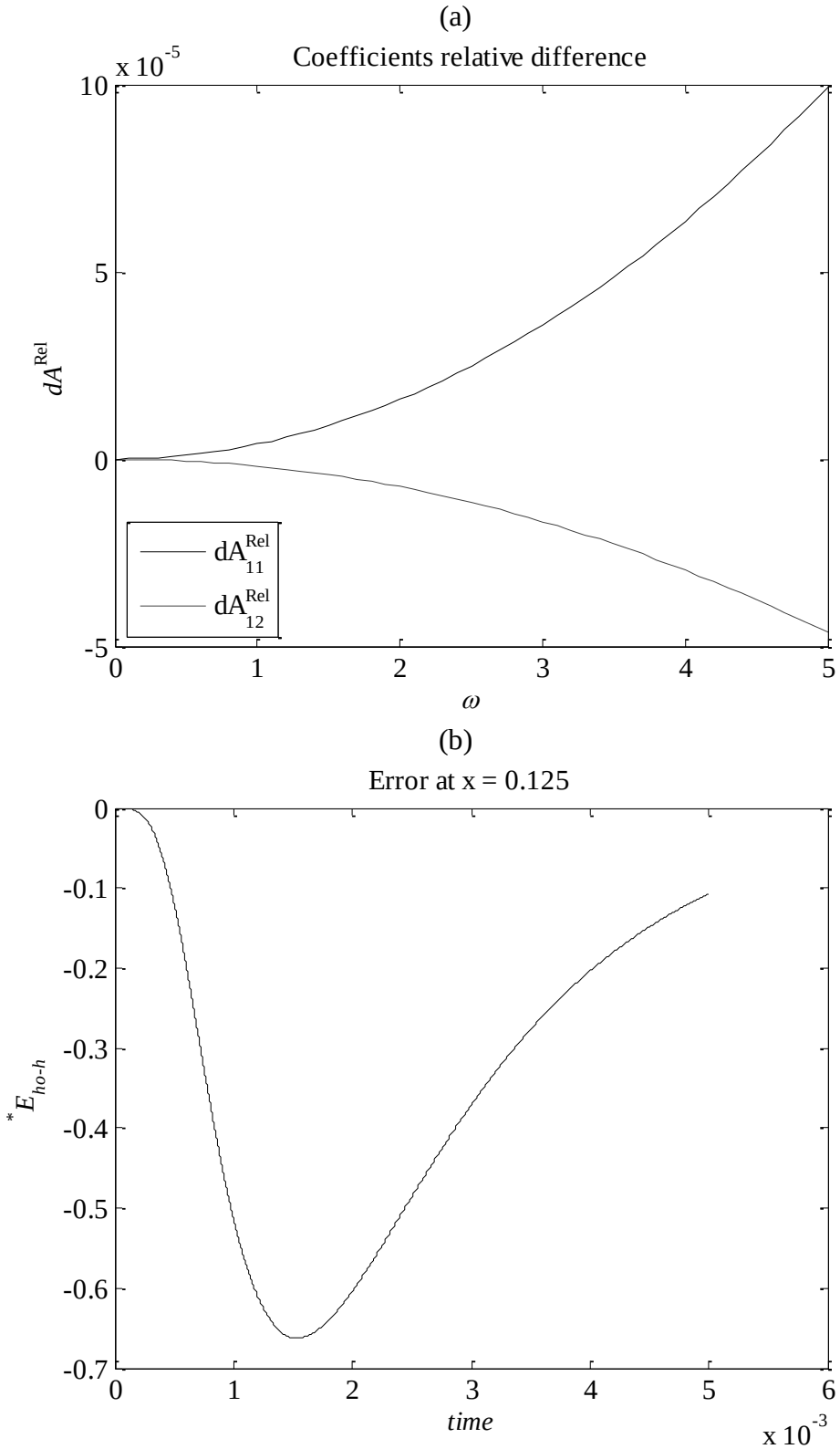

Figure 36: Relative difference between the coefficients of TL and LC I/O equations, (a) and the approximate error in the solution, (b).

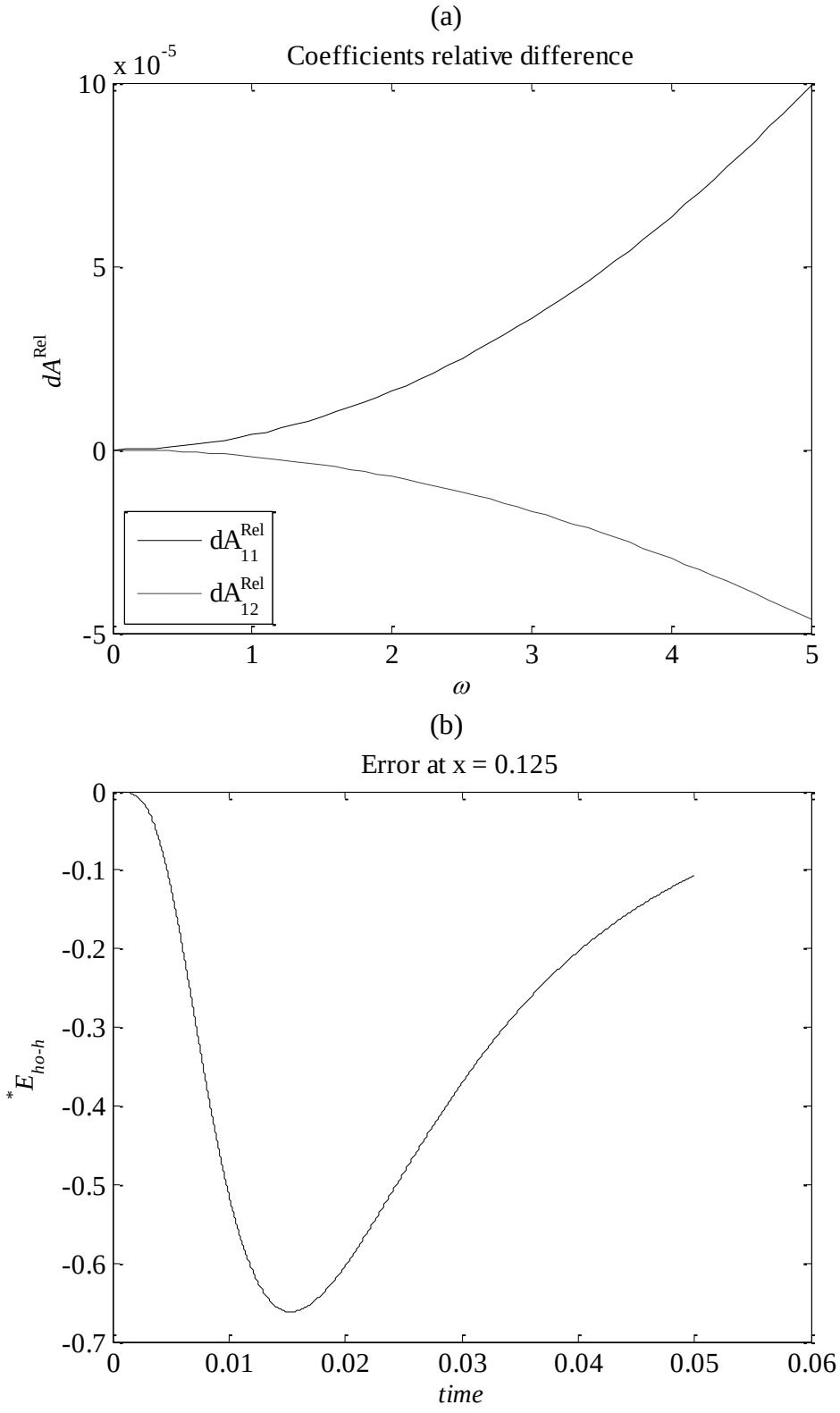

Figure 37: Relative difference between the coefficients of TL and LC I/O equations, (a), and the approximate error in the solution, (b).

Now consider the same problem as above, i.e. with R_d = 10, C_d = 1, h = 1/32 and $\omega \in [0,5]$, but with G_d = 10 instead of zero. The results are shown in Figure 38. The effect of this increase in G_d is a small reduction in the relative differences for a given

value of ω. The effect of the increase in G_d on the frequency content of the transient voltages is not clear, but the rate of change of the solution is not changed significantly. The error in the LCM solution, as shown in Figure 38(b), is slightly reduced. This has been further tested by increasing G_d to 100 for the same problem. The results are shown in Figure 39.

In this case, the relative differences have decreased significantly and so have the solution errors. The unknown in this analysis is again the effect of increasing G_d (i.e. increasing K) on the frequency content of the solution. Further work is required to derive that relationship, at least for simple reaction-diffusion problems, and to then establish if the formulas for the relative differences are useful in predicting spatial discretization errors for simple problems with constant coefficients, and more complex problems with piecewise-constant coefficients.

The next test examines the effect of changing h (i.e. the length of the TL segment) for a given set of parameters ($R_d = 1$, $C_d = 1$, $G_d = 1$, $\omega = 1$). Values of the relative differences, and the corresponding values of the estimated order of convergence, are listed in in Table 17. It is clear that the relationships between the two relative differences and the segment length are fourth order.

Table 17: Relative differences between the TL and LC circuit equation coefficients. The estimated orders of the differences are highlighted in bold.

h	dA_{11}^{Rel}	dA_{12}^{Rel}
0.5	2.08E-03	-1.17E-03
0.25	1.54E-04	-7.52E-05
0.125	1.00E-05	-4.74E-06
	3.7	**4.0**
0.0625	6.34E-07	-2.97E-07
	3.9	**4.0**
0.03125	3.97E-08	-1.85E-08
	4.0	**4.0**
0.015625	2.48E-09	-1.16E-09
	4.0	**4.0**
0.0078125	1.55E-10	-7.24E-11
	4.0	**4.0**
0.00390625	9.70E-12	-4.53E-12
	4.0	**4.0**
0.001953125	6.06E-13	-2.83E-13
	4.0	**4.0**

Further testing and analysis is detailed in the next chapter in which the LCM scheme is extended to model convection-reaction-diffusion.

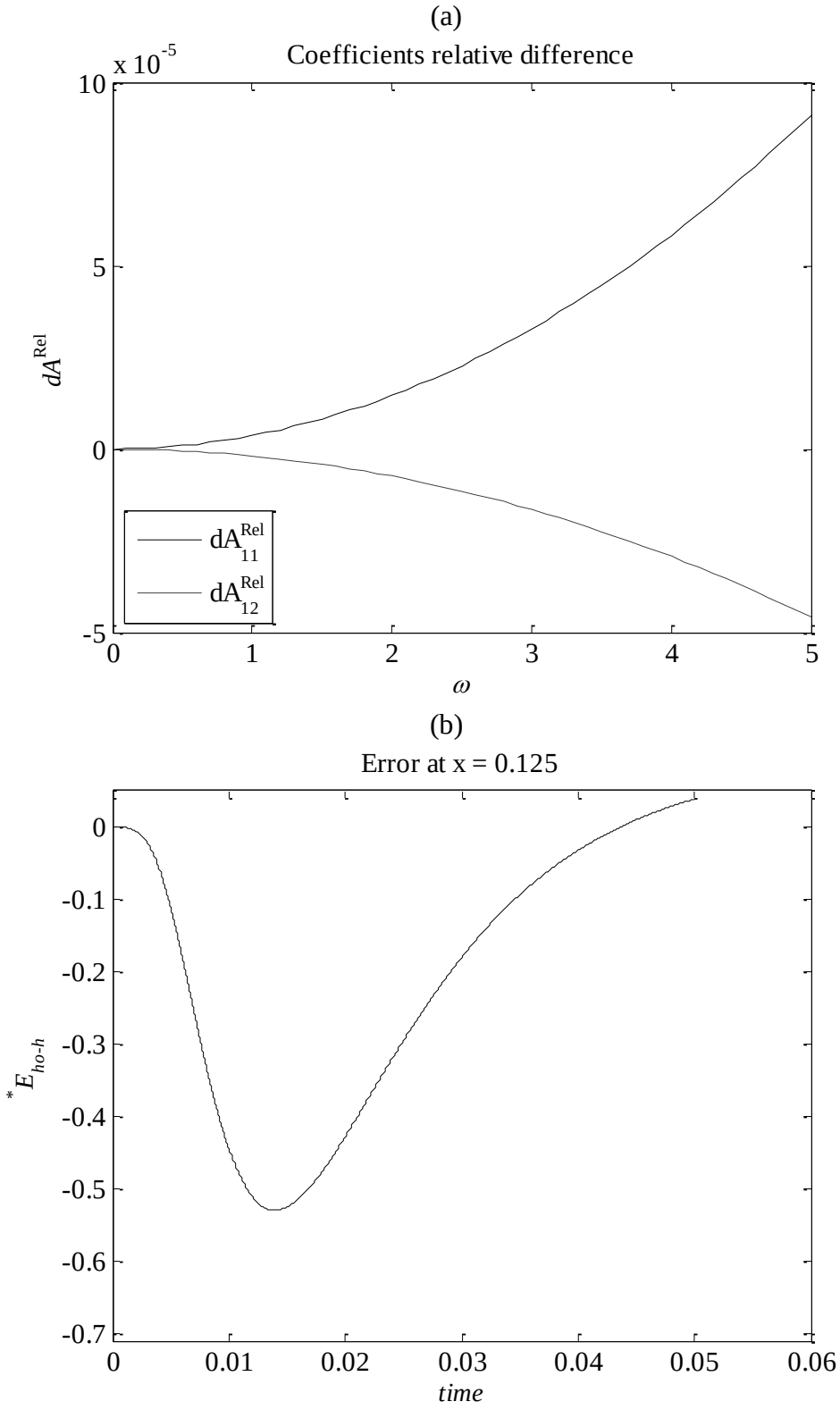

Figure 38: Relative difference between the coefficients of TL and LC I/O equations, (a), and the approximate error in the solution, (b)..

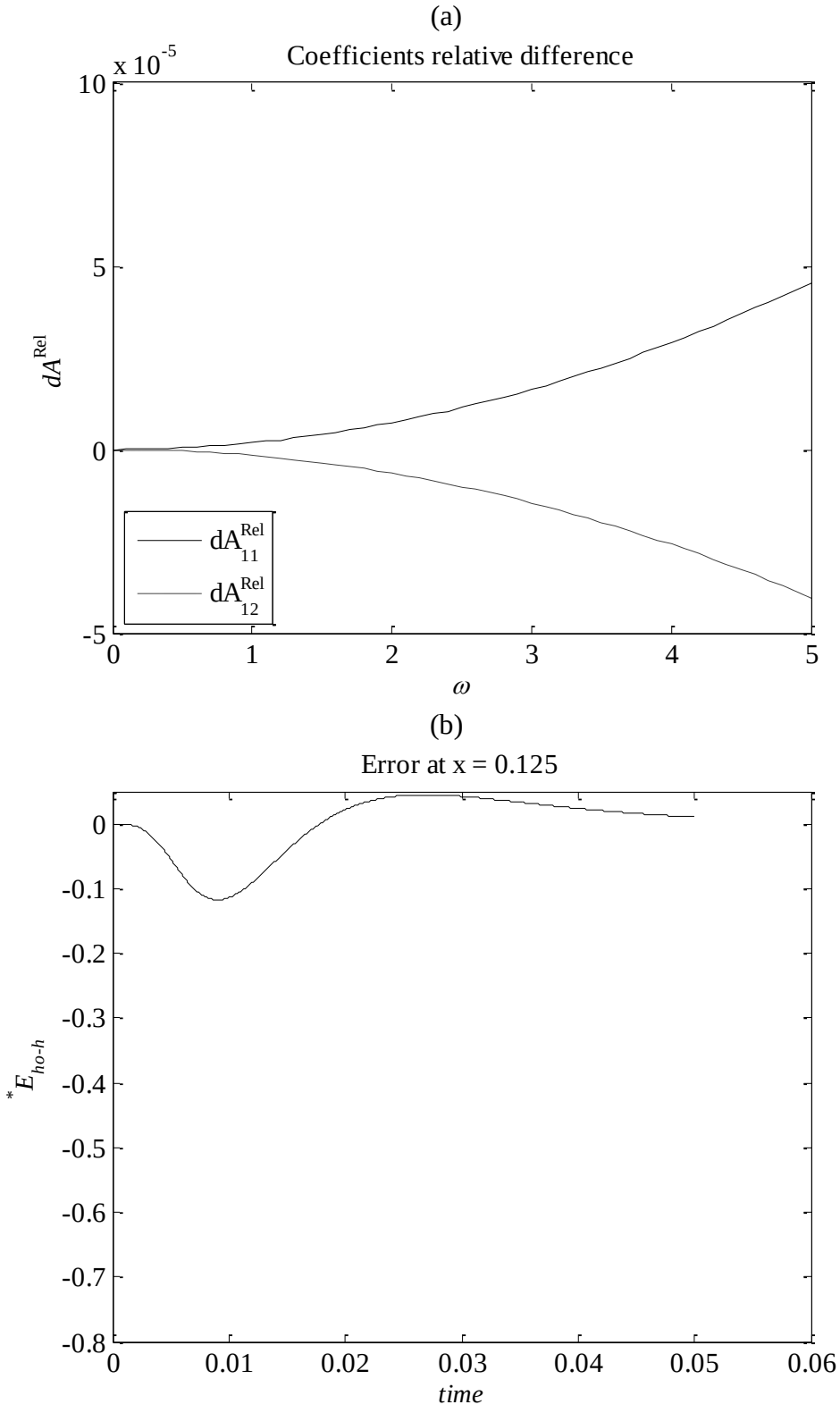

Figure 39: Relative difference between the coefficients of TL and LC I/O equations, (a), and the approximate error in the solution, (b).

Chapter 5

5 One-dimensional convection-reaction-diffusion

5.1 Introduction

In a convection-reaction-diffusion problem, the diffusant is transported (or "convected") through space while diffusing and reacting. That convection may be due to the movement of the medium (e.g. the motion of air or water in the case of pollution transport) or because of external forces that cause the diffusant to move (e.g. an electric field causing the "drift" of electrons or holes through a semiconductor).

The rate of transportation is defined by the convection velocity. As with other coefficients, this can vary over space and time, and can be dependent on the solution. In this study, however, only constant and spatially varying velocity coefficients are considered.

The form of the one-dimensional convection-reaction-diffusion equation (CRDE) solved here is

$$\frac{\partial \phi}{\partial x} = \frac{\partial}{\partial x}\left(D \frac{\partial \phi}{\partial x} \right) - K\phi - v\frac{\partial \phi}{\partial x} + S \tag{5.1}$$

Note that this has a non-conservative convection term (i.e. $v d\phi/dx$ as opposed to a conservative convection term, $d(v\phi/dx)$. This has a similar form to the equation for the voltage along a general transmission line with zero inductance derived in Appendix B

$$\frac{\partial V}{\partial t} = \frac{\partial}{\partial x}\left(\frac{1}{R_d C_d}\frac{\partial V}{\partial x}\right) - \frac{G_d}{C_d}V - \frac{1}{R_d}\frac{\partial}{\partial x}\left(\frac{1}{C_d}\right)\frac{\partial V}{\partial x} + \frac{I_d}{C_d} \tag{5.2}$$

As can be seen from comparing these two equations, modelling of the convection term requires that C_d must vary with x. As will be shown below, for a constant convection velocity and diffusion coefficient, it must vary exponentially (since C_d times the spatial derivative of $1/C_d$ must be a constant). This means that if K, D and S are all constant then G_d, R_d and I_d must also vary exponentially with x. In reaction-diffusion modelling using LCM, a piecewise-constant problem is first represented by a series of uniform TL segments. In convection-reaction-diffusion modelling, a piecewise-constant problem must be represented by a series of non-uniform TL segments with exponentially varying parameters. Such a TL segment is referred to here as an "exponential TL segment".

Convection dominant problems (i.e. problems in which the convection coefficient is significantly larger than the other coefficients) can be difficult to accurately solve using numerical techniques, and are, therefore, of particular interest. The ratio $v/D/\Delta x$ is called the Peclet number [51, 102]. For high Peclet numbers, many of the standard FVM, FDM and FEM schemes are prone to non-physical oscillations or 'wiggles' [9, 103]. There are FVM schemes for convection-diffusion that are bounded, such as the upwind differencing scheme or the exponential scheme [48-49, 61-62], but these are not tested here.

In this chapter, tests compare LCM results with those from QUICK FVM models (the details of how this scheme is implemented are given in Chapter 2). It is shown that LCM has advantages when solving CRDE problems.

5.1.1 Derivation of LCM equations for convection reaction diffusion

The first step in the process of deriving the LCM equations is determining the I/O relationship for the steady-state voltages and currents across a length of exponential transmission line. Equations (5.1) and (5.2) are equivalent when

$$D = \frac{1}{R_d C_d},\ v = \frac{1}{R_d}\frac{\partial}{\partial x}\left(\frac{1}{C_d}\right),\ K = \frac{G_d(x)}{C_d(x)} \text{ and } S = \frac{I_d(x)}{C_d(x)} \tag{5.3}$$

Combining two of these conditions relates the ratio v/D to the distributed capacitance

$$v / D = C_d \frac{\partial}{\partial x}\left(\frac{1}{C_d}\right) \tag{5.4}$$

Over the length of an exponential TL segment, *v*/*D* is constant, and so solving this gives

$$\frac{1}{C_d} = ce^{xv/D} \tag{5.5}$$

where c is a constant. The other TL parameters must then equal

$$R_d = \frac{ce^{xv/D}}{D},\ G_d = \frac{K}{ce^{xv/D}}, I_d = \frac{S}{ce^{xv/D}} \tag{5.6}$$

To establish the I/O relationship, as in the reaction-diffusion case, two first order equations must be solved:

$$\frac{dV}{dx} = -IR_d \tag{5.7}$$

and

$$\frac{dI}{dx} = -G_d V + I_d \tag{5.8}$$

Differentiating both with respect to *x* gives

$$\frac{d^2V}{dx^2} = -\frac{dR_d}{dx} I - R_d \frac{dI}{dx} \tag{5.9}$$

and

$$\frac{d^2I}{dx^2} = -\frac{dG_d}{dx} V - G_d \frac{dV}{dx} + \frac{dI_d}{dx} \tag{5.10}$$

Using Equations (5.7) and (5.8) to replace *dI*/*dx* and *dV*/*dx* in these then gives

$$\frac{d^2V}{dx^2} = \frac{1}{R_d}\frac{dR_d}{dx}\frac{dV}{dx} + R_d G_d V - R_d I_d \tag{5.11}$$

and

$$\frac{d^2I}{dx^2} = \frac{1}{G_d}\frac{dG_d}{dx}\frac{dI}{dx} - \frac{dG_d}{dx}\frac{I_d}{G_d} + G_d R_d I + \frac{dI_d}{dx} \tag{5.12}$$

Replacing G_d, I_d and R_d using Eq. (5.6), and simplifying, yields

$$\frac{d^2V}{dx^2} = \frac{v}{D}\frac{dV}{dx} + \frac{K}{D}V - \frac{S}{D} \tag{5.13}$$

and

$$\frac{d^2I}{dx^2} = -\frac{v}{D}\frac{dI}{dx} + \frac{K}{D}I \tag{5.14}$$

Equations (5.13) and (5.14) are second order ordinary differential equations that can be solved exactly giving the I/O relationship for an exponential TL segment. Assuming that the input is at $x = 0$, the output at $x = \Delta x$, and setting

$$V(0) = V_i \text{ and } I(0) = I_i \tag{5.15}$$

and, in order to satisfy Equations (5.7) and (5.8),

$$\frac{dV(0)}{dx} = -I_i R_d(0) \text{ and } \frac{dI(0)}{dx} = -G_d(0)V_i + I_d(0) \tag{5.16}$$

and solving Equations (5.13) and (5.14) gives the I/O relationship

$$\begin{bmatrix} V_o \\ I_o \end{bmatrix} = \begin{bmatrix} \beta\delta - \dfrac{\beta\gamma v}{\zeta} & -\dfrac{2c\beta\gamma}{\zeta} \\ -\dfrac{2DK\gamma}{c\beta\zeta} & \dfrac{\gamma v + \delta\zeta}{\beta\zeta} \end{bmatrix} \begin{bmatrix} V_i \\ I_i \end{bmatrix} + \begin{bmatrix} \dfrac{\zeta + \beta\gamma v - \beta\delta\zeta}{K\zeta} \\ \dfrac{2D\gamma}{c\beta\zeta} \end{bmatrix} S \tag{5.17}$$

where

$$\beta = \exp\left(\frac{v}{2D}\Delta x\right),\ \gamma = \sinh\left(\frac{\zeta}{2D}\Delta x\right), \text{ and } \delta = \cosh\left(\frac{\zeta}{2D}\Delta x\right) \tag{5.18}$$

and

$$\zeta = \sqrt{v^2 + 4KD} \tag{5.19}$$

In a situation where K is zero, the I/O relationship is

$$\begin{bmatrix} V_o \\ I_o \end{bmatrix} = \begin{bmatrix} 1 & \dfrac{c - c\chi}{v} \\ 0 & 1 \end{bmatrix} \begin{bmatrix} V_i \\ I_i \end{bmatrix} + \begin{bmatrix} \dfrac{\Delta x}{v} - \dfrac{D(\chi - 1)}{v^2} \\ \dfrac{D}{cv}\left(1 - \dfrac{1}{\chi}\right) \end{bmatrix} S$$

where

$$\chi = \exp\left(\frac{v}{D}\Delta x\right)$$

Note that the relationships above (when $v \neq 0$) include the constant c. In a model of a problem in which the physical capacitance (e.g. the thermal capacitance) is constant over space, the distributed capacitance of the transmission line must be continuous, i.e. the value of C_d at the end of one TL segment must equal the value of C_d at the start of the next segment. If, therefore, segment j has length Δx, the value of the constant for segment j+1 must be

$$c_{j+1} = c_j \exp\left(\frac{v_j}{D_j}\Delta x\right) \tag{5.20}$$

The value of c for the first segment in the TL can be any arbitrary constant.

The remaining steps involved in implementing the LCM method are identical to those required in reaction-diffusion modelling and detailed in Chapter 3 for steady-state problems and Chapter 4 for transient problems. In both cases, there can be many TL segments in any section joining two nodes, and so, firstly, the I/O relationships for each section must be calculated. Then equivalent lumped-component circuit elements can be found and the voltages at the nodes calculated. For steady-state piecewise-constant problems, the solutions obtained are exact.

5.2 Tests and results

In this section, the accuracy of the LCM method for convection-reaction-diffusion is examined and compared to that of FVM for a selection of problems. The tests show that the method does not produce spurious oscillations, is consistently convergent, and it can

be applied to general convection-reaction-diffusion problems. Time stepping is again implemented using both a first-order explicit scheme and TLM.

This section first looks at a straightforward transient application with constant coefficients. It then shows that the scheme is bounded (i.e. produces wiggle-free solutions), and that, as for reaction-diffusion modelling, the spatial discretization errors are second-order and LCM converges consistently even when the node positions do not correspond with coefficient discontinuities. The nature of the spatial discretization errors is examined further and TLM time stepping is tested for CRDE problems.

5.2.1 Modelling of charge carriers in semiconductors

Devices made from semiconductor materials such as Silicon and Germanium are used to amplify, convert and switch electric currents. This is due to the ability of the material's conductivity to change when subjected to electric fields, light, temperature and/or dopings [104].

Charge carriers (i.e. holes and electrons) within a semiconductor diffuse and recombine. They can also be caused to drift in a given direction by applying an electric field. Excess carriers can be generated through metal contact, which can act as an emitter, or through optical excitation such as by short laser pulses; the latter can produce electron-hole pairs instantaneously [4, 21].

The diffusion, drift and recombination of excess minority carriers in a p-type semiconductor is governed by a one-dimensional equation of the form

$$\frac{1}{D}\frac{\partial p}{\partial t} = \frac{\partial^2 p}{\partial x^2} - \frac{\mu E_x}{D}\frac{\partial p}{\partial x} - \frac{p}{D\tau} \tag{5.21}$$

where p is the concentration of carriers, D is the minority carriers diffusion constant, μ is its mobility, τ is its lifetime and E_x is the electric field strength [4, 21]. In practice, the electric field and other parameters may vary with position, time and/or temperature, however for modelling purposes they are generally considered constant.

First, consider a field-free (i.e. drift-free) diffusion and recombination problem where the equilibrium is disturbed by photo injection. The recombination process involves

excess holes recombining with free electrons, and this process can be modelled by the first order reaction term as in Eq. (5.21).

Consider a problem studied by Al-Zeben et al [4], with an initial injection of 1000cm^{-3} holes at $x = 0$ in an infinite medium (i.e. where the boundaries are located at $-\infty$ and $+\infty$). The sample is n-type silicon with a diffusion coefficient for the holes of $D = 50\text{cm}^2\text{s}^{-1}$ and a lifetime of 1μs. The LCM model must have $R_d = 1/D$ and $G_d = 1/\tau$.

The analytical solution for this problem is given as [4],

$$p(x,t) = \frac{p_0 A}{\sqrt{4\pi D t}} \exp\left(\frac{-(x-\mu E_x t)^2}{4Dt} - \frac{t}{\tau} \right) \tag{5.22}$$

with E_x equals zero in this case. The LCM solution (obtained with $h = 0.001$cm and $\Delta t = 0.005$μs) is shown at three points in time in Figure 40 along with the analytical solution.

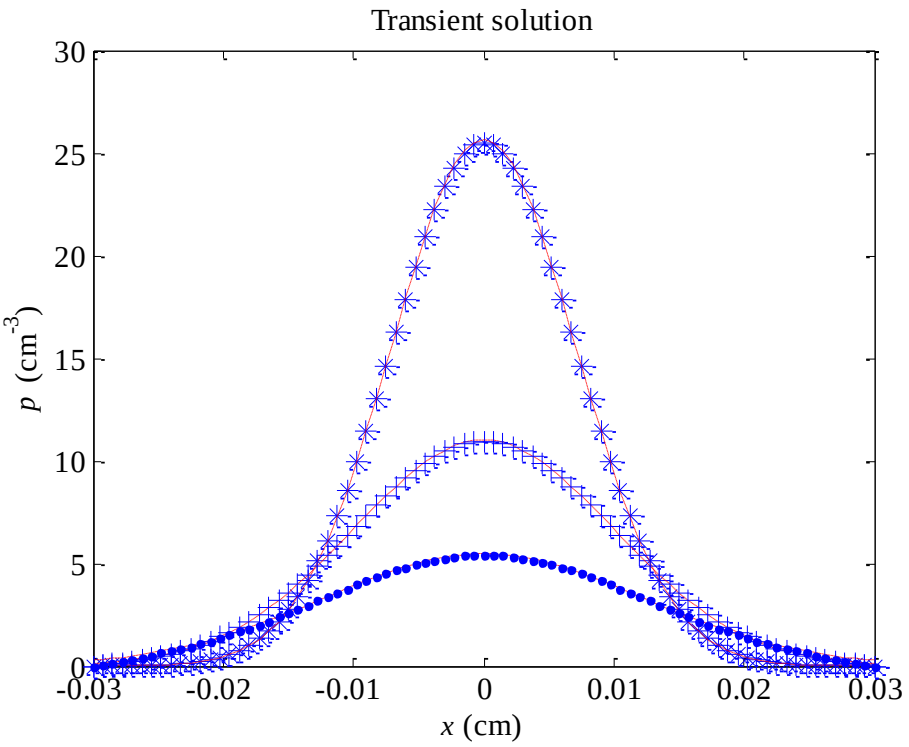

Figure 40: The result of minority carrier diffusion and recombination after 0.5μs (*), 1μs (+) and 1.5μs (•), as modelled using LCM, along with the equivalent analytical solutions (shown as dashed red lines).

Now consider the same problem but with $E_x \neq 0$ (i.e. where an electric field will cause the minority carriers to drift over space). The electric field considered by Al-Zeben is given as $E_x = 10$ V/cm. The "convection velocity" (required for the LCM equations

given above) is $v = \mu E_x/D$. The LCM solution is shown in Figure 41 along with the analytical solution (from Eq. (5.22)).

It is clear that the method produces accurate transient results for this problem with constant coefficients.

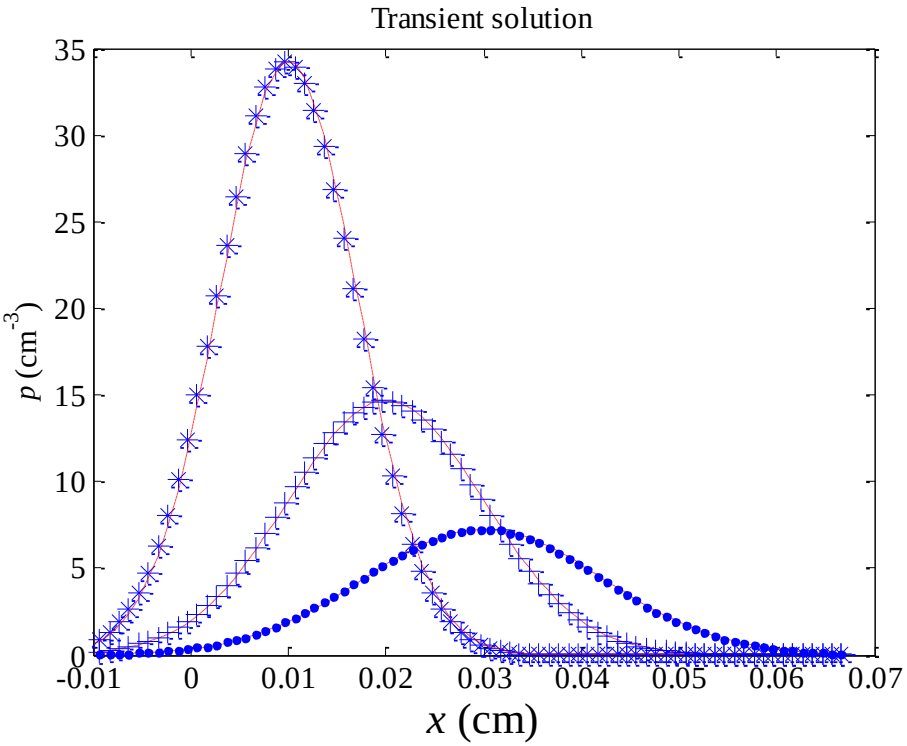

Figure 41: Results for minority carrier diffusion, drift and recombination after 0.5μs (*), 1μs (+) and 1.5μs (•), as modelled using LCM, along with the equivalent analytical solutions (shown as dashed red lines).

5.2.2 Spatial discretization errors

The method produces exact solutions in steady state when the coefficients are piecewise constant or constant. The spatial accuracy under transient conditions, and for more general problems, is dependent on both the coefficients of the convection-reaction-diffusion equation and on the spatial discretization.

5.2.2.1 Boundedness of LCM

Many of the standard FVM schemes used for solving convection-reaction-diffusion equations suffer from problems when the Peclet number, i.e. vh/D, is above a given limit [9, 105]. One method that can produce second-order accurate solutions is the QUICK FVM scheme, but it can exhibit wiggles when the Peclet number, and the node

spacing, is large. LCM, on the other hand, can produce both accurate and wiggle-free solutions of convection-dominant problems.

Consider a simple model of a problem with constant coefficients $D = 1$, $K = 2$, $v = 120$, and $S = 30$ modelled using $\Delta t = 1.0\times10^{-6}$ and $N = 5$ over the domain $x \in [0,1]$ with Dirichlet boundary conditions $V(0,t) = 0$ and $V(1,t) = 1$ and the initial condition $V(x,0) = 0$, $x \neq 1$. The Peclet number is 30. Figure 42 shows solutions at $t = 0.001$ and $t = \infty$. It can be observed that the QUICK FVM solution exhibits wiggles in both steady state and transient conditions. The steady-state LCM solution is exact, while the transient solution contains both spatial and temporal errors.

Physically, the values of the solution of a convection-diffusion problem should be bounded by the boundary values (e.g. all solution values, in this case, should be between 0 and 1). This is not the case if the scheme exhibits wiggles. One method of determining, for a particular scheme, the limit on the value of *Pe* below which the solution will be bounded, is Godunov's theorem [47]. If a reaction term is included in the problem with a positive reaction coefficient, then the solution will no longer always be bounded by the boundary values, but, if those boundary values are both positive, then all solution values must also be positive (i.e. the solution values must be bounded by zero and the larger of the two boundary values).

Consider the general discretized LCM equation for convection-reaction-diffusion equation without a source term and with constant coefficients in steady state as given in Eq. (3.29). Rearranging this equation gives

$$\left(\frac{1}{R_n}+\frac{1}{R_{n-1}}+G_{l,n}+G_{r,n-1}\right)V_n=\left(\frac{V_{n+1}}{R_n}\right)+\left(\frac{V_{n-1}}{R_{n-1}}\right) \tag{5.23}$$

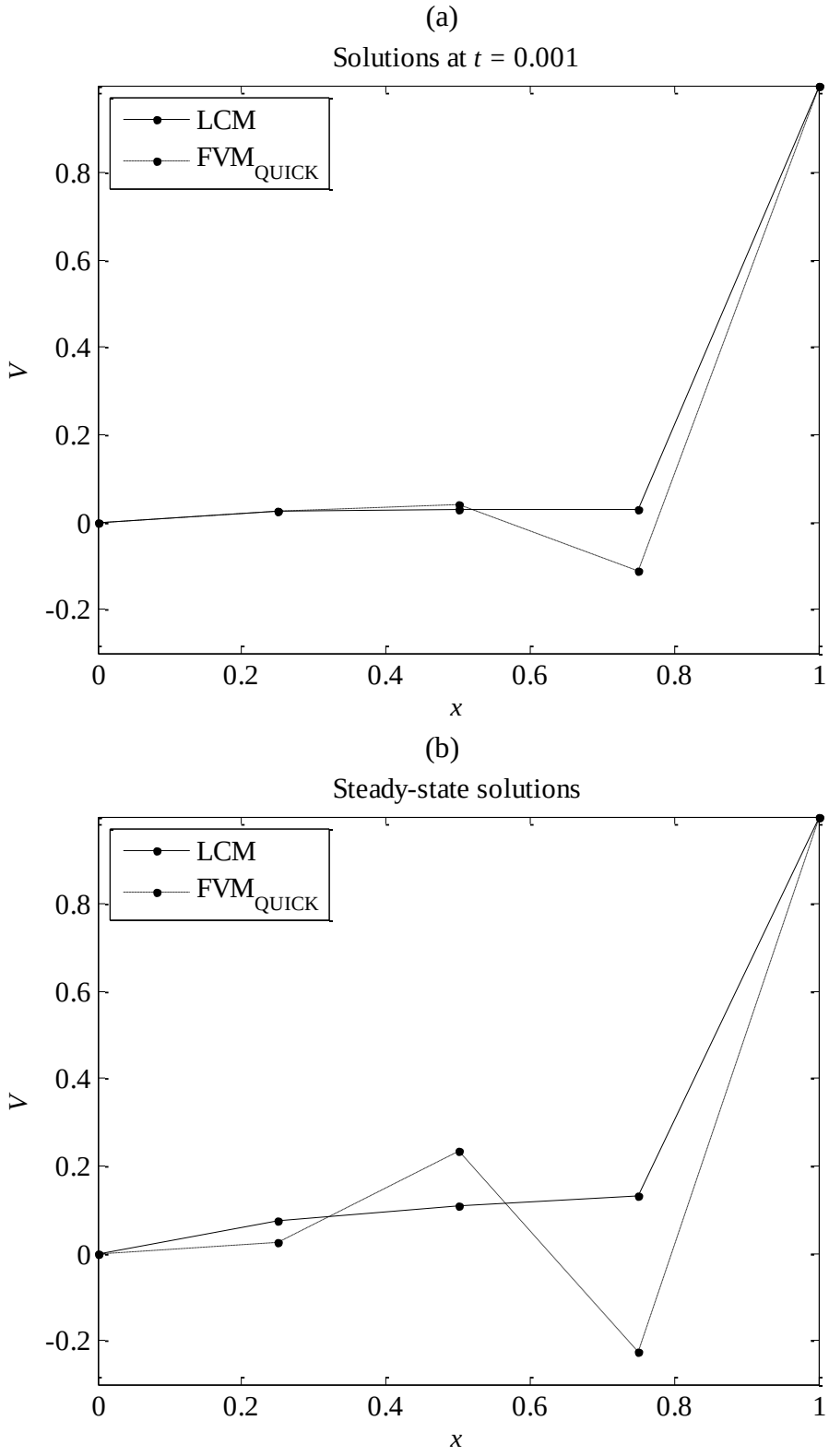

Figure 42: Transient, (a), and steady-state, (b), LCM and QUICK FVM solutions for a problem with constant coefficients.

Now combining Equations (3.18) to (3.20) and Equations (5.18) to (5.19) allows R_n (which equals R_{n-1} under those conditions) and $1/R_n + 1/R_{n-1} + G_{l,n} + G_{r,n-1}$ to be written as

$$R_n = \frac{2\alpha\beta\sinh\left(\frac{\zeta}{2D}h\right)}{\zeta} \tag{5.24}$$

$$\left(\frac{1}{R_n}+\frac{1}{R_{n-1}}+G_{l,n}+G_{r,n-1}\right)=\delta\left(\frac{1}{R_n}\beta+\frac{1}{R_{n-1}}\frac{1}{\beta}\right)+\frac{\gamma v}{\zeta}\left(-\frac{1}{R_n}\beta+\frac{1}{R_{n-1}}\frac{1}{\beta}\right) \tag{5.25}$$

where $\beta = e^{(hv/2D)}$, $\gamma = \sinh\left(h\zeta/2D\right)$, $\delta = \cosh\left(h\zeta/2D\right)$ and $\zeta = \sqrt{v^2+4KD}$.

Now v can be positive or negative but c, K, D and h are always positive. It is clear that β, γ, δ and ζ must also be positive, and so $R_n = R_{n-1}$ must be positive. Whether v is positive or negative, it can be easily shown that $1/R_n + 1/R_{n-1} + G_{l,n} + G_{r,n-1}$ will always be positive.

It is clear that all three coefficients in Eq. (5.23) are positive if K and D are positive. It is therefore clear that, if V_{n+1} and V_{n-1} are both positive, then V_n must also be positive. If the voltages at the boundary nodes are positive, the voltages at all internal nodes must also be positive. The method is therefore bounded.

This property of the scheme can also be inferred from knowledge of the behaviour of electrical circuits. In an LCM circuit composed of just resistors, conductors and capacitors (since there is no source term in this case) the voltage will be positive relative to the ground at all points along it if the voltages at both ends are positive. If the shunt conductances are also zero (i.e. if $G_l = G_r = 0$ for each element) then the voltages at all points will lie between the voltages at the two ends.

It is clear that this boundedness will apply whether the problem has constant or piecewise-constant coefficients (i.e. it does not matter how the values of the capacitors, resistors and conductors vary along the length of the circuit).

5.2.2.2 Order and consistency of convergence

To examine the consistency of convergence and the orders of the errors for the two methods with respect to the node spacing, two tests are presented here, one with all coefficients constant over space and one in which $v(x)$ is piecewise-constant.

The first model tested has $D = 5$, $K = 2$, $v = 8$, and $S = 3$, with $V(0,t) = 0$ and $V(1,t) = 1$ and $V(x,0) = 0$, $x \neq 1$. The time step length, $\Delta t = 1.0\times10^{-6}$, ensures that time-stepping errors are insignificant. Figure 43(a) shows the solution at $t = 0.01$ obtained with $h = 0.25$. The test parameters have been chosen so that there are no wiggles in the FVM solution. Figure 43(b) shows the convergence of the solution at $x = 0.5$ as the node spacing is reduced. The corresponding values of the estimated order of convergence are given in Table 18 (along with the solution values used to calculate them). It is clear from Table 18 that both schemes converge consistently and are second order. The LCM solutions are more accurate than the FVM solutions (by a factor of approximately two for small node spacings) but not significantly.

Table 18: The data plotted in Figure 43(b) and the corresponding estimates of the orders of the errors in the values of the solutions at $x = 0.5$ for both LCM and FVM.

N	LCM	FVM_{QUICK}
5	0.109365	0.113402
9	0.103028	0.104665
17	0.101537	0.102045
	2.1	**1.7**
33	0.101182	0.101322
	2.1	**1.9**
65	0.101095	0.101131
	2.0	**1.9**
129	0.101073	0.101083
	2.0	**2.0**
257	0.101068	0.101070
	2.0	**2.0**

The second test is similar to the first but with $v = \{2,25,5\}$, the discontinuities located at $x = 0.3$ and $x = 0.6$. Figure 44(a) shows that both the FVM and LCM solutions at $t = 0.01$ are again wiggle-free. Estimated order of convergence values are given in Table 19, along with the solution values (at $x = 0.5$ and $t = 0.01$) used to calculate them. These results show that, as is the case when modelling reaction-diffusion, the FVM scheme

does not converge consistently when the nodes are not positioned to correspond to the discontinuities in the problem coefficients, but the LCM scheme does.

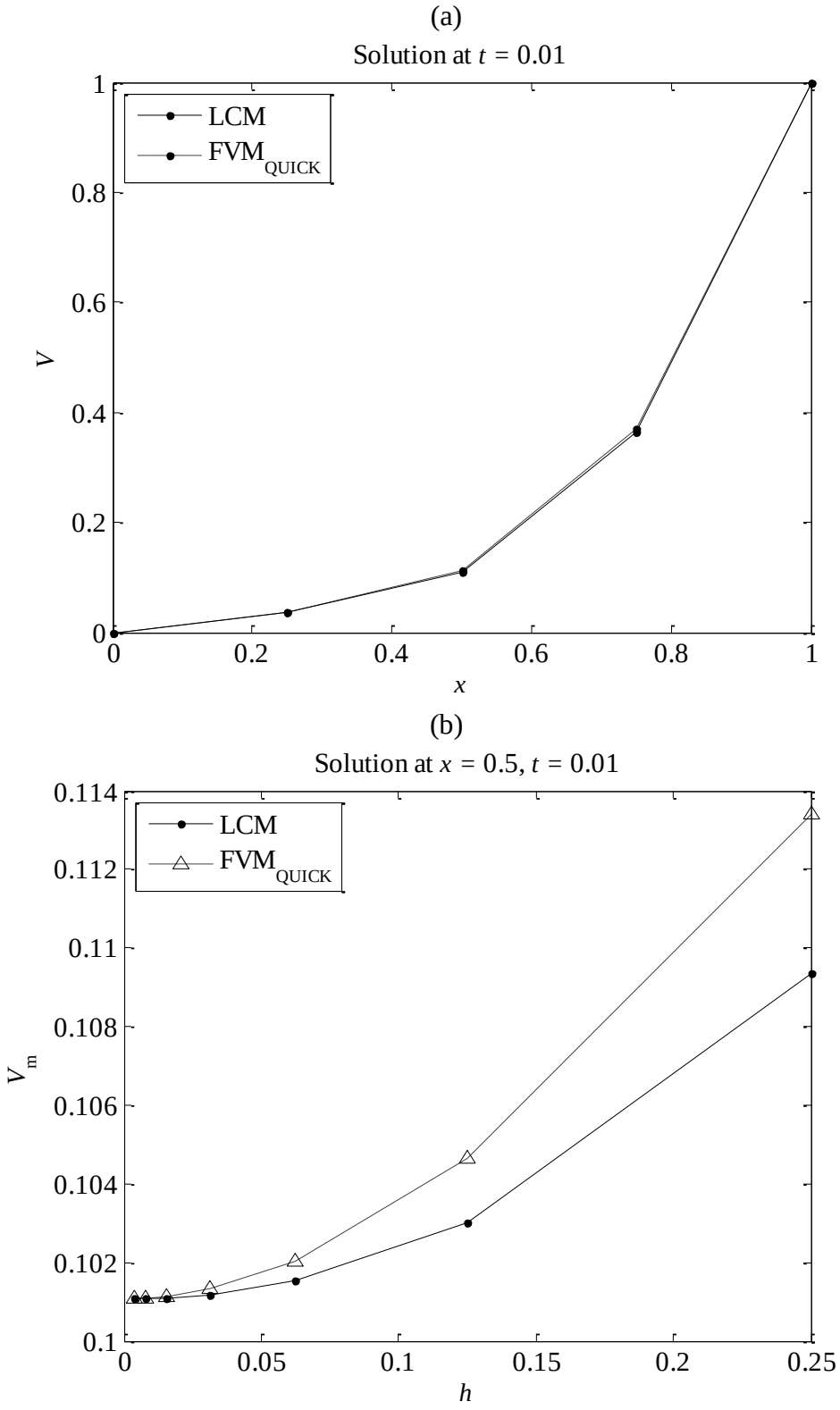

Figure 43: Solutions for a problem with constant coefficients, (a), and the variation in the values of the LCM and FVM solutions at the midpoint of the domain (i.e. x = 0.5) with changes in h, (b).

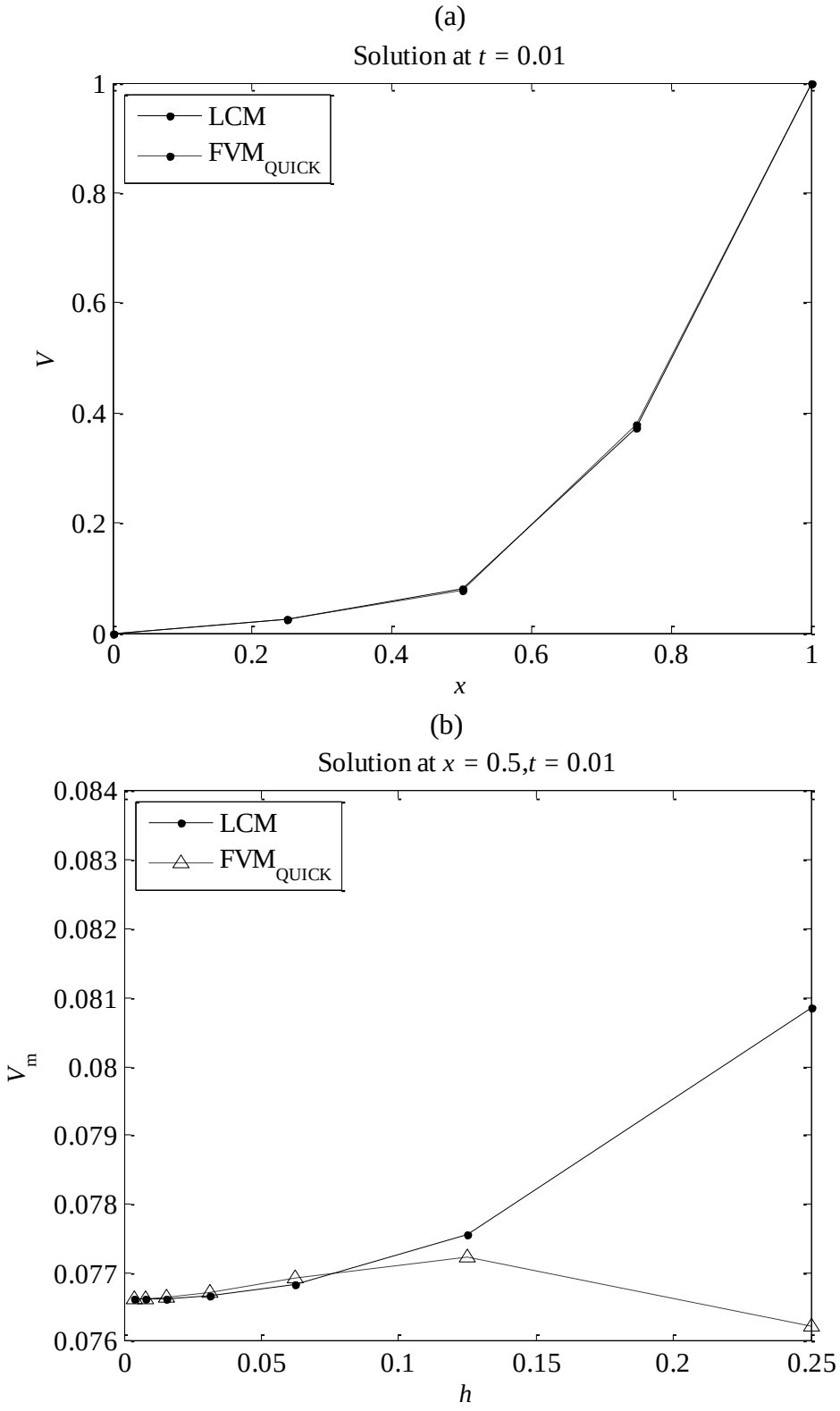

Figure 44: Solutions for a problem with piecewise-constant coefficients, (a), and the variation in the values of the LCM and FVM solutions at the midpoint of the domain (i.e. x = 0.5) with changes in h, (b).

Table 19: The data plotted in Figure 44(b) and the corresponding estimates of the orders of the errors in the values of solution at $x = 0.5$ for both LCM and FVM.

N	LCM	FVM_{QUICK}
5	0.080863	0.076221
9	0.077558	0.077223
17	0.076831	0.076918
	2.2	**1.7**
33	0.076665	0.076714
	2.1	**0.6**
65	0.076625	0.076641
	2.0	**1.5**
129	0.076615	0.076620
	2.0	**1.8**
257	0.076613	0.076614
	2.0	**1.9**

The LCM results are, in general, more accurate than those obtained using the FVM scheme, but, again, the difference is only a factor of approximately two when h is small. The next section explores the sources and nature of the spatial discretization errors in LCM (already briefly explored in the previous chapter), and looks at the relative accuracy of the two schemes as solutions develop over time.

5.2.2.3 Spatial discretization errors

When the coefficients are piecewise constant, there is no error in the steady-state solution calculated using LCM. The situation is different under transient conditions. The first step in LCM involves modelling exactly the physical problem using exponential TL segments. The second step involves modelling those TL segments with lumped-component circuit elements. This step introduces errors that are dependent on the lengths of the elements and on how the solution is varying over time. The error in the solution is always zero at the moment of initialization and must return to zero when the solution reaches a steady-state (i.e. when it is no longer varying). This section examines what happens between those points in time.

If time-stepping errors are negligible then there is one other source of errors in LCM for a transient piecewise-constant problem. It is due to model initialization; only the values of the solution at the nodes are specified and that will potentially introduce errors. Such errors will exist in any numerical solution and will depend on the initial conditions.

In the tests presented here, the time step length is such that time-stepping errors are negligible. The spatial discretization errors in a solution value obtained using a node spacing h are estimated using

$$^{*}E_{h-h_0} = V^h - V^{h_0} \tag{5.26}$$

where V^{h_0} is the equivalent solution value calculated using a significantly smaller node spacing, where $h_0/h \ll 1$. Care has been taken in all cases to ensure that the error values calculated in this way are significantly larger than the errors in the V^{h_0} values used (those errors having been estimated using Richardson extrapolation).

Results from a number of tests are presented below. All are from models with $N = 65$ and with a time step length of $\Delta t = 2\times10^{-6}$ (ensuring that the time-stepping errors are negligible), $h_0/h = 1/4$, boundary conditions $V(0, t) = 0$ and $V(1, t) = 100$, and initial conditions $V(x, 0) = 0$. All models tested have discontinuities at $x = 0.3$ and $x = 0.6$. Other details of the tests are listed in Table 20.

The estimated errors in the LCM and FVM solutions for Test 1a at $x = 0.5$ are plotted over time in Figure 45a. Since it is expected that the errors will be dependent on how the solution is changing over time, and in order to give some indication of that, $\partial^2V/\partial t^2$ has also been measured at $x = 0.5$ and is plotted against time in Figure 45b. From the results the following observations can be made:

- The errors are similar for both methods up to a point in time.
- The FVM error is significantly larger than that for LCM over most of the transient (and in steady state as expected), and the shapes of the two error-time curves are somewhat different in nature.
- The shape of the LCM error-time curve in Figure 45(a) and that of the plot of $\partial^2V/\partial t^2$ at $x = 0.5$ against time in Figure 45(b) are, to some extent, similar.

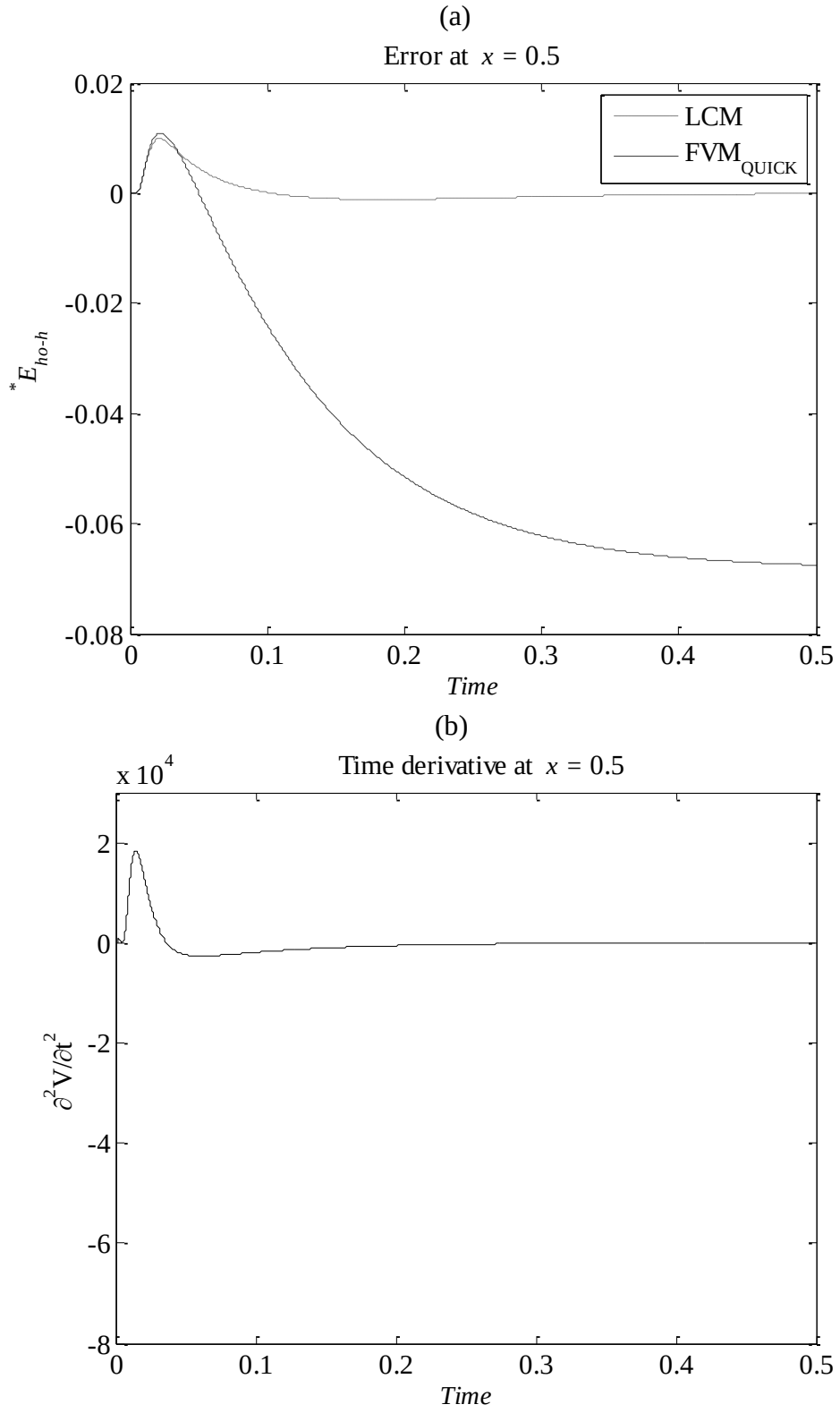

Figure 45: LCM and FVM errors at x = 0.5 for Test 1a (details in Table 20), (a), and the second time derivative at x = 0.5, (b).

Table 20: Details of test problems.

Test No.	$D(x)$	$S(x)$	$K(x)$	$v(x)$	Description
1a	{1, 2, 1}	{5, 20, 35}	{1, 1.5, 2}	{0.8, 1.6, 0.4}	Small Peclet numbers
1b	{1, 2, 1}	{5, 20, 35}	{1, 1.5, 2}	{8, 16, 4}	Large Peclet numbers
2	{1, 2, 1}	{5, 20, 35}	{40, 60, 80}	{0.8, 1.6, 0.4}	Large reaction coefficients
3	{1, 1.1, 1}	25	{0.02, 0.03,0.04}	0.04	Small jump in coefficients at discontinuities

Similar plots are shown in Figure 46 for Test-1b which has Peclet numbers ten times larger than in Test-1a. The LCM errors have decreased significantly in this case as a result of the increase in v and so have the FVM errors over the initial part of the transient. The decrease in the LCM errors corresponds to a decrease in the values of $\partial^2 V/\partial t^2$ as shown in Figure 46(b).

While, in many cases tested, there is some correspondence between the shape of the LCM error-time curve at $x = 0.5$ and the shape of corresponding second time derivative-time curve at $x = 0.5$, there is no straightforward relationship between the two. This is illustrated by the results from Test 2 (details of which are given in Table 20) shown in Figure 47.

A source of spatial errors in transient piecewise-constant LCM models is the difference between the TL segments and the lumped-component circuit elements used to model them. This difference depends on the frequency content of the voltage variations. It is clear that, while the second time derivative may be linked to this frequency content, the link is not straightforward. It is also clear that the solution error at a given point in space will not just be dependent on how the solution is changing at that point, but will also depend on what is happening to the solution at other points in space. In addition, the LCM error is always zero at $t = 0$, but that is not generally true for $\partial^2 V/\partial t^2$ (as in Test 2). Under such circumstances, the two curves may have qualitatively different shapes.

What these tests do support, however, is the suggestion that the errors in LCM are fundamentally different in nature to those in FVM, and that they are possibly linked to how the solution changes over time in a more straightforward way than the errors in FVM (since, unlike with FVM, the LCM solution errors approach zero as the time derivatives of the solution approach zero, i.e. as the solution reaches a steady-state).

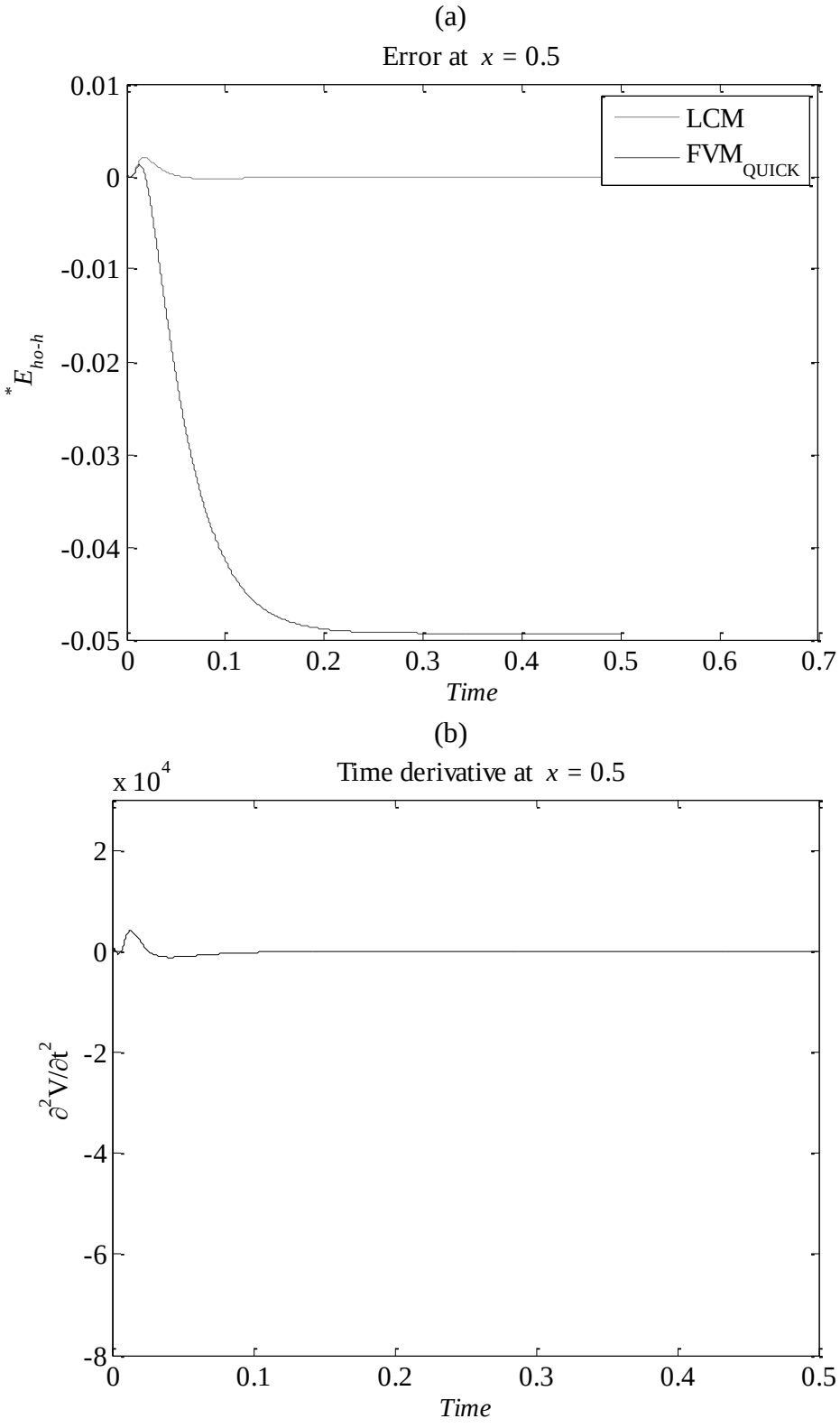

Figure 46: LCM and FVM errors at $x = 0.5$ for Test 1b (details in Table 20), (a), and the second time derivative at $x = 0.5$, (b).

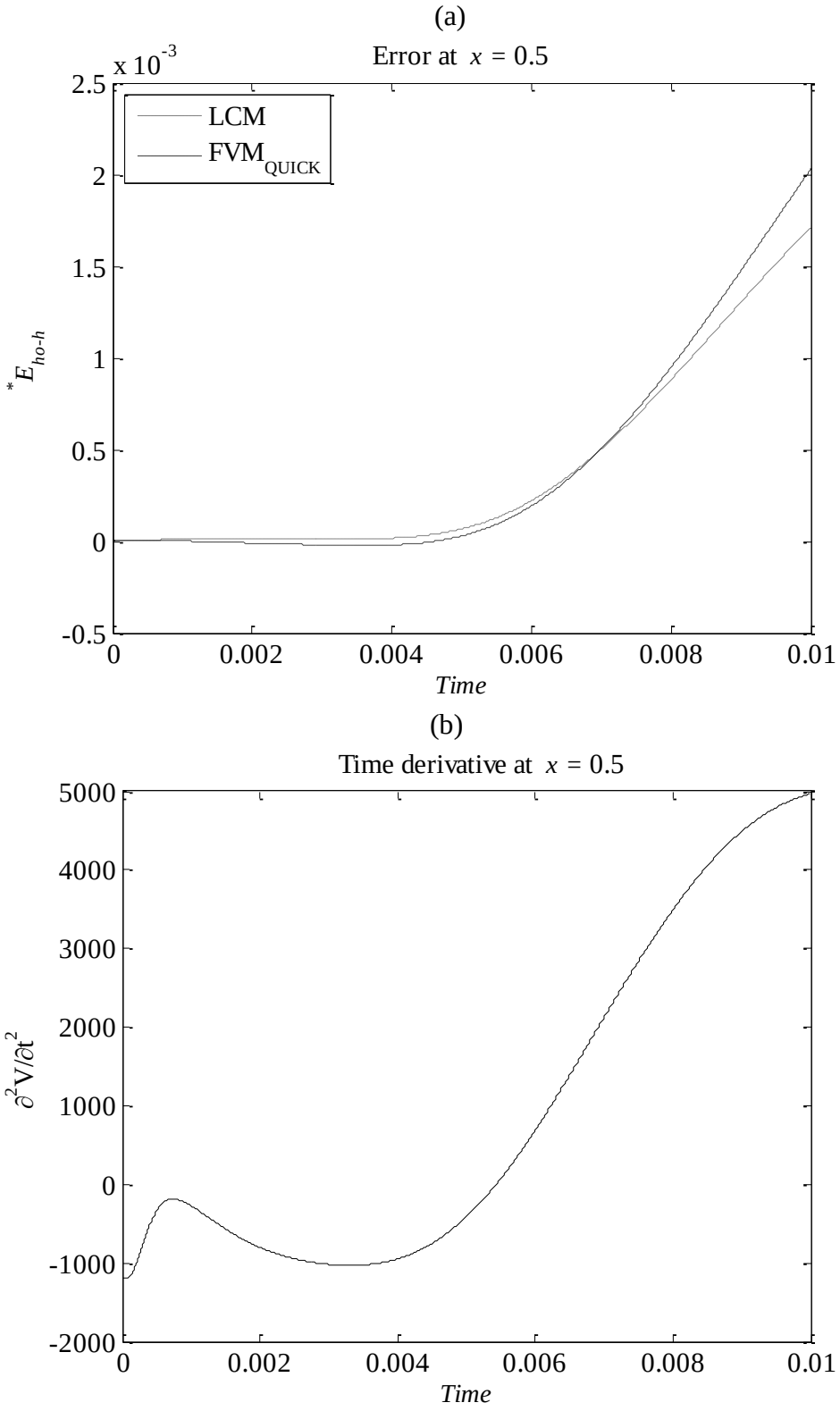

Figure 47: LCM and FVM errors at $x = 0.5$ for Test 2 (details in Table 20), (a), and the second time derivative at $x = 0.5$, (b).

While the transient LCM results are significantly better than those obtained using FVM over much of the length of the transient for the tests presented above, that is not always the case. In Test 3, the solution is dominated by the source and the diffusion terms, the

discontinuities in the coefficients are small, and the steady-state solution is almost a straight line (because of which, the steady-state FVM errors are small). The solution at $t = 0.5$, at which point it is still changing over time but has almost reached a steady state, is shown in Figure 48(a). The plots of errors over time are shown in Figure 48(b). Unlike in the other tests presented here, the difference between the LCM and FVM errors is insignificant over most of the transient.

It is clear that the LCM spatial discretization errors are dependent on how the solution is changing over time and that they can be significantly lower than those obtained using the FVM scheme tested here. Note that in the tests presented above, the problem coefficients are piecewise constant, and so the steady-state LCM errors are zero.

As mentioned above, there is some correspondence between the shape of the LCM error-time curve and the shape of corresponding second-time-derivative-time curve for the problems tested; however, there is no straightforward relationship between the two. The correspondence between the time and space derivatives and the LCM errors depends on the problem examined.

The variation of the time stepping errors over the length of the domain is examined next, along with possible relationships between those errors and derivatives of the solution.

Consider again the problems outlined in section 5.2.1 above. The first of those problems, with zero convection, is examined here again using a very small time-step of 1×10^{-10}. It can be assumed that any errors in the solution are due to the spatial discretization. The solution at $t = 1\times10^{-6}$ is given above in Figure 40 and the errors in the solution are plotted in Figure 49(a). Figure 49(b) shows the derivative $\partial^3 V/\partial x^2 \partial t$ at that instant estimated from the solution values.

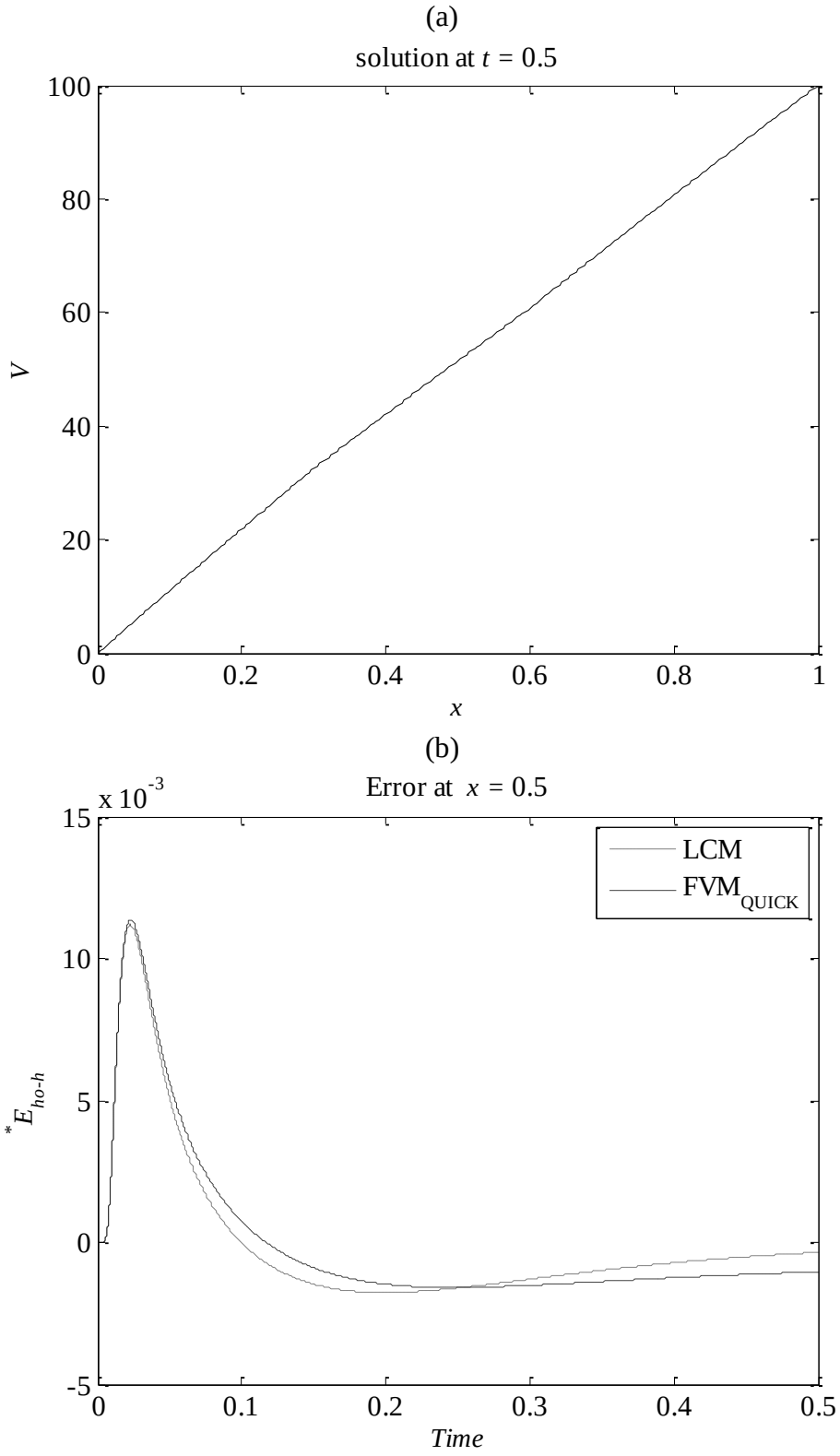

Figure 48: The solution of the problem in Test 3 (detailed in Table 20) at t = 0.5, (a), and the LCM and FVM errors at x = 0.5, (b).

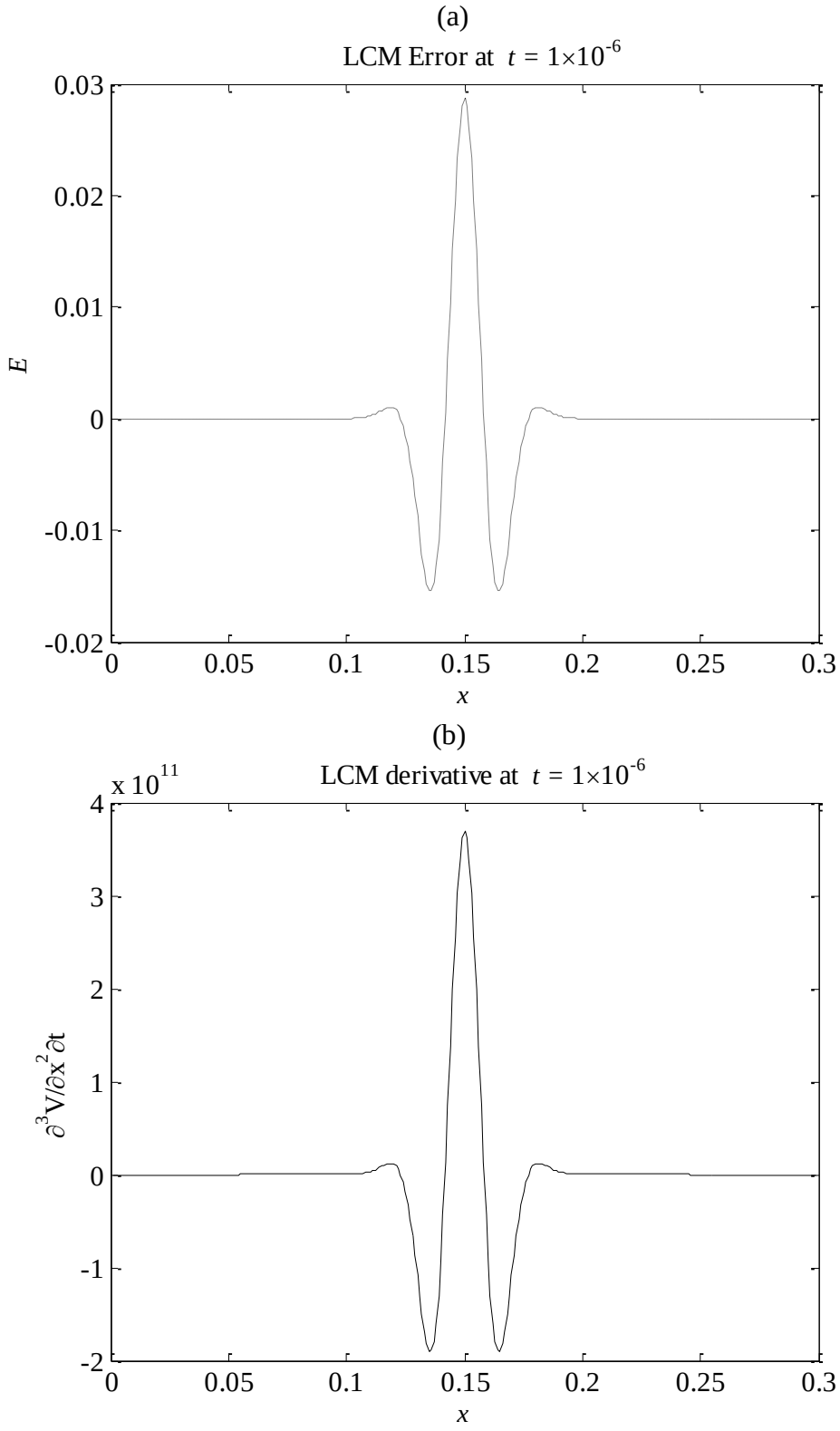

Figure 49: Error in the LCM solution, (a), and $\partial^3V/\partial x^2\partial t$ at the same instant, (b).

It is clear that there is a very strong correspondence between the shape of the error curve and that of $\partial^3V/\partial x^2\partial t$ for this case. Tests show that the ratio of one to the other is dependent on time (i.e. while the shapes of the error curve and the $\partial^3V/\partial x^2\partial t$ curve are

very similar at any point in time, the ratio of the values of one to the values of the other changes as the solution progresses).

When $v \neq 0$, the relationship between the LCM error and $\partial^3 V/\partial x^2 \partial t$ is no longer so straightforward. This is clear from which Figure 50 shows both for a model with non-zero convection (as in the second problem modelled in section 5.2.1 above) at $t = 1\times10^{-6}$.

Comparison of Figure 50(a) and Figure 50(b) clearly shows that the two shapes no longer correspond. Tests suggest that a linear combination of $\partial^2 V/\partial x \partial t$ and $\partial^3 V/\partial x^2 \partial t$ can more closely match the shape of the error plot. An example of such a combination is shown in Figure 51. It is clear that this match is not exact, and there is no reason to expect that it would be. What it, and other similar tests, do suggest, however, is that there is some relationship between the spatial variation in the discretization error and derivatives of the solution.

Since the magnitude and spatial variation of such derivatives can be easily estimated over time from a solution, it may be possible for a modeller to use them when deciding on node spacing and on where to concentrate nodes if an uneven grid is used. Further investigation is required.

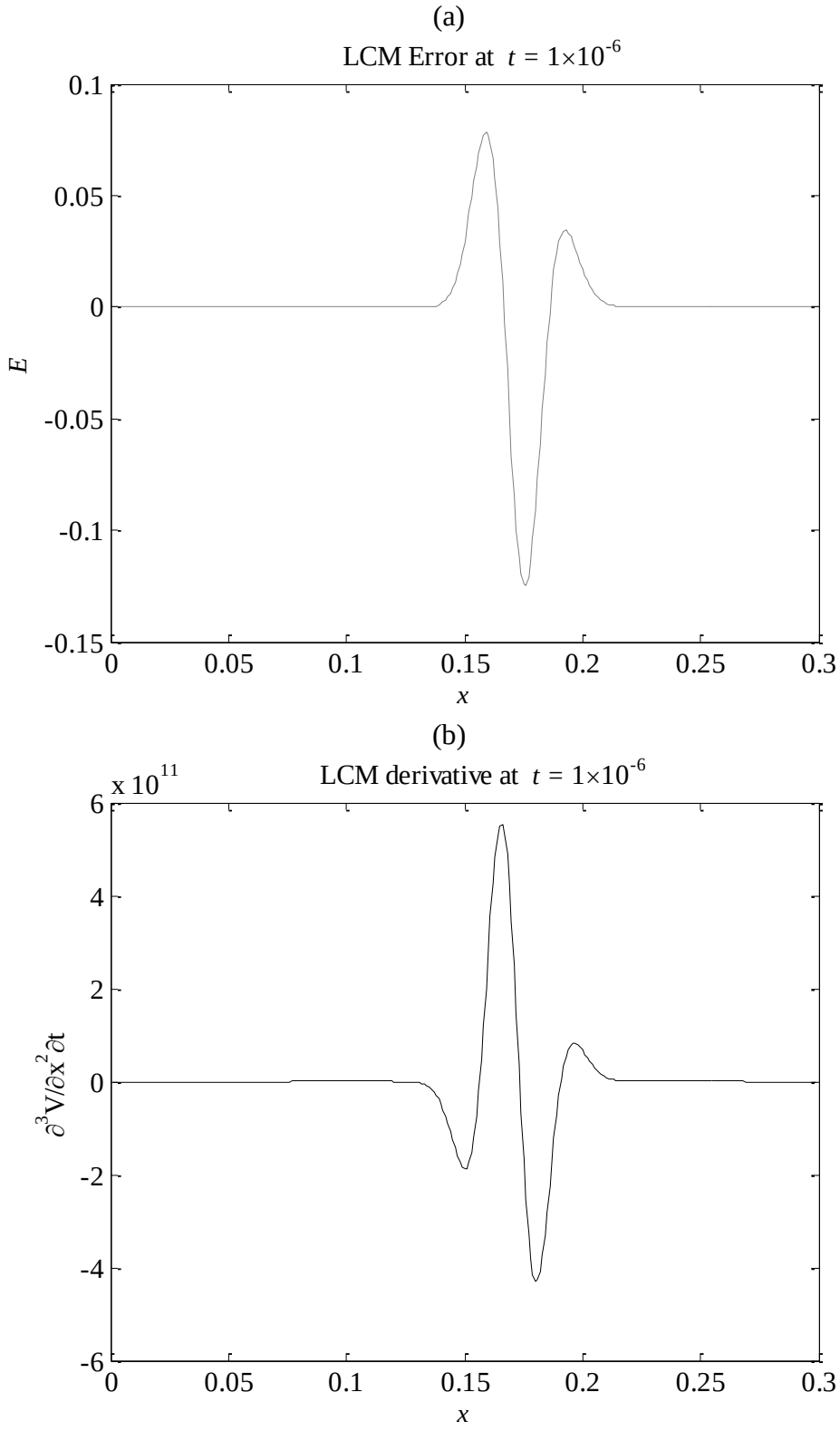

Figure 50: Error in the LCM solution, (a), and $\partial^3V/\partial x^2\partial t$ at the same instant, (b).

If there is a relatively straightforward relationship between errors and partial derivatives of the solution, this may allow the order of the errors to be established anaytically.

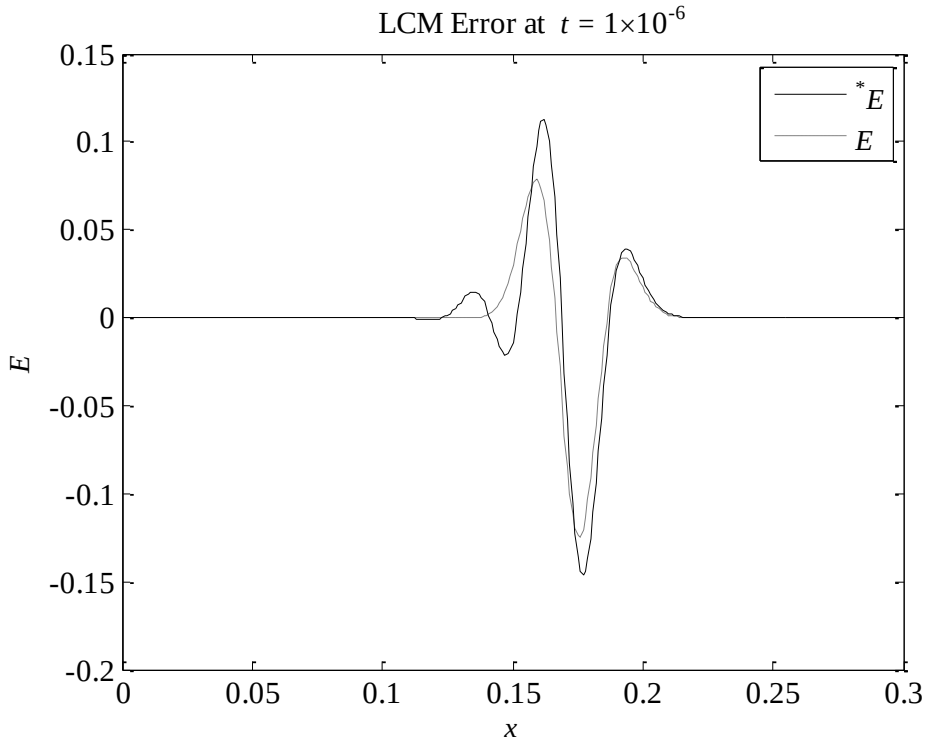

Figure 51: Actual error (labelled E), as in Figure 50(a), and a linear combination of $\partial^2 V/\partial x \partial t$ and $\partial^3 V/\partial x^2 \partial t$ (labelled ${}^*E$).

5.2.3 Reducing computational cost by changing *h* over time

The plots in Figure 52 show how estimated errors in the solutions at the midpoint of equivalent LCM and FVM models for a given problem with piecewise-constant coefficients (specified below) vary over time. The time-stepping errors are negligible so the errors shown are the result of the spatial discretization alone. The number of nodes used is $N = 65$. If the node spacing is increased, then the errors for both schemes increase. Figure 53 shows the effect on the errors of doubling the node spacing. With LCM, the shape of the error-time curve is not changed, but the magnitude of the errors increases by a factor of approximately four (as would be expected). The FVM error-time curve, in this case, changes shape when the node spacing is increased and the magnitude of the errors (both transient and steady state) increases by a factor much greater than four (due to the inconsistent convergence of the solution). As expected, for a problem with piecewise-continuous coefficients, the LCM errors approach zero as the solution approaches a steady state, no matter what node spacing is used. That is because LCM produces exact steady-state solutions for such problems.

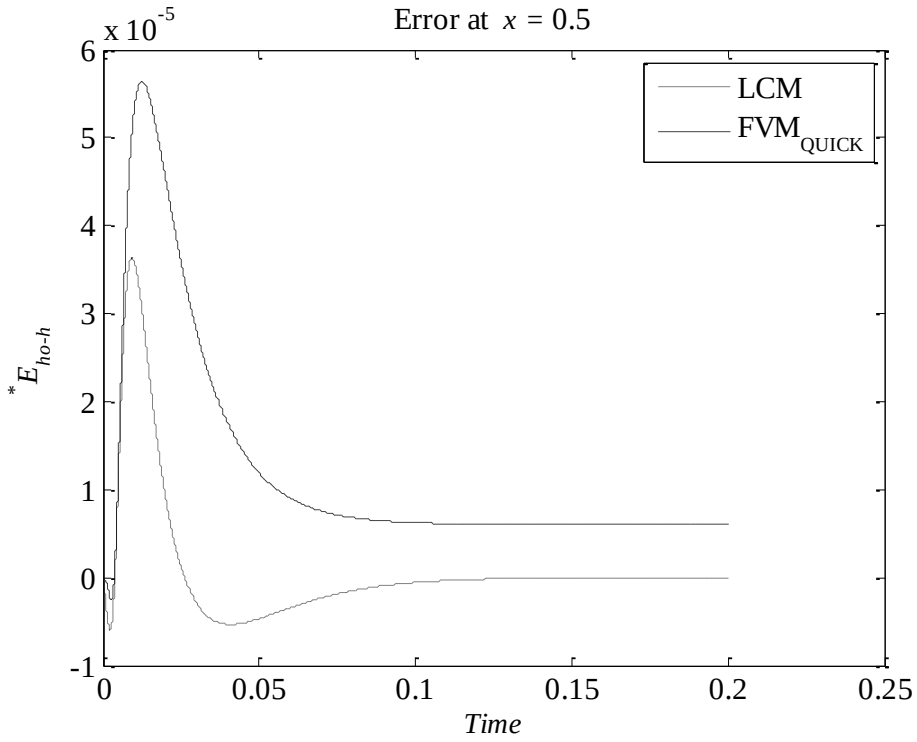

Figure 52: LCM and FVM errors at $x = 0.5$ for a model with $N = 65$.

In both cases, the LCM errors increase to an initial peak value and then decrease. A modeller may wish to keep errors at every time step within a specified limit. The required node spacing will be dictated by the initial peak. Looking at the LCM errors, the peak in this case occurs at approximately $t = 0.01$ and the errors have reduced again significantly at $t = 0.025$. The problem does not reach a steady state until after $t = 0.1$. If the node spacing was doubled at $t = 0.025$, for example, it would be expected that the subsequent errors would be approximately 4 times higher than just prior to the doubling, but these errors would still be well below the peak values. The computational cost of running the model until $t = 0.1$ would be reduced by a factor of approximately 1.6 compared with what it would be if the node spacing was left unchanged.

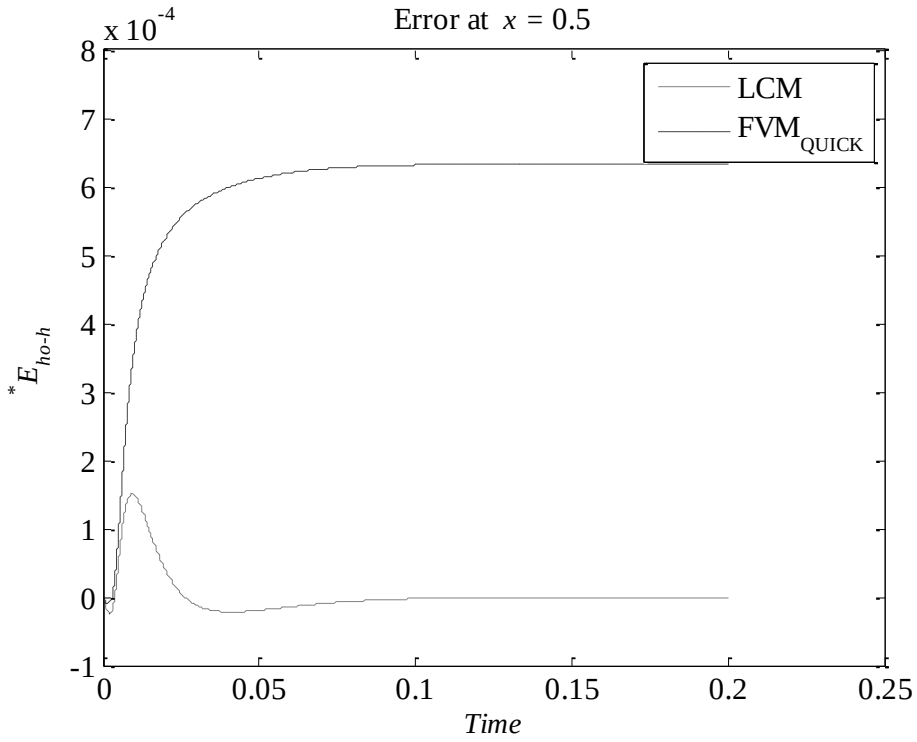

Figure 53: LCM and FVM errors at $x = 0.5$ for a model with $N = 33$.

The boundary conditions for the problem presented here are $V(0,t) = 0$ and $V(1,t) = 1$ and the initial conditions are $V(x,0) = 0$, $x \neq 1$. It has discontinuities at $x = 0.3$ and $x = 0.6$ and the coefficients are $D(x) = \{2,4,2\}$, $S(x) = \{6,12,9\}$, $K(x) = \{40,50,30\}$ and $v(x) = \{5,4,5\}$. The results presented here have been calculated with a time step of $\Delta t = 2\times10^{-6}$. If the number of nodes is initially 65, but is reduced to 33 at $t = 0.025$ for both the FVM and LCM models, then the errors are as shown in Figure 54.

It is clear that the desired outcome has been achieved for the LCM errors in this case, in that the node spacing has been increased, but the errors with the larger node spacing are lower than the maximum error with the smaller node spacing. The accuracy of the results when the node spacing is changed is not significantly lower than the accuracy achieved when N is kept at 65, but the computational cost is lower.

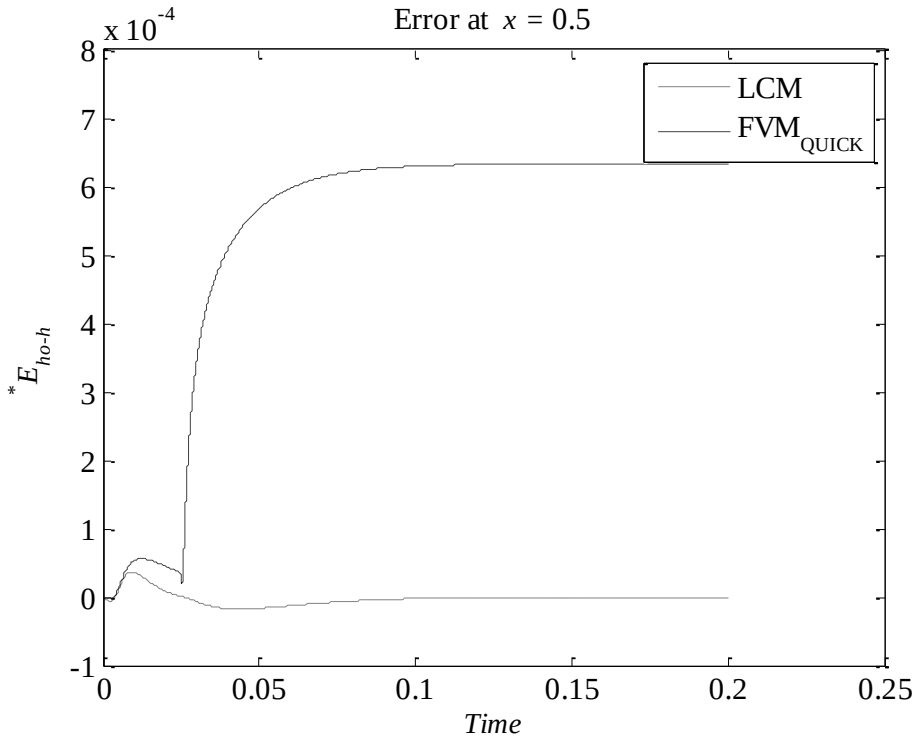

Figure 54: LCM and FVM errors at $x = 0.5$ for a model with $N = 65$ initially and a change to $N = 33$ at $t = 0.025$.

The change in node spacing was made at $t = 0.025$ in this example. That decision to choose that time was based on plots of estimated errors, which, normally, a modeller, who wishes to solve a problem with minimal computational cost, would not have. If a modeller had, however, some qualitative feedback on how the spatial discretization errors rise and fall over time, then that could be useful in determining when a change in node spacing may be beneficial.

Such a change would only be worthwhile if the steady-state spatial-discretization errors are significantly lower than the peak errors (for all node spacings used), and if the peak errors occur well before the solution reaches a steady state. As can be seen from the results above, the FVM errors in this example do not satisfy the first of these criteria, and, as illustrated in Figure 52, even when they do reduce significantly after the peak, they take longer to do so than the LCM errors.

5.3 Time-stepping errors

In Chapter 4, TLM is used as a time-stepping method in both LCM and FVM models. In this section, TLM is used in LCM for a convection-reaction-diffusion problem, the

results are compared with those obtained using the first-order explicit time-stepping scheme, and the order of the TLM time-stepping errors is estimated.

Since the lumped-component circuit for LCM for convection-reaction-diffusion is similar to that for reaction-diffusion, the TLM time-stepping method is the same as that described in Chapter 4. The problem tested has $D = \{2,3,5\}$, $K = \{2,1,4\}$, $v = \{2,8,5\}$ and $S = \{2,3,5\}$, with discontinuities at $x = 0.3$, $x = 0.6$. The boundary and initial conditions are $V(0,t) = 0$, $V(1,t) = 0$ and $V(x,0) = 0$, $x \neq 1$. The node spacing used is $h = 1/32$. The solution values at $x = 0.5$ and $t = 0.01$ are given in Table 21 for LCM and FVM using first-order explicit time-stepping, and for LCM using TLM time-stepping, for a range of time step lengths. Estimates of the orders of the errors are also presented. These are as expected with the TLM time-stepping errors being second order.

Table 21: LCM and FVM solutions calculated using a range of values of Δt, and the corresponding estimates of the orders of the errors.

Δt	LCM	FVM^{HA}_{QUICK}	LCM_{TLM}
1/20000	0.103370	0.104267	0.103165
1/40000	0.103333	0.104229	0.103264
1/80000	0.103315	0.104210	0.103289
	1.0	**1.0**	**2.0**
1/160000	0.103306	0.104200	0.103295
	1.0	**1.0**	**2.0**
1/320000	0.103301	0.104196	0.103296
	1.0	**1.0**	**2.0**
1/640000	0.103299	0.104193	0.103297
	1.0	**1.0**	**2.0**
1/1280000	0.103298	0.104192	0.103297
	1.0	**1.0**	**2.0**
1/2560000	0.103297	0.104191	0.103297
	1.0	**1.0**	**2.0**

Modelling of the capacitors in the lumped-component circuit elements using TL segments introduces additional sources of errors. One of these is a result of the inductance in the TL segments which introduces wave-like behavior in the solution as in standard TLM. The size of the resultant "wave-term errors" is dependent on $\Delta t^2/\Delta x^2$ [67-68]. These time-stepping errors will decrease as Δt is decreased, but unlike with other errors, will increase as Δx is decreased (if Δt is not decreased at the same time).

In the following test, the model settings have been selected so that the wave-term error dominates the solution. The time-step length used is $\Delta t = 1\times10^{-5}$. The problem modelled is the same as the previous one in this section. The solution at the midpoint of the domain is plotted against Δx in Figure 55. It is clear that as Δx is reduced, the error in the TLM solution increases. This is consistent with the error being largely due to the TLM wave-term. If Δt is decreased sufficiently for this problem, then the time-stepping errors will be negligible when compared to the spatial discretization errors, and so the errors will decrease as Δx is decreased, but only up to the point where the wave-term becomes significant again.

It is clear that, as expected, using TLM as a time-stepping technique can prevent a scheme from converging consistently as the node spacing is decreased. For consistent convergence, the time step length and the node spacing must be reduced at the same time.

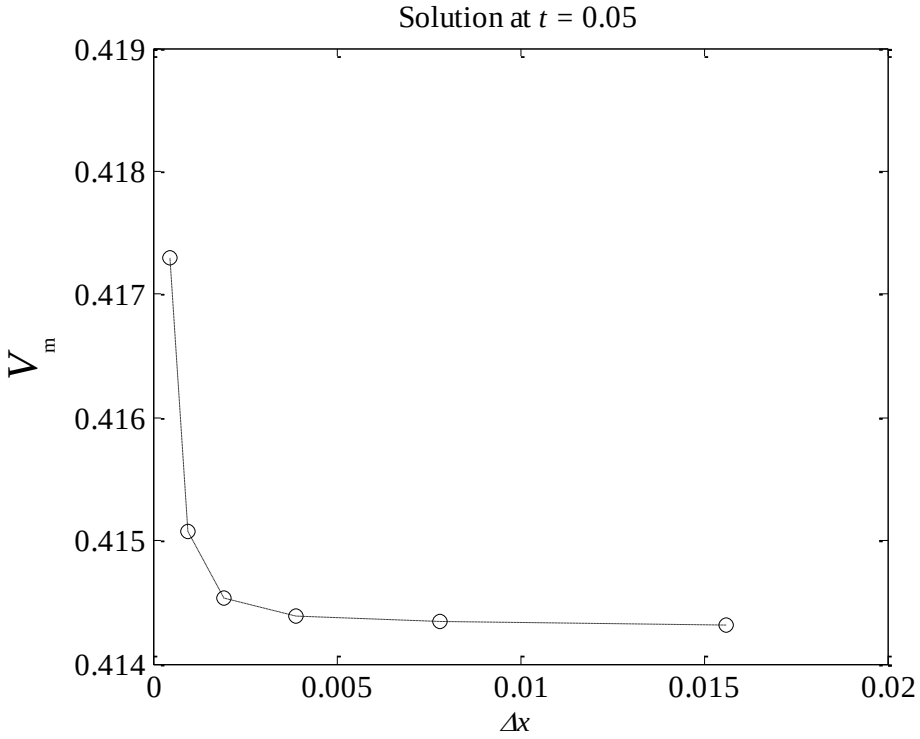

Figure 55: Variation in the LCM solution (with TLM time-stepping) at $x = 0.5$ and $t = 0.05$ for a problem with piecewise constant parameters.

To summarize, in this section it is shown that LCM is able to produce accurate solutions for general convection-reaction-diffusions problems, that the solutions produced are bounded, that it converges consistently when discontinuities in coefficients do not

correspond to the nodes, and that the spatial discretization errors are second order. It is shown that TLM is an efficient time-stepping scheme but that the wave-term errors mean that the solutions obtained in that way no longer converge consistently as Δx is reduced.

Chapter 6

6 2D convection-reaction-diffusion

6.1 Introduction

Few problems of interest can be modelled accurately in just one dimension. It is therefore important that any scheme for solving CRDEs can be extended to two and three dimensions. In this chapter, LCM is extended to solve 2D problems by first modelling them (as in TLM) using a network of interlinked one-dimensional TLs, as illustrated in Figure 56.

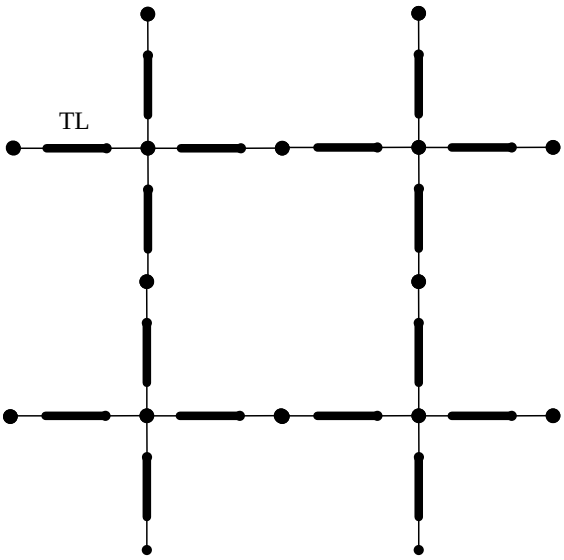

Figure 56: A 2D network of interlinked (i.e. joined at nodes) transmission lines, as used as an analogue for 2D convection-reaction-diffusion problems.

The first step is the derivation of the equation for the voltage on such a network, which can have the same form as a two-dimensional CRDE with non-conservative convection terms

$$\frac{\partial \phi}{\partial t} = \frac{\partial}{\partial x}\left(D_x \frac{\partial \phi}{\partial x} \right) + \frac{\partial}{\partial y}\left(D_y \frac{\partial \phi}{\partial y} \right) - v_x \frac{\partial \phi}{\partial x} - v_y \frac{\partial \phi}{\partial y} - K\phi + S \tag{6.1}$$

Comparison of the equation for the voltage with the CRDE gives the required TL parameters for a given problem. The next step is to model the one-dimensional TL sections between nodes using lumped-component circuit elements, and the final step is the calculation of the node voltages in a network of such circuit elements. Many of the steps involved are very similar to those in one-dimensional LCM.

Unlike with 1D steady-state LCM, there is no possibility that the 2D scheme (or any numerical scheme) can produce, in general, exact solutions, even when the coefficients are constant or piecewise-constant. That is because, with, for example, Dirichlet boundary conditions, the exact solution to a given problem is dependent on the solution value at all points on the boundary, but only the values at the boundary nodes are specified when solving numerically.

6.2 Derivation of the analogue equation

To derive the equation for a voltage across a two-dimensional network of transmission lines, analogous to the CRDE in 2D, consider a small section of a TL network, of dimensions $\Delta x \times \Delta y$, as shown in Figure 57.

First, consider the voltage drop along the short TL section in the x-direction. According to Kirchhoff's voltage law

$$V - \frac{\partial V}{\partial x}\Delta x - \left(I_x - \frac{\partial I_x}{\partial x}\Delta x \right) R_{dx} \Delta x - V = 0 \tag{6.2}$$

As Δx approaches zero, this simplifies to

$$-\frac{1}{R_{dx}} \frac{\partial V}{\partial x} = I_x \tag{6.3}$$

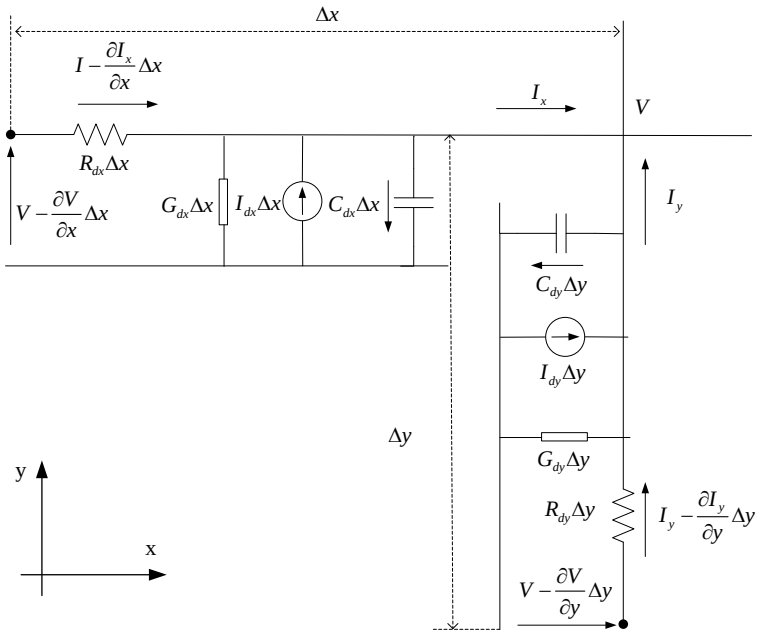

Figure 57: A small segment of a 2D TL network with distributed properties represented by lumped components. The diagram shows only one conductor in each TL connected at a point, but the second conductors are also connected; that connection is not shown in order to make the diagram as clear as possible.

Let the distributed capacitance at any point, whether on the TL in the *x*-direction or the *y*-direction, equal

$$C_d = C_{dx} = C_{dy} r \tag{6.4}$$

where *r* is a ratio equal to

$$r = \frac{\Delta y}{\Delta x} \tag{6.5}$$

The reason for doing this is explained below. Dividing Eq. (6.3) by C_d, gives

$$-\frac{1}{R_{dx} C_d}\frac{\partial V}{\partial x} = \frac{I_x}{C_d} \tag{6.6}$$

which, when differentiated with respect to *x*, gives

$$-\frac{\partial}{\partial x}\left(\frac{1}{R_{dx} C_d}\frac{\partial V}{\partial x}\right) = \frac{1}{C_d}\frac{\partial I_x}{\partial x} + \frac{\partial}{\partial x}\left(\frac{1}{C_d}\right) I_x \tag{6.7}$$

Replacing I_x using Eq. (6.6) and rearranging the resulting equation gives

$$-\frac{\partial}{\partial x}\left(\frac{1}{R_{dx}C_d}\frac{\partial V}{\partial x}\right)+\frac{1}{R_{dx}}\frac{\partial}{\partial x}\left(\frac{1}{C_d}\right)\frac{\partial V}{\partial x}=\frac{1}{C_d}\frac{\partial I_x}{\partial x} \tag{6.8}$$

Similarly, for the *y*-direction,

$$-\frac{\partial}{\partial y}\left(\frac{1}{R_{dy}C_d}\frac{\partial V}{\partial y}\right)+\frac{1}{R_{dy}}\frac{\partial}{\partial y}\left(\frac{1}{C_d}\right)\frac{\partial V}{\partial y}=\frac{1}{C_d}\frac{\partial I_y}{\partial y} \tag{6.9}$$

Now, according to Kirchhoff's current law, the sum of the currents entering the junction of the two TLs must equal zero, and so

$$\begin{aligned}\left(I_x-\frac{\partial I_x}{\partial x}\Delta x\right)+\left(I_y-\frac{\partial I_y}{\partial y}\Delta y\right)+I_{dx}\Delta x+I_{dy}\Delta y-\left(G_{dx}\Delta x+G_{dy}\Delta y\right)V\ldots\\ \ldots-\left(C_{dx}\Delta x+C_{dy}\Delta y\right)\frac{\partial V}{\partial t}=I_x+I_y\end{aligned} \tag{6.10}$$

which simplifies to

$$\left(C_{dx}\Delta x+C_{dy}\Delta y\right)\frac{\partial V}{\partial t}=-\frac{\partial I_x}{\partial x}\Delta x-\frac{\partial I_y}{\partial y}\Delta y+I_{dx}\Delta x+I_{dy}\Delta y-\left(G_{dx}\Delta x+G_{dy}\Delta y\right)V \tag{6.11}$$

Using Equations (6.8) and (6.9) to replace the derivatives of the currents gives

$$\begin{aligned}&\left(C_{dx}\Delta x+C_{dy}\Delta y\right)\frac{\partial V}{\partial t}=C_d\Delta x\frac{\partial}{\partial x}\left(\frac{1}{R_{dx}C_d}\frac{\partial V}{\partial x}\right)\ldots\\ &+C_d\Delta y\frac{\partial}{\partial y}\left(\frac{1}{R_{dy}C_d}\frac{\partial V}{\partial y}\right)-\frac{C_d\Delta x}{R_{dx}}\frac{\partial}{\partial x}\left(\frac{1}{C_d}\right)\frac{\partial V}{\partial x}\ldots\\ &-\frac{C_d\Delta y}{R_{dy}}\frac{\partial}{\partial y}\left(\frac{1}{C_d}\right)\frac{\partial V}{\partial y}-\left(G_{dx}\Delta x+G_{dy}\Delta y\right)V+I_{dx}\Delta x+I_{dy}\Delta y\end{aligned} \tag{6.12}$$

From Eq. (6.5), $r\Delta x = \Delta y$, and so this can be rewritten as

$$\begin{aligned}\left(C_{dx}+C_{dy}r\right)\frac{\partial V}{\partial t}=C_d\frac{\partial}{\partial x}\left(\frac{1}{R_{dx}C_d}\frac{\partial V}{\partial x}\right)+C_dr\frac{\partial}{\partial y}\left(\frac{1}{R_{dy}C_d}\frac{\partial V}{\partial y}\right)-\frac{C_d}{R_{dx}}\frac{\partial}{\partial x}\left(\frac{1}{C_d}\right)\frac{\partial V}{\partial x}\ldots\\ \ldots-\frac{C_dr}{R_{dy}}\frac{\partial}{\partial y}\left(\frac{1}{C_d}\right)\frac{\partial V(x,y,t)}{\partial y}-\left(G_{dx}+G_{dy}r\right)V+I_{dx}+I_{dy}r\end{aligned} \tag{6.13}$$

Now, from Eq. (6.4), $C_{dx}+C_{dy}r=2C_d$, and so this becomes

$$\frac{\partial V}{\partial t}=\frac{\partial}{\partial x}\left(\frac{1}{2R_{dx}C_d}\frac{\partial V}{\partial x}\right)+r\frac{\partial}{\partial y}\left(\frac{1}{2R_{dy}C_d}\frac{\partial V}{\partial y}\right)-\frac{1}{R_{dx}}\frac{\partial}{\partial x}\left(\frac{1}{2C_d}\right)\frac{\partial V}{\partial x}\ldots$$
$$\ldots-\frac{r}{R_{dy}}\frac{\partial}{\partial y}\left(\frac{1}{2C_d}\right)\frac{\partial V(x,y,t)}{\partial y}-\left(\frac{G_{dx}+G_{dy}r}{2C_d}\right)V+\frac{I_{dx}+I_{dy}r}{2C_d} \tag{6.14}$$

It is clear that a transmission line network of this kind is analogous to the CRDE in two dimensions

$$\frac{\partial\phi}{\partial t}=\frac{\partial}{\partial x}\left(D_x\frac{\partial\phi}{\partial x}\right)+\frac{\partial}{\partial y}\left(D_y\frac{\partial\phi}{\partial y}\right)-v_x\frac{\partial\phi}{\partial x}-v_y\frac{\partial\phi}{\partial y}-K\phi+S \tag{6.15}$$

when

$$D_x=\frac{1}{2R_{dx}C_d}=\frac{1}{2R_{dx}C_{dx}} \tag{6.16}$$

$$D_y=\frac{1}{2R_{dy}C_d}=\frac{1}{2R_{dy}C_{dy}} \tag{6.17}$$

$$v_x=\frac{1}{R_{dx}}\frac{\partial}{\partial x}\left(\frac{1}{2C_d}\right)=\frac{1}{R_{dx}}\frac{\partial}{\partial x}\left(\frac{1}{2C_{dx}}\right) \tag{6.18}$$

$$v_y=\frac{r}{R_{dy}}\frac{\partial}{\partial y}\left(\frac{1}{2C_d}\right)=\frac{1}{R_{dy}}\frac{\partial}{\partial y}\left(\frac{1}{2C_{dy}}\right) \tag{6.19}$$

$$K=\frac{G_{dx}+G_{dy}r}{2C_d}=\frac{G_{dx}}{2C_{dx}}+\frac{G_{dy}}{2C_{dy}} \tag{6.20}$$

$$S=\frac{I_{dx}+I_{dy}r}{2C_d}=\frac{I_{dx}}{2C_{dx}}+\frac{I_{dy}}{2C_{dy}} \tag{6.21}$$

It is also clear that these equations are very similar to the equivalent ones for one-dimensional LCM. This similarity allows, as will be shown below, the calculation of the lumped-component circuit element parameters to proceed largely as in one dimension. That is only achieved because the relationship between the distributed capacitances of the *x*-direction and *y*-direction TLs is as specified in Eq. (6.4).

It should be noted that the relationship given in Eq. (6.4) cannot generally be satisfied over a domain for a given convection-reaction-diffusion problem (although it could be satisfied for a reaction-diffusion problem), because modelling of convection requires C_{dx} and C_{dy} to vary over space in a specified way (e.g. exponentially over a section with a uniform convection velocity). To illustrate this, consider the situation represented in Figure 58 which shows 4 TLs with $h_x = h_y$ that are an approximate analogue for a problem with constant Pe_x and Pe_y. The values of Pe_x and h_x are such that the exponentially varying C_{dx} must double over the length of each horizontal TL section. The values of Pe_y and h_y are such that C_{dy} must increase by a factor of three over the length of each vertical TL section. The value of C_{dx} at the start of any horizontal line affects the values at every other point along that line. Changing it simply scales the values at all points. The same is true for the vertical lines. In a two-dimensional model, it is assumed that $C_d = C_{dx} = C_{dy}r$, where, as will be seen below, r must equal one when a square grid is used as in this example. It is clear that this cannot be the case at all points. Just considering the values at the nodes in Figure 58, the following would have to be satisfied:

$$2c_{1,x} = 9c_{1,y}$$

$$4c_{1,x} = 9c_{2,y}$$

$$2c_{2,x} = 3c_{1,y}$$

$$4c_{2,x} = 3c_{2,y}$$

which is not possible while satisfying the requirement that C_{dx} and C_{dy} cannot be zero. This is discussed further below.

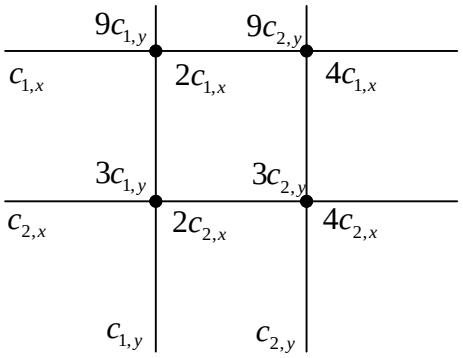

Figure 58: A two-dimensional model composed of two vertical and two horizontal TLs. The distributed capacitance at the left-hand end of each section of horizontal line is indicated below the line with a subscript *x*. The distributed capacitance at the lower end of each section of vertical line is indicated to the left of the line with a subscript *y*.

6.3 Derivation of the 2D LCM equation

The next step in the modelling process is to represent the sections of TLs linking adjacent nodes using lumped-component circuit elements, but, before explaining how that is done, the equation for the node voltages in a network of such elements must be derived.

To determine the node voltage at any node numbered *n*, *m* in terms of the voltages at the surrounding nodes, consider the four lumped-component circuit elements shown in Figure 59. From Kirchhoff's current law, the sum of the currents at node *n*, *m* is zero, and so.

$$C_{n,m}\frac{\partial V}{\partial t}=\left(\frac{V_{n+1,m}-V_{n,m}}{R_{x,n,m}}\right)-\left(\frac{V_{n,m}-V_{n-1,m}}{R_{x,n-1,m}}\right)+\left(\frac{V_{n,m+1}-V_{n,m}}{R_{y,n,m}}\right)-\left(\frac{V_{n,m}-V_{n,m-1}}{R_{y,n,m-1}}\right)\ldots$$
$$\ldots-V_{n,m}\left(G_{rx,n-1,m}+G_{lx,n,m}+G_{ry,n,m-1}+G_{ly,n,m}\right)+I_{rx,n-1,m}+I_{lx,n,m}+I_{ry,n,m-1}+I_{ly,n,m} \quad (6.22)$$

where

$$C_{n,m}=C_{rx,n-1,m}+C_{lx,n,m}+C_{ry,n,m-1}+C_{ly,n,m} \quad (6.23)$$

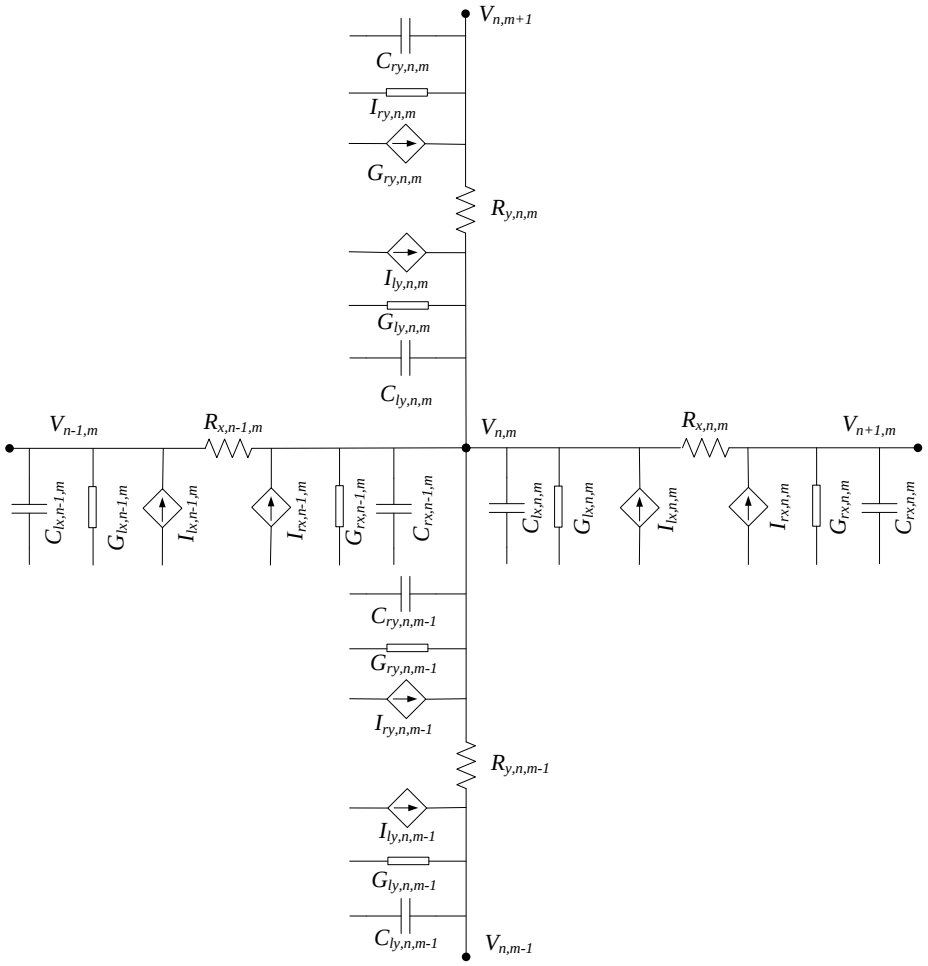

Figure 59: Part of a 2D lumped-component circuit model.

This can be rewritten as

$$R_{C,n,m}\frac{\partial V}{\partial t} = P_{x,n,m}\left(V_{n+1,m} - V_{n,m}\right) - \left(V_{n,m} - V_{n-1,m}\right) + P_{y,n,m}P_{xy,n,m}\left(V_{n,m+1} - V_{n,m}\right) - r_{n,m}\left(V_{n,m} - V_{n,m-1}\right) - R_{G,n,m}V_{n,m} + R_{I,n,m} \tag{6.24}$$

where

$$P_{x,n,m} = \frac{R_{x,n-1,m}}{R_{x,n,m}} \tag{6.25}$$

$$P_{y,n,m} = \frac{R_{y,n,m-1}}{R_{y,n,m}} \tag{6.26}$$

$$P_{xy,n,m} = \frac{R_{x,n-1,m}}{R_{y,n,m-1}} \tag{6.27}$$

and

$$R_{C,n,m} = R_{x,n-1,m}\left(C_{rx,n-1,m} + C_{lx,n,m}\right) + R_{x,n-1,m}\left(C_{ry,n,m-1} + C_{ly,n,m}\right) \tag{6.28}$$

$$R_{G,n,m} = R_{x,n-1,m}\left(G_{rx,n-1,m} + G_{lx,n,m}\right) + R_{x,n-1,m}\left(G_{ry,n,m-1} + G_{ly,n,m}\right) \tag{6.29}$$

$$R_{I,n,m} = R_{x,n-1,m}\left(I_{rx,n-1,m} + I_{lx,n,m}\right) + R_{x,n-1,m}\left(I_{ry,n,m-1} + I_{ly,n,m}\right) \tag{6.30}$$

6.4 Calculation of lumped-component circuit parameters

The first four equations derived above for the relationship between the problem coefficients and the TL parameters, i.e.

$$D_x = \frac{1}{2R_{dx}C_d},\ D_y = \frac{r}{2R_{dy}C_d},\ v_x = \frac{1}{R_{dx}}\frac{\partial}{\partial x}\left(\frac{1}{2C_d}\right),\ v_y = \frac{r}{R_{dy}}\frac{\partial}{\partial y}\left(\frac{1}{2C_d}\right) \tag{6.31}$$

are identical to the equivalent equations for a one-dimensional line derived in Chapter 5

$$D = \frac{1}{R_d C_d},\ v = \frac{1}{R_d}\frac{\partial}{\partial x}\left(\frac{1}{C_d}\right) \tag{6.32}$$

so long as the distributed capacitance in the *x*- and *y*-directions is half what it would be for an equivalent one-dimensional model. Similarly

$$K = \frac{G_{dx} + G_{dy}r}{2C_d},\ S = \frac{I_{dx} + I_{dy}r}{2C_d} \tag{6.33}$$

are similar to the equivalents for one dimension

$$K = \frac{G_d(x)}{C_d(x)},\ S = \frac{I_d(x)}{C_d(x)} \tag{6.34}$$

given that G_{dx} will equal zero along a vertical TL line (i.e. one aligned in the *y*-direction), and G_{dy} will equal zero along a horizontal TL.

The relationship between the problem coefficients and the TL distributed parameters is therefore identical, for each line, to what it is in one dimension, except for a factor of one half. The relationship between the distributed parameters of a TL section in a 2D model and the equivalent lumped-component circuit element is also the same as in one dimension (since the relationship is derived from the I/O relationships of the two circuit elements which are independent of what those elements are connected to).

It is therefore possible to calculate the lumped-component circuit parameters for each line, whether in the *x*- or *y*-direction, in exactly the same way as is done for a one-dimensional problem. The only things that need to be done differently are to take the factor of one-half into account for the capacitance, and to try to ensure that the distributed capacitances in the horizontal and vertical lines satisfy $C_{dx} = C_{dy}r$. As shown below, both of these adjustments can be made after the lumped-circuit parameters are calculated.

In one dimension, the calculations start by specifying a value of C_d at the boundary node. This value can be one. It is indicated as $C_{dx,0}$ in Figure 60. The value at node 2 is then $f_{x1}C_{dx,0}$, where f_{x1} is a function of the problem coefficients along the segment between nodes 1 and 2. Similarly, the value of C_d at node 3 will be $f_{x2}f_{x1}C_{dx,0}$, where f_{x2} is a function of the problem coefficients between nodes 2 and 3.

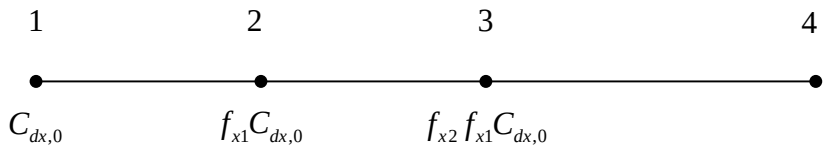

Figure 60: A section of one-dimensional transmission line with four nodes marked and the values of the distributed capacitance at three of those nodes indicated.

When the lumped-component circuit parameters are calculated, they are all inversely proportional, or proportional, to the value of $C_{dx,0}$, i.e. the value of C_d at the start of the line. They can therefore be easily recalculated for any given value of $C_{dx,0}$ by simply scaling their values by the correct amount.

Assume that the lumped-component parameter values have already been calculated for each of the TLs in a 2D network using arbitrary starting values for C_d for each line. Assume also that the values of the distributed capacitance for both the horizontal and vertical TLs have been recorded at each node. The relevant values are indicated in

Figure 61 for the elements surrounding node n, m. It is necessary, when calculating the LCM parameters for that node, to have $C_{dx,n,m} = C_{dy,n,m} r_{n,m}$ at the node, where $r_{n,m}$ is the necessary value for the ratio r at node n, m. In this case, that means that the distributed capacitance of the horizontal line at the node must be changed from the current value of $C_{dx,n,m}$ to $C_{dy,n,m}\, r_{n,m}$, which means that it must be scaled by a factor of

$$S_{n,m} = \frac{C_{dy,n,m} r_{n,m}}{C_{dx,n,m}}$$

While the distributed capacitance of the line must be increased by this factor, the distributed resistance, conductance and current source must all be reduced by the same factor. To take that into account, the lumped-component parameters for the circuit elements to the left and right of the node must simply be scaled in the same way (i.e. the capacitances must be increased by a factor of $S_{n,m}$, and all of the other parameters must be decreased by the same factor). Once that adjustment is made for node n, m, the 2D LCM equation parameters, defined by Equations (6.25) to (6.30), can be calculated for that node.

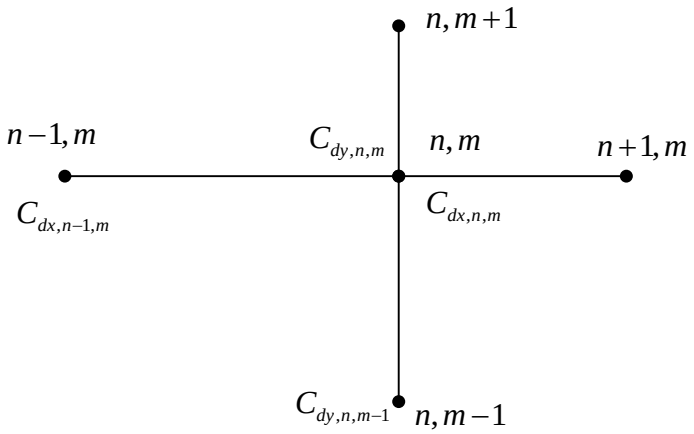

Figure 61: Part of a 2D TL network around node n, m. The values of the distributed capacitance at the nodes to the left and below are indicated, along with the two values (i.e. one for the horizontal line and one for the vertical line) at node n, m.

It should be noted that the values of the 2D LCM equation parameters, defined by Equations (6.25) to (6.30), are independent of any scaling of the distributed capacitances of the vertical and horizontal TLs, but that $P_{xy,n,m}$, $R_{C,n,m}$, $R_{G,n,m}$ and $R_{I,n,m}$ are all dependent on the ratio of the distributed capacitances of the two lines at node n, m.

There is a factor of one half in the equations relating the 2D TL network distributed properties and the problem coefficients, that is not in the equivalent equations for 1D modelling. As a result, a 2D lumped-component circuit with parameters calculated as described above (i.e. largely as for a one-dimensional model) will model

$$\frac{\partial \phi}{\partial t} = \frac{1}{2}\left\{\frac{\partial}{\partial x}\left(D_x \frac{\partial \phi}{\partial x}\right) + \frac{\partial}{\partial y}\left(D_y \frac{\partial \phi}{\partial y}\right) - v_x \frac{\partial \phi}{\partial x} - v_y \frac{\partial \phi}{\partial y} - K\phi + S\right\}$$

instead of

$$\frac{\partial \phi}{\partial t} = \frac{\partial}{\partial x}\left(D_x \frac{\partial \phi}{\partial x}\right) + \frac{\partial}{\partial y}\left(D_y \frac{\partial \phi}{\partial y}\right) - v_x \frac{\partial \phi}{\partial x} - v_y \frac{\partial \phi}{\partial y} - K\phi + S$$

For a steady-state problem, this makes no difference. For a transient model, this issue can be resolved by simply halving the values of the capacitors in the lumped-component circuit network.

It should be noted that the parameter r, introduced above in the derivation of the equation for the voltage across a small section of TL network of dimensions $\Delta x \times \Delta y$, equals the aspect ratio of the section (i.e. $r = \Delta x/\Delta y$). As seen above, using r as the ratio of the distributed capacitance of the horizontal and vertical lines at a given node, allows the 2D lumped-component circuit parameters to be calculated in a similar way to that used in 1D modelling. The question arises as to what value it should have for a given node. The answer, found through testing, is that it should equal the aspect ratio of the rectangular area corresponding to the node. For example, for the node shown in Figure 62, the ratio should be

$$r_{n,m} = \frac{h_{y,n,m-1} + h_{y,n,m}}{h_{x,n-1,m} + h_{x,n,m}}$$

As mentioned above, this equals one if the area is square.

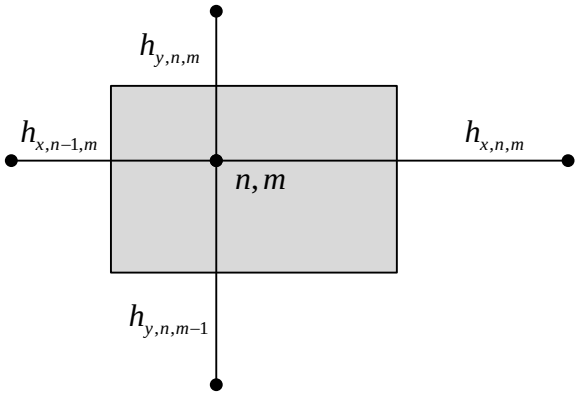

Figure 62: The rectangular area corresponding to node *n*, *m* in an unevenly spaced grid, with all node spacings labelled

6.5 Slug injection into a uniform groundwater flow field

Water supply contaminations can cause serious health problems and have environmental, economic and social impacts. As a result, it is important to understand the groundwater contaminant transport process [106]. One experimental method used involves injecting a slug tracer (e.g. a quantity of dye) into the groundwater flow field and monitoring its movement over time and space through a sampling process.

The transport of contaminant in the ground water system can be modelled using a CRDE, the equation often being simplified so as to aid solution. In this example, a single injection of a miscible contaminant fluid into an infinite homogenous medium is modelled, with a uniform flow field, anisotropic diffusion (i.e. $D_x \neq D_y$), and with no reactions or other sources of diffusant. In two dimensions, the equation to be solved is

$$\frac{\partial C}{\partial t} = D_x \frac{\partial^2 C}{\partial x^2} + D_y \frac{\partial^2 C}{\partial y^2} - v_x \frac{\partial C}{\partial x} - v_y \frac{\partial C}{\partial y} \tag{6.35}$$

The analytical solution is [106-107]

$$C(x, y, t) = \frac{C_o A}{4\pi t \sqrt{D_x D_y}} \exp\left(-\frac{\left(x - x_0 - v_x t\right)^2}{4 D_x t} - \frac{\left(y - y_0 - v_y t\right)^2}{4 D_y t} \right)$$

where an initial injection at a point (x_0, y_0) gives an initial concentration of C_0 at that point. In this example, $C_0 = 600$ mg/L, $D_x = 20$ m^2/day, $D_y = 80$ m^2/day, and $v_x = v_y = 0.1$ m/day. The node spacings are $h_x = h_y = 0.045$ m. The LCM solutions at $t = 1$ years, $t = 3$ years and $t = 5$ years, calculated using a time step length of 0.001

years, are shown in Figure 63. The problem domain is infinite but the model domain is 4500 m × 4500 m. The initial injection is made at $x = y = 2250$ m.

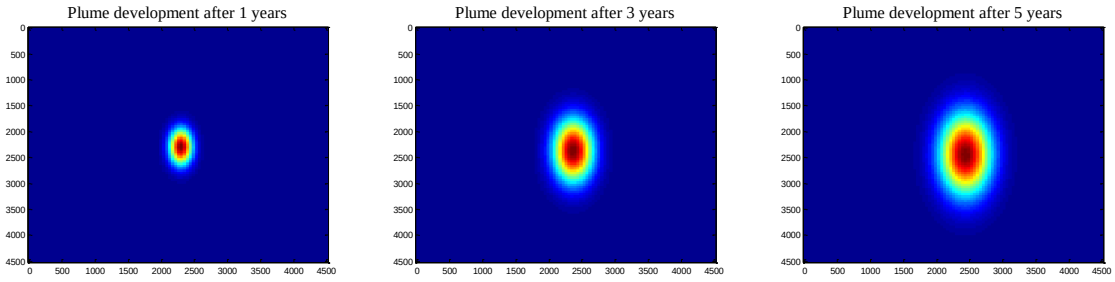

Figure 63: Plume development after 5 years, 10 years and 15 years, as calculated using LCM.

For comparison, solutions have also been calculated using FVM and are presented below. The central difference technique has been used for implementing convection for the sake of convenience and because it is capable of providing accurate results for a problem, like this, in which the Peclet number is low.

The LCM and FVM solutions along the line $y = 2250$ m at $t = 5$ years are plotted in Figure 64, along with the analytical solution. It is clear that they are in close agreement with each other. The corresponding errors are shown in Figure 65. It is clear that, for this problem, LCM has no clear advantage over FVM

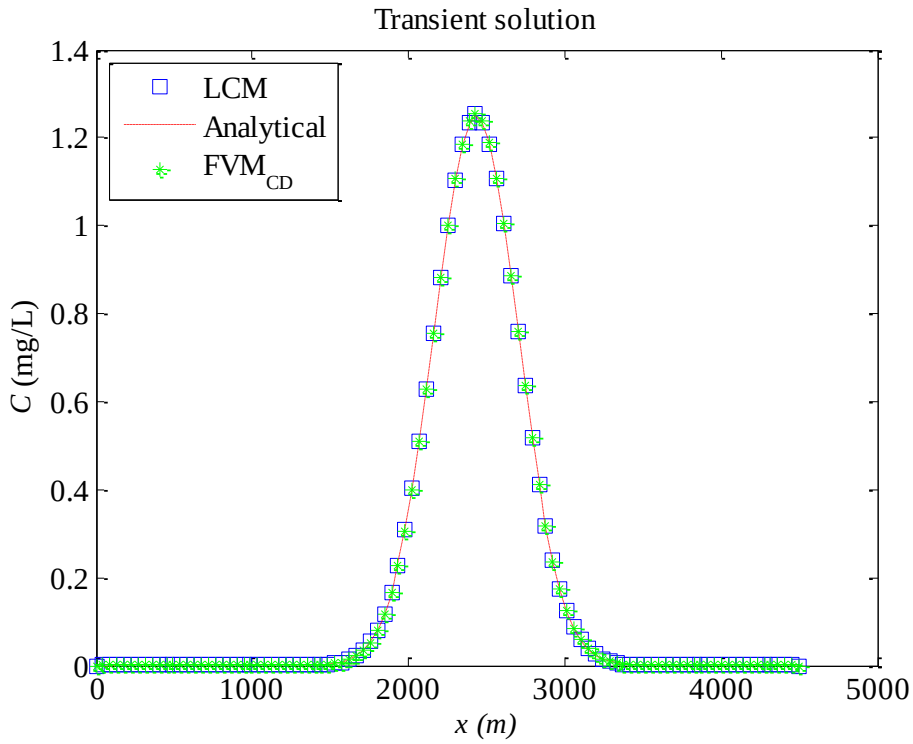

Figure 64: LCM, FVM and analytical solutions along the line y = 2250 m at t = 5 years.

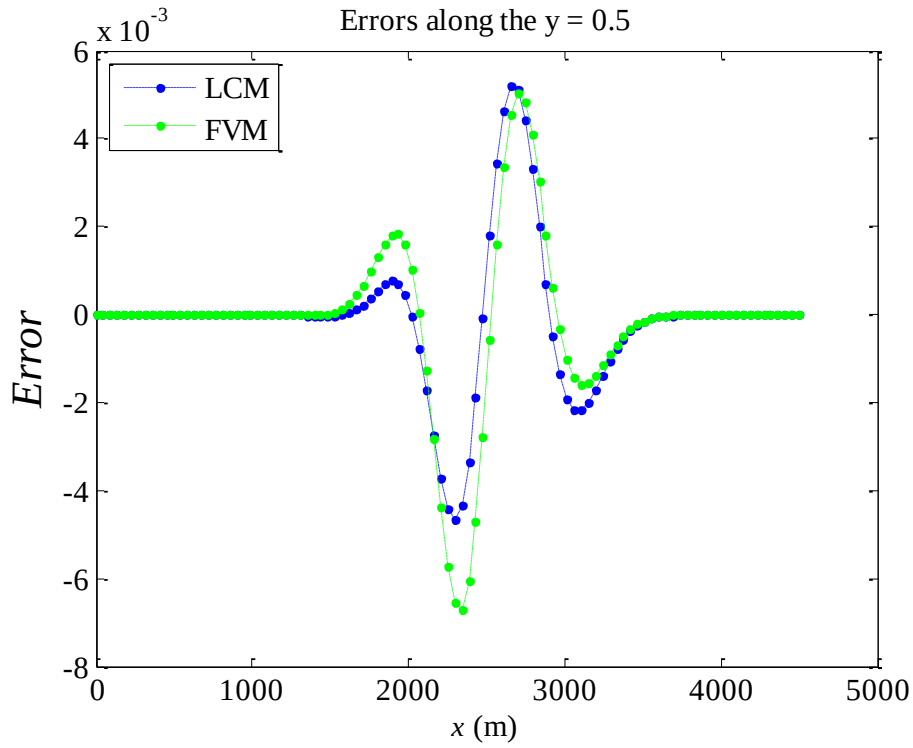

Figure 65: Absolute errors in the LCM and FVM solutions along the line y = 2250 m at t = 5 years.

6.6 Spatial errors in 2D LCM

This section examines the spatial errors in 2D LCM solutions, the order of convergence of those errors, and the consistency of convergence when nodes do not correspond to

discontinuities. Little effort is made here to compare the accuracy of the method with that of FVM; instead, the primary purpose of the tests presented is to validate the method outlined above by showing that 2D LCM models behave as expected under a variety of conditions.

All tests involve transient convection-reaction-diffusion problems, and the values presented are from solutions that have not reached a steady state, calculated with time-step lengths sufficiently short to ensure that time-stepping errors are insignificant.

The domain for the first test is illustrated in Figure 66 along with the values of the coefficients and the dimensions of the two media that comprise the domain. The nodes are positioned so that one vertical TL corresponds to the discontinuity. One section of this TL is highlighted in the diagram. The values of D, v_y, etc. used to calculate the required distributed parameters for this section (and the other sections along the discontinuity) are simply the averages of the values on either side. For example, the value of D is taken as (7 + 2)/2 = 4.5.

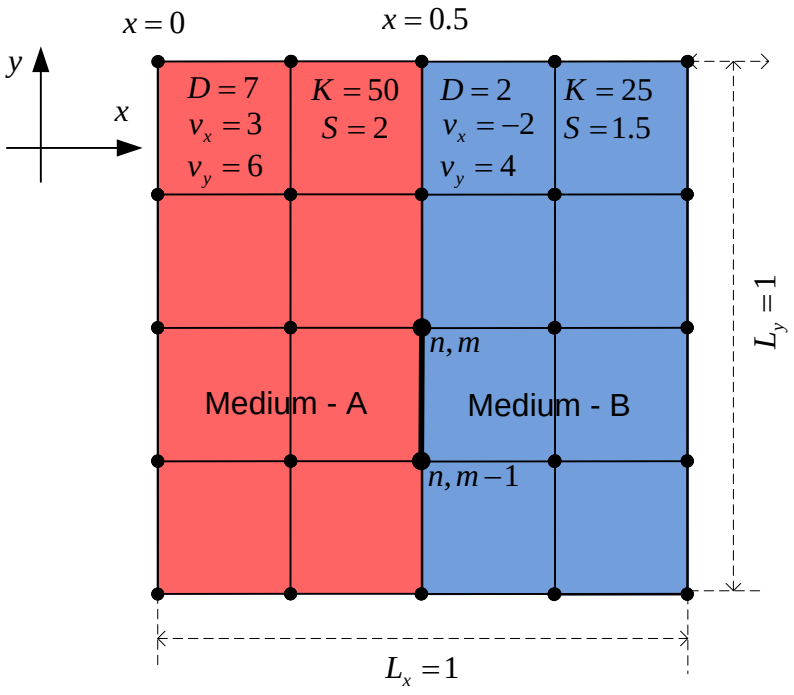

Figure 66: A 2D domain with piecewise-constant properties, in which nodes correspond to the interface where the two media meet.

The initial and boundary conditions for the model are $V(x, y; 0) = 0$, and $V(0, y; t) = 0$, $V(x, 0; t) = 0$, $V(1, y; t) = 1$ and $V(x, 1; t) = 1$, respectively. The meshes used are square (i.e. $h_x = h_y = h$) and the time-step is $\Delta t = 1\times10^{-6}$. LCM and FVM solution values of

$V(0.5, 0.5; 0.02)$ are plotted against h in Figure 67. Corresponding values of the estimated order of convergence are listed in Table 22 (along with the solution values used to calculate them, i.e. the values plotted in Figure 67).

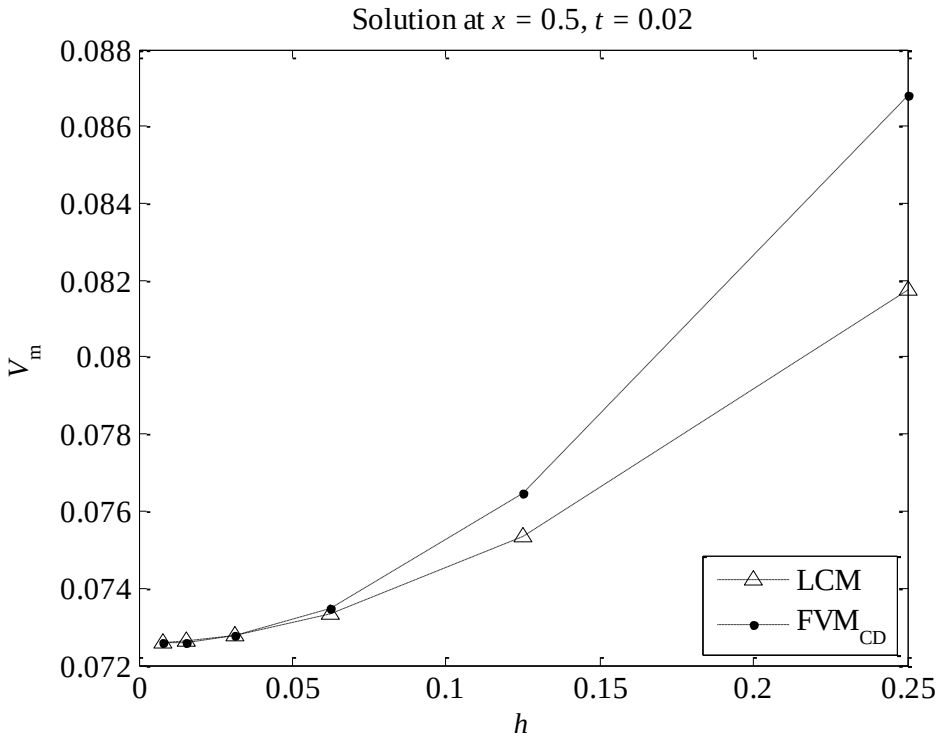

Figure 67: Estimated values of $V(0.5, 0.5; 0.02)$ plotted against h for a model with two media and nodes corresponding to the discontinuity.

Table 22: The values plotted in Figure 67 and the corresponding values of the order of convergence. Note that N is the total number of nodes in the model, so each row corresponds to a node spacing that is half that of the row above.

N	LCM	FVM_{CD}
25	0.081772	0.086812
81	0.075334	0.076462
289	0.073315	0.073478
	1.7	**1.8**
1089	0.072777	0.072752
	1.9	**2.0**
4225	0.072640	0.072600
	2.0	**2.3**
16641	0.072606	0.072579
	2.0	**2.8**

The results in Table 22 suggest a clear second order convergence of the LCM solutions, but the behaviour of the FVM solutions is less clear. The LCM solutions are more, but not significantly more, accurate than those obtained using the FVM scheme.

The next test examines the same problem but using an uneven grid as illustrated in Figure 68. Again, there is a vertical TL corresponding to the discontinuity, and the coefficients used to calculate the TL distributed parameters for that line are averages (but weighted according to the node spacings on either side). For example, the value of D at any point along the line is calculated as

$$D(0.5, y) = \frac{h_x \times 7 + (h_x/2) \times 2}{h_x + h_x/2}$$

LCM and FVM solution values of $V(0.5, 0.5; 0.02)$, calculated using $\Delta t = 8\times10^{-7}$ (shorter than for the first test above so as to avoid instability of the explicit time-stepping scheme), are listed in Table 23.

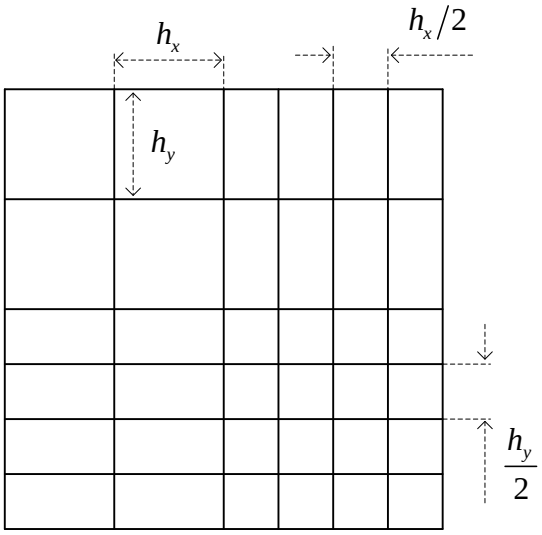

Figure 68: Illustration of the uneven mesh used to calculate the results in row 1 of Table 23.

Table 23: Values equivalent to those listed in Table 22 but calculated using uneven meshes.

N	LCM	FVM_{CD}
49	0.073750	0.071708
169	0.072774	0.072723
625	0.072632	0.072916
	2.8	**2.4**
2401	0.072603	0.072828
	2.3	**1.1**
9409	0.072596	0.072730
	2.0	**-0.2**
37249	0.072594	0.072666
	2.0	**0.6**

The LCM solution convergence is second order. The FVM solution convergence, expected to be first order, is not clear from the results. The reason for that has not been investigated to date. For small node spacings, the LCM scheme is significantly more accurate, in this case, than the FVM scheme tested.

To further validate the LCM method, a problem with four different media (as illustrated in Figure 69), and therefore more discontinuities, is examined next. The initial and boundary conditions are the same as for the previous two tests. In this case, averaging of coefficients is required for the horizontal TL corresponding to $y = 0.5$ and for the vertical TL corresponding to $x = 0.5$. LCM solutions for $V(0.5, 0.5; 0.02)$ and $V(0.375, 0.375; 0.02)$, and their corresponding orders of convergence, are listed in Table 24.

Table 24: Estimated values of $V(0.5, 0.5; 0.02)$ and $V(0.375, 0.375; 0.02)$ calculated using LCM with a range of node spacings, and the corresponding orders of convergence.

N	$V_{LCM}(0.5, 0.5; 0.02)$	$V_{LCM}(0.375, 0.375; 0.02)$
25	0.158430	
81	0.156836	0.094483
289	0.156274 **1.5**	0.093331
1089	0.156041 **1.3**	0.092995 **1.8**
4225	0.155953 **1.4**	0.092902 **1.9**
16641	0.155921 **1.5**	0.092877 **1.9**

The estimated order of the solution convergence is less than two when estimated using solution values at the central discontinuity, but is more clearly two when measured at other points in space. In order to investigate why this is the case, a similar model is tested but with the coefficients shown in Figure 70. In this case, the diffusion in each of the four media is anisotropic. The values of D_x, D_y, v_x and v_y have been chosen so that no averaging of coefficients is required, i.e. the values of D_x, v_x, K and S above and below the TL sections along $y = 0.5$, used to calculate the parameters for those sections, are equal, and so are the values of D_y, v_y, K and S to the left and right of the TL along $x = 0.5$. Estimated values of the order of convergence of the LCM solutions are listed in Table 25, along with the values of $V(0.5, 0.5; 0.02)$ from which they have been calculated.

The results show that the convergence is more clearly second order in this case. This suggests that the averaging of the coefficients may be affecting the convergence in the problem above, but this requires further investigation

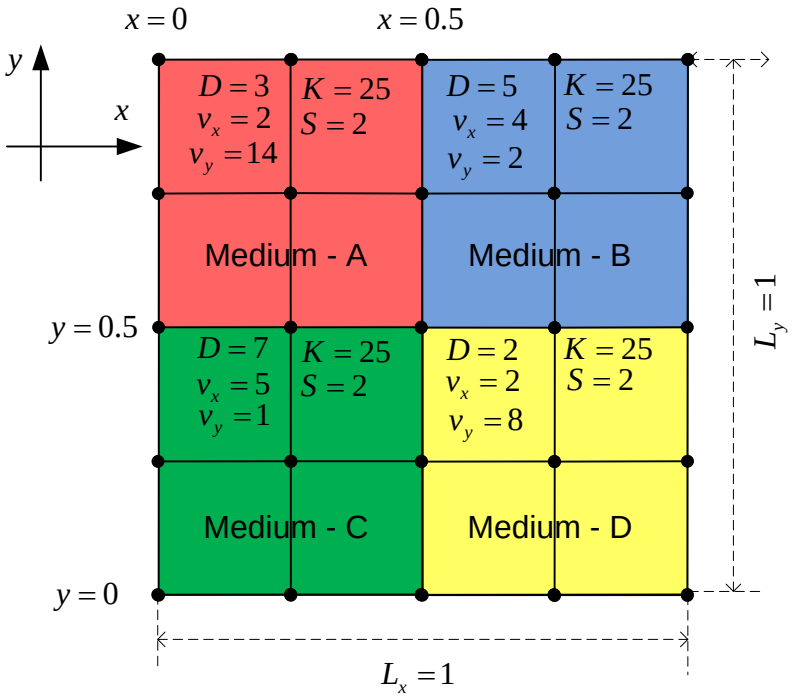

Figure 69: A two-dimensional domain with piecewise-constant coefficients, in which nodes correspond to the media interfaces.

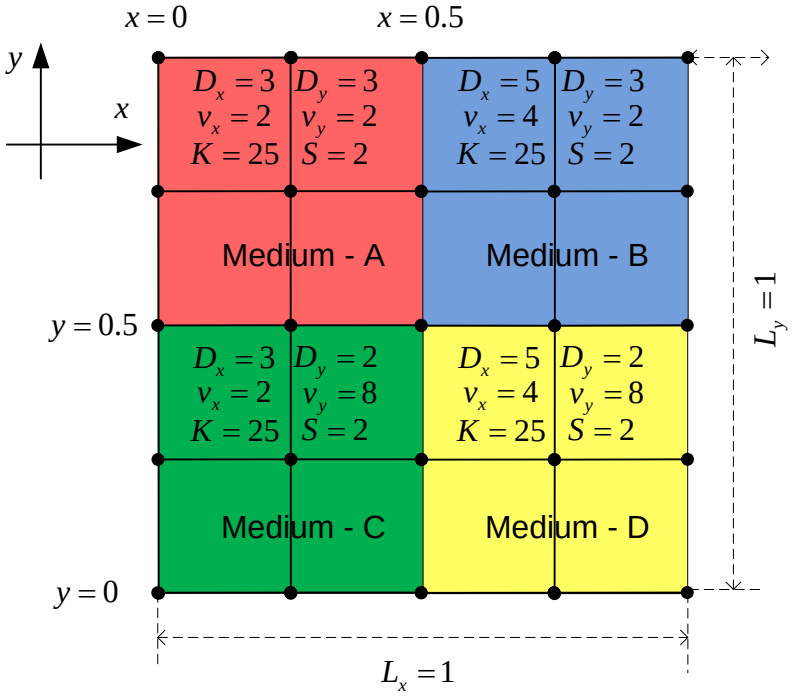

Figure 70: A 2D domain with piecewise-constant materials properties, in which the element and nodes correspond to the boundaries of the materials, and where some material properties are equal between two of the mediums in order to avoid averaging of the coefficient. For example, coefficients in the y-direction for the red and blue are equal.

Table 25: Estimated values of $V(0.5, 0.5; 0.02)$ calculated using LCM with a range of node spacings, and the corresponding order of convergence, for the problem illustrated in Figure 70.

N	LCM
25	0.156100
81	0.151197
289	0.149758 **1.8**
1089	0.149383 **1.9**
4225	0.149289 **2.0**
16641	0.149265 **2.0**

In a 2D model of a problem with coefficients that vary continuously over space, the coefficients would have to be approximated using piecewise-constant functions (as in one dimension). The number of discontinuities would then increase as the node spacing is decreased. The tests above suggest that an increased number of discontinuities may affect the order of convergence. Other tests, however, not presented here, have shown that convergence is closer to second order if the differences in the coefficients at the media interfaces were reduced, which would happen in such a model as the node spacing is reduced.

The results presented above validate the 2D LCM scheme, to some extent, in that they show that it is second-order convergent, but only for problems in which there is only one TL segment in each TL section linking adjacent nodes. The following test examines a situation in which this is not the case (i.e. there are no nodes at the discontinuity).

This test is similar to the first test above except that the discontinuity is located at $x = 0.3$, as shown in Figure 71. The coefficient values used to calculate the TL distributed parameters at any point in space, in this case, are simply the problem coefficients at that point in space. So, for example, the parameters for the section of vertical line between nodes (3, 3) and (3, 2) are calculated using the coefficients for medium B and are the same as for the section between nodes (4, 3) and (4, 2). The section of horizontal TL between nodes (2, 3) and (3, 3) for example, is comprised of two TL segments, the first with parameters calculated using the coefficients for medium A, and the second calculated using the coefficients for medium B.

For this test, the estimated order of convergence of the LCM solutions are listed in Table 26, along with the values of $V(0.5, 0.5; 0.02)$ from which they have been calculated. It is clear that the solution does not converge in a consistent manner. This is not surprising because the method used does not consistently take into account the variation in the problem coefficients between the nodes. The variation in the coefficients along the horizontal line section between node (2, 3) and (3, 3), for example, is taken into account, but the parameters for the vertical line between node (2, 3) and (2, 2) takes no account of the proximity of that line to the interface with medium B.

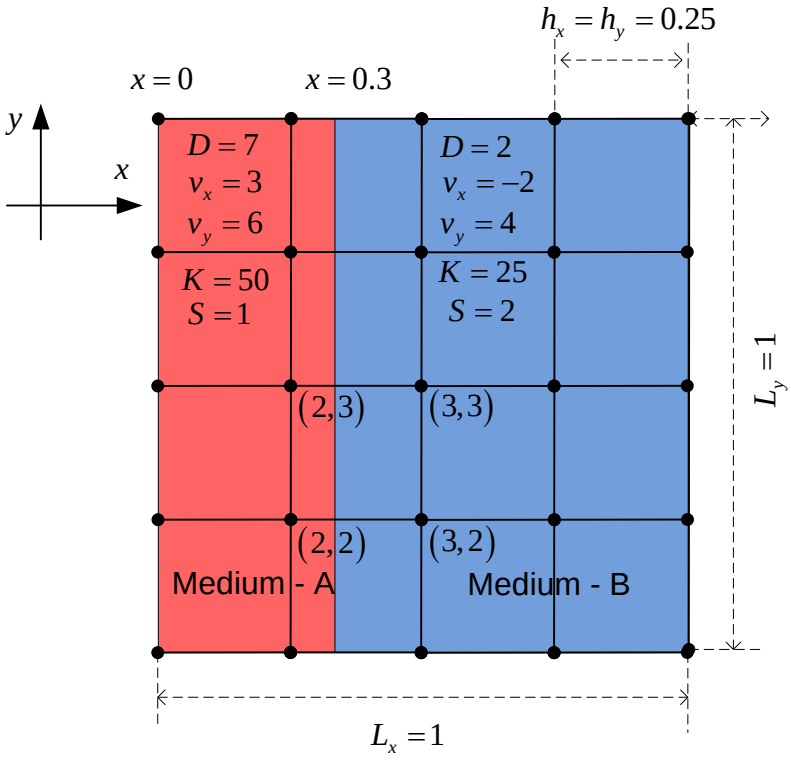

Figure 71: A 2D domain with piecewise-constant coefficients, in which no node positions correspond to the media interface.

Table 26: Estimated values of $V(0.5, 0.5; 0.02)$ calculated using LCM with a range of node spacings, and the corresponding order of convergence, for the problem illustrated in Figure 71.

N	LCM
25	0.109322
81	0.101167
289	0.098287 **1.5**
1089	0.098050 **3.6**
4225	0.098075 **3.2**
16641	0.097952 **-2.3**

The next test is similar, except in the way in which the problem coefficients are used to calculate the parameters of TL segments. Consider the section of vertical transmission line linking nodes (2, 3) and (2, 2) in Figure 71, shown again in Figure 72 (with dimensions indicated for the case where $h = 0.25$). In the previous test, the value of D used to calculate the parameters for the section is 7, i.e. the value for medium A. In this test, the value used is the average of D over the area highlighted in Figure 72, i.e., with $h = 0.25$,

$$D = \frac{0.25 \times \left(0.175 \times 7 + 0.075 \times 2\right)}{0.25 \times 0.25} = 5.5$$

Estimated values of the order of convergence for solutions calculated in this way are listed in Table 27 (equivalent to those in Table 26 calculated without averaging of coefficients), along with the solution values from which they have been calculated.

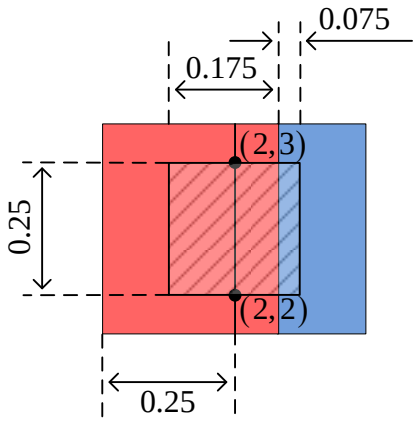

Figure 72: A section of the domain showing nodes (2, 3) and (2, 2) with dimensions indicated for the case in which $h = 0.25$. The coefficients averaged over the highlighted area are used to calculate the parameters for the section of vertical TL between the two nodes indicated.

Table 27: Estimated values of $V(0.5, 0.5; 0.02)$ as in Table 26, but calculated using models in which coefficients are averaged as indicated in Figure 72.

N	LCM
25	0.104826
81	0.100109
289	0.098548 **1.6**
1089	0.098077 **1.7**
4225	0.097958 **2.0**
16641	0.097931 **2.1**

It is clear that the method converges in a consistent second-order manner for this case. Further investigation is required to explore whether alternative averaging techniques could improve the accuracy of the scheme while maintaining consistent convergence of the solutions.

It is envisaged that the averaging method presented above could be used for any piecewise-constant problem. This is illustrated here using the example shown in Figure 73. The horizontal TL section between nodes (1, 2) and (2, 2) is composed of two segments (as highlighted indicated by the red and yellow lines in Figure 73(a)). The properties of the yellow segment are determined by the averages of the problem coefficients over the area indicated by the square grid (which, in this case, simply equal the coefficients for medium B). The properties of the red TL segment are similarly determined by the averages of the problem coefficients over the hashed area (and are therefore dependent on the coefficients of both medium A and medium B). The vertical

TL section between nodes (2, 1) and (2, 2) is composed of three segments as shown in Figure 73(b). The area over which averaging is required to determine the properties of the red segment is highlighted.

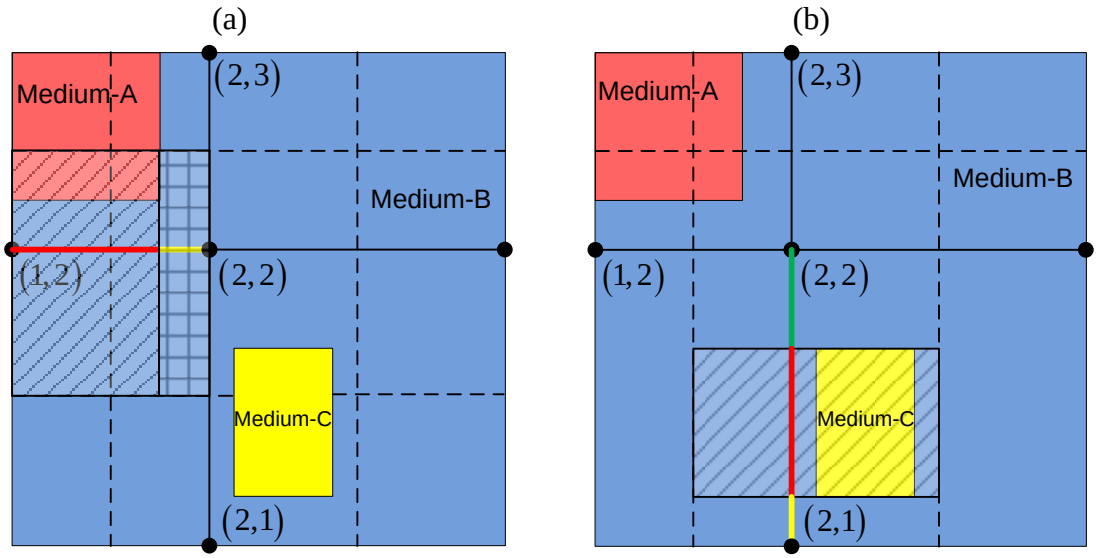

Figure 73: Part of a 2D domain with a section of horizontal transmission line highlighted comprising two segments, and the corresponding areas indicated over which coefficients are averaged, (a), and with a section of vertical transmission line highlighted comprising three segments, with the area indicated over which coefficients are averaged for one of those segments, (b).

Chapter 7

7 Discussion

7.1 Introduction

This thesis introduces and tests a novel numerical method called LCM, developed for solving convection-reaction-diffusion equations, in particular for applications in which physical properties (and, therefore, the coefficients of the CRDE) are piecewise-constant. The method can be applied to more general problems where coefficients vary continuously over space and time; however, this study is confined to the examination of problems in which they only vary over space. It is expected that any scheme for implementing time-varying coefficients would add similar errors to the results of any solution method (in the same way as different time-stepping schemes produce similar time-stepping errors in both LCM and FVM).

The method has first been established for one-dimensional steady-state reaction-diffusion problems. This has been followed by its extension for solving transient reaction-diffusion problems. It has also been extended to solve convection-reaction-diffusion problems and to two dimensions. It has not been extended to three dimensions but there is no reason to suggest that such an extension would be problematic.

The basis for the method is similar to that of TLM, but the resulting scheme resembles, to some extent, the Finite Volume Method. The method allows the use of TLM time-stepping for transient problems, as well as standard explicit and implicit schemes.

In general, for all tests, the one-dimensional LCM results are more accurate than equivalent FVM results. In some cases, especially where one or more of the problem

coefficients is piecewise constant, the difference in the accuracies is significant. The computational cost of calculating the LCM parameters is higher than that for the FVM schemes tested, but the results suggest that the LCM scheme is generally more efficient. That would be particularly true for transient linear problems since the lumped-component circuit parameters must only be calculated once, and the cost of that calculation, although higher than that for FVM, would, in general, be insignificant when compared to the overall solution cost.

The LCM scheme has other potentially significant advantages for a modeller. The solutions are bounded, even for high Peclet numbers. Evenly spaced nodes can be used for solving problems with discontinuities (as can unevenly spaced nodes, where the spacing is chosen for maximum efficiency instead of being dictated by the positions and thicknesses of the physical layers being modelled) without the problem of inconsistent convergence. This is a significant advantage because consistent convergence is required for the successful use of Richardson extrapolation and other techniques used by modellers, including techniques used for estimating the magnitude of errors in solutions and the node spacing required for a desired level of solution accuracy.

When solving a transient problem with one or more very thin physical layers, the need for consistent convergence in FVM may dictate that at least two nodes are very closely spaced. If an explicit time-stepping scheme is used (as is often the case in commercial solvers because of the large memory requirements associated with unconditionally stable implicit time-stepping) then a very short time step length may be required to ensure stability. That is not the case when using LCM.

Some of the results and analysis presented above suggest that there may be straightforward ways, when using LCM, of estimating when and where spatial discretization errors are highest during a transient solution. It may be possible, in the future, for modellers to use this information to optimize node positions so as to efficiently produce accurate solutions. It may also be possible to use this information to increase efficiency by varying the node spacing for a given problem over time.

7.2 Steady-state LCM

The method produces exact solutions for piecewise-constant one-dimensional problems. Where one of the coefficients varies continuously over space while the others are piecewise-constant, it is shown that the method produces significantly more accurate solutions than the FVM schemes tested. In general, when all coefficients vary continuously over space, the advantage of LCM over FVM is smaller, especially considering the higher cost of calculating the lumped-component circuit parameters.

As mentioned above, one-dimensional LCM solutions are bounded, and consistently converge no matter where the nodes are located. Testing suggests that two-dimensional LCM shares these properties.

7.3 Transient LCM

The technique used for determining the transient LCM circuit parameters produces highly accurate solutions in general. However, the lumped-component circuit elements do not exactly model the TL segments representing the problem to be solved when the voltage is varying over time. As a result, spatial discretization errors are introduced, even for problems with piecewise-constant coefficients.

LCM and FVM are identical for diffusion problems in which any discontinuities in the coefficients occur at nodes. That is not surprising since the steady-state solutions of such problems are piecewise quadratic (or piecewise linear if there is no source term), and the truncation errors in FVM are therefore zero.

For piecewise-constant transient one-dimensional problems, there are only two sources of errors in LCM, one due to the initialization and the one mentioned above (i.e. the difference between the behavior of the lumped-component circuits and the TL segments). Results suggest that it may be possible to relate the latter source of errors to the solution errors, and to how the solution is changing over time and space. If that is possible then it would potentially be very useful for modellers (e.g. in indicating when and where a change in node spacing may be of benefit).

TLM has been used as a time-stepping scheme for both LCM and FVM. It is simple to implement, explicit (and therefore efficient in terms of memory requirements),

unconditionally stable, second order and accurate. Its one principal limitation is that one source of errors, the wave term, is related to $\Delta t^2/\Delta x^2$, and so the solution does not converge consistently as Δx is reduced.

The ability to use TLM as a time-stepping technique for FVM in the manner outlined above arises from the similarity between the FVM equation and the equation for the voltage at a node in a simple lumped-component circuit. Such a similarity does not exist if the FVM equation for node n includes solution values other than those at nodes n+1 and n−1. TLM cannot, therefore, be used when convection is modelled using the QUICK scheme.

It should be noted that LCM with TLM time-stepping is essentially a TLM scheme, despite having been derived in a different manner to other TLM schemes.

7.4 Two-dimensional LCM

Two-dimensional LCM cannot produce exact solutions of steady-state problems with piecewise-constant coefficients. Tests suggest that it generally converges consistently in a second order manner, but further testing is required. Very limited comparison has been made to date with FVM, and further work is required to compare the accuracy of the two schemes. It may be possible to improve the accuracy of the LCM scheme outlined here by developing alternative methods for calculating the TL parameters when the problem coefficients vary over space.

7.5 Validation using real physical applications and analytical solutions

The real physical applications to which LCM has been applied in this thesis are limited in nature. For example, many of them are problems with constant coefficients. The difficulty in finding appropriate problems that fully show the benefits of LCM (for example, either one- or two-dimensional transient problems with piecewise-constant coefficients), for which solutions have been published, and which could be modelled using the method as outlined here, could be seen as undermining its value. It is partly due to the fact that many of the problems detailed in the literature involve coupled non-linear equations, time-varying coefficients, or more complex geometries, and the implementation of these is beyond the scope of the work presented here.

Analytical solutions have also been used for validation purposes. One-dimensional steady-state solutions can be found for some problems; however, it is difficult to find suitable transient 1D or 2D analytical solutions in the literature, especially for problems with discontinuities.

7.6 Future work

Some future work involving further development and analysis of the method is suggested and discussed here.

7.6.1 Variations in physical capacitance

In reaction-diffusion models, when C_d is a constant, its value does not affect the LCM parameters. In models of transient thermal problems involving heat conduction through different materials, however, the different thermal capacitances of those materials have to be taken into account, and that would be done in LCM by varying the distributed capacitance of the TL/TLs over space. The method derived in Chapters 4 and 5 allows such variations, but no problem of that type has been tested to date.

Spatial variations in capacitance may also be required in transient convection-reaction-diffusion models. One example is the modelling of heat flow during extrusion processes in which the convection term takes account of the movement of the extruded material relative to the extruder. There would appear to be no reason why different thermal capacitances could not be modelled in such problems using LCM, but, again, this has not been tested to date.

7.6.2 Implementation of different boundary-condition types

Modelling of few real physical problems can be done using only Dirichlet boundary conditions. Many problems require the implementation of Neumann boundaries and/or other boundary types. Along a transmission line, at any point, the value of dV/dx is related to the current in the TL by

$$\frac{dV}{dx} = -IR_d$$

Since, for a given problem, it is possible to calculate R_d at any point along the TL used to model the problem, setting the value of dV/dx at a point is equivalent to setting the current, I, at that point. It would be relatively straightforward to derive the LCM equation for the node next to a boundary in terms of the current at that boundary (instead of the voltage at that boundary as used above for implementing Dirichlet boundary conditions), thereby allowing the implementation of a Neumann boundary. There appears to be no reason why other boundary types (such as Robin boundaries) could not be implemented in a similar way.

7.6.3 LCM for solving CRDEs with conservative convection terms

As mentioned in Chapter 1, a CRDE with a conservative convection term, i.e. one similar to Eq. (1.3), could be solved using LCM by approximating $\nabla \cdot \mathbf{v}$ and adding it to the reaction term. That, however, would introduce errors resulting from the approximation. One type of problem that could potentially be solved without such errors is one in which the convection velocity is piecewise linear (while D, K and S are piecewise constant). That would make, for example, in the one-dimensional case, dv/dx piecewise constant, allowing the dv/dxV term to be included in the reaction term with no loss of accuracy. To adapt LCM for the solution of such problems, the equations for a TL segment capable of modelling convection-reaction-diffusion with a linearly varying convection velocity would first have to be solved. A somewhat similar derivation has been done previously for the varied impedance TLM method, but only for situations in which there is no reaction term [51]. It is not clear, at present, if it would be possible to extend LCM in this way for models with $K \neq 0$.

7.6.4 Spatial discretization errors

For piecewise-constant transient problems, there are two sources of errors other than time-stepping errors. There appear to be two possible approaches that may allow a more complete analysis of one of these, i.e. the errors that result from the differences between the TL segments used to model a problem and the lumped-component circuit elements used to model those segments. The first approach would build on the phasor analysis presented in Chapter 4. The second approach would involve an examination of the errors in solutions of problems for which the analytical solution is the fundamental solution (i.e. problems in which there is a single initial injection of diffusant at one point

in an infinite domain) as partially explored in Chapter 5. The aim of the analysis would be to relate the solution errors in more general problems to the nature of the problem (and its solution) in a way that could be useful for modellers in choosing what mesh to use (or, possibly, on deciding how a mesh might be changed over time to keep the spatial errors for a particular problem within limits while reducing computational cost).

7.6.5 Analysis of spatial discretization errors on uneven grids

With steady-state LCM, errors can occur if the coefficients of the problem being modelled are not piecewise constant and have to be approximated by piecewise-constant functions. Results in Chapter 3 show that it is not possible to clearly establish the order of these errors empirically for LCM with unevenly-spaced nodes. An analysis of how these approximations affect the solution errors is required.

For transient LCM models with piecewise-constant coefficients, errors occur because the lumped-component circuit elements act differently to the segments of TL they are modelling. The order of these errors, when implemented with unevenly spaced nodes, has also not yet been established. Analysis presented in Chapter 4 suggests that differences between the I/O coefficients for the TL segments and the lumped-component circuit elements are proportional to h^4 as h approaches zero. Further work is required to establish fully how these differences affect the solution values.

7.6.6 Investigation of LCM with time- and solution-dependent coefficients

There would be no need to change the LCM method in order to allow the solution of CRDEs with time- and/or solution-dependent coefficients. Techniques used in FVM modelling of such problems could be used with LCM. The main question that requires investigation is how the additional solution errors resulting from such techniques would compare to errors arising from the LCM method itself. It is reasonable to assume that, for example, the errors associated with implementing time-varying coefficients would be similar in both an LCM solution and an equivalent FVM solution. If the total solution errors for both schemes were then similar, there would be no advantage from the use of LCM.

7.6.7 Comparison with other schemes

The only comparison made here is with standard FVM schemes that, in general, have a lower computational cost than LCM for a given node spacing and time-step length. No attempt has been made to evaluate or compare the computational costs. A more comprehensive comparison is required to establish whether the LCM scheme is an efficient method for general problems with, for example, coefficients that vary over space and/or time, or if it only has significant advantages for particular types of problems. Furthermore, work is required to test the accuracy of 2D LCM against that of comparable FVM schemes for problems with piecewise constant, and continuously varying, coefficients.

7.6.8 Improving the accuracy and convergence of 2D LCM

As shown in Section 6.6, a technique is required in 2D LCM for averaging problem coefficients before calculating TL section parameters. The method tested involves straightforward averaging over areas. This does not fully take into account the position of discontinuities.

To illustrate this, consider Figure 74(a), which represents part of a thermal model with a small heating element indicated in red. Consider the two TL sections that are highlighted, one vertical and one horizontal. The parameters for the vertical section are calculated using the problem coefficients averaged over the hashed area in the diagram. The horizontal section will comprise three TL segments, one of which will take into account the properties and position of the heating element.

Now consider the situation shown in Figure 74(b) in which the location of the heating element has been changed. The parameters for the highlighted horizontal TL section are different in this case because the TL segment that accounts for the heating element properties has moved. The parameters for the vertical segment, however, are the same. If the heating element is moved a little further to the right as in Figure 74(c), the horizontal TL section parameters changes again, as do those for the vertical section highlighted (which is no longer affected by the heating element properties).

As the heating element is moved gradually to the right, therefore, the parameters for the horizontal transmission line section change gradually (the current source in the

equivalent lumped-component element at the left-hand element decreases while the current source at the right-hand end increases). The parameters for the vertical TL section, however, remain constant as the heating element is moved to the right, so long as it is entirely within the area highlighted or entirely outside that area.

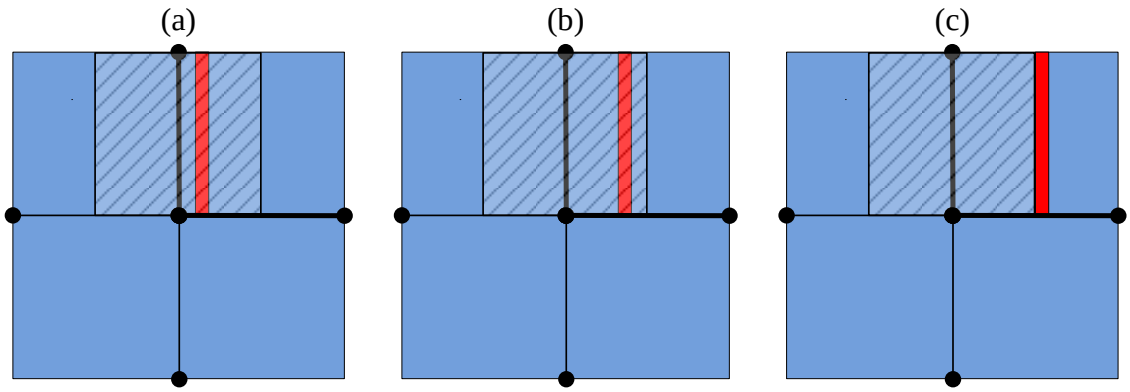

Figure 74: Part of a thermal model that includes a narrow heating element (i.e. a narrow area in which the source term in the corresdponding differential equation is not zero) indicated by the red rectangle. The heating element is shown in three different positions. Two TL sections are highlighted in each case, along with the area over which coefficients are averaged when calculating the parameters of the highlighted vertical TL section.

An alternative approach would average the coefficients over a larger area (as indicated in Figure 75) but would use a weighted average so that, for example, the problem coefficients close to the vertical TL section would be given a higher weighting than those further away. That would be similar to an approach used in the one-dimensional varied impedance TLM scheme [51], and would cause the vertical TL section parameters to vary gradually as the heating element is moved in this example. It is expected that such a scheme could be more accurate than the one described and tested in Section 6.6.

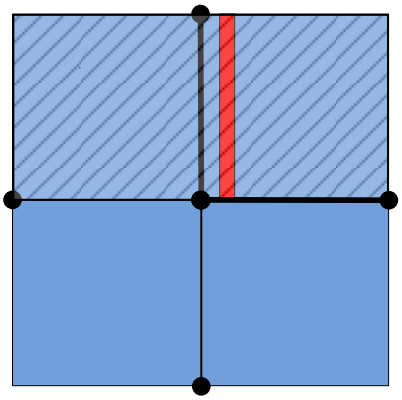

Figure 75: The area over which coefficients would be averaged, when calculating the parameters of the highlighted vertical TL section, in an alternative scheme

7.6.9 Complex geometries and non-orthogonal grids

The two-dimensional scheme outlined in Chapter 6 can only be implemented on graded orthogonal meshes (as illustrated in Figure 76(a)) and has only been tested with rectangular geometries. Graded meshes could be used with non-rectangular domains (as in Figure 76 (b)) but further work is required to implement it and test it for such problems.

The ability of the finite volume and finite element schemes to be implemented on unstructured triangular meshes is a very significant one. It is not known whether LCM could be adapted for use on such meshes, or, if it was, whether it would still exhibit its favourable properties.

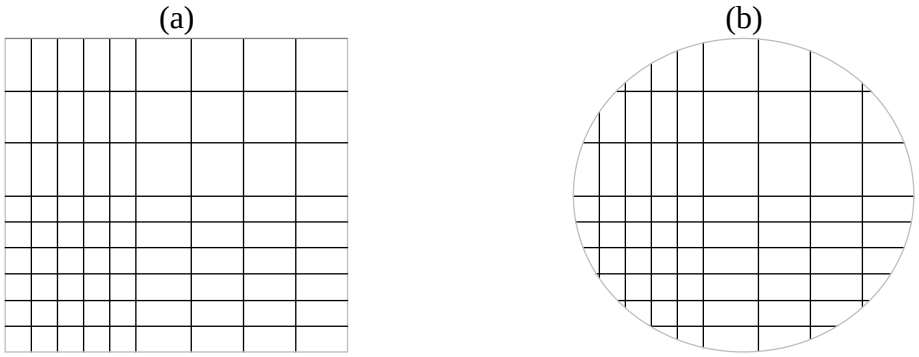

Figure 76: A graded orthogonal mesh for a rectangular domain, (a), and for a non-rectangular domain, (b).

Chapter 8

8 Conclusions

A new method for the solution of convection-reaction-diffusion equations has been successfully developed and implemented. The method is similar to TLM in that the CRDE is solved through an indirect process in which a transmission line is used as an analogue of the physical problem being solved. This transmission line is then modelled.

For steady-state modelling, the advantage of LCM, in terms of accuracy, over the FVM schemes tested, depends on the problem coefficients and how they vary over space. If they are all piecewise constant then the LCM solution is exact. If they all vary continuously over space, then the accuracy of LCM may not be significantly better than that of FVM (especially when the additional computational cost involved in calculating the LCM parameters is taken into account). If one or more of the coefficients is piecewise constant, however, LCM may be significantly more accurate.

For transient modelling, the spatial discretization errors for LCM and FVM can be very similar over a short initial part of the solution time. What happens after that depends on the relative accuracy of the two schemes for the equivalent steady-state problem. In general, LCM is significantly more accurate as the solution approaches a steady state. In practice, the advantage of LCM (in terms of accuracy) could depend on the purpose of the model. If, for example, a modeller is only interested in what happens to the solution as it changes rapidly from the initial conditions, then LCM may have little or no advantage over standard FVM schemes for him/her. If, on the other hand, a modeller is interested in what happens as the solution approaches a steady-state (for example, a

chemical engineer wishing to investigate how long it takes for 99% of a substance to undergo a given reaction, and what effect changes in process parameters may have on that time), then their use of LCM may be highly advantageous.

For problems with piecewise-constant coefficients, the solutions of the FVM schemes tested do not converge consistently if the nodes are not positioned to correspond to the discontinuities. That is not the case for LCM, which may be useful for a modeller in that, for example, they can position nodes in order to minimize errors, or concentrate nodes where the values of the solution are of particular interest, without needing to take into account the positions of discontinuities. The ability of LCM to account accurately for the properties of very narrow layers within the domain, and exhibit consistent convergence, without the need for closely spaced nodes, may be particularly advantageous in transient modelling in which, if a conditionally stable time-stepping technique is used, the node spacing may dictate the time step length required, and closely spaced nodes may lead to excessive computational costs.

The order of the steady-state discretization errors in LCM, resulting from the approximation of continuously varying coefficients by piecewise-constant functions, when implemented on uneven grids, has been investigated using results from one-dimensional models. While the scheme may be second order under such conditions, it is not possible to draw any conclusion at present (since the FVM results also appear to be second order on the same grids while it is known that FVM has first-order truncation errors when nodes are unevenly spaced). Further work is required.

Further work is also required to determine whether the nature of the solution over space and time can be used to determine, at least qualitatively, how LCM solution errors vary. Results suggest that transient LCM spatial discretization errors reach an initial peak and then fall, and that there may be a significant benefit in terms of reduced computational cost from changing the number of nodes once the errors have reduced to a certain degree. That would only be useful in practice if there was some way of monitoring how the solution errors are changing over time.

TLM has been used as a time-stepping technique in both LCM and FVM. While it may have significant advantages over many traditional techniques, the nature of the wave-term errors associated with it may limit its use in practice.

Further work is required to establish if, and under what conditions, LCM has significant advantages, in terms of accuracy, over equivalent FVM schemes in two dimensions.

Piecewise-constant convection-reaction-diffusion problems are common, and often occur in situations where numerical modelling is particularly necessary due to practical difficulties associated with experimentation (e.g. difficulties involved in making measurements without significantly altering the problem being examined). Further development of the method is required, but the results presented here suggest that such work may be worthwhile.

Appendices

Appendix A: Transmission and reflection coefficients in TLM

Consider a section of a TLM model between two nodes as shown in Figure 77 with a single incident pulse arriving from the left at the impedance discontinuity.

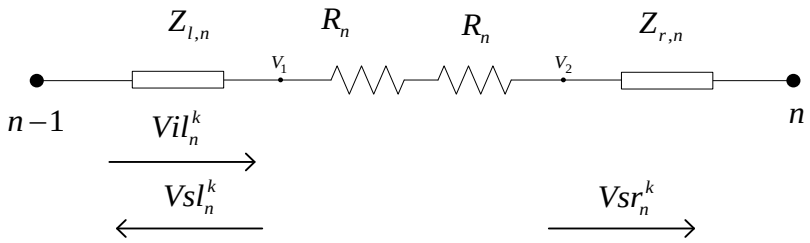

Figure 77: A section between two nodes in a link-resistor configuration for lossy TLM network in one-dimension.

The voltage scattered from any point in a given direction equals the voltage at that point minus the voltage incident from that direction at that instant. As a result, the voltages at the two points indicated in Figure 77 will be

$$V_1 = Vil_n^k + Vsl_n^k \tag{A.1}$$

$$V_2 = Vsr_n^k \tag{A.2}$$

According to Kirchhoff's current law, current at any point must be conserved. As a result

$$\frac{Vil_n^k}{Z_{l,n}} = \frac{Vsl_n^k}{Z_{l,n}} + \frac{Vsr_n^k}{Z_{r,n}} \tag{A.3}$$

The current flowing to the right through the two resistors is $Vsr_n^k / Z_{r,n}$. As a result

$$V_1 = 2R_n \frac{Vsr_n^k}{Z_{r,n}} + V_2 \tag{A.4}$$

From Equations (A.2) and (A.4), V_1 can be written as

$$V_1 = 2R_n \frac{Vsr_n^k}{Z_{r,n}} + Vsr_n^k$$

which simplifies to

$$V_1 = Vsr_n^k \left(\frac{Z_{r,n} + 2R_n}{Z_{r,n}} \right) \tag{A.5}$$

Equations (A.3) and (A.5) gives

$$Vsl_n^k = Vil_n^k - \frac{Z_{l,n}}{Z_{r,n} + 2R_n} V_1 \tag{A.6}$$

Substituting for Vsl_n^k in Eq. (A.1) using Eq. (A.6) gives

$$V_1 = \frac{2Z_{r,n} + 4R_n}{Z_{r,n} + 2R_n + Z_{l,n}} Vil_n^k \tag{A.7}$$

Replacing V_1 in Eq. (A.5) by that in Eq. (A.7) results in

$$Vsr_n^k = \frac{2Z_{r,n}}{Z_{r,n} + 2R_n + Z_{l,n}} Vil_{n1}^k \tag{A.8}$$

This is equivalent to

$$Vsr_n^k = \tau_{LR,n} Vil_{n1}^k \tag{A.9}$$

which means that the transmission coefficient for a voltage incident from left to right is given as

$$\tau_{LR,n} = \frac{2Z_{r,n}}{Z_{r,n} + Z_{l,n} + 2R_n} \tag{A.10}$$

Combining Equations (A.3) and (A.9) gives

$$\frac{Vil_n^k}{Z_{l,n}} = \frac{Vsl_n^k}{Z_{l,n}} + \frac{\tau_{LR,n}}{Z_{r,n}} Vil_{n1}^k \tag{A.11}$$

which can be simplified to

$$Vsl_n^k = \left(1 - \frac{Z_{l,n}}{Z_{r,n}} \tau_{LR,n}\right) Vil_{n1}^k \tag{A.12}$$

and it is equivalent to

$$Vsl_n^k = \rho_{LR} Vil_{n1}^k \tag{A.13}$$

This means that the reflection coefficient for a voltage incident from the left to right is given as

$$\rho_{LR} = \left(1 - \frac{Z_{l,n}}{Z_{r,n}} \tau_{LR,n}\right) \tag{A.14}$$

Similarly, the transmission coefficient for a voltage incident from the right can be shown to be

$$\tau_{RL,n} = \frac{2Z_{l,n}}{Z_{r,n} + Z_{l,n} + 2R_n} \tag{A.15}$$

and the equivalent reflection coefficient is

$$\rho_{RL,n} = 1 - \frac{Z_{r,n} \tau_{RL,n}}{Z_{l,n}} \tag{A.16}$$

Appendix B: Derivation of the equation for voltage along a general TL

Consider a short segment of a TL on length Δx with its distributed parameters represented by lumped components as shown in Figure 78. To avoid unduly cumbersome notation, the dependency on the parameters on position, x, is not indicated (for example, R_d is written instead of $R_d(x)$).

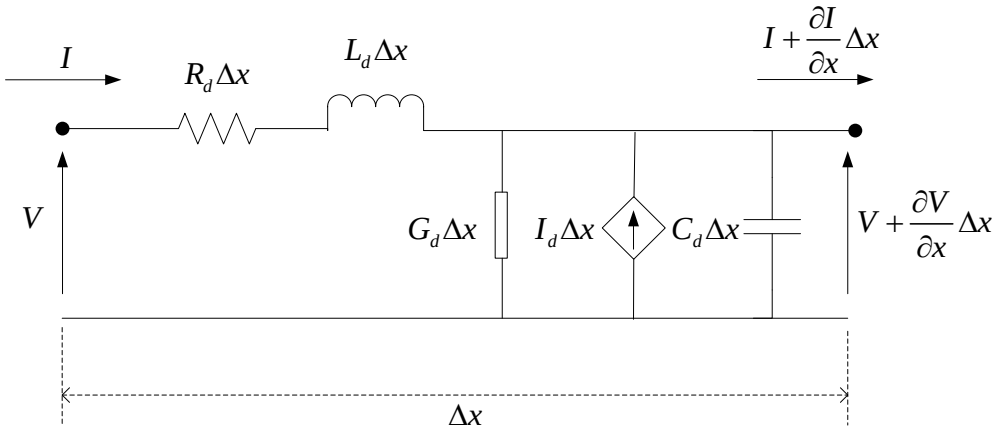

Figure 78: A short section of uniform TL of length Δx .

The voltage drop across the segment is

$$\left(V+\frac{\partial V}{\partial x}\Delta x\right)-V=-IR_d\Delta x-L_d\Delta x\frac{\partial I}{\partial t} \tag{B.1}$$

The sum of the currents entering the point at the right-hand side must be zero, and so

$$I-G_d\Delta xV+I_d\Delta x-C_d\Delta x\frac{\partial V}{\partial t}-\left(I+\frac{\partial I}{\partial x}\Delta x\right)=0 \tag{B.2}$$

Rearranging Eq. (B.1) gives

$$-I=\frac{1}{R_d}\frac{\partial V}{\partial x}+\frac{L_d}{R_d}\frac{\partial I}{\partial t} \tag{B.3}$$

Also, simplifying Eq. (B.1) and dividing across by C_d yields

$$\frac{1}{R_dC_d}\frac{\partial V}{\partial x}+\frac{I}{C_d}=-\frac{L_d}{R_dC_d}\frac{\partial I}{\partial t} \tag{B.4}$$

Differentiating Eq. (B.4) with respect to x gives

$$\frac{\partial}{\partial x}\left(\frac{1}{R_d C_d}\frac{\partial V}{\partial x}\right)+\frac{1}{C_d}\frac{\partial I}{\partial x}+\frac{\partial}{\partial x}\left(\frac{1}{C_d}\right)I=-\frac{L_d}{R_d C_d}\frac{\partial^2 I}{\partial x \partial t}-\frac{\partial}{\partial x}\left(\frac{L_d}{R_d C_d}\right)\frac{\partial I}{\partial t} \quad \text{(B.5)}$$

While differentiating Eq. (B.2) with respect to t results in

$$\frac{\partial^2 I}{\partial x \partial t}=-G_d\frac{\partial V}{\partial t}-C_d\frac{\partial^2 V}{\partial t^2} \quad \text{(B.6)}$$

Using Equations (B.2), (B.3) and (B.6) to replace the terms in Eq. (B.5)

$$\begin{aligned}\frac{\partial}{\partial x}\left(\frac{1}{R_d C_d}\frac{\partial V}{\partial x}\right)+\left(-\frac{G_d}{C_d}V+\frac{I_d}{C_d}-\frac{\partial V}{\partial t}\right)-\frac{\partial}{\partial x}\left(\frac{1}{C_d}\right)\left(\frac{1}{R_d}\frac{\partial V}{\partial x}+\frac{L_d}{R_d}\frac{\partial I}{\partial t}\right)=\ldots \\ \ldots\frac{L_d}{R_d C_d}\left(G_d\frac{\partial V}{\partial t}+C_d\frac{\partial^2 V}{\partial t^2}\right)-\frac{\partial}{\partial x}\left(\frac{L_d}{R_d C_d}\right)\frac{\partial I}{\partial t}\end{aligned} \quad \text{(B.7)}$$

If $L_d = 0$, Eq. (B.7) simplifies to

$$\frac{\partial V}{\partial t}=\frac{\partial}{\partial x}\left(\frac{1}{R_d C_d}\frac{\partial V}{\partial x}\right)-\frac{G_d}{C_d}V-\frac{1}{R_d}\frac{\partial}{\partial x}\left(\frac{1}{C_d}\right)\frac{\partial V}{\partial x}+\frac{I_d}{C_d} \quad \text{(B.8)}$$

Appendix C: Accuracy of LCM solution for steady-state reaction-diffusion

This section shows that the LCM solution of a reaction-diffusion problem with Dirichlet boundary conditions and piecewise-constant coefficients, with a single discontinuity in those coefficients, matches the corresponding analytical solution.

Figure 79 illustrates a RDE problem with boundary conditions $V(x_1) = V_L$ and $V(x_3) = V_R$. The problem has two physical layers of lengths h_1 and h_2 with the coefficients shown. The corresponding LCM model has nodes at x_1, x_2 and x_3. For simplicity, this analysis has been limited to the case where $x_2 - x_1 \leq h_1$.

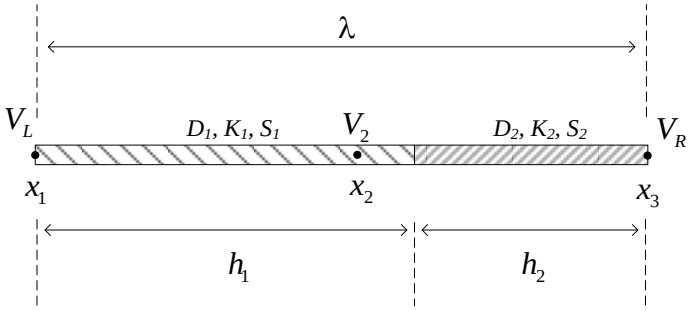

Figure 79: A representation of a problem with two physical layers and the locations of the nodes in the equivalent model.

Solving for V_2 using the LCM equation (Eq. (3.29)) gives the LCM solution in terms of the lumped-component circuit parameter values and the boundary voltages

$$V_2^{LCM} = \frac{\left(\frac{V_L}{R_1} + \frac{V_R + I_{l,2} + I_{r,1}}{R_2}\right)}{\left(G_{l,2} + G_{r,1} + \frac{1}{R_1} + \frac{1}{R_2}\right)} \tag{C.1}$$

Equations for $G_{l,2}$, $G_{r,1}$, R_1, R_2, $I_{l,2}$and $I_{r,1}$ can be found in terms of layer properties and x_2 from Eq. (3.18) to (3.22) once the I/O relationships for the two TL sections are found. These are not presented here because of their length. These can then be combined with Eq. (C.1) to give the LCM solution at node 2.

An analytical solution for the voltage along the domain for a scenario where $x_2 - x_1 = h_1$, can be found by solving equations (3.6) and (3.7) for each physical layer. This equation gives the solution in terms of V_2.

$$V_{x_2,x_1}(x) = \frac{(V_2K_1 - S_1)\sinh\left(\frac{\sqrt{K_1D_1}(x_1 - x)}{D_1}\right) - (V_LK_1 - S_1)\sinh\left(\frac{\sqrt{K_1D_1}(x_1 - x)}{D_1}\right)}{K_1\sinh\left(\frac{\sqrt{K_1D_1}(x_1 - x_2)}{D_1}\right)} + \frac{S_1}{K_1} \quad \text{(C.2)}$$

$$V_{x_3,x_2}(x) = \frac{(V_RK_2 - S_2)\sinh\left(\frac{\sqrt{K_2D_2}(x_2 - x)}{D_2}\right) - (V_2K_2 - S_2)\sinh\left(\frac{\sqrt{K_2D_2}(x_3 - x)}{D_2}\right)}{K_1\sinh\left(\frac{\sqrt{K_2D_2}(x_2 - x_3)}{D_2}\right)} + \frac{S_2}{K_2} \quad \text{(C.3)}$$

The diffusive flux, J, leaving layer 1 must equal that entering layer 2. Fick's Law [10] gives

$$J = -D\frac{\partial V}{\partial x} \quad \text{(C.4)}$$

and so $D_1 dV(x_2)/dx$ for layer 1 must equal $D_2 dV(x_2)/dx$ for layer 2. That gives

$$V_{2,exact} = \frac{\sqrt{D_1K_1}(K_1K_2\alpha_2V_L - K_2S_1\alpha_2 + K_2S_1\alpha_2\alpha_3) + K_1\alpha_1\sqrt{D_2K_2}(K_2V_R - S_2 + S_2\alpha_4)}{K_1K_2\left(\alpha_2\alpha_3\sqrt{D_1K_1} + \alpha_1\alpha_4\sqrt{D_2K_2}\right)} \quad \text{(C.5)}$$

where

$$\alpha_1 = \sinh\left(\frac{h_1\sqrt{D_1K_1}}{D_1}\right)$$

$$\alpha_2 = \sinh\left(\frac{h_2\sqrt{D_2K_2}}{D_2}\right)$$

$$\alpha_3 = \cosh\left(\frac{h_1\sqrt{D_1 K_1}}{D_1}\right)$$

and

$$\alpha_4 = \cosh\left(\frac{h_2\sqrt{D_2 K_2}}{D_2}\right) \qquad \text{(C.6)}$$

The LCM solution, derived as described above, equals this analytical solution for the voltage at node 2.

Further testing has shown that this is true for any number of physical layers of arbitrary lengths and any number of arbitrarily positioned nodes in the equivalent models. In all such tests, the errors in the LCM solutions are of a level consistent with them being solely the result of round-off errors in the computers used.

Appendix D: Details of FVM implementations of diffusion term

This section details the methods used to approximate the diffusion coefficient at the control volume boundaries when the diffusion coefficient is piecewise constant and either known over the entire domain or known only at the nodes.

Average of node value

This standard method uses simple linear interpolation to estimate the diffusion coefficient at the control volume boundaries using the values of D at the adjacent nodes [9-10]. It is implemented here in situations where D is only known at the nodes but is also used where D is piecewise constant. In the piecewise-constant case, it makes no use of the fact that $D(x)$ is known between the nodes. The general equation for the diffusion coefficient at the boundary between nodes n and n+1 is

$$D^{An}_{n+\frac{1}{2}} = \frac{h_n}{h_n + h_{n+1}} D_n + \left(1 - \frac{h_{n+1}}{h_n + h_{n+1}}\right) D_{n+1}$$

(where the superscript *An* refers to "average of the node values") which, for uniform node spacing, simplifies to

$$D^{An}_{n+\frac{1}{2}} = \frac{D_n + D_{n+1}}{2} \tag{D.1}$$

Average of average values

The second non-standard approach denoted using a superscript *AA*, and only used where D is piecewise-constant, takes account of the diffusion coefficient at all points by first calculating the average values of D over each volume using

$$\overline{D}_n = \frac{\int_{x_{n-\frac{1}{2}}}^{x_{n+\frac{1}{2}}} D dx}{x_{n+\frac{1}{2}} - x_{n-\frac{1}{2}}} \tag{D.2}$$

The diffusion coefficient at a control volume boundary is then calculated as

$$D^{AA}_{n+\frac{1}{2}} = \frac{\overline{D}_n + \overline{D}_{n+1}}{2} \tag{D.3}$$

Average between the nodes

The third, non-standard, method, denoted using a subscript *BA*, is used for problems with piecewise-constant $D(x)$. This method uses the average of $D(x)$ between nodes n and $n+1$ as the value of D at the control volume boundary between those nodes, i.e.

$$D^{BA}_{n+\frac{1}{2}} = \frac{\int_{x_n}^{x_{n+1}} D dx}{x_{n+1} - x_n} \tag{D.4}$$

Harmonic mean

The Harmonic mean, denoted here using a superscript *Hn*, is a standard method that gives a higher weight to low D values [10] and is calculated as

$$D^{Hn}_{n+\frac{1}{2}} = \frac{2D_n D_{n+1}}{D_n + D_{n+1}} \tag{D.5}$$

It can be used in all situations but cannot take into account values of $D(x)$ between the nodes.

Harmonic mean of average values

A fifth, non-standard, method, denoted by a superscript *Ha*, is used where D is piecewise constant and known at all points in space. The formula used is similar to Eq. (D.5) but average D values over the volumes (calculated using Eq. (D.2)) are used instead of values at the nodes

$$D^{HA}_{n+\frac{1}{2}} = \frac{2\overline{D}_n \overline{D}_{n+1}}{\overline{D}_n + \overline{D}_{n+1}} \tag{D.6}$$

Alternative harmonic average

A sixth non-standard method of calculating a harmonic mean value, denoted here by superscript *BHA*, uses one over the average value of 1/*D* between nodes *n* and *n* + 1 as the value of *D* at the boundary between the two nodes: i.e.

$$D_{n+\frac{1}{2}}^{BHA} = \frac{1}{\sum_{j=1}^{N_s} \frac{L_j / h}{D_j}} \tag{D.7}$$

Appendix E: FVM implementation of reaction term

In piecewise-constant problems where $K(x)$ is known, the integral $\int_{CV} K\phi$ must be estimated using some approximation of $\phi(x)$. One possibility is to assume a piecewise-linear variation in $\phi(x)$. Consider the situation shown in Figure 80 in which linear interpolation using the ϕ values at the nodes allows $\phi(x)$ to be estimates at other points.

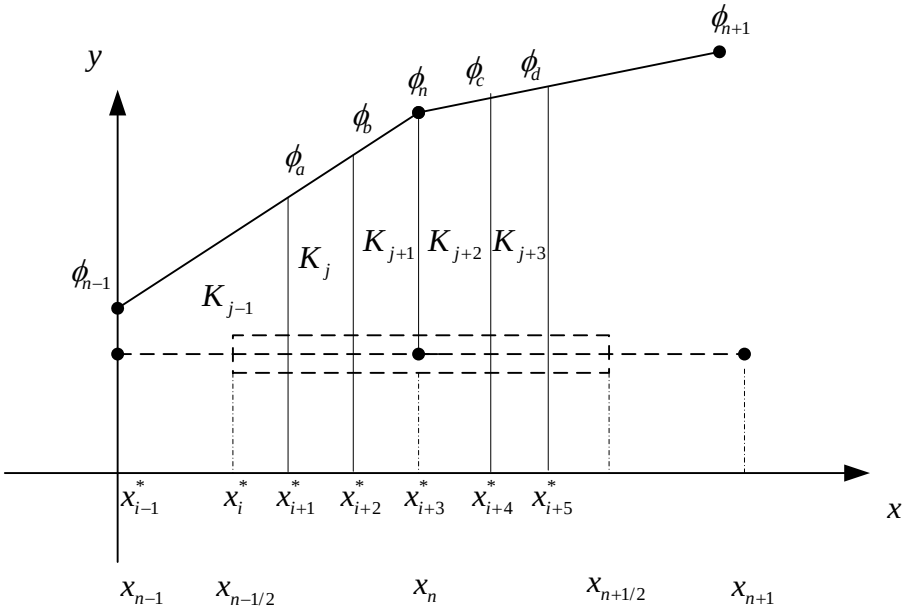

Figure 80: Plot of the voltage for a section of a domain for a problem with many layers. The dashed rectangle indicates the extent of control volume *n*.

The values K_{j-1}, K_j, K_{j+1}, K_{j+2} and K_{j+3} are the reaction coefficients for the layers shown. First, consider the section of the CV between $x_{n-½}$ and x_n where ϕ_a and ϕ_b are the interpolated values of $\phi(x)$ at the layer boundaries. Assuming a piecewise-linear variation in ϕ between x_{n-1} and x_n, the integral $K_{i+2}\int_{x^*_{i+1}}^{x^*_{i+2}} \phi\, dx$ can be written as,

$$K_{i+2}\int_{x^*_{i+1}}^{x^*_{i+2}} \phi dx = K_{\alpha,i+2}\phi_{n-1} + K_{\beta,i+2}\phi_n \qquad \text{(E.1)}$$

where

$$K_{\alpha,i+2} = K_{i+2}\frac{\left(x^*_{i+2} - x^*_{i+1}\right)\left(x^*_{i+2} - x^*_{i+1} - 2x_n\right)}{2\left(x_{n-1} - x_n\right)} \tag{E.2}$$

$$K_{\beta,i+2} = K_{i+2}\frac{\left(x^*_{i+2} - x^*_{i+1}\right)\left(x^*_{i+2} - x^*_{i+1} - 2x_{n-1}\right)}{2\left(x_{n-1} - x_n\right)} \tag{E.3}$$

where K_{i+2} is the value of K between x^*_{i+1} and x^*_{i+2}, which is equal to K_j in this case. Similar equations can be found for the integrals of $\int K\phi$ for the other layers between $x_{n-½}$ and x_n. As a result, adding the integrals for all segment between $x_{n-½}$ and x_n gives,

$$\int_{x_{n-\frac{1}{2}}}^{x_n} K\phi dx = \sum_{j=1}^{N_s|^n_{n-\frac{1}{2}}} K_{\alpha j}\phi_{n-1} + \sum_{j=1}^{N_s|^n_{n-\frac{1}{2}}} K_{\beta j}\phi_n \tag{E.4}$$

where j indicates the segment and $N_s|^n_{n-\frac{1}{2}}$ is the number of segments between $x_{n-½}$ and x_n.

A similar approach is used to get the integral $\int_{x_n}^{x_{n+\frac{1}{2}}} K\phi dx$, where the integral for the segment between x^*_{i+4} and x^*_{i+5} is given by,

$$K_{i+5}\int_{x^*_{i+1}}^{x^*_{i+2}} \phi dx = K_{\chi,i+5}\phi_{n-1} + K_{\delta,i+5}\phi_n$$

and where

$$K_{\chi,i+5} = K_{i+5}\frac{\left(x^*_{i+5} - x^*_{i+4}\right)\left(x^*_{i+5} - x^*_{i+4} - 2x_{n+1}\right)}{2\left(x_n - x_{n+1}\right)}$$

$$K_{\delta,i+5} = K_{i+5}\frac{\left(x^*_{i+5} - x^*_{i+4}\right)\left(x^*_{i+5} - x^*_{i+4} - 2x_n\right)}{2\left(x_n - x_{n+1}\right)}$$

Adding the integrals for all segments between x_n and x_{n+1} gives,

$$\int_{x_n}^{x_{n+\frac{1}{2}}} K\phi dx = \sum_{j=1}^{N_s|_n^{n+\frac{1}{2}}} K_{\chi,j}\phi_n + \sum_{j=1}^{N_s|_n^{n+\frac{1}{2}}} K_{\delta,j}\phi_{n+1} \tag{E.5}$$

The overall integral for the control volume is found by adding Equations (E.4) and (E.5)

$$\int_{n-\frac{1}{2}}^{n+\frac{1}{2}} K\phi dx = \sum_{j=1}^{N_s|_{n-\frac{1}{2}}^{n}} K_{\alpha j}\phi_{n-1} + \sum_{j=1}^{N_s|_{n-\frac{1}{2}}^{n}} K_{\beta j}\phi_n + \sum_{j=1}^{N_s|_n^{n+\frac{1}{2}}} K_{\chi,j}\phi_n + \sum_{j=1}^{N_s|_n^{n+\frac{1}{2}}} K_{\delta,j}\phi_{n+1} \tag{E.6}$$

References

1. Salas, A.H., L.J.M. H, and O.F. S, *Reaction-diffusion equations: A chemical application.* Scientia et Technica, 2010. **XVII**(46): p. 134-137

2. Volpert, V. and S. Petrovskii, *Reaction-diffusion waves in biology*. Physics of Life Reviews, 2009. **6**(4): p. 267-310.

3. Eslamian, M. and M.Z. Saghir, *Thermodiffusion (thermomigration) and convection in molten semiconductor-metal layers.* International Journal of Thermal Sciences, 2011. **50**(7): p. 1232-1242.

4. Al-zeben, M.Y., A.H.M. Saleh, and M.A. Al-Omar, *TLM modelling of diffusion, drift and recombination of charge carriers in semiconductors.* International Journal for Numerical Modelling, 1992. **5**(1992): p. 219 - 225.

5. Guin, L.N., *Existence of spatial patterns in a predator-prey model with self-and cross-diffusion.* Applied Mathematics and Computation, 2014. **226**(0): p. 320-335.

6. Rodrigo, M.R.M., Rogemar S., *An alternative approach to solving the Black-Scholes equation with time-varying parameters.* Applied Mathematics Letters, 2006. **19**(4): p. 398-402.

7. Cen, Z. and A. Le, *A robust and accurate finite difference method for a generalized Black-Scholes equation.* Journal of Computational and Applied Mathematics, 2011. **235**(13): p. 3728-3733.

8. Li, Y. and J. Wu, *Convergence of solutions for Volterra-Lotka prey-predator systems with time delays.* Applied Mathematics Letters, 2009. **22**(2): p. 170-174.

9. Versteeg, H.K. and W. Malalasekera, *An introduction to computational Fluid Dynamics. The Finite Volume Method*. 1995, Harlow: Pearson Education Limited.

10. Majumdar, P., *Computational methods for heat and mass transfer*. 2005, New York, London: Taylor & Francis.

11. Duffy, D.G., *Solutions of partial differential equations*. First ed. 1986: TAB Professional and Reference books.

12. Gockenback, M.S., *Partial differential equations: Analytical and numerical methods*. Second ed. 2011: siam.

13. Sen, S., *A new family of (5,5)CC-4OC schemes applicable for unsteady Navier–Stokes equations.* Journal of Computational Physics, 2013. **251**(0): p. 251-271.

14. Wesseling, P., *Principles of computational fluid dynamics*. 2001, Berlin: Springer.

15. J. H. Ferziger, M.P., *Computational method for fluid dynamics*. Third ed. 2002, Berlin: Springer.

16. Cussler, E.L., *Diffusion: Mass transfer in fluid systems*. Third ed. 2009: Cambridge University Press.

17. Frank P. Incropera, D.P.D., Theodore L.Bergman, Adrienne S. Lavine, *Fundamentals of heat and mass transfer*. Sixth ed. 2007: John Wiley & Sons. Inc.

18. Rohsenow, W.M., J.P. Hartnett, and E.N. Ganic, *Handbook of heat transfer fundamentals*. Second ed. 1988: McGraw–Hill.

19. Frank Kreith, R.F.B., George D. Raithby, K. G. T. Hollands et al, *Heat and mass transfer*. Inverse Engineering Handbook, ed. K.A. Woodbury. 1999, Boca Raton: CRC Press LLC.

20. Boris Baeumera, M.K., Mark M. Meerschaertb, *Numerical solutions for fractional reaction-diffusion equations.* Computers & Mathematics with Applications, 2008. **55**(10): p. 2212 - 2226.

21. de cogan, D. and M. Henini, *Transmission–line matrix (TLM): a novel technique for modelling reaction kinetics.* J. Chem. Soc., Faraday Trans, 1987. **2**(83): p. 843-855.

22. Bekhit, H.M., M. E-Kordy, and A. E.Hassan, *Contaminant transport in groundwater in the presence of colloids and bacteria: model development and verification.* Journal of Contaminant Hydrology, 2009. **108**(3-4): p. 152-167.

23. Lanser, D. and J.G. Verwer, *Analysis of operator splitting for advection-diffusion-reaction problems from air pollution modelling.* Journal of Computational and Applied Mathematics, 1999. **111**(February 1998): p. 201-216.

24. Lee, Y.H., et al., *Bifurcation diagrams of population models with nonlinear, diffusion.* Journal of Computational and Applied Mathematics, 2006. **194**: p. 357-367.

25. Sun, Y.-M., M.T. Liang, and T.P. Chang, *Time/depth dependent diffusion and chemical reaction model of chloride transportation in concrete.* Applied Mathematical Modelling, 2012. **36**(3): p. 1114-1122.

26. Amri, A., A. Saidane, and S. Pulko, *Thermal analysis of a three–dimensional breast model with embedded tumour using the transmission line matrix (TLM) method.* Computers in Biology and Medicine, 2011. **41**(2): p. 76-86.

27. Hocine, R., et al., *TLM method for thermal investigation of IGBT modules in PWM mode.* Microelectronic Engineering, 2009. **86**(10): p. 2053-2062.

28. Barona, R., et al., *Dynamical modelling of a reactive extrusion process: Focus on residence time distribution in a fully intermeshing co-rotating twin-screw*

extruder and application to an lginate extraction process. Chemical Engineering Science, 2010. **65**(10): p. 3313-3321.

29. Vaidya, D.S., et al., *Convection-diffusion of solutes in media with piecewise constant transport properties.* Chemical Engineering Science, 1996. **51**(24): p. 5299-5312.

30. Company, R., et al., *Explicit solution of Black-Scholes option pricing mathematical models with an impulsive payoff function.* Mathematical and Computer Modelling, 2007. **45**(1–2): p. 80-92.

31. Verwer, J.G., J.G. Blom, and W. Hundsdorfer, *An implicit-explicit approach for atmospheric transport-chemistry problems.* Applied Numerical Mathematics, 1996. **20**(1-2): p. 191-209.

32. Spee, E.J., et al., *A numerical study for global atmospheric transport-chemistry problems.* Mathematics and Computers in Simulation, 1998. **48**(2): p. 177-204.

33. Nicolas Fiétiera, Y.K., Matthieu Vialard, *New methods for the fast simulations of the extrusion process of hot metals.* Journal of Materials Processing Technology, 2009. **209**(5): p. 2244 - 2259.

34. Yang, L. and I. Epstein, *Oscillatory turing patterns in reaction-diffusion systems with two coupled layers.* Physical Review Letters, 2003. **90**(17): p. 1-4.

35. Linninger, A.A., et al., *Prediction of convection-enhanced drug delivery to the human brain.* Journal of theoretical biology, 2008. **250**(1): p. 125-138.

36. Bajracharya, K. and D.A. Barry, *Accuracy criteria for linearised diffusion wave flood routing.* Journal of Hydrology, 1997. **195**(1-4): p. 200-217.

37. Vitrac, O., A. Mougharbel, and A. Feigenbaum, *Interfacial mass transport properties which control the migration of packaging constituents into foodstuffs.* Journal of Food Engineering, 2007. **79**(3): p. 1048-1064.

38. Alcino Resende Almeida, R.M.C., *Integral transform methodology for convection-diffusion problems in petroleum reservoir engineering.* International Journal of Heat and Mass Transfer, 1995. **38**(18): p. 3359-3367.

39. Roques, L., M.-A. Auger-Rozenberg, and A. Roques, *Modelling the impact of an invasive insect via reaction-diffusion.* Mathematical biosciences, 2008. **216**(1): p. 47-55.

40. Khalid Alhumaizi, R.H., Mostafa Soliman, *Numerical analysis of a reaction diffusion convection system.* Computers and Chemical Engineering, 2003(27): p. 579 - 594.

41. Ellad B. Tadmore, R.E.M., Ryan S. Elliott, *Continuum mechanics and thermodynamics*. 2012: Cambridge University Press.

42. Lewis, R.W., P. Nithiarasu, and K.N. Seetharamu, *Fundamentals of the finite element method for heat and fluid flow*. 2004, West Sussex: Wiley.

43. Campo, A., M. R. Salimpour, and J. Ho, *The method of lines with numerical differentiation of the sequential temperature-time histories for a facile solution of 1-D inverse heat conduction problems.* Heat and Mass Transfer, 2013. **2013**(49): p. 369 - 379.

44. Wolfram, S., *A new kind of science*. 2002: Wolfram Media, Inc.

45. Patankar, S., *Numerical heat transfer and fluid flow*. 1980, New York: Hemisphere Publishing Corporation.

46. Johns, P.B., *A simple explicit and unconditionally stable numerical routine for the solution of the diffusion equation.* International Journal for Numerical Methods in Engineering, 1977. **11**(1307 - 1328).

47. Editors: Gabi Ben-Dor, O.I., Tov Elperin, *Handbook of shock waves*. Vol. 1. 2001, San diego: Academic Press.

48. Tian, Z.F. and S.Q. Dai, *High-order compact exponential finite difference methods for convection-diffusion type problems.* Journal of Computational Physics 2007. **2007**(220): p. 952-974.

49. Luo, C., et al., *Modified exponential schemes for convection-diffusion problems.* Communications in Nonlinear Science and Numerical Simulation, 2008. **13**: p. 369-379.

50. Anguelov, R., J.M.S. Lubuma, and F. Minani, *Total variation diminishing nonstandard finite difference schemes for conservation laws.* Mathematical and Computer Modelling, 2010. **51**(3–4): p. 160-166.

51. Kennedy, A. and W.J. O'Connor, *A transmission line modelling (TLM) method for steady-state convection-diffusion.* International Journal of Numerical Methods in Engineering, 2007. **72**(9): p. 1009-1028.

52. Kennedy, A. and W.J. O'Connor, *A TLM method for steady-state convection-diffusion: Some additions and refinements.* International Journal of Numerical Methods in Engineering, 2009. **77**(4): p. 518-535.

53. de Cogan, D., *Transmission line matrix (TLM) techniques for diffusion applications*. 1998: Gordon and Breach Science Publishers.

54. Pulko, S.H. and H.R. Newton, *Modelling diffusion based processes using TLM*. 1991, TLM, IEE colloquium, Transmission line matrix modelling: London. p. 3/1 - 3/6.

55. S. H. Pulko and A.O. Olashore, *Modelling of heat transfer from fluid sources using TLM technique.* International Journal of Modelling & Simulation, 1989. **9**(4): p. 96 - 100.

56. Pulko, S.H. and P.B. John, *Application of Transmission-line modelling (TLM) to thermal diffusion in bodies of complex geometry.* International Journal for Numerical Methods in Engineering, 1986. **23**: p. 2303 - 2312.

57. Pulko, S.H., W.A. Green, and P.B. Johns, *An extension of the application of transmission line modelling (TLM) to thermal diffusion to include non-infinite heat sources.* International Journal for Numerical Methods in Engineering, 1987. **24**: p. 1333 - 1341.

58. Morton, K.W., *Numerical solution of convection-diffusion problems*. First ed, ed. R.J. Knops and K.W. Morton. 1996, Oxford: Chapman & Hall.

59. Leonard, B.P., *Order of accuracy of quick and related convection-diffusion schemes.* Applied Mathematical Modelling, 1995. **19**(11): p. 640-653.

60. Hoffman, J.D., *Numerical methods for engineering and scientists*. 1992, McGraw-Hill, Inc.

61. Y.N. Reddy, P.P.C., *An exponentially fitted finite difference method for singular perturbation problems.* Applied Mathematics and Computation, 2004(154): p. 83 - 101.

62. Ramos, J.I., *An exponentially-fitted method for singularly perturbed, one-dimensional, parabolic problems.* Applied Mathematics and Computation, 2005(161): p. 513-523.

63. Feng, Q., *Explicit finite difference method for convection-diffusion equations*, in *Proceedings of the World Congress on Engineering 2009*. 2009: London, U.K.

64. Al-Sanea, S.A., M.F. Zedan, and S.N. Al-Hussain, *Effect of thermal mass on performance of insulated building walls and the concept of energy savings potential.* Applied Energy, 2012. **2012**(89): p. 430 -442.

65. Anderson, J.D., *Computational fluid dynamics: the basics with applications*. 1995, New york: McGraw-Hill.

66. Pulko, S.H. and P.B. Johns, *Modelling of thermal diffusion in three dimensions by the transmission line matrix method and the incorporation of nonlinear thermal properties.* Communications in Applied Numerical Methods, 1987. **3**(1987): p. 571-579.

67. Ian, A., D. Russel, and P.W. Webb, *Automatic time step control in TLM difusion modelling for problems with time-varying load conditions.* International Journal of Numerical Modelling, 1996. **9**(1996): p. 417-428.

68. R. Hocine, A.B. Stambouli, and A. Saidane, *A three-dimensional TLM simulation method for thermal effect in high power insulated gate bipolar transistors.* Microelectronic Engineering, 2002. **2003**(65): p. 293-306.

69. Fawwaz T. Ulaby, E.M., Umberto Ravaioli, *Fundamentals of applied electromagnetics*. Vol. 6th, Upper Saddle River: Pearson.

70. Enders, P., S.H. Pulko, and D.M. Stubbs, *TLM for diffusion: consistent first time step. Two-dimensional case.* International Journal of Numerical Methods in Engineering: Electronic Networks, Devices and Fields, 2002. **15**: p. 251 - 259.

71. Kennedy, A. and W.J. O'Connor, *Error analysis and reduction in lossy TLM.* International Journal of Numerical Methods in Engineering, 2008. **73**(7): p. 1027-1045.

72. Gui, X. and D. de Cogan, *Transmission-line matrix models for solving transient problems of diffusion with recombination.* international Journal of Numerical Methods in Engineering: Electronic Networks, Devices and Fields, 2003. **464**: p. 453-464.

73. Aliouat Bellia, S., et al., *Transmission line matrix modelling of thermal injuries to skin.* Burns, 2008. **34**(5): p. 688-697.

74. Kennedy, A. and W.J. O'Connor, *An alternative TLM method for steady-state convection-diffusion.* International Journal of Numerical Methods in Engineering, 2009. **79**(10): p. 1264-1283.

75. Barbeiro, S., *Supraconvergent cell-centered scheme for two dimensional elliptic problems.* Applied Numerical Mathematics, 2009. **59**(1): p. 56-72.

76. Min, C., F. Gibou, and H.D. Ceniceros, *A supra-convergent finite difference scheme for the variable coefficient Poisson equation on non-graded grids.* Journal of Computational Physics, 2006. **218**(1): p. 123-140.

77. William L. Oberkampf, C.J.R., *Verification and validation in scientific computing*. 2010, Cambridge: Cambridge.

78. Clavero, C. and J.L. Gracia, *A higher order uniformly convergent method with Richardson extrapolation in time for singularly perturbed reaction-diffusion parabolic problems.* Journal of Computational and Applied Mathematics, 2013. **252**(0): p. 75-85.

79. Richard L. Burden, J.D.F., *Numerical Analysis*. 9th Internation Edition ed. 2011, Australia: Brooks/Cole, Cengage Learning.

80. Kumar, R. and J. Kumar, *Numerical simulation and convergence analysis of a finite volume scheme for solving general breakage population balance equations.* Applied Mathematics and Computation, 2013. **219**(10): p. 5140-5151.

81. J. Kacur, B.M., M. Remešíková, *Convergence of an operator splitting method on a bounded domain for a convection-diffusion-reaction system.* Journal of Mathematical Analysis and Applications, 2008(348): p. 894-914.

82. Natividad, M.C. and M. Stynes, *Richardson extrapolation for a convection–diffusion problem using a Shishkin mesh.* Applied Numerical Mathematics, 2003. **45**(2–3): p. 315-329.

83. Mukherjee, K. and S. Natesan, *Richardson extrapolation technique for singularly perturbed parabolic convection-diffusion problems.* Computing, 2011. **92**(1): p. 1-32.

84. G I Shishkin, L.P.S., *The Richardson extrapolation technique for quasilinear parabolic singularly perturbed convection-diffusion equations.* Journal of Physics, 2006. **2006**(55): p. 203 -213.

85. Pozrikidis, C., *Numerical computation in science and engineering*. 1998, Oxford: Oxford Universtiy Press.

86. Baruch, G., G. Fibich, and S. Tsynkov, *High-order numerical method for the nonlinear Helmholtz equation with material discontinuities in one space dimension.* Journal of Computational Physics, 2007. **227**(1): p. 820-850.

87. Al-Sanea, S.A. and M.F. Zedan, *Effect of insulation location on initial transient thermal response of building walls.* Journal of building physics, 2001(24): p. 275 - 299.

88. Song Jiangfenga, H.Z., Li Lianxiab, Chen Chang'ana, Luo Delia, *One-dimensional simulation of hydrogen isotopes diffusion in composite materials by FVM.* International Journal of Hydrogen Energy, 2011(36): p. 5702 - 5706.

89. Price, B.A. and T.F. Smith, *Thermal response of composite building envelopes accounting for thermal radiation.* Energy Conversion and Management, 1994. **36**(1): p. 23-33.

90. Sakai, G., et al., *Theory of gas-diffusion controlled sensitivity for thin film semiconductor gas sensor.* Sensors and Actuators B: Chemical, 2001. **80**(2): p. 125-131.

91. Matsunaga, N., et al., *Formulation of gas diffusion dynamics for thin film semiconductor gas sensor based on simple reaction-diffusion equation.* Sensors and Actuators B: Chemical, 2003. **96**(1–2): p. 226-233.

92. Cruz, P., et al., *Comparison of finite difference and control volume methods for solving differential equations.* Computers & Chemical Engineering, 2005. **29**(10): p. 2256-2258.

93. Diskin, B. and J.L. Thomas, *Notes on accuracy of finite-volume discretization schemes on irregular grids.* Applied Numerical Mathematics, 2010. **60**(3): p. 224-226.

94. Wöllenstein, J. *Semiconductor gas sensors using thin and thick film technology*. 12/04/2014]; Available from: http://www.ipm.fraunhofer.de/content/dam/ipm/en/PDFs/Product%20sheet/GP/ISS/Metalloxid-Sensor_en_V3.pdf.

95. Ashino, R., M. Nagase, and R. Vaillancourt, *Behind and beyond the Matlab ODE suite.* Computers & Mathematics with Applications, 2000. **40**(4–5): p. 491-512.

96. Mathworks. *Section on MATLAB help: ODESET*. 2011; 7.12.0.635 (R2011a):[Available from: http://www.mathworks.co.uk/help/matlab/ref/odeset.html.

97. Pulko, S.H., et al., *Automatic timestepping in TLM routines for the modelling of thermal diffusion processes.* International Journal of Numerical Methods in Engineering: Electronic Networks, Devices and Fields, 1990. **3**: p. 127 - 136.

98. de Cogan, D., *Time-step changes and parity effects in TLM thermal models*, in *International Conference on Simulation*. 1998, Simulation '98. International Conference on (Conf. Publ. No. 457): York. p. 325 - 328.

99. Gui, X. and P.W. Webb, *An error parameter in TLM diffusion modelling.* International Journal of Numerical Methods in Engineering: Electronic Networks, Devices and Fields, 1992. **5**: p. 129 - 137.

100. Borchartt, T.B., et al., *Breast thermography from an image processing viewpoint: A survey.* Signal Processing, 2013. **93**(10): p. 2785-2803.

101. Tan, T.Z., et al., *A novel cognitive interpretation of breast cancer thermography with complementary learning fuzzy neural memory structure.* Expert Systems with Applications, 2007. **33**(3): p. 652-666.

102. Grigoriev, M.M. and G.F. Dargush, *Boundary element methods for transient convective diffusion. Part I: General formulation and 1D implementation.* Computer Methods in Applied Mechanics and Engineering, 2003(192): p. 4281-4298.

103. Nadukandi, P., E. Oñate, and J. Garcia, *A high-resolution Petrov-Galerkin method for the 1D convection-diffusion-reaction problem.* Computer Methods in Applied Mechanics and Engineering, 2010(199): p. 525-546.

104. Robbins, A.H. and W.C. Miller, *Circuit analysis: theory and practice*. second ed. 2004: Thomas/Delmar Learning.

105. Ferreira, V.G., et al., *A bounded upwinding scheme for computing convection-dominated transport problems.* Computers & Fluids, 2012(57): p. 208-224.

106. Edited by : Mustafa M. Aral, S.W.T., *Groundwater Quantity and Quality Management*. 2011: ASCE.

107. Martinus Th. van Genuchten, F.J.L., Todd H. Skaggs, Nobuo Toride, Scott A. Bradford, Elizabeth M. Pontedeiro, *Exact analytical solutions for contaminant transport in rivers: The equilibrium advection-dispersion equation.* J. Hydrol. Hydromech., 2013. **61**(2): p. 146-160.